Universidad Autónoma de Madrid
Facultad de Ciencias
Departamento de Física Teórica

Isocurvature perturbations and Model Selection in Inflationary Cosmology

Memoria realizada por
María Beltrán Moreno,
presentada ante el Departamento de Física Teórica
de la Universidad Autónoma de Madrid
para la obtención del título de Doctora en Ciencias.

Proyecto dirigido por el
Dr. Juan García-Bellido Capdevila,
del Instituto de Física Teórica y
de la Universidad Autónoma de Madrid

Madrid, Abril 2007.

He was nothing like any human teacher Harry had ever had. His priority did not seem to be to teach them what he knew, but rather, to impress upon them that nothing, not even centaurs's knowledge, was foolproof.

A mis padres.

Contents

Motivation and Goals

Isn't everyone amazed when staring at the sky during a starry night?

Doesn't everyone wonder why all those stars, galaxies and planets are there? What forces sustain them? Will they be there forever? Have they been there forever? When did *forever* start?

I believe these are questions that every human being must have wondered about at some point, no matter their education, social class or temporal locus. It seems to me that this puzzlement about the cosmos, is one of the most important chapters in the book of the interaction between men and Nature. It is inherent to us to wonder about everything that surrounds us. The sky is therefore a natural place to begin looking. That is why this is a science that, under different names and tints has existed since men are men. Definitely, times and methods have changed. In particular, Cosmology is going through an epoch of unprecedented success. The steady progress of observations allows us to check our model of the Universe up to the point where we are able to describe what was the nature of matter at the beginning of our cosmological era and how it has evolved to the present day. It seems amazing that something as insignificant as a few people inside the Universe are able to disentangle such a mystery. Nevertheless not only are we doing it, but the future outlook is very promising.

The Universe as we know it, is about 13700 million years old. The theory of the *Hot Big Bang* describes its evolution since all the matter contained reached thermodynamic equilibrium, even before the Universe was one second old. This thermodynamical description together with particle physics, allows us to study all the particles present after the quark-hadron transition ($t_{\mathrm{q-h}} \sim 10^{-4}$s) from a theoretical point of view. These were neutrinos, electrons, nucleons, photons and other transmitters of the Electroweak force, and possibly dark matter. Specifically one of the greatest success was the description in 1950 of the Primordial Nucleosynthesis (the creation of all the light nuclei of H and He less than two minutes after the Universe was born) that lead to the accurate prediction of the abundances of light elements in the Universe.

Generally speaking, it could be said that the thermodynamical homogeneous evolution of the Universe is known and controlled since then. A number of experiments have confirmed our knowledge.

Also, thanks to the theory of General Relativity and Perturbation theory, we are able to describe the evolution of the inhomogeneities until these reach a non-linear regime[1]. All these developments unveil for us the process of structure formation in the Universe which along with the description of the homogeneous evolution allow us to talk about a Standard Cosmological Model for the first time in history.

In fact, there still remain a number of questions to be solved, and so this picture should be taken with a grain of salt. However, we can say that we nearly have a model that describes the evolution of the Universe. This description is unique when the values of the most important parameters, namely the total density of matter, Ω_0, the Hubble parameter H_0 and the amplitude of the primordial perturbations are specified.

This chain of successes currently lacks an essential ingredient which is the primordial origin of the universe. Perhaps, one can always go back in time to ask about the origin of the origin, and never settle for a given *beginning of time*, but it is important to explain the origin of the primordial inhomogeneities that seed the observed structures. We need to find a mechanism which is able to produce them with the appropriate amplitude and spatial distribution to agree with current observations. Also, this mechanism should explain the homogeneity and flatness that, as we will see during this thesis, hold in the Universe.

During the last thirty years there have been a great number of attempts to solve all these enigmas. Cosmic strings were a good candidate as seeders of inhomogeneities, however the spatial correlation in the temperature anisotropies in the Cosmic Microwave Background radiation they would generate does not agree with that observed by COBE in 1992[2] [1]. Besides, this theory did not solve the flatness and horizon problems. Also, the theory of the varying speed of light could clarify the problem of the homogeneity in the temperature but does not explain how homogeneities were formed.

So this was the situation when in 1980, the Inflationary paradigm arose. It was put forward by Alan Guth and promptly developed by Andrei Linde [2, 3]. In it, an effective scalar field induces an de Sitter phase in the Universe that drives it through a period of exponential expansion. This makes the picture change because the starting point of the the Hot Big Bang is a stretched piece of the space that existed before inflation, with all the consequences it implies.

This way, Inflation solves several of the problems that used to concern cosmologists. Inflation inevitably predicts a flat an homogeneous Universe. On the other hand, and according to quantum field theory, a nearly massless field fluctuates quantum mechanically, perturbing its own energy density in a scale invariant way giving

[1]Even after they enter the non-linear regime, their evolution can be traced thanks to the numerical simulations to which many supercomputers around the globe are devoted.

[2]As a matter of fact, the observation of the anisotropies in the CMB awarded G. F. Smoot and J. C. Mather the 2006 Nobel Prize in Physics as the PIs of the project.

the power spectrum that may be inferred from the galaxy distribution in the Universe.

Almost without asking for it, three very important questions, namely flatness, homogeneity and anisotropies, were solved. Since then many theoretical and observational efforts were aimed at refining the original inflationary paradigm.

It is now time to remark on the essential role played by experiments. The measurement of the anisotropies in the CMB, which are microscopically small, is one of the main pillars upon which this unprecedented step forward is based. If in 1992, the COBE satellite confirmed their existence and correlation, in 2003 the Wilkinson Microwave Anisotropy Probe, WMAP [4], measured their magnitude with an accuracy that allowed us to bound the values for the main cosmological parameters with errors smaller than 10% of their value. In 2006 a second data release of WMAP [5] allowed for a tighter constraint of the parameters with the additional measurement of the anisotropies in the CMB polarization.

Apart from other, ground based experiments that measure the CMB anisotropies, it has also been crucial the contribution of two other kinds of experiments: the supernovae of type Ia and the elaboration of accurate maps of large scale structures in the Universe (see, for example, [6] y [7]).

All this experimental progress, together with the Hot Big Bang Model and Inflation, allows us to observe a Universe which, according to what was expected theoretically, shows a gaussian and scale invariant spectrum of primordial anisotropies. Also, we observe that the nature of the anisotropies is *adiabatic*. That is, the perturbations in the energy density have a direct correspondence with perturbations in the number density of particles. This means that the fluid may be wholly described just by knowing its temperature.

However, this is by no means the end of the story. The inflationary paradigm still allows for many extensions and the implications of some of them are tightly related to physics beyond the standard model (of particle physics). For example, the possible presence of cosmic defects and their effect on the observations, the observation of a tensor component in the CMB spectrum or the nature of Dark Energy are issues of different relevance for cosmology but all of them still need to be solved.

At a different epistemological level, and probably more easily accessible, there is the problem of knowing the exact nature of the primordial anisotropies. There is no direct proof of the existence of anisotropies of nature other than adiabatic, but observations do not rule out that a small fraction of them were seeded by *isocurvature* primordial seeds. If more than two fields were present during inflation, there is the possibility that some of the primordial perturbations were seeded by perturbations in the *entropy* of the fluid and not in its energy density.

This thesis is devoted to the study of the possible signatures of isocurvature anisotropies. From a theoretical point of view, their existence would open up a whole

spectrum of possibilities since it would be necessary to find another scalar field that could exist during inflation. Such is the case of the axion in Quantum Chromodynamics, which, under a number of circumstances, would generate an isocurvature spectrum observable today. This is only an example of the power of the cooperation of Cosmology and particle physics. We believe it should be investigated and exploited and more so today that there are so many new born experimental projects.

The Planck satellite, which will be launched into space during the next few months, and international collaborations such as DES are remarkable examples of all the machinery which will be put to work in a very promising future. We should be ready to digest the new volume of data theoretically as well as experimentally.

This thesis mainly compares the phenomenology expected from theory to experiments, thus it is needed to develop the appropriate tools. The relatively short time that experiments have been accessible has not allowed Cosmology to prepare powerful and unique techniques for data analysis. We also deal with this problem during the thesis by studying which are the optimal parameters one should constrain given a set of data. This is an information inference problem which has been tackled for a long time by expert statisticians but had never been applied to Model Selection in Cosmology. We believe that parameter extraction from data should deal equally with Model selection and parameter determination. In order to do that, we develop new computational techniques that allow us to classify a model according to their ability to fit a set of data.

The thesis is organised as follows: in the first chapter, we summarize some major aspects of the Hot Big Bang model and Cosmological perturbation theory. This will be used as a frame for chapter 2 in which a review of single-field inflation is given, describing its successes and predictions. In Chapter 3 the theory of isocurvature perturbations in cosmology is discussed, presenting some of the parametrizations for parameter constraining. In the next chapter we describe some of the major experiments from which cosmological information is extracted and in chapter 5 we present the basic theory of Bayesian Model Selection, and our particular tools developed to attack the problem. Finally, before concluding we present all our results on isocurvature parameter determination, giving all the bounds found after using different assumptions and different sets of data.

Chapter 1

Introduction

The natural evolution of Cosmology as a science, has driven it towards the study the physics of higher and higher energies. Lately, and thanks to the amazing improvement of observations, cosmology has opened a new and very productive line of research in cooperation with particle physics.

One of the products of this synergy between particle physics and Cosmology has been the birth of an extremely successful paradigm: *the Inflationary Cosmology*. Still a paradigm, the phenomenology associated to the dynamics of an effective primordial scalar field, existing after the Planck time $t_{\rm P} \sim 10^{-43}$, agrees rather accurately with observations. The nature of the **inflaton field** is not fixed by the inflationary paradigm. Some models of physics beyond the standard model do propose some some theoretical candidates, nevertheless none of them have been authenticated observationally. We must study the field by its effects on the background evolution of the universe and the formation of structure.

Let us review the status of cosmology before inflation was proposed. The **Hot Big Bang** model describes an expanding universe that was born sometime before primordial nucleosynthesis ($t_{\rm nucl} \simeq 1$s) [8]. This allows for an accurate and successful prediction of the abundances of the light elements. The universe was then a radiation dominated hot plasma in expansion that progressively cooled down. Since radiation is a relativistic fluid it loses energy faster than the cold dust fluid while the Universe is expanding. Thus, the matter energy density grew with respect to radiation until it became dominant. When the temperature cooled to about 0.2eV photons decoupled from matter and travelled (almost[1]) freely ever since. Now we observe them as a background radiation with a blackbody spectrum with temperature $T_{\rm CMB} = 2.728K$.

The Hot Big Bang model has been successful on explaining all this phenomenology. However, there exist some small (of $\mathcal{O}(10^{-5})$) fluctuations in the magnitude of the temperature. They carry a vast amount of information about the distribution

[1]When the first stars formed ($t \sim 10^9$yr), the intergalactic medium became highly ionized (with a very low optical depth) and the photons of the CMB were partially reescattered.

of matter at the time of decoupling. These small inhomogeneities would give rise to large scale structure (LSS) later on. Before the inflationary paradigm was established there were only vague ideas about how these were seeded. Topological defects was the preferred solution but nowadays we know that this possibility is ruled out by data. Even though their existence is not completely ruled out, their role as main seeders of primordial anisotropies is discarded.

As we shall see, inflation does make an unavoidable prediction about the primordial seeds of LSS. And this is another of its great successes. Although it is expected to gather more and more experimental evidence in favour of Inflation, predicting the primordial power spectrum for anisotropies and fixing the horizon and flatness problems make this paradigm the ideal candidate.

The basic inflationary idea can be extended in many ways. One of them is by allowing more than one scalar field to be present during inflation [9, 10]. In some cases this would induce anisotropies in the entropy of the fluid in addition to those in the energy density expected in one-field models. The inclusion of new fields arises as a natural possibility, why not having more than one field? moreover, there exist models of particle physics beyond the Standard Model, such as the QCD axion, that also suggest the idea [11, 12]. Thus, its study opens a wide window for new physics. The phenomenology associated with this kind of models is much richer, and although they have not been discarded by experiments [13, 14, 15], they are not strictly required to explain the data. The upper bound on this models allows for a contribution of up to 40% (95% c. l.) of the power of the anisotropies at a scales of $k = 0.05h^{-1}\mathrm{Mpc}^{-1}$. Hopefully,future analyses and experiments will allow us to discriminate between models.

In this chapter, we perform a quick review of the tools used for studying the Standard Model in Cosmology, and set the basis and notation for further extensions such as isocurvature perturbations. We discuss General Relativity and Cosmological perturbation theory, the two basic ingredients to explore both the homogeneous and inhomogeneous evolution of the Universe. We prepare the road for the discussions held in chapters 2 and 3 in which we present the simplest Single-field inflationary model and the Isocurvature model extension respectively. As we will see, we then explore the phenomenology of experiments in chapter 4 and the debate and problematics of statistic and Model Selection in Cosmology in chapter 5. Finally, we present our results in chapter 6.

1.1 Background evolution of the universe

The mathematical structure for cosmology, the theory of General Relativity (GR), was put forward by Albert Einstein in 1916. Further, cosmologically aimed, developments of the theory were implemented by Alexander Friedmann and Georges Lemaitre.

Since then, there have been some new theoretical proposals to modify GR, however observations so far have not been able to discriminate between models. Many theoretical and experimental progresses are studying the problem; for the time being, the simplest, original GR theory remains in force.

The observational side of cosmology has suffered a very different evolution. New technologies have made possible a dramatic development and we are currently able of discussing a Standard Model of Cosmology with a fixed, set of parameters bounded to at least a few percent accuracy in their values.

Now we can make use of all the old and new knowledge to describe the background evolution of the universe, or "Hot Big Bang Cosmology". This section will only cover the basics about the the hot big bang model that will be needed for the rest of the review.

Working inside a general relativistic framework, we need to define a metric tensor, $g_{\mu\nu}$, in order to characterize the evolution and properties of spacetime. Once specified, we measure the spacetime interval between two points as:

$$ds^2 = g_{\mu\nu} dx^\mu dx^\nu \tag{1.1}$$

In general $g_{\mu\nu}$ is coordinate dependent, and it must be so in such a way that the interval ds^2 is invariant under a change of coordinates or a *change of gauge*.

Supported by the Copernican principle and observations, we impose **homogeneity** and **isotropy** at sufficiently large scales to arrive at the dynamic Friedmann-Robertson-Walker (FRW) form [8] of the metric (throughout the whole text we will stick to this signature convention):

$$ds^2 = -dt^2 + a^2(t)[\frac{dr^2}{1 - Kr^2} + r^2(d\theta^2 + \sin^2\theta d\phi^2)] \tag{1.2}$$

where t is the physical cosmic time, $a(t)$ is the scale factor, and the rest of the coordinates are **comoving** or time independent. A comoving observer is that who measures zero momentum at its own location or that who sees an isotropic universe around. It is useful to keep in mind the relationship between physical, $\mathbf{r}(t)$, and comoving coordinates $\mathbf{x}$, which applies to any cosmic distance:

$$\mathbf{r}(t) = a(t)\mathbf{x} \tag{1.3}$$

The value of the constant K determines the spatial curvature of the universe. The Ricci scalar for the spatial part of the metric is:

$${}^{(3)}R = \frac{6K}{a^2(t)} \tag{1.4}$$

As we will see in the next sections, present experiments point towards a zero or almost zero value for this parameter.

Using the **conformal time** τ, defined as $d\tau = dt/a$ we arrive at a form of the metric which is conformal to a static metric:

$$ds^2 = a^2(\tau)[-d\tau^2 + \gamma_{ij}dx^i dx^j] \tag{1.5}$$

(we have conveniently expressed the spatial part of the metric by the three dimensional tensor γ_{ij}). This form of the metric is often useful in theoretical cosmology.

The matter content of the universe at large scales can be described as a **perfect fluid**. A perfect fluid is one that is isotropic in the local rest frame and in an arbitrary frame, its energy momentum tensor takes the form:

$$T^{\mu\nu} = (\rho + P)u^\mu u^\nu + Pg^{\mu\nu} \tag{1.6}$$

where u^μ is the four-velocity ($u^\mu = \frac{dx^\mu}{ds}$) of the fluid, which in the local rest frame takes the form $u^\mu = (1, 0, 0, 0)$. The factor P is the pressure of the fluid, and ρ is its energy density.

The conservation of the energy-momentum tensor, and in particular, conservation of energy, is ensured as long as the continuity equation holds:

$$3\frac{\dot{a}}{a}(\rho + P) + \dot{\rho} = 0 \tag{1.7}$$

This ensures the conservation of energy inside a comoving volume $\mathcal{V} \propto a^3$ during the adiabatic expansion of the universe.
Equation (1.7) is easily solvable if the equation of state of the fluid is specified. We know the universe went through at least two successive epochs of radiation and matter domination. We can compute the evolution of the energy density of the universe as a function of the scale factor during these two epochs:

$$\begin{aligned} P_{rad} = \frac{1}{3}\rho_{rad} \Rightarrow \rho_{rad} \propto a^{-4} \\ P_{mat} = 0 \Rightarrow \rho_{mat} \propto a^{-3} \end{aligned} \tag{1.8}$$

As we will see later, the energy density of an oscillating scalar field evolves as that of a presureless dust fluid. When the field is away from its minimum and its potential energy is much bigger than its kinetic energy its energy density is a constant and its equation of state is $w = -1$, *i. e.* $P_{field} = -\rho_{field}$, as shown in Chapter 2.

Understanding the different rates at which the different fluids evolve is necessary to study the dynamics of the universe as a multi-component fluid.

In cosmology time and distances are measured in terms of the **redshift**. It is defined by:

$$1 + z = \frac{\lambda_{obs}}{\lambda} = \frac{a(t_0)}{a(t)} \tag{1.9}$$

When we use it referred to time, it means the time when the scale factor of the universe was $(z + 1)$ times smaller than it is today. The value of the scale factor today is conveniently taken to be $a(t_0) \equiv a_0 = 1$.

Once the metric and the energy content of the universe have been specified, we can study the dynamics by solving Einstein's field equations[2]:

$$G_{\mu\nu} \equiv R_{\mu\nu} - \frac{1}{2} g_{\mu\nu} R + \Lambda g_{\mu\nu} = 8\pi G T_{\mu\nu} \tag{1.10}$$

where R is the Ricci scalar:

$$R = 6\left(\frac{\ddot{a}}{a} + \frac{\dot{a}^2}{a^2} + \frac{K}{a^2}\right) \tag{1.11}$$

and $R_{\mu\nu}$ is the Ricci tensor, with components [18][3]:

$$\begin{aligned} R_{00} &= -3\frac{\ddot{a}}{a}; \quad R_{0i} = 0; \\ R_{ij} &= \left(\frac{\ddot{a}}{a} + 2\frac{\dot{a}^2}{a^2} + 2\frac{K}{a^2}\right) g_{ij} \end{aligned} \tag{1.12}$$

Λ is the cosmological constant term, originally proposed by Einstein in 1917 in an attempt to balance the forces and preserve the previously accepted picture of a static universe. If we move it to the rhs of (1.10) we can see that the equation is equivalent to one with no cosmological constant but with an energy-momentum tensor for the vacuum energy of the form:

$$T_{\mu\nu} = -\frac{\Lambda}{8\pi G} g_{\mu\nu} \tag{1.13}$$

that has a form of perfect fluid with: $P = w\rho$ and $w = -1$. We can associate this energy momentum tensor to that of the vacuum because it contains all the possible symmetries, as the vacuum does. Current analyses try to constrain the equation of state of the dark energy, or w. We have seen that a pure cosmological constant would have a value of $w = -1$ whereas some other more exotic[4] form of dark energy would have a different value. Current observations are in good agreement with $w = -1$ (see [17]).

Inserting Eqns. (1.2) and (1.6) into (1.10) we arrive at the Friedmann equations:

$$\frac{\dot{a}^2}{a^2} = \frac{8\pi G}{3}\rho - \frac{K}{a^2} + \frac{\Lambda}{3} \tag{1.14}$$

$$\frac{\ddot{a}}{a} = -\frac{4\pi G}{3}(\rho + 3P) + \frac{\Lambda}{3} \tag{1.15}$$

[2]We are using the convention c=1 throughout the text unless otherwise specified. The index convention will also be fixed: 0 refers to the temporal coordinate whereas $i, j = 1, 2, 3$ refer to the spatial coordinates.

[3]Note that a sign convention different from the one in the reference has been used. That is the only departure from it.

[4]We believe that the cosmological constant term is rather exotic by itself, in the sense that it could be the hint for a modified general relativity in which one could not measure energy absolutely.

The rate of expansion of the universe, given by $\frac{\dot{a}}{a}$ is called the **Hubble parameter**, H. It can also be written as:

$$H^2(z) = H_0^2[(1+z)^3\Omega_{\rm M} + (1+z)^4\Omega_{\rm R} + (1+z)^2\Omega_K + (1+z)^{3(1+w)}\Omega_X] \quad (1.16)$$

where w is the equation of state of the dark energy, Ω_X, assuming it is constant in time.

The quantity cH^{-1} is called the Hubble distance and it gives an estimate of the distance that light has travelled since the beginning of the universe[5]. More precisely, we can compute the comoving radial distance travelled by a light ray ($ds^2_{\rm light} = 0$) or **particle horizon** $x_h(t)$:

$$dx_h(t) = \frac{dt}{a(t)} \Rightarrow x_h(t) = \int_0^t \frac{dt'}{a(t')} \quad (1.17)$$

The particle horizon gives the size of the largest causally connected region at time t.

There are two other cosmological distances that will turn out to be useful in the forthcoming chapters: the angular diameter distance, $D_{\rm A}$ and the luminosity distance $d_{\rm L}$.

Both of them depend on the redshift at which they are measured and the underlying cosmological model as follows.

The angular diameter distance is the quotient between the angle subtended by an object in the sky and its physical size, and it can be computed from:

$$D_A(z) = \frac{1}{(1+z)H_0}\int_0^z \frac{dz'}{\sqrt{(1+z)^3\Omega_{\rm M} + (1+z)^4\Omega_{\rm R} + (1+z)^2\Omega_K}} \quad (1.18)$$

The *luminosity distance* is related to $D_{\rm A}$ as:

$$d_{\rm L} = (1+z)^2 D_{\rm A} \quad (1.19)$$

The two $(1+z)$ factors in the previous equation come from the energy redshift and the time delay suffered by the photons [18]. It is defined by the relationship between the flux $\mathcal{S}$ and intrinsic luminosity $\mathcal{L}$ of an object:

$$d_{\rm L} = \sqrt{\frac{\mathcal{L}}{4\pi\mathcal{S}}} \quad (1.20)$$

Intuitively, $d_{\rm L}$ measures the distance a photon would "think" it has travelled from the source with luminosity $\mathcal{L}$ to us. We need to calculate its value to compute the physical distance that separates us from a Supernova, which we will eventually use to measure the expansion rate of the universe, as we will see in chapter 4.

[5]When computing distances and times using the value of the Hubble parameter at the present time (H_0) it is sometimes useful to parametrize its uncertainty by h, such that $H_0 = 100\ h$ km/s Mpc^{-1}.

Solving for equations (1.7), (1.14) and (1.15) we find the expression for the evolution of the scale factor with time. The solution for these equations is generally dependent on K, the spatial curvature. As said before, experiments point towards a zero value of this constant. Thus we only solve them for the $K = 0$ case.

For a radiation filled universe we find:

$$a(t) \propto t^{\frac{1}{2}} \tag{1.21}$$

For a cold dust (conventional matter) filled universe:

$$a(t) \propto t^{\frac{2}{3}} \tag{1.22}$$

We clearly see how the equation of state of the content of the universe does affect its evolution.

It is useful to define the **critical density** of the universe. This is the energy density the universe would have if it was completely flat ($K = 0$). Using equation (1.14) and including the cosmological constant as a part of the total energy density, we find:

$$\rho_{\text{crit}} = \frac{3H^2}{8\pi G} \tag{1.23}$$

with the current measurements of the hubble parameter, this density corresponds to about 5.8 ± 0.3 protons per cubic meter.

The total energy density of the universe is made of all the energy densities of the different species present at the different epochs: photons, baryons, dark matter, dark energy, neutrinos and so on. Thus we can write the total energy density as a sum:

$$\rho = \rho_B + \rho_{DM} + \rho_\nu + \rho_\gamma + \rho_\Lambda ... \tag{1.24}$$

The individual energy densities are better expressed as a fraction of the critical density:

$$\Omega_i = \frac{\rho_i}{\rho_{\text{crit}}} \tag{1.25}$$

These are also called **density parameters**. We see then that if the universe is flat, we can write equation (1.24) as:

$$\frac{\rho}{\rho_{\text{crit}}} = \Omega_B + \Omega_{DM} + \Omega_\nu + \Omega_\gamma + \Omega_\Lambda ... \equiv \Omega \tag{1.26}$$

The parameter Ω is the value of the total energy density. When we refer to its value at the present epoch, we write Ω_0. Inserting (1.26) into (1.14), we obtain its simplified version:

$$\Omega - 1 = \frac{K}{a^2 H^2} \tag{1.27}$$

For a closed universe $\Omega > 1$ ($K > 0$) whereas for an open infinite universe $\Omega_0 < 1$ ($K < 0$).

Quick history of the universe

It will be useful to bear in mind the energy and time scales we are dealing with at the different cosmological epochs. The following table will help us on that [8]:

t	T-Energy	Event
10^{-43} s	10^{19}GeV?	Planck Scale, Inflation Begins?
...	...	Inflation ends, Physics beyond SM???
10^{-10} s	10^{2} GeV	EW symmetry breaking
10^{-2} s	10 MeV	γ, ν, e, $\bar{e}$ and p in thermal equilibrium
10 s	1 MeV	ν decoupling, e $\bar{e}$ annihilation.
100 s	0.1 MeV	Nucleosynthesis
10^{4} yrs	1 eV	Matter-radiation equality
10^{5} yrs	0.1 eV	Photon decoupling
$\sim 10^{9}$ yrs	10^{-3} eV	First bound structures form
$\sim 8.2 \cdot 10^{9}$ yrs	~ 3.8 K	Vacuum-matter equality
$13.6 \cdot 10^{9}$ yrs	2.728 K	Today

With this summary, we get a quick idea of some of the parameters needed to have a satisfying description of the background evolution of the universe. As we will see in the following chapters, current cosmological analyses are focused on determining the values of parameters such as Ω_B, Ω_{DM}, H_0 and $H(z)$ as accurately as possible.

Nevertheless, a complete theory describing the universe must, somehow explain the existence of the observed inhomogeneities in the universe. Clusters of galaxies, galaxies, stars, and ultimately... us. If the universe were completely homogeneous none of these would be present. We need to slightly drop the assumption of homogeneity and allow for small perturbations in the distribution of the primordial energy density of the universe. That way we will be able to explain the formation of LSS as well as the observed anisotropies int the CMB. We cover this topic in the next section.

1.2 Theory of Cosmological Perturbations

Cosmologists use a perturbative approach to solve the problem of structure formation in the universe. Current LSS is the product of the gravitational evolution of what once were small perturbations in the primordial universe.

This hypothesis is well founded upon one of the most fruitful pieces of data we can count on, the anisotropies on the CMBR. The CMB is a probe for the homogeneity of the universe during the radiation and matter domination epochs, as well as a smoking gun for the presence of some small perturbations (of order 10^{-5}) in the distribution of the matter during that time. We can follow them forward in time until now when they have evolved to conform the observed structures.

We will review this evolution in Chapter 4, but for the moment, let us set the basis of the cosmological perturbation theory and develop a formalism to follow the linear evolution of these perturbations (up to first order). Inside the general relativistic frame we see that the form of the metric determines the behaviour and distribution of matter but the reverse mechanism is also true. The matter distribution also back-reacts on the metric:

$$\text{METRIC TENSOR} \Longleftrightarrow \text{MATTER DISTRIBUTION}$$

In order to rigorously track the evolution of the perturbations we will take into account the perturbations on the metric tensor as well as the perturbations on the distribution of the energy density.

A given tensor can be perturbed with tensors of rank equal or smaller than its own. Since the metric $g_{\mu\nu}$ is a tensor of rank two, its perturbations can be sorted as scalar, vectorial and tensorial under the Lorentz subgroup of 3D rotations[6] [19]:

$$g_{\mu\nu} = {}^{(0)}g_{\mu\nu} + \delta g_{\mu\nu} = {}^{(0)}g_{\mu\nu} + \delta^{(s)}g_{\mu\nu} + \delta^{(v)}g_{\mu\nu} + \delta^{(t)}g_{\mu\nu} \tag{1.28}$$

Now we see the explicit expressions for each of the perturbative terms for the metric tensor (1.5).

Scalar perturbation In order to perturb the metric in the most general way, we need to define the four scalar quantities ϕ, ψ, B, E which in general are dependent on $(\mathbf{x}, t)$. Then, this term of the perturbation takes the form:

$$\delta^{(s)}g_{\mu\nu} = a^2(\tau) \begin{pmatrix} -2\phi & B_{|i} \\ B_{|i} & 2(-\psi\gamma_{ij} + E_{|ij}) \end{pmatrix} \tag{1.29}$$

where $_{|i}$ denotes a covariant derivative with respect to the coordinate i.

As we see later, in the simplest inflationary scenario the quantum fluctuations of the scalar inflaton field induce this kind of perturbations in the metric. These will eventually seed the potential wells into which matter falls to create the observed structures.

[6] The reason why this transformations are picked is because of the time-like foliation of the FRW universe.

Vector perturbation The vector perturbation takes the form:

$$\delta^{(v)} g_{\mu\nu} = a^2(\tau) \begin{pmatrix} 0 & -S_i \\ -S_i & F_{i|j} + F_{j|i} \end{pmatrix} \tag{1.30}$$

where S_i and F_i are two divergenceless three-vectors. If they were not divergenceless it would be possible to write them as the rotational of another vector plus the gradient of a scalar. Then we would not completely separate the scalar and the vectorial contributions to the global perturbation.

In the basic inflationary scenario vector perturbations are not created. If present, they must have been generated by some other more exotic primordial mechanism such as primordial magnetic fields or topological defects. They would seed vortical fluid perturbations which would survive up to now only under some special (though not impossible) conditions imposed on the streaming of the different fluids in the universe [20].

There is currently no observational strong evidence for the existence of primordial vector perturbations. Therefore we will not pursue their study further in this work. This does not mean that they were not there and any progress in this field could provide us with a very powerful insights about high energy particle physics.

Tensor perturbations They are constructed using the symmetric three-tensor h_{ij} satisfying the constraints:

$$h^i_i = 0; \quad h_{ij}{}^{|i} = 0 \tag{1.31}$$

Again, conditions (1.31) are imposed so that nothing inside h_{ij} is transformed as a three vector or a scalar. The tensor perturbation takes the form:

$$\delta^{(t)} g_{\mu\nu} = a^2(\tau) \begin{pmatrix} 0 & 0 \\ 0 & h_{ij} \end{pmatrix} \tag{1.32}$$

Tensorial perturbations are generically predicted by inflation. The intensity of the gravitational waves that would be generated could be so low that they would not be directly detected by interferometers. However, depending on the energy scale at which inflation took place, their effects could be observable in the B-mode polarization on the CMB spectrum of anisotropies [21].

The four dimensional metric tensor $g_{\mu\nu}$ has 10 different components ($g_{\mu\nu} = g_{\nu\mu}$). Due to the freedom of choice of coordinates, it turns out that 4 out of these components are non physical. We are thus left with 6 independent components of $g_{\mu\nu}$.

Six degrees of freedom which are evenly distributed so that two physical quantities of each nature can be defined (2 scalar, 2 vectors and 2 tensors).

The three different parts in which we splitted the metric perturbations are completely decoupled to linear order. Thus we can safely take care of the scalar perturbations alone which are the ones required for the rest of the work. The next section is devoted to them and their transformation properties under a change of coordinates.

1.2.1 Gauge invariant scalar perturbations

Perturbative methods are known to have a wide variety of applications inside the physical and mathematical sciences. In General Relativity we encounter two major obstacles when using them.

The first one comes one one encounters the complexity of its equations but this can be solved by using the appropriate numerical methods, and does not represent an insurmountable problem. The second, more subtle one, stems on the covariance requirement that must be imposed on every equation. Spacetime itself is perturbed as well as the quantities defined on it. The unperturbed quantity, ${}^{(0)}Q$ and the perturbed quantity Q, *live* in different manifolds, and thus the perturbation $\delta Q = Q - {}^{(0)}Q$ is ill-defined under a general change of coordinates[7].

As a matter of fact, it can be showed [22] that the general change of coordinates:

$$\begin{aligned} \tau &\rightarrow \tilde{\tau} = \tau + \xi^0(\tau, \mathbf{x}) \\ x^i &\rightarrow \tilde{x}^i = x^i + \gamma^{ij}\xi_{|j}(\tau, \mathbf{x}) \end{aligned} \tag{1.33}$$

induces a change in the perturbation δQ of:

$$\Delta Q = \tilde{\delta Q} - \delta Q = \mathcal{L}_\xi Q \tag{1.34}$$

Where $\mathcal{L}_\xi Q$ is the Lie derivative in the direction of the vector ξ.

Now, applying (1.34) to the scalarly perturbed line element:

$$ds^2 = a^2(\tau)[-(1+2\phi)d\tau^2 + 2B_{|i}dx^i d\tau + [(1-2\psi)\gamma_{ij} + 2E_{|ij}]dx^i dx^j] \tag{1.35}$$

we get the transformation under gauge change of each of the scalar quantities. As an example, we will explicitly write the change for ϕ, up to linear order:

$$\begin{aligned} \tilde{\delta g_{00}} &= \delta g_{00} + \Delta g_{00} = \delta g_{00} + \mathcal{L}_\xi {}^{(0)}g_{00} \\ \mathcal{L}_\xi {}^{(0)}g_{00} &= \xi^{\lambda (0)}g_{00|\lambda} + 2\xi^{\lambda}_{|0}{}^{(0)}g_{\lambda 0} = -2a^2(\frac{a'}{a}\xi^0 + \xi^{0\prime}) \\ &\Longrightarrow \tilde{\phi} = \phi - \frac{a'}{a}\xi^0 - \xi^{0\prime} \end{aligned} \tag{1.36}$$

[7]The manifold in which the perturbed quantity is defined, changes as the coordinates change

where the prime denotes differentiation with respect to the conformal time τ.
Using the same procedure, we can compute the changes for ψ, B and E:

$$\tilde{\psi} = \psi + \frac{a'}{a}\xi^0 \tag{1.37}$$

$$\tilde{B} = B + \xi^0 - \xi' \tag{1.38}$$

$$\tilde{E} = E - \xi \tag{1.39}$$

These transformation laws can also be derived by directly transforming the line element and expanding up to first order in the perturbations of the coordinates:

$$ds^2(\tilde{\tau}, \tilde{\eta}) = ds^2(\tilde{\psi}, \tilde{\phi}, \tilde{B}, \tilde{E}) \simeq ds^2(\tau, \eta) + \delta ds^2(\tau, \eta)$$

As we see, in the presence of cosmological perturbations, we are free to choose any gauge. This means that there is no way in which observers sitting in different causally disconnected regions could agree in the magnitude of a perturbation.
In cosmology, we deal with regions which are bigger than the Hubble radius so this ambiguity, intrinsic to the theory, is actually annoying.

However, it was shown by Bardeen in [23] that it is possible to define two gauge invariant scalar quantities which are enough to completely describe the scalar cosmological perturbations (as we saw before, only two physical degrees of freedom correspond to the scalar perturbations). The scalar potentials:

$$\Phi = \phi + \frac{1}{a}[(B - E')a]' \tag{1.40}$$

$$\Psi = \psi + \frac{a'}{a}(B - E') \tag{1.41}$$

are invariant under a change of coordinates such as (1.33). Due to their role inside the perturbed FRW metric, Φ is referred to as the **Newtonian potential** and Ψ is the **Intrinsic Curvature perturbation**. Also called the **Bardeen potentials**, they are extremely useful for cosmological perturbation theory since they allow us to track perturbations in the gravitational potential in a unique way. We shall see, through this thesis, the substantial role played by them as the center of the theory of cosmological perturbations.

As a matter of fact, we can write any perturbation of a scalar quantity in a gauge invariant way (gi). Take $Q(\tau, \mathbf{x})$ that can be decomposed into its background value and a perturbation:

$$Q(\tau, \mathbf{x}) = {}^{(0)}Q(\tau) + \delta Q(\tau, \mathbf{x}) \tag{1.42}$$

it is always possible to construct a combination of $\delta Q(\tau, \mathbf{x})$ and metric perturbations that is gi:

$$\delta Q(\tau, \mathbf{x})^{(gi)} = \delta Q(\tau, \mathbf{x}) + {}^{(0)}Q(\tau)'(B - E') \tag{1.43}$$

We will be using the formalism of gi perturbations for studying the cosmological perturbations and will be now applied to the field equations (1.10). We can split each of the tensors into their background and perturbation parts:

$$G^{\mu\nu} \rightarrow {}^{(0)}G^{\mu\nu} + \delta G^{\mu\nu}; \quad T^{\mu\nu} \rightarrow {}^{(0)}T^{\mu\nu} + \delta T^{\mu\nu} \tag{1.44}$$

The perturbed Einstein equations are then:

$$\delta G_{\mu\nu} = 8\pi G \delta T_{\mu\nu} \tag{1.45}$$

Their is calculation quite a dull task, nevertheless no sophisticated mathematics are needed and we can get them straightforwardly if we are patient enough. We write them now in a gauge invariant form and in conformal time, making use of the Bardeen potentials:

$$\begin{aligned} -3\mathcal{H}(\mathcal{H}\Phi + \Psi') + \nabla^2\Psi &= 4\pi G a^2 \delta T_0^{0(gi)} \\ (\mathcal{H}\Phi + \Psi')_{,i} &= 4\pi G a^2 \delta T_i^{0(gi)} \\ [(2\mathcal{H}' + \mathcal{H}^2)\Phi + \mathcal{H}\Phi' + \Psi'' + 2\mathcal{H}\Psi' + \frac{1}{2}\nabla^2 D]\delta_j^i - \gamma^{ik} D_{|kj} &= -4\pi G a^2 \delta T_j^{i(gi)} \end{aligned} \tag{1.46}$$

where $D = \Phi - \Psi$. The prime denotes a derivative with respect to the conformal time and $\mathcal{H} = \frac{a'}{a} = \frac{1}{a}H$ is the hubble factor in conformal time. This set of equations will be completed once we state what kind of matter fills the universe. In particular, for hydrodynamical matter treated as a perfect fluid, the perturbations on the energy-momentum tensor:

$$\delta T_0^{0(gi)} = \delta\rho^{(gi)}, \quad \delta T_i^{0(gi)} = (\rho_0 + P_0)a^{-1}\delta u_i^{(gi)}, \quad \delta T_j^{i(gi)} = -\delta P^{0(gi)}\delta_j^i \tag{1.47}$$

where $\delta\rho$, δP and δu_i are the perturbations on the energy density, the pressure and the three velocity of the fluid respectively.
The pressure fluctuation can be expressed in terms of $\delta\rho$ and the entropy perturbation δS:

$$\delta P = c_s^2 \delta\rho + \epsilon \delta S \tag{1.48}$$

where:

$$c_s^2 = \frac{1}{3}(1 + \frac{3}{4}\rho_m/\rho_r)^{-1}; \quad \epsilon = c_s^2 \rho_m / S \tag{1.49}$$

As we see from (1.48), $c_s^2 = \frac{\partial P}{\partial \rho}$ is the velocity of sound for hydrodynamical matter.

Inserting (1.47) into (1.46) and taking into account (1.48), we can combine the 00 and ij parts of the perturbed field equations to give:

$$\Phi'' + 3\mathcal{H}(1 + c_s^2)\Phi' - c_s^2\nabla^2\Phi + [2\mathcal{H}' - (1 + c_s^2)\mathcal{H}^2]\Phi = 4\pi G a^2 \epsilon \delta S \tag{1.50}$$

(in the absence of anisotropic stress, we have $\Phi = \Psi$). If we consider scales much larger than the Hubble radius, and pure adiabatic perturbations in which $\delta S = 0$, equation (1.50) can be written as a neat gauge invariant conservation law:

$$\dot{\zeta} = 0; \text{ with } \zeta = \frac{2}{3}(H^{-1}\dot{\Phi} + \Phi)/(1+w) + \Phi \tag{1.51}$$

This last equation is rather significant. Our goal is to track the amplitude of the perturbations from the time they leave the horizon and become classical until they become causally connected. If the perturbation on the entropy is negligible, as long as we know the value of ζ at horizon exit, its value will be know at all times. On the comoving gauge ζ takes on the physical meaning of a curvature perturbation. We will be using this variable and will refer to it as $\mathcal{R}$. For future convenience, we will also define the curvature perturbation on uniform total density slices. In this gauge the spatial line element is written as:

$$dl^2 = a^2(t)(1-2\zeta)\delta_{ij}dx^i dx^j \tag{1.52}$$

with:

$$\zeta = H\frac{\delta\rho}{\dot{\rho}} = \mathcal{H}\frac{\delta\rho}{\rho'} \tag{1.53}$$

In [24] the authors prove that the curvature perturbation defined on uniform density spatial hyper-surfaces is conserved on super hubble scales if the non adiabatic pressure is negligible and as long as the energy-momentum tensor is covariantly conserved. That is, the conservation of ζ is a direct consequence of the general coordinate invariance of the gravity theory, and not of the gravity theory itself.
It was shown in [25] that this quantity might not be conserved if more than one field was present during inflation. We will see in Chapters 2 and 3 how useful this quantity becomes for inflationary phenomenology.

Chapter 2

Single field inflation

In 1980 Alan Guth was the first to propose a new mechanism that seemed to solve some of the achings of cosmology at the time [2]. It was based on the idea that the universe underwent some supercooled phase transition at its very first stages. This would lead to a huge increase of the entropy of the universe which would solve the homogeneity and flatness problems However, this model had some unavoidable drawbacks (as a matter of fact, some of them were outlined on [2]).

Nevertheless the idea of a very early accelerated expansion of the universe appears quite plausible. Matter in the form of a scalar field would have this effect on the early universe. Many different models of inflation have been built since then [29, 30]. Most of them are of phenomenological nature. As pointed out in the introduction, the energy scale for inflation as well as the nature of the inflaton field are still unknown to cosmologists and particle physicists therefore, it is via the phenomenology that we approach the problem of accepting or discarding models.

Now, let us review two serious problems that could not be solved inside the Hot Big Bang scenario.

The Horizon Problem

From equations (1.8) and (1.25) we can derive:

$$\Omega_{\mathrm{M}}(z)(1+z)^{-3}H(z)^2 = const = \Omega_{M,0}H_0 \tag{2.1}$$

to estimate the magnitude of the Hubble parameter at time $t < t_0$ during an epoch of matter domination. Knowing that $z_{rec} \simeq 1100$ *i. e.* $a_{rec} \simeq 1100^{-1}$, we can get a rough estimate of the particle horizon at the time of recombination. From Eq. (1.17):

$$x(a_{rec}) = \int_0^{a_{rec}} \frac{da}{a^2 H(a)} \tag{2.2}$$

from Eq.(1.16), for flat universes and taking into account that at that epoch the vacuum energy was negligible, we arrive at:

$$x(a_{rec}) = \frac{c\ \mathrm{h}^{-1}\ \mathrm{Mpc}}{100\sqrt{\Omega_{M,0}}} \int_0^{a_{rec}} \frac{da}{\sqrt{a_{eq}+a}} \tag{2.3}$$

where $c = 299792$ km s^{-1} is the speed of light and $a_{eq} \simeq (24000\Omega_{\mathrm{M}}h^{-2})^{-1}$ is the scale factor at the equality of matter and radiation. Solving the previous equation, we find $x(a_{rec}) \simeq 200h^{-1}$ Mpc.

The angular diameter distance to the last scattering surface is around $26100h^{-1}Mpc$ for a flat universe thus, this region subtends an angle of about $\delta\theta = x(a_{rec})/D_{\mathrm{A}}(a_{rec}) \sim 0.8$ degree on the sky. And here comes the horizon puzzle: we observe equal temperatures on the cosmic background microwaves that come from everywhere in the sky. In particular, regions that were not in causal contact during recombination had the exact same temperature. How come two causally disconnected regions communicated their temperature to each other?

The Flatness Problem

Using the definition of the density parameter (1.25), and absorbing the cosmological constant inside the global density ($\Omega = \Omega_{\mathrm{matter}} + \Omega_\Lambda$, with $\Omega_\Lambda = \frac{\Lambda}{3H_0^2}$,), we can write (1.14) as:

$$|\Omega - 1| = \frac{|K|}{a^2H^2} \tag{2.4}$$

Knowing evolution of the scale factor during both matter and radiation domination, and it is easy to see that the product a^2H^2 decreases with time, and the density parameter moves away from 1.
In order to satisfy the current observational bounds on Ω, $(\Omega_0 - 1) \sim 0.02$, it must have been equal to one to very high accuracy at earlier times, eg, at nucleosynthesis ($t \sim 1s$) its value should have been 1 up to a precision of $\mathcal{O}(10^{-17})$!
Since there is no reason why the density of the universe should be precisely the critical, the value of Ω at early times implies a clear problem of fine tuning.

When attempting to solve the flatness problem, we magically encounter the basic idea for inflation. Let us find a way in which the comoving hubble scale, $1/aH$ *decreases* with time:

$$\begin{aligned} &\frac{d}{dt}(1/aH) = -\frac{\ddot{a}}{\dot{a}^2} \text{ therefore,} \\ &\frac{d}{dt}(1/aH) < 0 \Longleftrightarrow \ddot{a} > 0 \end{aligned} \tag{2.5}$$

In order to achieve a decrease in the comoving hubble scale, all we need is accelerated expansion. There still remains the issue of making the value of $|\Omega - 1|$ so small that the subsequent increase due to Hot Big Bang expansion is not enough to move Ω significantly away from 1 at the present epoch. We will deal with this in the next section.

Assuming no cosmological constant [1] $\Lambda = 0$, we see from equation (1.15) that:

$$P < -\frac{1}{3}\rho \Longleftrightarrow \ddot{a} > 0 \tag{2.6}$$

Inside a GR framework, a negative pressure of the matter is needed in order to generate an accelerated expansion of the scale factor.

As we will see in the following subsection, energy in the form of a scalar field does exhibit this odd property as long as a few requirements are fulfilled. This very simple idea, for which we have to give the credit to Andrei Linde, has become an incredibly solid milestone for the new cosmology.
It turns out that working under this hypothesis not only solves many of the problems of the Hot Big Bang, but also enables us to make new predictions. In addition to gracefully solving these problems, inflation provides a mechanism to generate the primordial perturbations that later on will give rise to the observed structures. Current experiments fit the inflationary paradigm quite accurately.

2.1 Scalar Field Dynamics

The requirement $P < -\rho/3$ is naturally obtained in scalar field theories.

We define ϕ as an effective scalar field we call **inflaton**. We assume a lagrangian density described by:

$$\mathcal{L} = \frac{R}{16\pi G} - \frac{1}{2}D_\mu\phi D^\mu\phi - V(\phi) \tag{2.7}$$

D_μ is the covariant derivative. R is the Ricci scalar of the generic FRW metric with physical time coordinate. The gravity part of the lagrangian density becomes negligible after a few e-folds so we can safely ignore this part.

Applying the covariant Euler-Lagrange equations:

$$D_\mu \frac{\delta\mathcal{L}}{\delta(D_\nu\phi)} - \frac{\delta\mathcal{L}}{\delta\phi} = 0 \tag{2.8}$$

[1] Even if current observations indicate $\Lambda \neq 0$ we can safely ignore it during inflation because its effects only become important at very recent epochs $z < 0.5$ (see [6]).

We can compute the scalar field equation:

$$g^{\mu\nu}D_\mu(\partial_\nu\phi) = V_{,\phi};$$
$$g^{\mu\nu}D_\mu(\partial_\nu\phi) = \frac{1}{\sqrt{-g}}\partial_\mu(\sqrt{-g}g^{\mu\nu}\partial_\nu\phi) =$$
$$= \frac{1}{\sqrt{-g}}[-3a^2\dot{a}\dot{\phi}\sqrt{\gamma} - a^3\sqrt{\gamma}\ddot{\phi} + \partial_i(\sqrt{-g}g^{ij}\partial_j\phi)];$$
$$\Rightarrow \ddot{\phi} + 3H\dot{\phi} - \frac{1}{a^2}D^2_\gamma\phi = -V_{,\phi} \tag{2.9}$$

where we have used $\sqrt{-g} = a^3\sqrt{\gamma}$ where γ is the determinant of the spatial part of the metric, and D_γ stands for the covariant derivative with respect to the spatial part of the metric.

Knowing that the action generated by the scalar field part of (2.7) is:

$$\mathcal{S} = \int dx^4\sqrt{-g}\mathcal{L}_\phi \tag{2.10}$$

we can compute the energy momentum tensor by:

$$T_{\mu\nu} = \frac{-2}{\sqrt{-g}}\frac{\delta S_\phi}{\delta g^{\mu\nu}} \tag{2.11}$$

and comparing to (1.6) we get the pressure and energy density of the inflaton field:

$$\rho_\phi = -T^0_0 = \frac{1}{2}\dot{\phi} + V + \frac{1}{2a^2}(\nabla\phi)^2 \tag{2.12}$$
$$P_\phi = \frac{1}{3}T^i_i = \frac{1}{2}\dot{\phi} - V + \frac{1}{6a^2}(\nabla\phi)^2 \tag{2.13}$$

if we neglect the gradient terms and assume a weakly dependence on time (we will systematically enumerate the requirements imposed on the field), we get:

$$P_\phi \simeq -\rho_\phi \simeq -V(\phi) \tag{2.14}$$

Since the energy density of the scalar field is positive, we have obtained a fluid that fulfills (2.6).

... Bonus!! Solving the Horizon Problem

We now compute the time evolution of the scale factor, assuming that ρ_ϕ is approximately constant during some inflationary epoch $\Delta t = t_{end} - t_i$. The Friedmann equation is (1.14):

$$H^2 + \frac{K}{a^2} = \frac{8\pi G}{3}\rho_\phi \tag{2.15}$$

and has the solutions:

$$a(t)\cdot H_\phi = \begin{cases} \cosh(H_\phi t) & \text{for} \quad K = 1 \\ \exp(H_\phi t) & \text{for} \quad K = 0 \\ \sinh(H_\phi t) & \text{for} \quad K = -1 \end{cases} \tag{2.16}$$

with:

$$H_\phi = \sqrt{\frac{8\pi G}{3}\rho_\phi}$$

(as expected, for every solution, $\ddot{a}(t) > 0$).

All of the solutions behave exponentially after a reasonable amount of time, so we study the behaviour of the case $K = 0$: $a(t) = a(t_i)e^{(t-t_i)H_\phi}$.

The particle horizon at the end of inflation:

$$r_h(t_{\text{end}}) \simeq a_0 \int_{t_{\text{i}}}^{t_{\text{end}}} \frac{dt}{a(t)} \simeq \frac{a_0}{a(t_i)H_\phi} \tag{2.17}$$

If $r_h(t_{\text{end}})$ is bigger than the distance to the last scattering surface ($\sim H_0^{-1}$), the horizon problem fades away. Let us see how this is attained:

$$r_h(t_{\text{end}}) > H_0^{-1} \Longleftrightarrow a(t_i)H_\phi < a_0 H_0;$$
$$\frac{a_i}{a_{\text{end}}} < \frac{a_{\text{end}}H_\phi}{a_0 H_0} \Longleftrightarrow e^{\Delta t H_\phi} > \frac{a_{\text{end}}H_\phi}{a_{\text{eq}}H_{\text{eq}}} \cdot \frac{a_{\text{eq}}H_{\text{eq}}}{a_0 H_0}$$

Making the approximation that the universe is completely radiation dominated from t_{end} to t_{eq} and matter dominated from t_{eq} to t_0, we get:

$$e^{\Delta t H_\phi} > (1+z_{\text{eq}})\frac{T_{\text{end}}}{T_{\text{eq}}} = (1+z_{\text{eq}})^{-1/2}\frac{T_{\text{Planck}}}{T_0}\frac{T_{\text{end}}}{T_{\text{Planck}}} \tag{2.18}$$

With $(1+z_{\text{eq}}) \simeq 3600$ and the current temperature of the CMBR, we get:

$$\Delta t H_\phi > 70 + \ln(\frac{T_{\text{end}}}{T_{\text{Planck}}}) \tag{2.19}$$

The energy at the end of inflation is still unknown. For example, for $T_{\text{end}} \sim 10^{14} GeV$ we get the condition that inflation must last for N $= \Delta t H_\phi > 60$ e-folds.

It is easy to see that $N \sim 60$ is also enough to solve the flatness problem. If we include a 60 e-fold inflationary epoch in (2.4) we get $|\Omega_0 - 1| \sim \mathcal{O}(10^{-4})$.

2.2 Slow Roll approximation and background equations

We have just seen how, imposing some constraints on equations (2.12) and (2.13), two of the main problems of the Hot Big Bang model have vanished[2].

The initial cause to all these consequences is (2.14). This condition is achieved if the potential energy of the homogeneous scalar field dominates over the kinetic term, $\dot{\phi}^2 < V(\phi)$. And this is possible if the potential is flat enough so that the field *slowly rolls* towards the minimum of its potential.

There exists an attractor to the solution of the equations of motion of the field. Within this attractor, some of the terms of the equations of the dynamics of the scalar field can be dropped and they simplify to:

$$H^2 = \frac{8\pi G}{3} V(\phi) \tag{2.20}$$

$$3H\dot{\phi} = -V'(\phi) \tag{2.21}$$

where a prime denotes the derivative with respect to the field.
When we work in the vicinity of this solution, we say we are working under the **slow roll approximation** (SRA).

If we define the **slow roll parameters** [8]:

$$\epsilon(\phi) = \frac{1}{16\pi G}\left(\frac{V'}{V}\right)^2; \quad \eta(\phi) = \frac{1}{8\pi G}\frac{V''}{V} \tag{2.22}$$

It can be shown that the SRA holds as long as:

$$\epsilon \ll 1; \quad |\eta| \ll 1 \tag{2.23}$$

Under the SRA we can compute the amount of inflation, or the number of e-folds. In the previous section, we assumed $H \sim$ const. We drop this assumption now:

$$\mathrm{N} = \ln \frac{a(t_{\mathrm{end}})}{a_(t_i)} = \int_{t_i}^{t_{\mathrm{end}}} H(t)dt = \int_{\phi_i}^{\phi\mathrm{end}} \frac{V}{V'}d\phi \tag{2.24}$$

Eqns. (2.20) and (2.21) where used for the last equality.

[2]Inflationary expansion also predicts a negligible density of unwanted relics predicted by physics beyond the standard model such as monopoles or other topological defects

Now, we shall work under the **chaotic inflation** [26] framework. One of the potentials we can use is $V(\phi) = \frac{1}{2}m^2\phi^2$. The slow roll parameters are:

$$\epsilon = \eta = \frac{1}{4\pi G} \cdot \frac{1}{\phi^2} \tag{2.25}$$

So inflation will carry on until the field rolls down to $|\phi_{\rm end}| \gtrsim 1/\sqrt{4\pi G}$. The slow roll equations are:

$$H^2 = \frac{4\pi G}{3} m^2\phi^2; \quad 3H\dot{\phi} + m^2\phi = 0 \tag{2.26}$$

And the solutions are:

$$\phi(t) = \phi_i - \frac{m}{\sqrt{12\pi G}}t \tag{2.27}$$

$$a(t) = a_i \exp[\sqrt{\frac{4\pi G}{3}} m(\phi_i - \frac{m}{\sqrt{48\pi G}}t^2)] \tag{2.28}$$

For a general potential, the solution to the background equations is not so straight forward. It can be ensured that if the potential is such that the SR conditions are fulfilled then inflation will take place. However, bear in mind that the reverse is not true and even though we will not discuss them in this thesis, there are models in which one could could have inflation without SR conditions.

2.3 Perturbation equations

Apart from solving the problems we have already described, the inflationary paradigm gets its strength from a very powerful (and unavoidable) prediction about the formation of structure in the universe. Quantum fluctuations of the inflaton field are stretched out of the horizon and squeezed to classical perturbations during inflation. When they reenter the horizon they seed the potential wells in which matter falls to form the observed structures.
As we will see, the power spectrum predicted by inflation is almost scale invariant. This means that no scale is preferred among the others. The argument to arrive at this conclusion goes as follows: the amplitude of the curvature perturbation, ζ is proportional to the amplitude of the quantum fluctuation of the scalar field $\delta\phi$. Its expected value goes as $\delta\phi_k \sim \frac{H_k}{2\sqrt{2}k^{3/2}}$. Apparently, this magnitude is not scale invariant, however, during inflation the Hubble factor is basically constant and so are the amplitudes of the different wavelength modes. But we will see this in more

detail in what follows.

We now consider small deviations from the ideal Friedmann behaviour:

$$\phi = \phi_0 + \delta\phi \Longrightarrow \rho_\phi = \rho_0 + \delta\rho... \text{ and so on.} \tag{2.29}$$

we have dropped the 0 subindex for convenience.
Note that using (1.43), we can construct a gauge invariant field perturbation:

$$\delta\phi^{(gi)} = \delta\phi - \phi'(B - E') \tag{2.30}$$

To first order in the perturbations of the metric and the scalar fields, the energy momentum tensor is:

$$\begin{aligned} T^\mu_\nu &= \overbrace{{}^{(0)}g^{\mu\alpha}\phi_{0,\alpha}\phi_{0,\nu} - [\frac{1}{2}{}^{(0)}g^{\alpha\beta}\phi_{0,\alpha}\phi_{0,\beta} - V(\phi_0)]}^{{}^{(0)}T^\mu_\nu} + \\ &{}^{(0)}g^{\mu\alpha}2\phi_{0,\alpha}\delta\phi_{0,\nu} + \delta g^{\mu\alpha}\phi_{0,\alpha}\phi_{0,\nu} + \\ &[\frac{1}{2}{}^{(0)}g^{\mu\alpha}2\phi_{0,\alpha}\delta\phi_{0,\beta} + \delta g^{\alpha\beta}\phi_{0,\alpha}\phi_{0,\beta} + \delta\phi V(\phi)_{,\phi}] = \\ &= {}^{(0)}T^\mu_\nu + \delta T^\mu_\nu \end{aligned} \tag{2.31}$$

From this equation, we can read the different components of the perturbation of the energy-momentum tensor. In physical time:

$$\delta\rho = \dot\phi(\delta\dot\phi - \dot\phi A) + \delta\phi V_{,\phi} \tag{2.32}$$

$$\delta q_{,i} = -\dot\phi\delta\phi_{,i} = -\delta T^0_i \tag{2.33}$$

$$\delta P = \phi'\delta\phi' - \phi'^2 A - V_{,\phi}\delta\phi \tag{2.34}$$

(to avoid confusion we adopted a new notation for the scalar gravitational potential perturbation $\delta g_{00} = -2\phi \to -2A$).
The quantities (2.32) and (2.33) can be combined to form a gauge invariant quantity, the **comoving density perturbation**:

$$\epsilon_m \equiv \delta\rho - 3H\delta q \tag{2.35}$$

(it is called like that because an observer who measures zero momentum, would measure $\epsilon_m \equiv \delta\rho_{\text{comoving}}$).

We can now compute the perturbed Einstein equation for a scalar field using (2.32), (2.33), (2.32) and (1.46). We note that the perturbations on the field do not generate anisotropic stress, therefore we can use again $\Psi = \Phi$. We will now

write the equations in conformal time and comoving gauge as that parametrization becomes more convenient for solving the system:

$$\begin{aligned}
\Phi'' + 3\mathcal{H}\Phi' + (\mathcal{H} + 2\mathcal{H}^2)\Phi &= 4\pi G[\phi'\delta\phi' - a^2 V_\phi(\phi)\delta\phi] && (2.36)\\
-\nabla^2\Phi + 3\mathcal{H}\Phi' + (\mathcal{H} + 2\mathcal{H}^2)\Phi &= -4\pi G[\phi'\delta\phi' + a^2 V_\phi(\phi)\delta\phi] && (2.37)\\
\Phi' + \mathcal{H}\Phi &= 4\pi G\phi'\delta\phi' && (2.38)\\
\delta\phi'' + 2\mathcal{H}\delta\phi' - \nabla^2\delta\phi &= 4\phi'\Phi' - 2a^2 V_\phi(\phi)\Phi - a^2 V_{\phi\phi}(\phi)\delta\phi && (2.39)
\end{aligned}$$

It will be useful for later discussion to write equation (2.39) in the spatially flat gauge and physical time:

$$\begin{aligned}
&\ddot{\delta\phi} + 3H\dot{\delta\phi} + \left(\frac{k^2}{a^2} + V_{\phi\phi}\right)\delta\phi \\
&\quad = -2V_\phi A + \dot{\phi}\left[\dot{A} + 3\dot{\psi} + \frac{k^2}{a^2}(a^2\dot{E} - aB)\right], \qquad (2.40)
\end{aligned}$$

where we have used A instead of ϕ for the perturbation We can express these last equations in a more solvable way by using the variables:

$$u = -z\mathcal{R}; \quad z = \frac{a\phi'}{\mathcal{H}} \qquad (2.41)$$

where:

$$\mathcal{R} = \psi - \frac{\mathcal{H}}{\phi'}\delta\phi \qquad (2.42)$$

is curvature perturbation defined on comoving surfaces. That way, we arrive at a very simple equation for the amplitude of the curvature perturbation, u:

$$u'' - \Delta u - \frac{z''}{z}u = 0 \qquad (2.43)$$

which is the same as a harmonic oscillator with a time dependent mass. We discuss the solutions of this equation in the following section.

2.4 Quantum fluctuations of the inflaton

Equation (2.43) is the equation of motion of a lagrangian density:

$$\mathcal{L} = \frac{1}{2}[(u')^2 - (\nabla u)^2 + \frac{z''}{z}u^2] \qquad (2.44)$$

which is that of a free theory with a time varying mass: $m_u = -z''/z$. The problem of quantizing the fluctuations of the inflaton, and its back-reactions on the metric adds up to quantizing the variable u.

We will canonically quantize the field following the usual steps. First we write it in terms of its Fourier components:

$$\hat{u}(\eta, \mathbf{x}) = \frac{1}{(2\pi)^{3/2}} \int d^3k [u_{\mathbf{k}} \hat{a}_{\mathbf{k}} e^{i\mathbf{kx}} + u^*_{\mathbf{k}} \hat{a}^\dagger_{\mathbf{k}} e^{-i\mathbf{kx}}] \tag{2.45}$$

$\hat{a}_{\mathbf{k}}$ and $\hat{a}^\dagger_{\mathbf{k}}$ are the creation and annihilation operators, which follow the commutation relations:

$$[\hat{a}_{\mathbf{k}}, \hat{a}_{\mathbf{k}'}] = [\hat{a}^\dagger_{\mathbf{k}}, \hat{a}^\dagger_{\mathbf{k}'}] = 0; \quad [\hat{a}_{\mathbf{k}}, \hat{a}^\dagger_{\mathbf{k}'}] = \delta^{(3)}(\mathbf{k} - \mathbf{k}') \tag{2.46}$$

And the vacuum state of the theory is annihilated by $\hat{a}_{\mathbf{k}}$:

$$\hat{a}_{\mathbf{k}}|0\rangle = 0$$

The field equation in Fourier space becomes:

$$u''_{\mathbf{k}} + (k^2 - \frac{z''}{z})u = 0 \tag{2.47}$$

We can distinguish two wavelength regimes:

$$u_{\mathbf{k}} \propto \begin{cases} e^{i\mathbf{kx}} & \text{for} \quad k/aH \gg 1 \\ z & \text{for} \quad k/aH \ll 1 \end{cases} \tag{2.48}$$

The short wavelenght regime, are plane waves, as expected for a harmonic oscillator. For the long wavelength regime, the amplitude u is proportional to z. By equation (2.41), we can immediately see that for single field inflation, the amplitude of the comoving curvature perturbation is conserved at large scales.
For $\mathcal{R}$ we have:

$$\mathcal{R}(\tau, \mathbf{x}) = (2\pi)^{-3/2} \int \mathcal{R}_{\mathbf{k}}(\tau) e^{i\mathbf{k}\cdot\mathbf{x}} d^3k, \tag{2.49}$$

with

$$\mathcal{R}_{\mathbf{k}}(\tau) = \left[\frac{u_k(\tau)}{z} \hat{a}_{\mathbf{k}} + \frac{u^*_k(\tau)}{z} \hat{a}^\dagger_{-\mathbf{k}} \right]. \tag{2.50}$$

The *power spectrum* is defined by:

$$\langle 0|\mathcal{R}_{\mathbf{k}} \mathcal{R}^\dagger_{\mathbf{k}'}|0\rangle = \frac{2\pi^2}{k^3} P_{\mathcal{R}}(k) \delta^{(3)}(\mathbf{k} - \mathbf{k}'). \tag{2.51}$$

From (2.50) we obtain

$$\mathcal{P}_{\mathcal{R}}(k) = \frac{k^3}{2\pi^2} \frac{|u_k(\tau)|^2}{z^2} \tag{2.52}$$

The power spectrum for the anisotropies is the function we can observe in the universe. Thus, in order to compare data with the predictions of the theory, we need

to solve (2.43) to find $u_k(\tau)$. And we will do so under the slow roll approximation.

We rewrite the SR parameters (2.22) as a function of the new variables:

$$\epsilon = 4\pi G\frac{z^2}{a^2}; \quad \delta = 1 + \epsilon - \frac{z'}{\mathcal{H}\phi'} \tag{2.53}$$

where $\delta \simeq \eta - \epsilon$. For approximately constant SR parameters (they are constant up to $\mathcal{O}(\epsilon^2)$) one can find an expression for the mass term:

$$\frac{z''}{z} = \frac{1}{\tau^2}\left(\nu^2 - \frac{1}{4}\right), \quad \text{where} \qquad \nu = \frac{1+\epsilon-\delta}{1-\epsilon} + \frac{1}{2} \tag{2.54}$$

Then the solution for (2.43) can be found in terms of $H_\nu^{(1)}(z)$, the Hankel function of first kind:

$$u_k(\tau) = \frac{\sqrt{\pi}}{2}e^{i(\nu+\frac{1}{2})\pi/2}(-\tau)^{-1/2}H_\nu^{(1)}(-k\tau) \tag{2.55}$$

(this solution fulfills (2.48) as expected). For the modes well outside the horizon ($(k/aH) \ll 1$):

$$iH_\nu^{(1)}(z) \sim \frac{1}{\pi}\Gamma(\nu)\left(\frac{1}{2}z\right)^{-\nu} \qquad (z \to 0) \tag{2.56}$$

Inserting this into (2.52) we get the power spectrum for single field inflation and slow roll approximation:

$$\mathcal{P}_\mathcal{R}(k) = \frac{G}{\pi}\frac{H^2}{\epsilon}\left(\frac{k}{aH}\right)^{3-2\nu} \tag{2.57}$$

which is usually parametrized in terms of an amplitude A_s and a tilt n_s:

$$\mathcal{P}_\mathcal{R}(k) = A_s^2\left(\frac{k}{aH}\right)^{n_\mathrm{s}-1} \tag{2.58}$$

Under the slow-roll approximation:

$$n_s - 1 \equiv \frac{d\ln\mathcal{P}}{d\ln k} = -6\epsilon + 2\eta \tag{2.59}$$

That is, slow roll inflation predicts a scalar tilt n_s very close to one. One conservative analysis including many different data can be found in [17] with a value for the tilt of:

$$n_s = 0.966^{+0.025}_{-0.020} \tag{2.60}$$

The latest WMAP data release, under a ΛCDM assumption finds [5]:

$$n_s = 0.958 \pm 0.016 \tag{2.61}$$

Extensions to the standard inflationary model

For single field inflation, we arrive at a simple expression for the predicted power spectrum for the primordial anisotropies. In the most basic scenario this is an adiabatic, gaussian and scale invariant power spectrum. And all these features do agree with observations.

However, there exists the possibility that there exist some deviations from this standard model. We describe some of them in what follows:

- Running tilt: some models of inflation predict a scale dependent tilt. This is parametrized by $n_{\rm run}$, the running of the spectral tilt, defined by:

$$n_{\rm run} = \frac{d\ln n_{\rm s}}{d\ln k} = -16\epsilon\eta + 24\epsilon^2 + \xi^2 \tag{2.62}$$

  where:

$$\xi^2 \equiv (8\pi G)^{-2}\frac{V'(d^3V/d\phi)}{V^2}$$

  A positive running increases large scale power and a negative running has the opposite effect. Deviation from scale invariance may arise due to more complicated potentials for the inflation field. In in [17] they constrain its value to:

$$n_{\rm run} = -0.075^{+0.047}_{-0.055}$$

  though this result could be strongly model biased, as we discuss on Chapter 5.

- Deviations from gaussianity: These may arise from non linear interactions during inflation. There are several reasons why this should occur and their observation in the CMB anisotropies would open a window to new physics during inflation such as magnetic fields. A small deviation from gaussianity could be also generated in the curvaton model. The factor f_{NL} generally measures the non gaussian contribution to the Bardeen potential (1.40):

$$\Phi = \Phi_{\rm gauss} + f_{NL}\Phi^2_{\rm gauss} \tag{2.63}$$

  Single field models predict [27, 28]:

$$|f_{NL}| = |2\epsilon - 2\eta| \lesssim 0.1 \tag{2.64}$$

  Which is lost in the noise from the second-order correction to cosmological perturbation theory. This bound comes from the observational bound on the spectral index in the inflaton scenario (2.59).

- Deviations from adiabaticity The whole next chapter is devoted to this extension of the standard model. As we will see, there may exist some perturbations in the entropy of the fluid that would eventually seed their own curvature perturbations. Current analysis do not rule out the possibility of their existence but again, they are definitely not needed to explain data.

Chapter 3

Isocurvature perturbations in inflationary cosmology

In this chapter, we review the general scenario for isocurvature perturbations and present some of the most important models proposed in literature.

We also present the parametrisation of the amplitudes that will be used all throughout the thesis, and we study the signature that a particle such as the QCD axion could imprint in the CMB as an isocurvature signal.

3.1 General remarks

In the previous chapters we have studied the most basic inflationary mechanism. For single field inflation, the perturbation in the curvature is caused by quantum oscillations of the inflaton field. Its amplitude is practically constant for super hubble modes and remains so until the perturbations reenter the horizon. We will see the phenomenology associated to this in chapter 4.

In a different scenario in which there exists an additional field which is not necessarily coupled to the inflaton (only gravitationally coupled), the curvature perturbation might stop being conserved. Then, the observed anisotropies are not anymore a direct map of the inflaton primordial power spectrum. Instead, they are a mixture of curvature and entropy or isocurvature perturbations that may or may not be correlated with each other.

But what are isocurvature or entropy perturbations? Remember that the curvature perturbations are inhomogeneities in the distribution of the energy density. These seem to be the dominant cause of structure, but they may not be the only ones.

In general, if two or more fields are present during inflation, independently of whether or not all of them take the role of the inflationary field, they may induce

an additional perturbation mode. These isocurvature, or entropy perturbations are those for which the energy density is spatially uniform while the ratio of the number densities of two different species is not conserved throughout space. They are called *isocurvature* because they are those present on slices of uniform total energy density, or zero perturbation on the spatial curvature.

In the standard picture we assume the Universe to contain photons plus cold dark matter (CDM), the baryons and three species of neutrinos. If all of these different species are thermalized it will only be necessary to know the temperature of the universe in order to describe it. Thus, the pressure is practically a unique function of the energy density and the condition for adiabaticity:

$$\frac{\delta P}{\delta \rho} = \frac{\dot{P}}{\dot{\rho}} \tag{3.1}$$

is satisfied. Alternatively, if the species are not thermalized (maybe because one of the species is the decay product of a field that was always decoupled from the field giving rise to the rest of the matter) the adiabaticity condition (3.1) migth not be satisfied and an additional quantity is required in order to completely describe the evolution of the universe. We call this quantity the **entropy perturbation**:

$$\mathcal{S}_{i\gamma} = 3H\left(\frac{\delta\rho_i}{\dot{\rho}_i} - \frac{\delta\rho_\gamma}{\dot{\rho}_\gamma}\right) \tag{3.2}$$

Using (1.53) we get the curvature perturbations on uniform total density hypersurfaces for the different species (the perturbations $\delta\rho$ are defined in the comoving gauge):

$$\zeta = H\frac{\delta\rho}{\dot{\rho}} \tag{3.3}$$

$$\zeta_m = H\frac{\delta\rho_{\rm m}}{\dot{\rho}_{\rm m}} = \frac{\delta\rho_{\rm m}}{3\rho_{\rm m}} \tag{3.4}$$

$$\zeta_r = H\frac{\delta\rho_\gamma}{\dot{\rho}_\gamma} = \frac{\delta\rho_\gamma}{4\rho_\gamma} \tag{3.5}$$

The entropy perturbation can be now written as:

$$\mathcal{S}_{i\gamma} = 3(\zeta_i - \zeta_\gamma) \tag{3.6}$$

The number of new degrees of freedom is the same as the number of species with $\mathcal{S}_{i,\gamma} \neq 0$. One can grasp a very naive idea of the physical meaning of isocurvature or entropy perturbations in figures 3.1.

This inhomogeneity in the composition of the fluid, does not generate a curvature perturbation, but does indeed induce perturbations in the velocity of the fluid. These will be ultimately responsible for the inhomogeneities observed. Note that, because of this, the amplitude of the perturbations is naturally smaller than those generated adiabatically. We will see the difference in the power spectra on chapter 4.

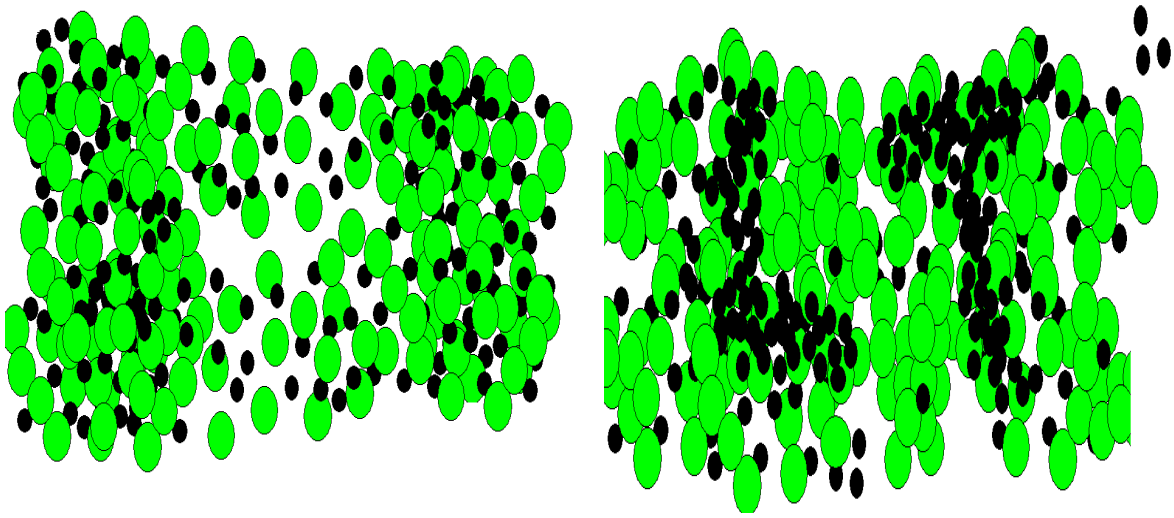

Figure 3.1: Artistic photon and neutrino soup. On the left hand side, the background energy density spatially fluctuates. However, the ratio n_γ/n_ν has a constant value in space. On the right hand side, we encounter the opposite scenario. Even though the background energy density is constant,n_γ/n_ν fluctuates throughout space.

The addition of new fields is well justified under the framework of particle physics beyond the standard model. Particles such as the axion could have an observable signature in the CMB anisotropies. However, in order to be able to detect isocurvature, two main conditions must be fulfilled:

- The two fields and their products must be totally decoupled from each other during the whole history of the universe. Otherwise, their products would thermalize and erase all the entropy perturbations [31].
- In some of the isocurvature generating models, the masses of the two fields must be similar so that both fields have similar contributions to the CMB anisotropies. There is no a priori reaso why this would happen. In the most general scenario, fields need not have similar masses.

These two caveats do remark the difficult life of an isocurvature observer, but the phenomenology hidden under them and the possibility of opening new windows to new physics, make this subject an interesting field of research.

Depending on the nature of the particles and the perturbations, different isocurvature modes arise [32]. The evolution of each fluid is determined by two first order differential equations, thus with four species present, we could expect eight perturbation modes; one adiabatic and seven isocurvature. However, three of those modes are pure gauge, and only four isocurvature modes are physical: Baryon, Cold Dark Matter, and neutrino isocurvature (BI, CDI, NID) are two modes generated by the spatial variations in the relative number densities of B or CDM with respect to

photons. A fourth mode, the neutrino velocity mode (NIV), may arise because the neutrinos do have a relativistic velocity, wich can be compared to that of the fotons. Therefore, we can measure perturbations *also* in the relative velocities of neutrinos and photons.

In order to observe as much as these five modes (one adiabatic and four isocurvature) five different fields (or more) must have been present during inflation *and* must satisfy the requirements stated above. In principle, thus, it could be possible to study the constraints on the existence of more than one mode at a time [33]. However, due to the a priori unlikeliness of all the conditions being fulfilled at the same time, we find it more sensible to try to constrain only one of them at a time. We stick to this conservative restriction throughout the whole analysis.

3.2 Multiple field models

A very convenient formalism for the study of multiple field models was developed in [34]. We summarise it now to get their major conclusions and equations. We use the lagrangian density:

$$\mathcal{L} = \sum_{i=1}^{N} \frac{1}{2} g^{\mu\nu} \phi_{i,\mu} \phi_{i,\nu} + V(\phi_1, \phi_2 ... \phi_N) \tag{3.7}$$

The background field equations for each of the fields are:

$$\ddot{\phi}_i + 3H\dot{\phi}_i + V_{,\phi_i} = 0 \tag{3.8}$$

where $V_{,\phi_i} = dV/d\phi_i$. Depending on the potential the two fields may or may not be coupled at zero order.
With a perturbed line element such as (1.35) (in which again, we change notation $\phi \to A$ in order to avoid confusion), we compute the perturbed field equation in the spatially flat gauge (see eq. (2.40)). Now we work with the Fourier components of the spatial perturbation. For the shake of clarity, will omit the subindex **k**.

$$\delta\ddot{\phi}_i + 3H\delta\dot{\phi}_i + \frac{k^2}{a^2}\delta\phi_i + \sum_j^N V_{,\phi_i,\phi_j}\delta\phi_j =$$

$$-2V_{\phi_i}A + \dot{\phi}_i[\dot{A} + 3\psi + \frac{k^2}{a^2}(a^2\dot{E} - aB)] \tag{3.9}$$

It is easy to extend equations (2.32) and (2.33) to the two field formalism, and we get:

$$\delta\rho = \sum_{j=1}^{N} \dot{\phi}_j(\delta\dot{\phi}_j - \dot{\phi}_j A) + \delta\phi_j V_{,\phi_j} \tag{3.10}$$

$$\delta q_{,i} = -\sum_j^N \dot{\phi}\cdot\delta\phi_{,i} = -\delta T_i^0 \tag{3.11}$$

For simplicity, we now restrain ourselves to the case $N = 2$. The formalism is easily extensible to more than two scalar fields.

In order to clarify the role of adiabatic and entropy perturbations, [34] defined two new fields, the **adiabatic field** σ and the **entropy field**, s. These fields come from a different decomposition of the total perturbation in the field space. Instead of using fields 1 and 2, one projects the perturbation along the field trajectory and perpendicular to it. For clarity see figure 3.2.

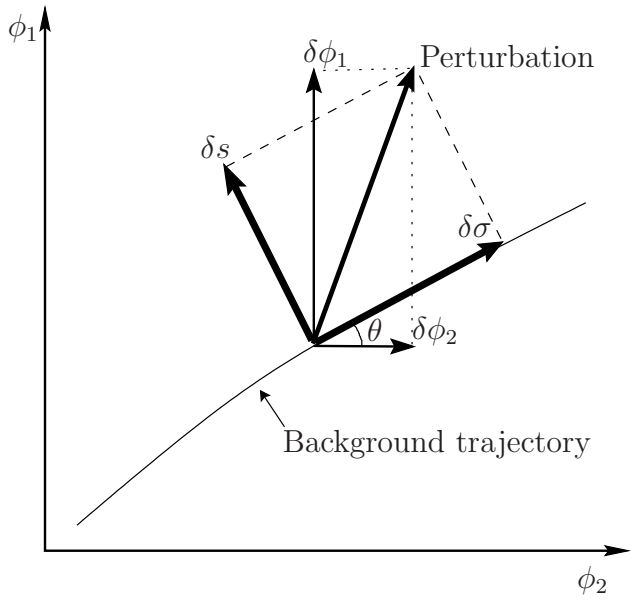

Figure 3.2: An illustration of the decomposition of an arbitrary perturbation into an adiabatic ($\delta\sigma$) and entropy (δs) component. The angle of the tangent to the background trajectory is denoted by θ. The usual perturbation decomposition, along the ϕ_1 and ϕ_2 axes, was shown for the first time in [34].

If perturbations were only along the background trajectory, some particular combination of the two fields ϕ_1 and ϕ_1 would not be distinguishable from a single field trajectory. The existence of a second field allows for an additional degree of freedom that needs to be tracked with an additional variable, the entropy perturbation $\mathcal{S}$. The perturbations on the new fields are the product of a rotation in the field space:

$$\begin{pmatrix} \delta\sigma \\ \delta s \end{pmatrix} = \begin{pmatrix} \sin\theta & \cos\theta \\ \cos\theta & -\sin\theta \end{pmatrix} \begin{pmatrix} \delta\phi_1 \\ \delta\phi_2 \end{pmatrix} \tag{3.12}$$

We now proceed to get all the previous field equations for the $\delta\sigma$ and δs fields.

The perturbed field equations are:

$$\begin{aligned}\delta\ddot{\sigma} + 3H\delta\dot{\sigma} + \left(\frac{k^2}{a^2} + V_{\sigma\sigma} - \dot{\theta}^2\right)\delta\sigma \\ = -2V_\sigma A + \dot{\sigma}\left[\dot{A} + 3\dot{\psi} + \frac{k^2}{a^2}(a^2\dot{E} - aB)\right] \\ + 2(\dot{\theta}\delta s)^{\cdot} - 2\frac{V_\sigma}{\dot{\sigma}}\dot{\theta}\delta s\,,\end{aligned} \tag{3.13}$$

and

$$\begin{aligned}\ddot{\delta s} + 3H\dot{\delta s} + \left(\frac{k^2}{a^2} + V_{ss} - \dot{\theta}^2\right)\delta s \\ = -2\frac{\dot{\theta}}{\dot{\sigma}}\left[\dot{\sigma}(\dot{\delta\sigma} - \dot{\sigma}A) - \ddot{\sigma}\delta\sigma\right]\,,\end{aligned} \tag{3.14}$$

where

$$V_{\sigma\sigma} = (\sin^2\theta)V_{\chi\chi} + (\sin 2\theta)V_{\phi\chi} + (\cos^2\theta)V_{\phi\phi}\,, \tag{3.15}$$

$$V_{ss} = (\sin^2\theta)V_{\phi\phi} - (\sin 2\theta)V_{\phi\chi} + (\cos^2\theta)V_{\chi\chi}\,. \tag{3.16}$$

Equation (3.11) becomes:

$$\delta q_{,i} = -\dot{\phi}_1\delta\phi_{1,i} - \dot{\phi}_2\delta\phi_{2,i} = -\dot{\sigma}\delta\sigma_{,i} \tag{3.17}$$

Comparing (3.13) and (3.14) to (2.40), one can see that if $\dot{\theta} = 0$ the equation of motion for $\delta\sigma$ becomes the equation of motion for a scalar field in a perturbed background whereas the field δs corresponds to a scalar field in an unperturbed background.

The perturbation in the curvature on comoving hypersufaces (2.42) for two fields becomes:

$$\mathcal{R} = \psi - H\frac{\dot{\phi}_1\delta\phi_1 + \dot{\phi}_2\delta\phi_2}{\dot{\phi}_1^2 + \dot{\phi}_2^2} = \psi + \frac{H}{\dot{\sigma}}\delta\sigma \tag{3.18}$$

where the last equality comes from the definition of the adiabatic field. We see then that the power spectrum of the quantum field σ is the direct responsible for the curvature perturbations, and thus the power spectrum may be calculated analogously to (2.58).

As a matter of fact, we show here the expression for the power spectra of both

quantities $\mathcal{R}$, and $\mathcal{S}$ and their correlation:

$$\begin{aligned}
\Delta^2_{\mathcal{R}}(k) &\equiv \frac{k^3}{2\pi^2}\langle\mathcal{R}^2_{\rm rad}\rangle = \frac{k_0^3}{2\pi^2}A^2\left(\frac{k}{k_0}\right)^{n_{\rm ad}-1}, \\
\Delta^2_{\mathcal{S}}(k) &\equiv \frac{k^3}{2\pi^2}\langle\mathcal{S}^2_{\rm rad}\rangle = \frac{k_0^3}{2\pi^2}B^2\left(\frac{k}{k_0}\right)^{n_{\rm iso}-1}, \\
\Delta^2_{\mathcal{RS}}(k) &\equiv \frac{k^3}{2\pi^2}\langle\mathcal{R}_{\rm rad}\mathcal{S}_{\rm rad}\rangle \\
&= \frac{k_0^3}{2\pi^2}A\,B\,\cos\Delta_{k_0}\left(\frac{k}{k_0}\right)^{n_{\rm cor}+\frac{1}{2}(n_{\rm ad}+n_{\rm iso})-1}.
\end{aligned} \tag{3.19}$$

Also, we get different contributions to the spectrum of the cosmic microwave background. We can compute three different anisotropy power spectra:

$$\begin{aligned}
C_l^{\rm ad} &\equiv \int\frac{dk}{k}\left[\Theta_l^{\rm ad}(k)\right]^2\left(\frac{k}{k_0}\right)^{n_{\rm ad}-1}, \\
C_l^{\rm iso} &\equiv \int\frac{dk}{k}\left[\Theta_l^{\rm iso}(k)\right]^2\left(\frac{k}{k_0}\right)^{n_{\rm iso}-1}, \\
C_l^{\rm cor} &\equiv \int\frac{dk}{k}\,\Theta_l^{\rm ad}(k)\,\Theta_l^{\rm iso}(k)\left(\frac{k}{k_0}\right)^{n_{\rm cor}+\frac{1}{2}(n_{\rm ad}+n_{\rm iso})-1}
\end{aligned} \tag{3.20}$$

Then, the total angular power spectrum reads

$$C_l = A^2\,C_l^{\rm ad} + B^2\,C_l^{\rm iso} + 2\,A\,B\,\cos\Delta_{k_0}\,C_l^{\rm cor}$$

which can be conveniently parametrised as [13]:

$$C_\ell = (A^2+B^2)\left[(1-\alpha)\,C_l^{\rm ad} + \alpha\,C_l^{\rm iso} + 2\beta\sqrt{\alpha(1-\alpha)}\,C_l^{\rm cor}\right] \tag{3.21}$$

where $\alpha = B^2/(A^2+B^2)$ represents the isocurvature fraction at the pivot scale k_0 (typically, $k_0 = 0.05{\rm hMpc}^{-1}$) and β defines the correlation coefficient at k_0, thus $\beta = \cos\Delta_{k_0}$.

This parametrisation will be used throughout the whole work. We assume different conditions on the values of α and β and the tilts in Eqns. (3.19), but this will be the basic isocurvature parameter space we will constrain in Chapter 6.

3.2.1 Double Inflation

This is a double field model in which the constraint of a quadratic potential is imposed for both fields. In particular:

$$V(\phi_1,\phi_2) = \frac{1}{2}m_h^2\phi_h^2 + \frac{1}{2}m_l^2\phi_l^2 \tag{3.22}$$

where $m_h > m_l$ are the masses of the ligth and heavy field. The model was first introduced in [35] to explain an apparent lack of power at small scales. This idea was further developed in [36], but as soon as observations improved and massive neutrinos were introduced in the analysis, it was realised that there was no need of any exotic inflationary mechanism to explain them.
However, double inflation is still a simple, rich on phenomenology multiple inflationary model that has been widely studied. Interest on this model raises due to the fact that double inflation is the most plausible model inside the multiple inflationary models. If more than two fields were present during inflation, it would be very unlikely that we got to observe the effects of any field other than the two last to decay. Thus, even if N fields are generically predicted during inflation, only two of them have relevant observable effects on our universe.
Note though, that an observable isocurvature contribution to the spectrum of fluctuations is not a generic prediction of these models. We will see under which conditions is isocurvature generated.

Background equations

We will work with the two unperturbed homogeneous scalar fields with masses $m_h > m_l$.
They are only gravitationally coupled, therefore the phenomenological Lagrangian is:

$$\mathcal{L} = \frac{R}{16\pi G} - \frac{1}{2}(\phi_{h|\mu}\phi_h^{|\mu} + m_h^2\phi_h^2) - \frac{1}{2}(\phi_{l|\mu}\phi_l^{|\mu} + m_l^2\phi_l^2) \tag{3.23}$$

Using the equations developed in section 1.3 we find:

$$H^2 = \frac{4\pi G}{3}(\dot{\phi}_h^2 + \dot{\phi}_l^2 + m_h^2\phi_h^2 + m_l^2\phi_l^2) \tag{3.24}$$

$$\dot{H} = -4\pi G(\dot{\phi}_h^2 + \dot{\phi}_l^2) \tag{3.25}$$

And the field equations:

$$\ddot{\phi}_h + 3H\dot{\phi}_h + m_h^2\phi_h = 0; \quad \ddot{\phi}_l + 3H\dot{\phi}_l + m_l^2\phi_l = 0 \tag{3.26}$$

In order to undergo an inflationary epoch in which $|\dot{H}| \ll H^2$ the following conditions need to be fulfilled:

$$H \gg m_h \tag{3.27}$$

$$\phi_h^2 \gg \frac{1}{2\pi G} \quad ; \quad \phi_l^2 \gg \frac{1}{2\pi G} \tag{3.28}$$

Now we impose the slow-roll regime and equations (3.24) and (3.26) become:

$$H^2 = \frac{4\pi G}{3}(m_h^2\phi_h^2 + m_l^2\phi_l^2) \tag{3.29}$$

$$3H\dot{\phi}_h + m_h^2\phi_h = 0; \quad 3H\dot{\phi}_l + m_l^2\phi_l = 0 \tag{3.30}$$

Performing the change of variables, from t, the physical time variable to $s = -\ln(a/a_f)$, the number of e-folds to the end of inflation (a_f is the value of the scale factor at the end of inflation) we can write:

$$\frac{d^2\phi_h^2}{ds^2} = \frac{m_h^2\phi_h^2}{m_l^2\phi_l^2} \cdot \frac{d^2\phi_l^2}{ds^2} \tag{3.31}$$

and solve for s:

$$s = 2\pi G(\phi_h^2 + \phi_l^2) \tag{3.32}$$

Using the parametrisation:

$$\phi_h^2 = \frac{s}{2\pi G}\sin^2\theta;\ \ \phi_l^2 = \frac{s}{2\pi G}\cos^2\theta \tag{3.33}$$

we can solve for the number of e-folds till the end of inflation as a function of θ:

$$s(\theta) = s_0\frac{(\sin\theta)^{2/(R^2-1)}}{(\cos\theta)^{2R^2/(R^2-1)}} \tag{3.34}$$

where s_0 is half of the number of e-folds left till the end of inflation, when both scalar fields have the same value ($\theta = \pi/4$). We have also defined the parameter $R \equiv \frac{m_h}{m_l}$ as it will become useful for the calculations below.
We see that while $s(\theta)$ is not strongly dependent on s_0, its evolution is mainly determined by R.
Of fig.3.3 we have plotted the trajectories on the field space for a fixed $s_0 = 62$ value and different values for the ratio of the masses, and fixed R value and varying s_0.

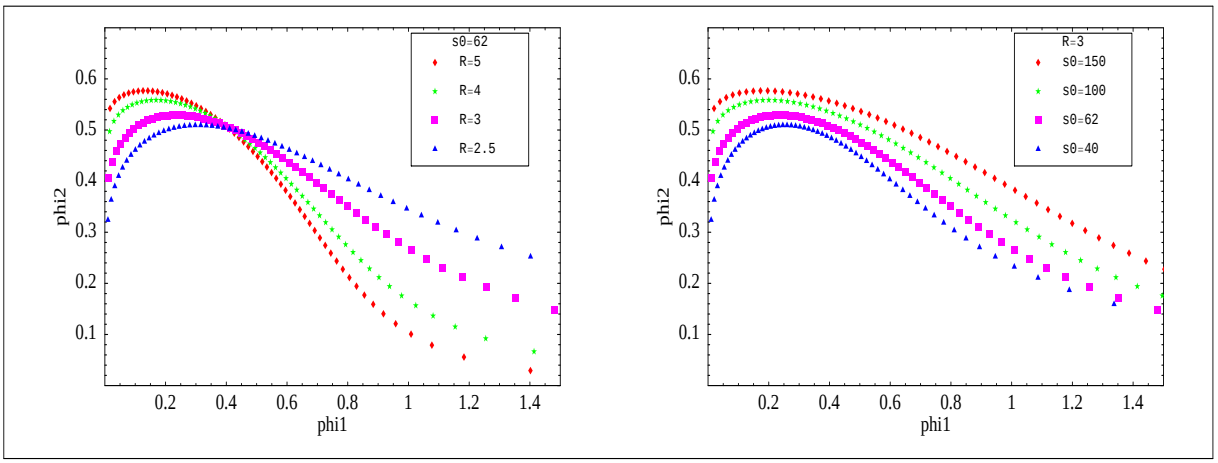

Figure 3.3: Trajectories on field space from $\theta = 0$ to $\theta = \frac{\pi}{2}$.The plot on the left shows the different trajectories for different values of R. The plot on the right does so for different values of s_0

Substituting (3.33) into (3.29) we find the temporal evolution of the scale factor:

$$H^2(\theta) = \frac{2}{3} m_l^2 s[1 + (R^2 - 1)\sin^2\theta] \tag{3.35}$$

So with equations (3.33), (3.34) and (3.35) we have the slow roll solution to the background equations (3.24) and (3.26).

Perturbation Equations

Now we take into account the non-homogeneous component of the fields and compute its evolution throughout inflation. We assume the fields can be decomposed into its homogeneous and a small inhomogeneous perturbation:

$$\phi_h(t, \mathbf{x}) = \phi_h(t) + \delta\phi_h(t, \mathbf{x}) \tag{3.36}$$
$$\phi_l(t, \mathbf{x}) = \phi_l(t) + \delta\phi_l(t, \mathbf{x}) \tag{3.37}$$

(for convenience, from now on the dependence on the coordinates will be omitted). The gauge fixing used during this whole section is the **longitudinal gauge** ($a^2\dot{E}_l - aB_l = 0$) even though we will not use the corresponding subindex.
With the perturbed line element:

$$ds^2 = -(1 + 2\Phi)dt^2 + a^2(1 - 2\Psi)\delta_{ij}dx^i dx^j \tag{3.38}$$

and (3.36), we can compute the perturbed Einstein and field equations:

$$\Phi = \Psi \tag{3.39}$$
$$\dot{\Phi} + H\Phi = 4\pi G(\dot{\phi}_h\delta\phi_h + \dot{\phi}_l\delta\phi_l) \tag{3.40}$$
$$\delta\ddot{\phi}_i + 3H\delta\dot{\phi}_i + (\frac{k^2}{a^2} + m_i^2)\delta\phi_i = 4\dot{\phi}_i\dot{\Phi} - 2m_i^2\phi_i\Phi \tag{3.41}$$

$i = h, l$ in Eq. (3.41).
We are only interested on the behaviour of perturbations outside the horizon. Therefore, we only track the evolution of the long wavelength modes taking the limit $k \to 0$. It is shown in [36] that the solutions are weakly time dependent. Therefore, we can neglect the terms $\dot{\Phi}$ and $\delta\ddot{\phi}_i$. Working under the slow roll assumption the equations take the form:

$$H\Phi = 4\pi G(\dot{\phi}_h\delta\phi_h + \dot{\phi}_l\delta\phi_l) \tag{3.42}$$
$$3H\delta\dot{\phi}_i + m_i^2\delta\phi_i = -2m_i^2\phi_i\Phi \tag{3.43}$$

The resolution of these equations is a bit involved so we will just write down the solutions:

$$\Phi = -\frac{C_1(k)\dot{H}}{H^2} + C_3(k)\frac{2(R^2-1)m_h^2\phi_h^2 m_l^2\phi_l^2}{3(R^2\phi_h^2 + \phi_l^2)} \tag{3.44}$$
$$\frac{\delta\phi_h}{\dot{\phi}_h} = \frac{C_1(k)}{H} + C_3(k)\frac{2\phi_l^2 H}{R^2\phi_h^2 + \phi_l^2} \tag{3.45}$$
$$\frac{\delta\phi_l}{\dot{\phi}_l} = \frac{C_1(k)}{H} - C_3(k)\frac{2R^2\phi_h^2 H}{R^2\phi_h^2 + \phi_l^2} \tag{3.46}$$

Since ϕ_1 and ϕ_2 are independent uncoupled scalar fields and essentially massless during inflation, we can use the general formalism of Chapter 2, and write, in the slow-roll approximation,

$$C_1(k) = -\frac{\kappa^2}{2}\frac{H_k}{\sqrt{2k^3}}\Big(\phi_1\, e_1(\mathbf{k}) + \phi_2\, e_2(\mathbf{k})\Big)\,, \tag{3.47}$$

$$C_3(k) = -\frac{3H_k}{2\sqrt{2k^3}}\left(\frac{e_1(\mathbf{k})}{m_1^2\phi_1} - \frac{e_2(\mathbf{k})}{m_2^2\phi_2}\right)\,, \tag{3.48}$$

where H_k is the rate of expansion when the perturbation of wavenumber

$$k \simeq k_H\, e^{s_H - s_k}\,, \tag{3.49}$$

left the horizon during inflation, where the scale of our present horizon is $k_H^{-1} = 3000\, h^{-1}$ Mpc.

We will now assume that the ligth scalar field decays at the end of inflation into the ordinary particles, giving rise to photons, neutrinos, electrons and baryons, while the cold dark matter (CDM) arises from the decay of the heavy field. In principle, part of the CDM could also be produced by the light field or the heavy field could also decay into ordinary particles, but we will ignore these possibilities here. Then, the perturbations in the comoving gauge take the form

$$\frac{\delta^{(c)} n_\gamma}{n_\gamma} = \frac{\delta^{(c)} n_\nu}{n_\nu} = \frac{\delta^{(c)} n_B}{n_B}\,,$$

and there is only one isocurvature mode, the CDI mode,

$$\mathcal{S} \equiv \delta^{(c)} \ln \frac{n_{\rm cdm}}{n_\gamma} = \delta^{(c)}_{\rm cdm} - \frac{3}{4}\delta^{(c)}_\gamma\,,$$

all of which are gauge invariant quantities. During the radiation era, the initial conditions of all these modes are described in terms of only two k-dependent quantities, Φ_k and S_k. The pure adiabatic initial conditions are given by the gravitational potential during the radiation era,

$$\Phi_{\rm rad}(k) = \frac{2}{3}\,\mathcal{R}_{\rm rad}(k) = \frac{2}{3}\,C_1(k)\,,$$

with $C_1(k)$ the amplitude of the growing adiabatic mode during inflation. On the other hand, the isocurvature initial conditions in the radiation era arise from the perturbations in the heavy field ϕ_1 at the end of inflation. In the long wavelength limit, the perturbations of this field during reheating follow closely the field itself, so that its energy density perturbations satisfy, in the comoving gauge,

$$\frac{\delta\rho^{(c)}}{\rho} = 2\frac{\delta\phi_1}{\phi_1} = -\frac{4}{3}C_3(k)\, m_1^2$$

which is constant during inflation, across reheating and into the radiation era. The entropy perturbation is dominated by the CDM density perturbation during the radiation era, $\mathcal{S}_{\rm rad} \simeq \delta^{(c)}_{\rm cdm}$. Using the values of $C_1(k)$ and $C_3(k)$ during inflation, we can finally write:

$$\begin{aligned} \mathcal{R}_{\rm rad}(k) &= -\sqrt{\frac{4\pi G}{k^3}} H_k s_k^{1/2} \Big(\sin\theta_k \, e_h(\mathbf{k}) + \cos\theta_k \, e_l(\mathbf{k}) \Big) \\ \mathcal{S}_{\rm rad}(k) &= \sqrt{\frac{4\pi G}{k^3}} H_k s_k^{-1/2} \left(\frac{e_h(\mathbf{k})}{\sin\theta_k} - \frac{R^2 \, e_l(\mathbf{k})}{\cos\theta_k} \right) \end{aligned} \tag{3.50}$$

where $e_i(\mathbf{k})$ are gaussian random fields associated with the quantum fluctuations of the fields and the subindex k implies the value at horizon crossing. One typically expects $s_k \simeq 60$ for our present hubble radius.

Inserting (3.50) into (3.19), we find the expression for the adiabatic and isocurvature amplitudes in this model. We see that a double inflation model predicts no scale dependence for the correlation spectrum, or $n_{\rm cor} = 0$.

In particular, we get:

$$\alpha = \frac{R^4 \tan^2\theta + 1}{s_k^2 \sin^2\theta + R^4 \tan^2\theta + 1} \,, \tag{3.51}$$

$$\beta = \frac{(R^2 - 1)\sin\theta}{\sqrt{R^4 \tan^2\theta + 1}} \,. \tag{3.52}$$

whose values are plotted in Fig. 3.4 as a function of the angle θ and for $s_k \simeq 60$.

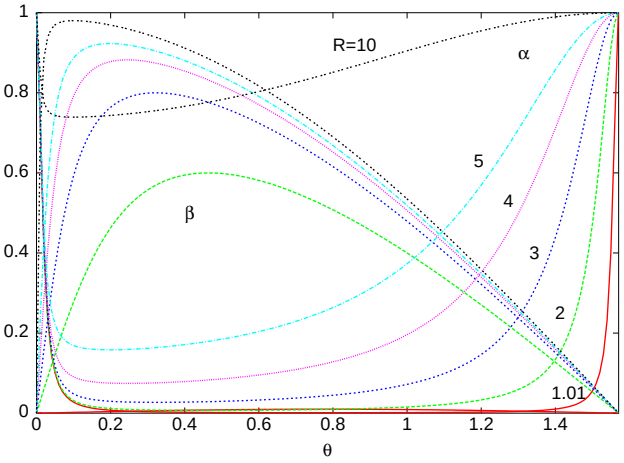

Figure 3.4: The values of parameters α and β as a function of the angle θ, for different values of the ratio $R = m_1/m_2$ in double inflation.

For the tilt, we get:

$$n_{\rm ad} = 1 - \frac{2}{s_k} + \frac{(R^2-1)\tan^2\theta}{2s_k(1+R^2\tan^2\theta)^2}\,, \tag{3.53}$$

$$n_{\rm iso} = 1 - \frac{(R^2-1)(R^2\tan^4\theta - 1)(1+\tan^2\theta)}{s_k(1+R^2\tan^2\theta)^2(1+R^4\tan^2\theta)}\,, \tag{3.54}$$

whose values, for $s_k = 60$, are typically $n_{\rm ad} = 0.97$ and $n_{\rm iso}$ in the range $[0.97, 0.90]$

From Eqns. (3.51) and (3.52), one can get the relationship [14]:

$$2\beta\sqrt{\alpha(1-\alpha)} = \frac{2(R^2-1)}{s_k}(1-\alpha)\,. \tag{3.55}$$

and easily impose bounds on this double field model, as we show in Chapter 6.

3.3 Curvaton Model

The models revised so far share a common mechanism for the generation of the primordial curvature perturbation. The quantum fluctuations of the field driving inflation, the inflaton, are converted to classical gaussian perturbations with an almost flat spectrum. The power spectrum of the observed anisotropies constrains the models by corresponding to a particular shape of the potential of the field.
It was noted in refs. [37, 38, 39] that the primordial curvature perturbation may have a completely different origin, namely, the quantum fluctuations of a light field other than the inflaton. This field is called the **curvaton** and its energy density is subdominant during inflation. After inflation ends the energy density of the curvaton field becomes dominant and the isocurvature perturbations convert to adiabatic even on super-horizon scales, through a mechanism studied in [37]. Then, the curvaton field decays and the product particles inherit the spectrum of anisotropies. The model does not generically predict isocurvature perturbations. As we shall see, the existence of isocurvature modes depends, on the nature of the curvaton field as well as the time of decay and its decay products. If entropy perturbations do exist, they must be totally correlated to the adiabatic ones because both are sourced by the same field. We see how the curvaton field perturbations are transferred to matter and radiation perturbations as the number of e-folds grows in figure 3.5 [40]. The precise evolution of these curves is strongly dependent on the initial densities of the components as well as on the decay rate of the curvaton field to the other species. Getting a particular value for any of the perturbations at a particular time requires strong fine tunning of the initial conditions.

The curvaton model suggests a rather different inflationary scenario, therefore we not only describe the mechanisms that give rise to isocurvature perturbations, but also we must summarise the curvature perturbation generation.

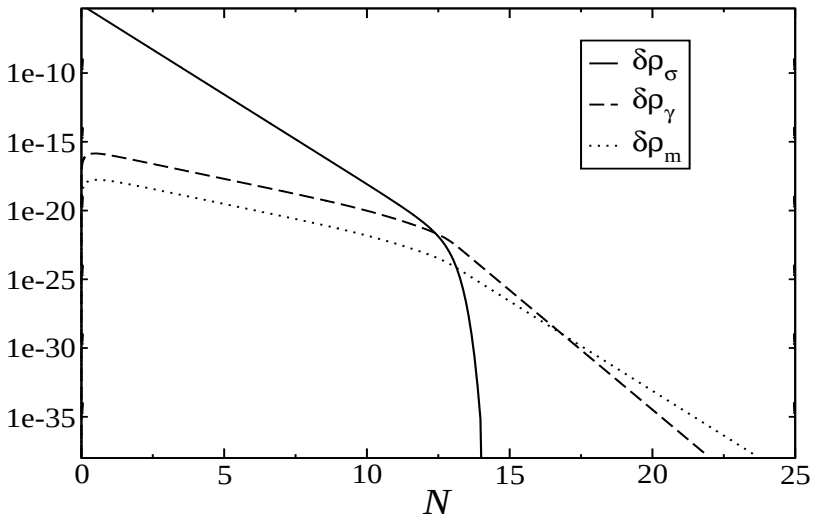

Figure 3.5: The evolution of the density perturbations on uniform-curvature hypersurfaces δ_σ,δ_γ and $\delta_{\rm m}$ against the number of e-foldings. The initial value of the curvaton energy density is $\Omega_{\sigma,{\rm rm}} = 10^{-4.6}$ [40].

In a very simple scenario, the two fields coexist uncoupled:

$$\mathcal{L} = \frac{1}{2}\phi_{,\mu}\phi^{,\mu} + V(\phi) + \frac{1}{2}\sigma_{,\mu}\sigma^{,\mu} + V(\sigma) \tag{3.56}$$

where ϕ is the inflaton field and σ is the curvaton. The properties and behaviour of ϕ are those described in Chapter 2, and the only requirement imposed is that the curvature perturbation generated by it is negligible compared to the one generated by the curvaton. In order to achieve this, the scale of inflation needs to be low enough, in particular [39]:

$$|V(\phi)|^{1/4} \leq 10^{-2}\frac{-\dot{H}}{H^2}M_{\rm P}$$

where $M_{\rm P} = \sqrt{8\pi G} = 2 \cdot 10^{18}$Gev. This allows a maximum scale for inflation of $V^{1/4} < 2 \times 10^{15}$Gev which would imply negligible gravity waves generation. The observation of gravity waves in the CMBR anisotropies would automatically rule out the curvaton model.

The curvaton field

The curvaton field lives in an unperturbed FRW spacetime (its energy density is so low that the back-reactions on the metric are negligible) and its lagrangian is defined

in (3.56). We are interested on the Fourier components of its quantum fluctuations, which follow equation (3.9) on the spatially flat gauge. Assuming we can ignore the fluctuations of the other field(s) present and taking the long wavelength limit, we get:

$$\ddot{\delta}\sigma_k + 3H\dot{\delta}\sigma_k + V_{\sigma\sigma}\delta\sigma_k = 0 \tag{3.57}$$

If the potential is sufficiently flat ($|V_{\sigma\sigma}| \ll H^2$) the perturbation is gaussian and its spectrum is given by

$$\mathcal{P}_{\delta\sigma} = \frac{H_*^2}{4\pi^2} \tag{3.58}$$

where the star denotes the epoch of horizon exit $k = a_* H_*$. Assuming $V \simeq \frac{1}{2}m^2\sigma^2$, the energy density of the curvaton field is:

$$\rho_\sigma = \frac{1}{2}m^2(\sigma+\delta\sigma)^2 = \overbrace{\frac{1}{2}m^2\sigma^2}^{\rho_0} + \underbrace{\frac{1}{2}m^2(2\sigma\delta\sigma + (\delta\sigma)^2)}_{\delta\rho} \tag{3.59}$$

(even if the potential is not quadratic, one can make this approximation after a few Hubble times). It is shown in [39] that non-gaussianity in the primordial power spectrum would arise if $\delta\sigma \gg \sigma$. Since the observed spectrum is basically gaussian, we assume $\delta\sigma \ll \sigma$ and the density contrast δ_σ is[1]:

$$\delta_\sigma \equiv \frac{\delta\rho_\sigma}{\langle\rho_\sigma\rangle} \simeq 2\frac{\delta\sigma}{\sigma} \tag{3.60}$$

and its power spectrum is therefore:

$$\mathcal{P}_\delta^{\frac{1}{2}} = \frac{H_*}{\sigma_*\pi} \tag{3.61}$$

After inflation ends, the universe is dominated by decay products of the inflaton, mainly radiation. The Hubble factor starts decreasing until $H \sim |V_{\sigma\sigma}|$ or in the case of a quadratic potential $H \sim m_\sigma$. Then the curvaton field starts oscillating around its minimum behaving as a cold dust fluid with energy density $\rho_\sigma \propto a^{-3}$. During the oscillation both the field equation for σ and Eq. (3.57) continue to be valid, and the quantity $\delta_\sigma \equiv \frac{\delta\sigma}{\sigma}$ remains constant. Since $\rho_{\rm rad} \propto a^{-4}$, even though the energy density of the curvaton started being subdominant, it can grow with respect to the radiation and become the dominant component of the universe.

Generation of the curvature perturbation.

As outlined in the previous paragraphs the curvature perturbation is generated by the existence of a non adiabatic pressure ($\delta P_{\rm nad}$) because of the curvaton field. It is

[1]It is also shown in [39] that $\delta\sigma \ll \sigma \Longleftrightarrow H_* \ll \sigma_*$

shown in [24, 25] that the time evolution of the curvature perturbation on uniform density hypersurfaces is proportional to $\delta P_{\rm nad}$:

$$\dot{\zeta} = -\frac{H}{\rho + P}\delta P_{\rm nad} \tag{3.62}$$

(ζ is related to the curvature perturbation in the comoving gauge by $\zeta = -\mathcal{R}$). As the curvaton energy density starts becoming comparable to $\rho_{\rm rad}$, $\delta P_{\rm nad}$ stops being negligible and ζ starts growing. When the curvaton energy density becomes dominant or it decays (whichever is earlier) the anisotropic pressure becomes zero again and the curvature perturbation is constant.
The total curvature perturbation at the end of inflation is composed by the contribution of the radiation and the curvaton:

$$\zeta = H\frac{\delta\rho}{\dot{\rho}} = H\frac{\delta\rho_r + \delta\rho_\sigma}{\dot{\rho}_r + \dot{\rho}_\sigma} = \frac{4\rho_r\zeta_r + 3\rho_\sigma\zeta_\sigma}{4\rho_r + 3\rho_\sigma} \tag{3.63}$$

We imposed the condition that the curvature perturbation generated by the inflaton field is negligible. It follows that:

$$\zeta = \frac{\rho_\sigma\delta_\sigma}{4\rho_r + 3\rho_\sigma} \tag{3.64}$$

If the curvaton dominates the energy density before decay, the final value of ζ:

$$\zeta = \frac{1}{3}\delta \tag{3.65}$$

On the opposite case, if $\rho_\sigma = r\rho_r$ with $r \ll 1$ when it decays then (and assuming the decay is instantaneous):

$$\zeta = \frac{1}{4}r\delta \tag{3.66}$$

On either case, the spectrum of the resulting curvature perturbations is a fraction of the spectrum of the curvaton field perturbation. Using (3.61):

$$\mathcal{P}_\zeta^{\frac{1}{2}} \simeq r\mathcal{P}_\delta^{\frac{1}{2}} = r\frac{H_*}{\sigma_*\pi} \tag{3.67}$$

In the next section, we describe the generation of isocurvature perturbations and its phenomenological signature.

Generation of the isocurvature perturbation

As outlined in the introduction of this chapter, non-thermalized species are needed in order to have $\mathcal{S}_{i\gamma} \neq 0$.
Non-thermalization can be achieved by decoupling species from each other. And this naturally occurs within the Hot Big Bang model due to the cooling of the expanding

universe. The particular time at which species decouple as well as the time at which the curvaton decays, determine the chances of existence of an observable isocurvature contribution.

At the end of inflation, and before the curvaton decays, from (3.2) the entropy perturbation is:

$$\mathcal{S}_{\sigma\gamma} = 3(\zeta_\sigma - \zeta_\gamma) \tag{3.68}$$

In the scenario described above for the curvature perturbations, the isocurvature perturbation reduces to $\mathcal{S}_{\sigma\gamma} = 3\zeta_\sigma$. As we see now, the way and time in which the curvaton field decays determines whether or not this isocurvature perturbation is inherited by the products.
Conceptually simpler, we will now focus on the Cold Dark Matter (CDM) entropy perturbations. Since all the perturbation previous to curvaton decay is equal to that on the radiation fluid, we can write:

$$\mathcal{S}_{\mathrm{cdm}\gamma} = 3(\zeta_{\mathrm{cdm}} - \zeta_\gamma) = 3(\zeta_{\mathrm{cdm}} - \zeta) \tag{3.69}$$

We define CMD creation as the time from which the number density of CDM matter particles starts being conserved. We assume that the CDM generating mechanism does not involve any quantity with an isocurvature perturbation. Therefore, the initial CDM perturbation must be zero. In the possible scenario that some isocurvature perturbation was intrinsic to the CDM creation mechanism, it could be completely unrelated to the curvaton-induced perturbation and thus, their amplitudes are not related either. Therefore, even in this case, it is safe to assume that $\mathcal{S}_{\mathrm{cdm}}$ is basically induced by the curvaton field.
We can differentiate two regimes based on the time when the curvaton field decays [28].

1. The curvaton field decays **before** the CDM is created.

   After decaying, the products of the field will naturally thermalize along with the rest of the constituents. In particular, with the field giving rise to CDM. Therefore the adiabaticity condition will be fulfilled before the CDM is created and no entropy perturbation will be generated.
   This case is observationally indistinguishable from a single field adiabatic model without gravitational waves, such as hybrid inflation or inverted hybrid inflation [12].

2. The curvaton field decays **after** the CDM is created, but its energy density is very subdominant. Then, equation (3.69) becomes:

   $$\mathcal{S}_{\mathrm{cdm}} = -3\zeta = 3\mathcal{R} \tag{3.70}$$

   The spectrum of the isocurvature perturbation has an amplitude three times bigger than the adiabatic curvature perturbation. Also, the spectra are totally

correlated. This corresponds to the amplitudes: $\alpha = 3^2/(1+3^2) = 0.9$ and $\beta = +1$ with $n_{\rm iso} = n_{\rm ad}$. Such a large correlated perturbation was first ruled out by [41], which required:

$$|\frac{\mathcal{S}_{\rm cdm}}{\zeta}| < 1.5 \ \text{ at } 95\% \text{ c.l.}$$

(more recent analysis impose an even more stringent bound on this ratio at two sigma [15]).

3. The curvaton field decays **after** the CDM is created, but its energy density is important.

4. The curvaton field decays **after** the CDM is created, but its energy density is important but does not dominate.

   On the other scenario, the CDM is created when the energy density of the curvaton field starts becoming dominant. Then, the CDM will inherit a curvature perturbation $\zeta_{\rm cdm} = \zeta_\sigma$. By the definition of the density contrast we see that $\zeta_\sigma \propto \delta_\sigma$. We now parametrise (3.66) with:

$$\zeta = q\zeta_\sigma \tag{3.71}$$

   and equation (3.69) becomes:

$$\mathcal{S}_{\rm cdm} = 3\left(\frac{1-q}{q}\right)\zeta \tag{3.72}$$

   The q factor is approximated [40] by:

$$q(p) \simeq 1 - \left(1 + \frac{0.924}{\mu}p\right)^{-\mu} \tag{3.73}$$

   where $p \equiv [\Omega_\sigma \sqrt{\frac{H}{\Gamma_{\gamma\sigma}}}]_{\rm in}$. $\Gamma_{\gamma\sigma}$ is the rate at which the curvaton decays into radiation. Fitting to a numerical simulation gives $\mu = 1.24$.

We see that requiring a small $\Omega_{\sigma,\rm in}$ implies a big decay rate for the curvaton into radiation. This is not a priori theoretically motivated, and thus the fine tunning becomes necessary. This is something not desirable and makes the allowed regime for the curvaton not very likely.

Caveats in the generation of observable isocurvature perturbations

It is worth a note on the subject of the possible elimination of the non-adiabatic perturbations, pointed out by S. Weinberg in [31]. As a matter of fact, there are no

flaws in his analysis, and one should take this as an indication of the rareness of an eventual isocurvature signal in the observations.

However, every argumentation is based on the assumption that the universe undergoes a phase in which all of the species present there are in local thermal equilibrium[2]. In particular it assumes that after inflation, whatever remnant of additional fields present (that could give rise to non-adiabatic modes) decays or annihilates approaching the number density at equilibrium thermally, with a rate of change:

$$Y \rightsquigarrow -\mathcal{K}(T)(n - n_{\rm eq}(T)) \tag{3.74}$$

where $\mathcal{K}$ is a positive rate and n and $n_{\rm eq}$ are the number densities of the extra species in and out of equilibrium [31]. This way, the original nature of the perturbation in the number density, gets erased and all the perturbations are adiabatic.

This thermalization process is the one usually undergone by many of the known species in the universe. However, there are particles beyond the standard model which may be generated by other mechanisms. In particular the QCD axion, may not be thermally generated, but by a displacement of the phase from the equilibrium point when the particle theoretically acquires its mass via non perturbative effects when the QCD symmetry is broken. In what follows, we concentrate directly on this specific particle physics model.

As mentioned in Chapter 1, one of the goals of this work, is to serve as a link between particle physics and cosmology which we believe, will provide mutual support for future advances in both fields.

The fact that the strong sector of the Standard Model conserves the discrete symmetries P and CP while the electroweak sector does not, also known as the *strong CP problem*, is considered a serious puzzle for modern particle physics [42]. In one of the most elegant solutions to the problem, a new particle arises, the axion. Its existence at very high energies, even during inflation, would have strong cosmological implications.

We believe this particular model represents a beautiful example of how constraints on the isocurvature fraction, may help discerning among different axionic scenarios. As we will see, also the CDM energy density measured in the universe provides a tight bound to the model.

3.4 The Axion as a candidate for CDM.

In 1977 R. D. Peccei and H. Quinn [11] proposed a compelling solution to the strong CP problem, in which they introduced a new $U(1)_{\rm PQ}$ global symmetry at

[2]The author clearly states in the article the extent to which his claims are valid. With this note we wish to remark which are the conditions that must be fulfilled in order to allow for the generation and subsequent observation of the isocurvature modes.

high energies. The symmetry is spontaneously broken in the early universe and the resulting Nambu-Goldstone boson is known as the *axion* [43]. Non perturbative effects at the QCD scale give a potential to the axion, whose minimum eliminates the CP-violating terms, thus agreeing with the observed electric dipole moment of the neutron [44]. Even though the existence of the axion was postulated soon after the Peccei-Quinn proposal this particle has never been detected by any direct or indirect searches, see e.g. [45].

The axion mass and couplings to the rest of the matter are inversely proportional to the scale, f_a, at which the $U(1)_{\rm PQ}$ symmetry is broken [46, 45]. Indeed, the mass is found to be

$$m_a = \frac{\sqrt{z}}{1+z}\,\frac{f_\pi m_\pi}{f_a} = 6.2\,\mu{\rm eV}\,\left(\frac{10^{12}\ {\rm GeV}}{f_a}\right)\,, \tag{3.75}$$

where $z = m_u/m_d \simeq 0.56$ is the mass ratio of up to down quarks, and m_π, f_π are respectively the pion mass and decay constant. The generic tree-level coupling to photons γ and fermions f reads

$$\mathcal{L}_{\rm int} = g_\gamma\,\frac{\alpha}{\pi}\,\frac{a(x)}{f_a}\,\vec{E}\cdot\vec{B} + i\,g_f\,\frac{m_f}{f_a}\,a(x)\,\bar{f}\,\gamma_5\,f\,, \tag{3.76}$$

where $\vec{E}$ and $\vec{B}$ are the electric and magnetic fields, α is the electromagnetic coupling constant, and for each species g_i is a model-dependent coefficient of order one. The different ways in which the symmetry is accomplished, and then broken, give rise to different axion models that forecast similar axion properties. Nevertheless, there exists one remarkable distinction between them, which is the predicted coupling to electrons; for the "hadronic" models, such as the KSVZ model [47], one has $g_e = 0$, while the tree-level coupling does not vanish for the non-hadronic DFSZ models [48]. The other couplings are of the same order. For example, $g_\gamma = -0.36$ in the DFSZ model, while $g_\gamma = 0.97$ in the KSVZ model.

In the original axion model a physical meaning was given to the symmetry breaking scale by fixing it to the electroweak scale, i.e. $f_a \sim 100$ GeV, which was soon ruled out by direct searches (see, for example [42, 45]). In the currently accepted *invisible axion* model, the scale f_a is in principle arbitrary, well above the electroweak scale so that the axion coupling to matter is weak enough to pass undetected, for the moment. There are at present several experiments searching for the axion in the laboratory, like ADMX [49] and CAST [50], which have recently reported bounds on the axion coupling to matter [51].

Since in the small coupling (large f_a) limit the axion remains effectively decoupled from the rest of the particle species, its fluctuations during inflation could induce isocurvature perturbations in the CMB anisotropies spectrum which would in principle be observable today. We will take into account these two facts, together with a detailed study of the quantum diffusion of the field during inflation, to put strong constraints on its relic density and its mass today.

The paper is organised as follows: in Section 3.4.1 we review the different production mechanisms, focusing on the misalignment angle and the consequences of the De Sitter stage during inflation; in Section 3.4.2 we study the induced isocurvature component. Later on, in Chapter 6, in Section 6.3 we present the additional constraints bounding the axionic window along with our results and conclusions.

3.4.1 Production mechanisms

As pointed out in the introduction, the Peccei-Quinn global $U(1)_{PQ}$ symmetry is spontaneously broken by some scalar symmetry breaking field $\psi = r/\sqrt{2}\, e^{i\Theta}$. The symmetry breaking potential is

$$V(\psi) = \frac{\lambda}{4}\left(r^2 - \frac{f_a^2}{N^2}\right)^2 = V_{\rm PQ} - \frac{1}{2}m_\psi^2 r^2 + \frac{\lambda}{4}r^4\,, \tag{3.77}$$

where N is the number of degenerate QCD vacua associated with the colour anomaly of the PQ symmetry and λ is an unknown energy scale.

Spontaneous symmetry breaking (SSB) occurs when the energy density of the universe falls below $V_{\rm PQ}$ and the field acquires a vacuum expectation value (*vev*), $r = f_a/N$. Note, however, that SSB is effective only when the typical fluctuations on δr are smaller than f_a/N. If either T or $H_{\rm inf}$ are of order f_a/N at reheating or during inflation, thermal or quantum fluctuations (respectively), will modify the effective potential and restore the PQ symmetry.

Let us focus now on the case where no symmetry restoration occurs, and the radial part of the field oscillates perturbatively around the value f_a/N after the symmetry is broken (we will come back to the case with symmetry restoration in later sections). The phase of the field, Θ, moves along the flat direction of the potential and remains massless. This is the Goldstone boson of the PQ symmetry breaking associated to a residual global $U(1)$ symmetry of the theory [42, 43]. The axion is related to the phase of the PQ field by

$$a(\vec{x}) = \frac{f_a}{N}\Theta(\vec{x})\,. \tag{3.78}$$

As the universe expands, and its energy decreases to about $\Lambda_{\rm QCD}$, the non-perturbative instanton effects *tilt* the previously flat potential and the phase symmetry is explicitly broken [44]. The new induced potential is

$$V(a) \simeq m_a^2 \frac{f_a^2}{N^2}(1 - \cos\Theta) \tag{3.79}$$

which is obviously no longer flat. The axion field acquires a mass about the minimum of the potential that depends on the temperature in the vicinity of $T \sim \Lambda_{\rm QCD}$ as [52, 53]

$$m_a(T) \simeq m_a C \left(\frac{\Lambda_{\rm QCD}}{200{\rm MeV}}\right)^{\frac{1}{2}} \left(\frac{\Lambda_{\rm QCD}}{T}\right)^4\,, \tag{3.80}$$

where m_a is the zero temperature axion mass (3.75) and C is a model-dependent factor calculated in Refs. [52, 53] to be of the order of $C \simeq 0.018$. The field equation of motion is

$$\ddot{a} + 3H\dot{a} + V'(a) + \frac{1}{R^2}\nabla^2 a = 0\,, \tag{3.81}$$

where $V'(a) = \partial V/\partial a$, with ∇^2 the comoving laplacian, and R is the scale factor of the universe. If the axion field is initially sufficiently close to the minimum of the potential when it acquires its mass, then $V'(a) \simeq m_a^2 a$. Otherwise, anharmonic effects should be taken into account by inserting in (3.81) the actual instanton contribution to the mass of the axion. In either case, the mass and the potential term are time-dependent.

Axions are produced in the early Universe by various mechanisms. A priori, any combination of them could be the one responsible for the present axion abundance. We will briefly describe here the different scenarios and production mechanisms. For detailed reviews see Refs. [42, 45].

Thermal production

If the coupling of axions to other species is strong enough (i.e. f_a low enough), then axions may be produced from the plasma in the early universe and it is possible that an axionic thermal population existed at high energy. If this is the case, a relic density of thermally generated axions would be present nowadays and could significantly contribute to the current cold dark matter component of the universe.

The two main processes that dominate the thermal production of axions are photo- and gluon-production and pion-axion conversion (the axion and the pion share the same quantum numbers and thus they can oscillate into each other). Since nucleons and mesons only exist after the quark-hadron transition, the second mechanism is only possible after $T \sim \Lambda_{\rm QCD} \simeq 200$ MeV. During the thermal equilibrium stage, the axion density normalized to the entropy of the universe ($Y \equiv n_a/s$) acquires an equilibrium value $Y_{\rm eq}$. Since it is assumed that the axion is relativistic during the epoch of interest, we have

$$Y_{\rm eq} = \frac{\zeta(3)T^3/\pi^2}{(2\pi^2/45)\ g_{*,{\rm eq}}T^3} \simeq \frac{0.27}{g_{*,{\rm eq}}}\,, \tag{3.82}$$

where $g_{*,{\rm eq}}$ is the number of relativistic degrees of freedom at the temperature where the axions reach their equilibrium distribution. The decoupling of axions from thermal equilibrium is described by the Boltzmann equation [54]:

$$Y' = \left(\frac{\Gamma_{\rm abs}}{xH}\right)(Y_{\rm eq} - Y)\,, \tag{3.83}$$

where $x^{-1} \equiv T/m$ represents the temperature normalized to a convenient energy scale $m \sim \Lambda_{\rm QCD}$, H is the Hubble expansion rate, and $\Gamma_{\rm abs}$ is the thermal-averaged

interaction rate for the process $a + i \leftrightarrow 1 + 2$, see Ref. [55]. Since $\Gamma_{\rm abs}/H$ decreases and acquires values < 1 for $T < \Lambda_{\rm QCD}$, the axions cease to be in thermal equilibrium with the rest of the species and they freeze out when the rate of the interactions cannot keep up with the expansion of the universe. More precisely, it is shown in Ref. [54] that $\Gamma_{\rm abs}/H$ presents a peak at the QCD scale and then decays exponentially. So, it is possible to find the relic abundance of thermal axions by integrating forward in time from $T \simeq 200$ MeV till today the solution to (3.83),

$$Y(x) = Y_{\rm eq}\left(1 - \exp\Big[-\int_0^x \frac{\Gamma_{\rm abs}}{x' H} dx'\Big]\right) . \tag{3.84}$$

Finally, the relic abundance of axions can be written as

$$Y_\infty = \frac{0.278}{g_{*,F}}\left(1 - \exp\Big[-\Big(\frac{m_a}{10^{-4}\,{\rm eV}}\Big)^2 x_{\rm qh}^{-5/2}\, e^{-x_{\rm qh}}\Big)\Big]\right) , \tag{3.85}$$

which depends on the number of relativistic degrees of freedom at the freeze-out temperature $g_{*,F}$ (and not at the equilibrium temperature) and on $x_{\rm qh} = m/\Lambda_{\rm QCD}$. We can thus extract the number density of thermal axions and their contribution to the matter density of the universe,

$$\Omega_{\rm a}^{\rm th} h^2 = \frac{m_a}{130\,{\rm eV}}\left(\frac{10}{g_{*,F}}\right) , \tag{3.86}$$

with $\Omega_{\rm a} \equiv \rho_a/\rho_c = 8\pi G\rho_a/3H_0^2$. This result applies only when $m_a > 10^{-3}$ eV: otherwise, the peak value of $\Gamma_{\rm abs}/H$ at the QCD scale is smaller than one, and the axions never reach thermal equilibrium. On the other hand, the current WMAP bound on the cold dark matter density [5]

$$\Omega_{\rm cdm} h^2 = 0.112^{+0.003}_{-0.006} ,$$

together with Eq. (3.86), imposes a bound on the axion mass $m_a < 14.5$ eV. As we will see in Section 6.3.1, this bound is overseeded by astrophysical data which forbid a mass range of $0.01\,{\rm eV} < {\rm m_a} < 200$ keV for the DFSZ axion [42, 45].

Hadronic axions are not so tightly constrained by astrophysical data because they do not take part (at tree level) in the processes that cause the anomalous energy loses in stars such as $\gamma + e^- \to e^- + a$ or the Primakoff effect [42]. Thus, a narrow mass window remained open until recently for thermal hadronic axions of $m_a \simeq$ several eV. However, a more detailed look at the freeze out temperature and a combination of cosmological data from CMB and LSS has allowed Ref. [56] to shut the window on the axion mass, $m_a < 1.05$ eV, in a model independent way. We will therefore ignore from now on the thermal axion contribution to cold dark matter.

Axion production via cosmic strings

We already mentioned that the PQ symmetry could be restored at high energy, e.g. by large quantum fluctuations during inflation, or large thermal fluctuations

after reheating. After each symmetry restoration phase, the spontaneous symmetry breaking (SSB) will produce a population of axionic cosmic strings. Let us review the three cases in which axionic strings are produced after, during or before inflation:

- *after inflation:* if the scale f_a/N is below the reheating temperature of the universe, the PQ symmetry is restored at reheating. Then, axionic cosmic strings will be produced when the temperature of the Universe falls below f_a/N. These strings typically decay into axion particles before dominating the energy density of the universe. The axions produced this way are relativistic until the QCD transition, where they acquire a mass and become non-relativistic. Eventually these axions may come to dominate the energy density after equality, in the form of cold dark matter. Estimates of their present energy density vary depending on the fraction of axions radiated by long strings versus string loops. Three groups have studied this issue and found agreement within an order of magnitude [57, 58, 59],

$$\Omega_{\rm a}^{\rm str} h^2 \simeq 4\Delta_{\rm QCD} \left(\frac{1\mu{\rm eV}}{m_a}\right)^{1.18} \tag{3.87}$$

  where $\Delta_{\rm QCD} = 3^{\pm 1}$ is a "fudge factor" which takes into account all the uncertainties in the QCD phase transition. Similar constraints are found in [60] in a global string decay model independent way.

- *at the end of inflation:* the PQ symmetry is restored during inflation whenever the typical amplitude of quantum fluctuations $H_{\rm inf}/2\pi$ exceeds the symmetry breaking scale f_a/N. If the inequality

$$\frac{H_{\rm inf}}{2\pi} > \frac{f_a}{N} \tag{3.88}$$

  holds throughout inflation, comic strings will be produced at the very end of this stage. The mechanism by which cosmic strings are produced at the end of inflation is very different from that of a thermal phase transition and could affect the number of infinite strings, and thus the approach to the scaling limit, with the subsequent estimate of the relic density of axions. If, after all, the scaling limit is approached, then the present energy density of axion will be approximately given by Eq. (3.87).

- *during inflation:* the PQ SSB could occur during inflation, when $H_{\rm inf}/2\pi$ falls below f_a. In this case, one expects axionic strings to be diluted during the remaining inflationary stage, and the relic density will be suppressed by an additional factor, $\exp(N_{\rm SSB})$, where $N_{\rm SSB}$ is the number of e-folds between PQ symmetry breaking and the end of inflation. As a consequence, this density should be negligible today, unless $N_{\rm SSB}$ is fine-tuned to small values by assuming that f_a/N is very close to the Hubble rate at the end of inflation.

- *before inflation:* if, for instance, the PQ symmetry is restored at very high energy and breaks before inflation is turned on e.g. at low scales, the axionic strings produced in that way, as well as the possible axions into which they may have decayed, will be diluted by inflation and can be safely neglected.

Note, however, that, apart from axionic strings, there are also axionic domain walls bounded by axionic strings. In the case that the PQ color anomaly corresponds to $N = 1$, the network of domain walls and strings decay away. However, for $N > 1$, the domain walls end up dominating the energy density of the universe, contrary to observations [61]. Solving this problem requires breaking the N degeneracy, by slightly lowering the energy of one of the N vacua and thus inducing the decay of the domain walls. However, this possibility seems far fetched from the point of view of model building, and we will ignore it here. A detailed discussion is given in Ref. [62]. From now on, we will assume that $N = 1$. We will also assume that the reheating temperature after inflation is not high enough to restore the PQ symmetry and thus reproduce the mesh of axionic strings. Thus we are left with only one production mechanism, misalignment.

Generation via misalignment angle

This production mechanism takes place at very early stages in the universe. When the PQ symmetry is explicitly broken, the phase of the field Θ may or may not be at the minimum of its potential. As explained above, a (or Θ) is a massless field during inflation and thus it fluctuates quantum-mechanically. If the typical amplitude of quantum fluctuations is large enough, Θ could take different values in different points of our observable universe after inflation, with a flat probability distribution in the range $[-\pi, \pi]$; otherwise, it could remain nearly homogeneous. In both cases, at the time of the QCD transition, the (local or global) value of the misalignment angle Θ_1 can differ from zero, leading to the sudden appearance of a potential energy term,

$$\begin{aligned} \rho_{\rm a} &= \frac{1}{2}\dot{a}^2 + \frac{(\vec{\nabla} a)^2}{2R^2} + \overbrace{m_a^2 f_a^2 (1 - \cos\Theta)}^{\text{new term}} , \\ &\simeq \frac{1}{2} f_a^2 \Big(\dot{\Theta}^2 + \frac{(\vec{\nabla}\Theta)^2}{R^2} + m_a^2 \Theta^2 \Big) \quad \text{for small } \Theta. \end{aligned} \tag{3.89}$$

Actually, the gradient energy can be safely neglected in Eq. (3.89). Indeed, even in the case in which the axion is maximally inhomogeneous, i.e. when the phase Θ is equally distributed in the range $[-\pi, \pi]$ in our observable universe at the end of inflation, it is straightforward to show that at any later time the coherence length (the physical size of the "homogeneity patches" for a) is always of the order of the Hubble radius. This can be checked e.g. by solving the equation of motion (3.81) in Fourier space. As a consequence, and recalling that a is defined in the range

$[-\pi f_a, \pi f_a]$, the typical size of the gradient $\vec{\nabla} a$ is given by $f_a H$. So, the gradient energy scales as $H^2 \propto R^{-4}$ during radiation domination, and at the time of the QCD transition it is at most of the order of $(f_a H_{\rm QCD})^2$. A quick estimate gives $H_{\rm QCD} \sim 10^{-11}$eV, while in the following we will always consider values of the axion mass much larger than this. So, when the axion mass is "switched on", the gradient energy is negligible with respect to the potential energy $V \sim (f_a m_a)^2$.

Since $m_a(T)$ grows suddenly to values much bigger than $H_{\rm QCD}$, one can also deduce from Eq. (3.81) that after acquiring its mass the field quickly rolls down towards the minimum of the potential, since the condition for rolling is $m_a(T) \gg 3H$. After a lapse of time that depends on the initial value of the misalignment angle, Θ_1, the field will reach the lowest energy point and start oscillating. For the latest stages of the oscillation we have $m_a(T) \gg 3H$ (and also $m_a(T) \simeq m_a$) so that the expression

$$\rho_a = \left\langle \frac{1}{2} f_a^2 \left(\dot{\Theta}^2 + m_a^2 \Theta^2 \right) \right\rangle = \frac{1}{2} f_a^2 m_a^2 \left\langle \Theta_1^2 \right\rangle \left(\frac{R_{\rm QCD}}{R} \right)^3 \tag{3.90}$$

becomes a good approximation for the spatial average of the axion density over our observable Universe.

However, for a precise estimate, it is necessary to take into account the time dependence of the mass when solving Eq. (3.81). In Ref. [63] the evolution equation is numerically solved for the case $m_a(T) \propto T^{-p}$, and it is found that (3.90) is corrected by a factor $f_c(p) \simeq 0.44 + 0.25p$, that we will take into account in the final computation of the energy density. After the QCD transition, the axionic energy density evolves with time as

$$\rho_a \frac{R^3}{m_a(T)} = \text{const.}\,, \tag{3.91}$$

where R is the scale factor of the universe. While the energy density varies with the temperature, the number density $n_a = \rho_a / m_a(T)$ is conserved in a comoving volume, which simply reflects axion number conservation. Thus, the current energy density of axions is related to the number density $n_{a,1}$ at the time t_1 where oscillations start by

$$\rho_a^{\rm today} = \gamma \frac{s_0}{s_1} m_a \, n_{a,1}\,, \tag{3.92}$$

where $s = (2\pi^2/45) g_* T^3$ is the entropy density, g_* counts the relativistic degrees of freedom present in the universe at a given temperature, and γ accounts for a possible entropy release after the axion starts oscillating [64]. Solving for T_1 from the condition $m_a(T_1) \simeq 3H(T_1)$, we find a relic axion density

$$\Omega_{\rm a} h^2 \simeq 7.24 \, g_{*,1}^{-5/12} \langle \Theta_1^2 \rangle \left(\frac{200{\rm MeV}}{\Lambda_{\rm QCD}} \right)^{\frac{3}{4}} \left(\frac{1 \mu{\rm eV}}{m_a} \right)^{\frac{7}{6}}\,. \tag{3.93}$$

If the axion begins oscillating roughly at the time when it acquires a mass, i.e. when the temperature of the universe is slightly larger than $\Lambda_{\rm QCD}$, then $g_{*,1} = 61.75$. In

Eq. (3.93), the spatial average $\langle\Theta_1^2\rangle$ of the initial misalignment squared angle is not given by any field theoretical reasoning; but by considerations about the stochastic behavior of the field during inflation, as explained below.

Quantum diffusion of the axion during inflation

Let us assume that the Peccei-Quinn symmetry was spontaneously broken above the energy scale of inflation, corresponding to the length scales that we observe in the CMB today. Thus we need to take into account the effect of the de Sitter quantum fluctuations [65] that induce a stochastic diffusion of the axion away from the initial value Θ_i.

The probability $\mathcal{P}(\Theta, N_e)$ of finding a certain value Θ at a time given by the number of e-folds N_e satisfies a Fokker-Planck equation with diffusion coefficient $D = H_{\rm inf}/(2\pi f_a)$,

$$\frac{\partial\mathcal{P}}{\partial N_e} = \frac{1}{2}D^2\,\frac{\partial^2\mathcal{P}}{\partial\Theta^2}\,, \tag{3.94}$$

whose solution is

$$\mathcal{P}(\Theta, N_e) = \frac{1}{\sqrt{2\pi D^2 N_e}}\,\exp\left[-\frac{(\Theta-\Theta_i)^2}{2D^2N_e}\right]\,. \tag{3.95}$$

Thus, as was also pointed out in [66, 67], a given inflationary domain that starts at a particular initial value Θ_i will be dispersed, after N_e e-folds of inflation, by

$$\langle(\Theta-\Theta_i)^2\rangle^{1/2} = \frac{H_{\rm inf}}{2\pi f_a}\times\sqrt{N_e}\,. \tag{3.96}$$

That is, the field will have randomly walked a distance proportional to the square root of the number of jumps, in this case given by the number of e-folds.

The Fokker-Planck equation provides a good description of the stochastic evolution of the phase at a given point in real space; however, it does not give any hint on the spatial structure and on the coherence length of the axion field. A straightforward analysis based on Fourier space reveals that the coherence length (or "scale of homogeneity") of any light or massless field during inflation at a given time is given by the Hubble radius at that time. Since the comoving Hubble radius $1/(aH)$ decreases with time during inflation, the stochastic evolution caused by quantum fluctuations can be seen as a process of fragmentation of an initially nearly homogeneous domain into several smaller nearly homogeneous patches.

In the present context, this remark is crucial, because it allows to identify the number of e-folds N_e which is really relevant in equation (3.96). When the scale corresponding to the observable universe crosses the Hubble length during inflation (i.e., typically, between 30 and 70 e-folds before the end of inflation), the axion field is nearly homogeneous over a length comparable to the size of the whole observable

universe. Therefore, we should start counting the number of jumps *starting from that moment* (there might be many e-folds of inflation before that time, but they are only relevant for comparing the axion field value in our observable universe with that in other inaccessible, disconnected universes). Let us call this number of e-folds $N_{\rm obs}$, and from now on, let us define Θ_i as the average value of Θ inside the observable universe $N_{\rm obs}$ e-folds before inflation ending.

At the end of inflation, the coherence length of the axion field is smaller than the size of the observable universe by approximately a factor $\exp[N_{\rm obs}]$. In other words, the initial domain of average value Θ_i has fragmented into many domains of average value Θ, with a dispersion $\langle(\Theta-\Theta_i)^2\rangle^{1/2}$ given by equation (3.96) with $N_e = N_{\rm obs}$.

Later on, causal diffusion tends to smooth the axion field over the Hubble length. Since after inflation, the comoving Hubble radius $1/(aH)$ increases with time, the number of homogeneity patches inside the observable universe decreases (after reaching its maximum at the end of inflation). In the next section, we will evaluate the dispersion of the phase Θ at the time of the QCD transition. By that time, fluctuations on scales smaller than the Hubble radius $H_{\rm QCD}^{-1}$ have been washed out. Therefore, the relevant dispersion $\langle(\Theta-\Theta_i)^2\rangle^{1/2}$ is given by the number of jumps during inflation between $N_{\rm obs}$ and $N_{\rm QCD}$, the time of Hubble exit for the comoving scale $k_{\rm QCD}$ which re-enters the horizon when $H = H_{\rm QCD}$. The number of e-folds between $N_{\rm obs}$ and $N_{\rm QCD}$ is given roughly by

$$\Delta N = \ln\frac{a_{\rm QCD}H_{\rm QCD}}{a_0 H_0} \sim \ln\frac{\Lambda_{\rm QCD}}{\Lambda_0} \sim 30. \tag{3.97}$$

So, the dispersion of the PQ phase at QCD transition and inside the observable universe is given by

$$\langle(\Theta-\Theta_i)^2\rangle^{1/2} \sim \frac{H_{\rm inf}}{2\pi f_a}\times\sqrt{30}\,. \tag{3.98}$$

At this point, we see that two situations can occur. First, if $f_a \gg H_{\rm inf}$, the right-hand-side in equation (3.96) can be much smaller than one at the end of inflation; then, the axion field is essentially homogeneous, and the background value Θ_1 in our universe is random but unique. Second, if $f_a \leq H_{\rm inf}$, the right-hand-side can be of order one or larger, which means that the Brownian diffusion of the axion is complete, and the misalignment angle at the QCD scale is randomly distributed with a flat probability distribution in the range $[-\pi,\pi]$. Note that in this case, the quantum perturbations of the radial part of the PQ field are also large enough for restoring the symmetry. In both cases, the mean energy density of the axion is proportional to

$$\langle\Theta_1^2\rangle = \frac{1}{2\pi}\int_{-\pi}^{\pi}\alpha^2 d\alpha = \frac{\pi^2}{3}\,, \tag{3.99}$$

where the average should be understood as holding over many realizations of the universe in the case of a nearly homogeneous Θ_1, or over our present Hubble radius in the case of complete diffusion.

Up until this point we have ignored the anharmonic corrections that could arise from the possibly large value of Θ_1. The calculations have been made using the approximation $(1-\cos\Theta) \simeq \frac{1}{2}\Theta^2$, which is obviously not valid for large angles. To take into account this uncertainty, we will use $\langle \Theta_1^2 f(\Theta_1)\rangle$ instead of the plain rms value of Θ_1. When included, one finds $\langle \Theta_1^2 f(\Theta_1)\rangle \simeq 1.2\,\pi^2/3$.

3.4.2 Isocurvature perturbations from axion fluctuations

If the PQ symmetry is spontaneously broken during inflation, while the scale of inflation is much higher than that of the quark-hadron transition, the flat direction associated with the massless Nambu-Goldstone boson will be sensitive to de Sitter quantum fluctuations. Indeed, quantum fluctuations are imprinted into every massless scalar field present during inflation, with a nearly scale invariant spectrum,

$$\langle |\delta a(k)|^2 \rangle = \left(\frac{H_{\rm inf}}{2\pi}\right)^2 \frac{1}{k^3/2\pi^2}\,. \tag{3.100}$$

If the scale of inflation is high enough, $H_{\rm inf}/2\pi > f_a$, it is possible that quantum fluctuations of the radial part of the PQ field restores the symmetry [67]. This symmetry restoration could have very different implications for cosmological perturbations than a possible thermal symmetry restoration taking place after inflation. Indeed, the effective mass-squared $V''(\rho)$ at the false vacuum $\rho = 0$ is much smaller than the Hubble rate, $V''(\rho) = H_{\rm inf}^2/48\pi^2 \ll H_{\rm inf}^2$. So, the PQ field behaves like a light complex field during inflation. The symmetry is restored in the sense that an average over a scale much larger than the coherence length $\lambda_\psi(t)$ of the field would give $\langle\psi\rangle = 0$. However, $\lambda_\psi(t)$ is of the same order as the Hubble radius $c/H(t)$ at a given time. In comoving space, the coherence length decreases by a huge factor $e^{\Delta N}$ during inflation, and the evolution of the field can be seen as a stochastic process of fragmentation into smaller and smaller homogeneity patches. But at the time when our observable universe crosses the Hubble scale, the PQ field is still nearly homogeneous inside our patch. Its quantum fluctuations become frozen beyond the horizon, and could thus leave a long wave perturbation which would still be described by Eq. (3.100). A detailed proof of this highly non-linear process requires a lattice simulation, whose analysis we leave for a future publication. In this paper, we will conservatively assume that isocurvature perturbations are erased when $H_{\rm inf}/2\pi > f_a$, as has been assumed so far in the rest of the literature [67].

The axion field perturbations δa do not perturb the total energy density, first because the potential energy is exactly zero, and second because as explained before, the gradient energy of the axion cannot exceed $\sim (f_a H_{\rm inf})^2$; for $f_a \ll M_P$ this is much smaller than the total energy density $(3/8\pi)M_P^2 H_{\rm inf}^2$. Since the total energy density, and thus the curvature, are unperturbed by these perturbations during inflation, they are of *isocurvature* type, and manifest themselves as fluctuations in

the number density of axions [68, 69, 12, 70, 71],

$$\delta\left(\frac{n_a}{s}\right) \neq 0\,. \tag{3.101}$$

In the absence of thermal symmetry restoration after inflation, i.e. if the temperature of the plasma does not reach f_a, the axion does not couple significantly to ordinary matter. Thus the fluctuations imprinted during inflation still do not change the total curvature/density of the universe on super-Hubble scales during radiation domination, but they may contribute to the temperature anisotropies of the CMB [72, 73, 74, 75].

Once the axions acquire a mass, it is in principle possible that their interactions with other particles could drive them into thermal equilibrium, thus converting their isocurvature perturbations into curvature or density perturbations. However, the axion coupling is so tiny that it effectively remains decoupled from the rest of the plasma throughout the history of the universe, even after acquiring a mass at the QCD transition. It cannot thermalize and this means that whatever fluctuations the axion has imprinted from inflation are truly isocurvature [31].

We will study here a scenario in which the observable power spectra of CMB anisotropypies and large scale structures are given by the sum of two contributions: an adiabatic mode seeded by the inflaton perturbation, and an isocurvature mode seeded by the axion perturbations. Since these two fields have independent quantum fluctuations during inflation, the adiabatic and isocurvature modes are totally uncorrelated.

Let us assume that the Universe contains photons (γ), approximately massless neutrinos (ν), baryons (b), axions (a), ordinary CDM such as neutralinos (x) and a cosmological constant. In the following, the subscript cdm will denote the total cold dark matter component, so that $\Omega_{\rm cdm} = \Omega_{\rm a} + \Omega_{\rm x}$.

- For the mode seeded by the inflaton, the perturbation evolution starts from the initial condition (during radiation domination and on super-Hubble modes) $\frac{3}{4}\delta_\gamma = \frac{3}{4}\delta_\nu = \delta_{\rm b} = \delta_{\rm x}$, while $\delta_{\rm a} = 0$. The perturbations in the relativistic components $\delta_\gamma = \delta_\nu$ are themselves related to the curvature perturbation $\mathcal{R}$. Since below the QCD scale the two types of cold dark matter share the same equation of state, they are equivalent to a single fluid obeying to the initial condition $\delta_{\rm cdm} = R_{\rm a}\delta_{\rm a} + (1 - R_{\rm a})\delta_{\rm x}$, with $R_{\rm a} \equiv \Omega_{\rm a}/\Omega_{\rm cdm}$. For the mode under consideration, $\delta_{\rm a} = 0$ and $\delta_{\rm x} = \delta_{\rm b}$, so that $\delta_{\rm cdm} = (1 - R_{\rm a})\delta_{\rm b}$. This initial condition is different from the standard adiabatic initial condition in a model without axions, $\delta_{\rm cdm} = \delta_{\rm b}$. However, this initial condition for $\delta_{\rm cdm}$ is irrelevant in practise, because cold dark matter perturbations do not leave a direct signature in the CMB anisotropies, while the observable matter power spectrum today is sensitive to the initial value of $\mathcal{R}$ but not of $\delta_{\rm cdm}$. This can be explicitly checked by running a Boltzmann code with the standard adiabatic initial condition replaced by $\delta_{\rm cdm} = (1 - R_{\rm a})\delta_{\rm b}$: one finds that for

fixed curvature spectrum and fixed $\Omega_{\rm cdm}$, the CMB and LSS power spectra do not depend on $R_{\rm a}$. Therefore, the mode seeded by the inflaton is equivalent to the usual adiabatic mode.

- For the isocurvature mode, the perturbation evolution starts from the initial condition $\frac{3}{4}\delta_\gamma = \frac{3}{4}\delta_\nu = \delta_{\rm b} = \delta_{\rm x} \simeq 0$ and $\delta_{\rm a} = \mathcal{S}_{\rm a}$, where $\mathcal{S}_{\rm a}$ is the gauge invariant entropy perturbation

$$\mathcal{S}_{\rm a} = \frac{\delta(n_{\rm a}/s)}{(n_{\rm a}/s)} = \frac{\delta n_{\rm a}}{n_{\rm a}} - 3\frac{\delta T}{T} \tag{3.102}$$

(indeed, after the QCD transition, the axion fluid is non-relativistic with $\rho_{\rm a} = m_{\rm a} n_{\rm a}$, so $\delta_{\rm a} = (\delta n_{\rm a})/n_{\rm a}$; furthermore, the fact that $\delta_{\rm a} \gg \delta_\gamma$ implies $(\delta n_{\rm a})/n_{\rm a} \gg 4(\delta T)/T$ and $S_{\rm a} = (\delta n_{\rm a})/n_{\rm a} = \delta_a$). Again, it is equivalent to consider the perturbations of a single cold dark matter fluid, obeying now to the initial condition $\delta_{\rm cdm} = R_{\rm a}\delta_{\rm a} + (1 - R_{\rm a})\delta_x = R_{\rm a}\mathcal{S}_{\rm a}$. If we compare with the initial condition for a usual "Cold Dark matter Isocurvature" (CDI) model, given by $\delta_{\rm cdm} = \mathcal{S}_{\rm cdm}$, we see that the axionic isocurvature solution is equivalent to the CDI solution with $\mathcal{S}_{\rm cdm} = R_{\rm a}\mathcal{S}_{\rm a}$.

In summary, an axionic model with axionic fraction $R_{\rm a} = \Omega_{\rm a}/\Omega_{\rm cdm}$, initial curvature spectrum $\langle \mathcal{R}^2 \rangle$ and initial entropy spectrum $\langle \mathcal{S}_{\rm a}^2 \rangle$ is strictly equivalent to a mixed adiabatic+CDI model with the same curvature spectrum and $\langle \mathcal{S}_{\rm cdm}^2 \rangle = R_{\rm a}^2 \langle \mathcal{S}_{\rm a}^2 \rangle$.

Let us now relate the curvature and entropy power spectrum to the quantum fluctuations of the inflaton and axion field during inflation. For the adiabatic mode, it is well-known that the curvature power spectrum reads

$$\langle |\mathcal{R}(k)|^2 \rangle = \frac{2\pi H_k^2}{k^3 M_P^2 \epsilon_k} \tag{3.103}$$

where ϵ is the first inflationary slow-roll parameter [8] and the subscript k indicates that quantities are evaluated during inflation, when $k = aH$. In first approximation this spectrum is a power-law with a tilt $n_{\rm ad}$ depending also on the second slow-roll parameter η [8],

$$n_{\rm ad} = 1 - 6\epsilon_k + 2\eta_k \ . \tag{3.104}$$

For the isocurvature mode, using the axion perturbation spectrum of Eq. (3.100), we obtain

$$\langle |\mathcal{S}_{\rm a}(k)|^2 \rangle = \left\langle \left| \frac{\delta n_{\rm a}}{n_{\rm a}} \right|^2 \right\rangle = 4 \left\langle \left| \frac{\delta a}{a} \right|^2 \right\rangle = \frac{2H_k^2}{k^3 f_a^2 \langle \Theta_1^2 \rangle} \, . \tag{3.105}$$

This power spectrum can be approximated by a power-law with a tilt

$$n_{\rm iso} = 1 - 2\epsilon_k \, , \tag{3.106}$$

which is related to the tilt n_t of tensor perturbations.

The relative amplitude of isocurvature perturbations at a given pivot scale in adiabatic+CDI models is often parametrized as [14, 76, 15]

$$\alpha = \frac{\langle|\mathcal{S}_{\rm cdm}(k)|^2\rangle}{\langle|\mathcal{S}_{\rm cdm}(k)|^2\rangle + \langle|\mathcal{R}(k)|^2\rangle} \ . \tag{3.107}$$

Since the axionic model is equivalent to an adiabatic+CDI model, we can still use the same parametrization. The parameter α is related to fundamental parameters by

$$\alpha = \frac{R_{\rm a}^2\langle|\mathcal{S}_{\rm a}(k)|^2\rangle}{R_{\rm a}^2\langle|\mathcal{S}_{\rm a}(k)|^2\rangle + \langle|\mathcal{R}(k)|^2\rangle} \simeq \frac{R_{\rm a}^2 M_P^2 \epsilon_k}{\pi f_{\rm a}^2\langle\Theta_1^2\rangle} \tag{3.108}$$

where in the last equality we assumed $\alpha \ll 1$.

We have finally arrived at an expression directly comparable to data. Eq. (3.108) will serve on Chapter 6 as our discriminator inside the parameter space spanned by the scale of inflation and the symmetry breaking scale.

As we mentioned at the beginning of this section, we have shown how a purely theoretical, particle physics model, gives rise to an observable isocurvature signal providing us with tools to test the theory, or at least, to put some important constraints.

Of course, this applies to the first two isocurvature models presented as examples, only that these are not so precisely predicted from a particle physics model.

Once we have laid the grounds for the theoretical part, we need to develop the phenomenological part, *i. e.* the experiments. It is not straightforward to go from observations to parameters such as α. We take care of this issue in the following chapter.

Chapter 4

Cosmological Probes

As has been stated many times before, Cosmology has entered a new era in which many different observations can validate or falsify the different theories for the history of the Universe. It is very important to control the extent to which these probes can help us, their potential and their limitations.

In this chapter, we review the main standardly used cosmological probes and focus on their implications for cosmology, paying special attention to what can be learnt from them about the nature of the primordial seeds.

4.1 CMB anisotropies

Up until the universe was about $3 \cdot 10^5$ years old, its energy budget is saturated by three species: photons, baryons and dark matter. The temperature then, $T \sim 1 - 0.1$eV, is high enough to keep a very effective Thomson scattering rate that holds the photons and the baryons tightly coupled. Due to the very high sound speed (eq.1.49) in the photon-baryon plasma, perturbations in it propagate efficiently causing the baryons to vibrate in a harmonic way with a principal mode that has the size of the sound horizon at that epoch. The dark matter, a fluid with zero equation of state and no acoustic propagation of the perturbations, absorbs part of the shocks in the plasma and makes this photon-baryon-dark matter fluid a damped oscillator. Of course, many subtleties need to be taken into account but this is the main picture of what was going on during the first stages of the universe.

At the recombination epoch ($z_{\rm rec} \sim 1100$) the universe has expanded and cooled so much that the power of the Thomson scattering is not enough to keep the baryons and the photons oscillating together. The latter decouple from the rest of the species and travel freely ever after because the gravitational interaction with the matter is too weak to modify their trajectories. The baryonic fluid from which the photons decouple is not homogeneously distributed in space and these footprints are recorded in the energy distribution of the photons. They permeate the universe now and reach

us from all directions, containing valuable information about the spatial distribution of matter at the recombination epoch.

But this is not the only piece of information one can get from the anisotropies in the CMB radiation. In spaces that are expanding with time, the ratio of physical distances measured at different epochs, provides us with clues about the expansion history, the amount of energy contained and its nature.

The location of the peaks in the CMB anisotropies power spectrum is approximately proportional to the inverse of the angular separation $\theta_s \equiv \frac{r_s}{D_A(z_{\rm rec})}$ [79].

4.1.1 Theory and experiments

The goal of the theory of the CMB anisotropies is to relate the perturbations in the gravitational potential to the fluctuations in the CMB temperature observed by satellites or ground based experiments. Cosmologists measure the temperature of the background radiation in different patches and directions in the sky. It is extremely homogeneous[1], its tiny variations being of order $\frac{\delta T}{T_{\rm CMB}} \sim 10^{-6}$ where $\delta T = T - T_{\rm CMB}$ and $T_{\rm CMB} = 2.728K$. Since the sky is a sphere, this map of temperatures may be decomposed into the spherical harmonics:

$$\frac{\delta T(\mathbf{e})}{T} \equiv \Theta(\mathbf{e}) = \sum_{\ell m} a_{\ell m} Y_{\ell m}(\mathbf{e}) \tag{4.1}$$

where $\mathbf{e}$ is the vector on the direction of observation. If the initial conditions are gaussian, we have:

$$\langle a_{\ell m} a^*_{\ell' m'} \rangle = C_\ell \ \delta_{\ell \ell'} \delta_{m m'} \tag{4.2}$$

and all of the off-diagonal terms ($l \neq l';\ m \neq m'$) of the correlation matrix vanish because of isotropy. We assume gaussian initial conditions all throughout this work, and in this case, the *angular power spectrum* of the anisotropies, the C_ℓ's, is enough to describe the whole sky map. Since their values are uncorrelated to each other for a given realization they are the quantities generally used for comparing experiments to theory.

Using equations (4.1) and (4.2), and the theorem of the sum of spherical harmonics, we find an expression for the angular correlation function in the anisotropies. If α is the angle between directions $\mathbf{e}$ and $\mathbf{e}'$, then:

$$C(\alpha) \equiv \langle \frac{\delta T(\mathbf{e})}{T} \frac{\delta T(\mathbf{e}')}{T} \rangle = \sum_\ell C_\ell \left(\frac{2\ell + 1}{4\pi} \right) P_\ell(cos\alpha) \tag{4.3}$$

is the correlation function for the anisotropies.

[1]This is once the dipole contribution due to our motion with respect to the galaxy has been removed.

Note that each possible value of m corresponds to the different direction of observation in which lay each patch of the sky from which temperature is being measured. The total number for each ℓ is $(2\ell+1)$ thus, for a low multipole number ℓ, very few samples of the sky can be taken and we are left with not enough data to perform statistics. In particular, for each amplitude [78]:

$$\Delta C_\ell = \sqrt{\frac{2}{(2\ell+1)}} \tag{4.4}$$

This is known as the problem of *cosmic variance* which limits the accuracy to which low multipoles may be measured.

The anisotropies observed today must be also a function of the present time η_0 and position $\mathbf{x}_0$, thus:

$$\Theta(\mathbf{e}) \rightarrow \Theta(\mathbf{x}_0, \eta_0, \mathbf{e}) \tag{4.5}$$

which can be expressed in its Fourier series and in terms of the Legendre polynomials:

$$\Theta(\mathbf{x}_0, \eta_0, \mathbf{e}) = \int \frac{d^3\mathbf{k}}{(2\pi)^3} e^{i\mathbf{k}\mathbf{x}_0} \sum_\ell (-i)^\ell (2\ell+1) a_\ell(\mathbf{k}, \eta_0) P_\ell(\hat{\mathbf{k}} \cdot \mathbf{e}) \tag{4.6}$$

Thus, the power spectrum is:

$$C(\alpha) = \sum_\ell \frac{2}{\pi} \int \frac{dk}{k} k^3 \langle |a_\ell(k, \eta_0)|^2 \rangle \frac{2\ell+1}{4\pi} P_\ell(\cos\alpha) \tag{4.7}$$

Comparing this expression to (4.3), we arrive at a relation for the C_ℓ's and the a_ℓ coefficients.

$$C_\ell = \frac{2}{\pi} \int \frac{dk}{k} k^3 \langle |a_\ell(k, \eta_0)|^2 \rangle \tag{4.8}$$

Now that we know how experimentalists report their data, we need to relate the primordial potential that describes initial inhomogeneities according to Eq.(1.50) to the a_ℓ coefficients and to the C_ℓ's themselves via Eq.(4.8).

There are many subtleties to this calculations and since it is not our main point to describe the physics of the CMB anisotropies but rather its implications for cosmology, we will follow [77] and [8] closely but will use some of the beautiful, hand waving simplifications presented in [78]. All the illustrations of the anisotropies are done using the `camb` fortran code [80].

To study the "primordial soup" present before recombination, we need to bear in mind that this is a fluid in which many species coexist. Each one of them with a different equation of state and holding different interactions with the rest. Fortunately, there are a few (not too simple) equations that fully describe the behavior of each of the fluids. These are the Continuity and Euler equations for the non relativistic fluids and the Boltzmann equation for the relativistic gases. In the most general scenario, the non-relativistic species are the cold dark matter (cdm), that

interacts with the rest of the species only gravitationally, and the baryons (b). As relativistic species, we count the neutrinos (ν) and the photons (γ).

All of the subsequent equations, are written using the gauge invariant formalism described on 1.2.1 where the gravitational backreaction of the matter in the metric is expressed in terms of Φ, the Newtonian potential, and Ψ the intrinsic curvature perturbation.

Relativistic fluid: photons

Under the gas dynamics formalism, there is one fundamental function that describes the whole state of a gas, and this is the distribution function $f(t, \mathbf{r}, \mathbf{p})$ where $\mathbf{r}, \mathbf{p}$ are the position and momentum of the particle respectively. The number of particles, N, in a given section of the volume in the phase space is:

$$dN = \frac{1}{2\pi} g_i f(t, \mathbf{r}, \mathbf{p}) d\mathbf{r} d\mathbf{p}$$

where g_i is the number of spin states of the particle.

If the fluid is collisionless, and therefore there is no momentum exchange with other particle species, the Liouville equation or the conservation of the volume in the phase space applies, and we have:

$$\frac{df}{dt} = 0 \tag{4.9}$$

We can write the Liouville equation in an explicitly covariant form:

$$\frac{\delta f}{\delta t} + \frac{\delta f}{\delta x^i}\frac{dx^i}{dt} + \frac{\delta f}{\delta t}\frac{dp}{dt} = 0 \tag{4.10}$$

where we have ignored variations in the direction of propagation of the photon, γ^i because we assume flat space times for simplicity[2]. The effects of gravity on equation (4.10) are taken into account via the geodesic equation computed up to order one in the perturbations[81].

Assuming thermalization, a *not so straight forward* calculation [81], probes that, to zero order, the distribution function $f(t, \mathbf{r}, \mathbf{p})$ is, as a matter of fact, that of a blackbody:

$$f(\mathbf{r}, \mathbf{p}) = \frac{1}{\exp[E/T] - 1} \tag{4.11}$$

where E is the energy ($E = p$) and the slight dependence on the spatial coordinates comes through T. The perturbation in the photon density, $\delta\rho_\gamma$, is directly translated

[2]In any case, the term generated in the equation is of second order in the perturbations, and it could be dropped even for non flat spacetimes.

as a perturbation in the temperature, $\frac{\delta\rho_\gamma}{\delta\rho_\gamma} = 4\frac{\delta T}{T}$ because $n_\gamma \propto T^3$.Therefore, the function f gets a shift:

$$f(p, T + \Theta) = f(p, T) + \delta f \tag{4.12}$$

with $\Theta \equiv \frac{\delta T}{T}$. More explicitly:

$$\begin{aligned} f(\mathbf{p}) &= \frac{1}{\exp[p/T(1+\Theta)] - 1} \simeq \frac{1}{\exp[p/T] - 1 - \frac{\Theta p}{T}\exp[p/T]} \\ &\simeq \frac{1}{\exp[p/T] - 1} + \frac{\Theta p}{T}\exp[p/T]\frac{1}{(\exp[p/T] - 1)^2} \end{aligned} \tag{4.13}$$

Thus, to first order [8] :

$$\delta f = -p\Theta\frac{df(p)}{dp} \tag{4.14}$$

Using the perturbed geodesic equation, equation (4.10) and the relation (4.14), we can write the collisionless perturbed liouville equation in terms of Θ [81]:

$$\dot{\Theta} + \gamma^i\frac{\delta}{\delta x^i}(\Theta + \Phi) + \dot{\gamma}^i\frac{\delta}{\delta\gamma^i}\Theta + \dot{\Psi} = 0 \tag{4.15}$$

Not that in this case, we are studying the perturbations as they where happening at time η, thus:

$$\Theta \to \Theta(\mathbf{x}, \eta, \mathbf{e})$$

If we go to Fourier space, and writing the dependence explicitly:

$$\Theta(\mathbf{x}, \eta, \mathbf{e}) = \frac{1}{(2\pi^3)}\int d\mathbf{k}^3 e^{i\mathbf{kx}}\Theta_\mathbf{k}(\eta, \mathbf{e}) \tag{4.16}$$

We can still decompose each Fourier component into the Legendre polynomials:

$$\Theta_\mathbf{k}(\eta, \mathbf{e}) = \sum_{\ell=0}^{\infty}(-i)^\ell(2\ell + 1)\Theta_\ell(\mathbf{k}, \eta)P_\ell(\mu) \tag{4.17}$$

where μ is the cosine of the angle formed by the vectors $\mathbf{k}$ and $\mathbf{e}$, *i. e.* $\mu = \frac{\mathbf{k}}{k}\cdot\mathbf{n}$. Also, we drop the explicit temporal dependence.

$P_\ell(\cos\theta)$ are the Legendre polynomials:

$$\begin{aligned} P_0(\cos\theta) &= 1 \\ P_1(\cos\theta) &= \cos\theta \\ P_2(\cos\theta) &= \frac{1}{4}(1 + 3\cos 2\theta) \\ &\ldots \end{aligned}$$

This way, the component Θ_0 picks up a constant component, and Θ_1 and Θ_2 pick up the linear and quadratic term respectively, also known as the monopole, dipole and quadrupole.

With all of the above considerations, Eq. (4.15) becomes, for each of the Fourier modes:

$$\dot{\Theta}_{\mathbf{k}} + ik\mu(\Theta_{\mathbf{k}} + \Phi_{\mathbf{k}}) + \dot{\Psi}_{\mathbf{k}} = 0 \tag{4.18}$$

From now on, we work on Fourier space but drop the $\mathbf{k}$ in the notation.

Fortunately, Nature is not that simple, and photons and baryons do interact via Thomson scattering. Then, one must include a *collision* term, $C[f]$ in Eq. (4.9) to get:

$$\frac{df}{dt} = C[f] \tag{4.19}$$

the **Boltzmann equation** for the distribution. The particular form of the collision factor depends on the intervening species and the interactions among them.

It is out of the reach of this thesis to explain in great detail the origin of the collision term. Under some general assumptions such as the thermalization of the electronic fluid and working in the non relativistic Thomson limit, *i.e.* $\frac{\delta p}{p} \ll 1$, we finally, we arrive at the equation for the evolution of Θ [77]:

$$\dot{\Theta} + ik\mu(\Theta + \Psi) = -\dot{\Psi} + \dot{\tau}[\Theta_0 - \Theta - \frac{1}{10}\Theta_2 P_2(\mu) - i\mu v_b] \tag{4.20}$$

where we drop once again, the explicit dependence on the $\mathbf{k}$ mode and the subindices denote the coefficient in the Legendre expansion. The factor τ is the optical depth which is mainly determined by the number of free electrons $n_e(t)$ present in the fluid. During the very early stages, at $z \ll 1100$, $n_e(t)$ ∼constant but its value falls abruptly at recombination. Fortunately, we can use approximations that capture the main effects of this behaviour, but it is important to keep in mind that corrections to the current antsazts could add up to be important and many efforts are focused on determining to what extent this could be so. So far cumulative results add up to $\sim 0.3\%$ in x_e, the free electron fraction [82].

Even though we have not explicitly mentioned the influence of the polarization in the fluid, it does matter. Thomson scattering is proportional to the scalar product of the initial and final polarization vector, therefore polarization must be included in this analysis. This is reflected in the fact that the dipole and quadrupole do appear explicitly in equation (4.20)

Now we take care of the other two components of the primordial Universe: the cold dark matter and the baryons.

Cold Dark Matter

To first order in the perturbations, the conservation of the energy-momentum tensor, $D_\mu T^\mu_\nu = 0$, gives the continuity and Euler equations:

$$\dot{\delta_{\rm b}} = -k(v_b - \Theta_1) + \frac{3}{4}\dot{\delta_\gamma} \tag{4.21}$$

Since they only interact with the rest of the species gravitationally, its effects are only reflected through the gravitational potentials in the final equations, and never show up explicitly.

Baryons

In the total matter rest frame, the continuity and Euler equations are:

$$\begin{aligned} \dot{\delta}_b &= -k(v_b - \Theta_1) + \frac{3}{4}\dot{\delta}_\gamma \\ \dot{v}_b &= -\frac{\dot{a}}{a}v_b + k\Phi + \dot{\tau}(\Theta_1 - v_b)/R \end{aligned} \tag{4.22}$$

Now, we have the three sets of equations that along with the Poisson and the anisotropic stress equations, describe the dynamics in the early Universe.

The general picture is that of a tightly coupled fluid oscillating on top of a gravitational potential field. In the tight coupling limit, the Compton scattering time, $\dot{\tau}^{-1}$, is much smaller than the expansion of the Universe or the gravitational infall and equations (4.20) through (4.22) can be expanded in powers of it [83, 77]. In this limit, $\Theta_\ell = 0$ for all the $\ell \geq 2$.

We finally arrive at a single differential equation of second order for the monopole:

$$\ddot{\Theta}_0 + \frac{\dot{a}}{a}\frac{R}{1+R}\dot{\Theta}_0 + k^2 c_s^2 \Theta_0 = F(\Phi, \Psi, \eta) \tag{4.23}$$

with:

$$F(\Phi, \Psi, \eta) = -\ddot{\Psi} - \frac{\dot{a}}{a}\frac{R}{1+R}\dot{\Psi} - \frac{k^2}{3}\Phi \tag{4.24}$$

an "external force" term that arises from the gravitational potential field [77]. R is the momentum density ratio $R \equiv \frac{p_b+\rho_b}{p_\gamma+\rho_\gamma} = \frac{3\rho_b}{4\rho_\gamma}$. The lhs of the equation is a damped harmonic oscillator with time dependent coefficients - we see that thanks to the isotropy, the linear nature of the modes, and in the tight coupling limit the complicated dynamics of a fluid such as our primordial soup, can be described as a damped oscillator! Isn't the Universe beautiful?!

Solving (4.23) and initial conditions, is all we need for the simplest prediction of the CMB anisotropies. Note that since the CDM and the other two species do not interact thermodynamically, its effects only enter the final equation through the effect they have on the Bardeen potentials.

In the absence of any anisotropic stress, we have $\Psi = \Phi$, so we will unify the two potentials. Rearranging (4.23), we arrive at:

$$(\ddot{\Theta}_0 + \ddot{\Psi}) + \frac{\dot{a}}{a}\frac{R}{1+R}(\dot{\Theta}_0 + \dot{\Psi}) + k^2 c_s^2(\Theta_0 + \Psi) = -\Psi(k^2 c_s^2 + \frac{k^2}{3}) \tag{4.25}$$

The solution to this equation can be derived with the WKB approximation [77]:

$$\begin{aligned}[1+R(\eta)]^{1/4}\Theta_0^{\rm tc}(\eta) &= \Theta_0(0)\cos(kr_s(\eta)) + \frac{\sqrt{3}}{k}[\dot{\Theta}(0) + \frac{1}{4}\dot{R}(0)\Theta(0)]\sin(kr_s(\eta)) \\ &+ \frac{\sqrt{3}}{k}\int_0^\eta d\eta'[1+R(\eta')]^{3/4}\sin[kr_s(\eta)-kr_s(\eta')]F(\Psi,\eta')\end{aligned} \tag{4.26}$$

If we now drop the tight coupling assumption and take into account one more order in the expansion of powers in $\dot{\tau}^{-1}$, we arrive at a solution where the damping due to photon diffusion is reflected:

$$(\Theta_0(\eta)+\Psi(\eta)) = (\Theta_0^{\rm tc}(\eta)+\Psi(\eta))e^{-[k/k_D(\eta)]^2} \tag{4.27}$$

where $k_D(\eta)$ is the diffusion scale or the distance a photon can random walk by the time η.

We should be ready to compute now the C_ℓ via Eq.(4.3). Comparing Eq.(4.3) to Eq.(4.17), it could be thougth that this step is straight forward. However, we need to take into account that in reality, we are observing the anisotropies that free streamed towards us from a finite spherical shell of radius $D_* = \eta_0 - \eta$. This makes the relation not exact.

A plane wave can be decomposed in terms of the Bessel spherical functions $j_\ell(kx)$ and the spherical harmonics:

$$e^{i\mathbf{kx}} = 4\pi\sum_{\ell=0}^{\infty} i^\ell j_\ell(kx)\sum_{m=\ell}^{m=-\ell} Y_{\ell m}(\Omega_x)Y^*_{\ell m}(\Omega_k) \tag{4.28}$$

where Ω_x and Ω_k define the directions of the position and momentum vectors respectively. Inserting (4.28) in (4.16):

$$\Theta(\mathbf{x}) = \sum_{\ell m} Y_{\ell m}(\Omega_x)\underbrace{\int \frac{d^3k}{(2\pi)^3} i^\ell j_\ell(kD_*)\Theta_{\mathbf{k}}Y^*_{\ell m}(\Omega_k)}_{a_{\ell m}(k)} \tag{4.29}$$

because the radial component of the position vector is indeed D_*. The relationship to $a_{\ell m}$ comes from comparing to Eq. (4.1). Finally, using Eq.(4.2), we arrive at the expression for the coefficients of the correlation function [78]:

$$C_\ell = \frac{2}{\pi}\int dk k^2 a^2_{\ell m}(k) \tag{4.30}$$

It must also be noted that other effects apart from the anisotropies due to gravitational perturbations should be taken into account.

In order to derive some of the implications for cosmology, and to get a physical taste of equation 4.25, we follow the simplifications done in [78].

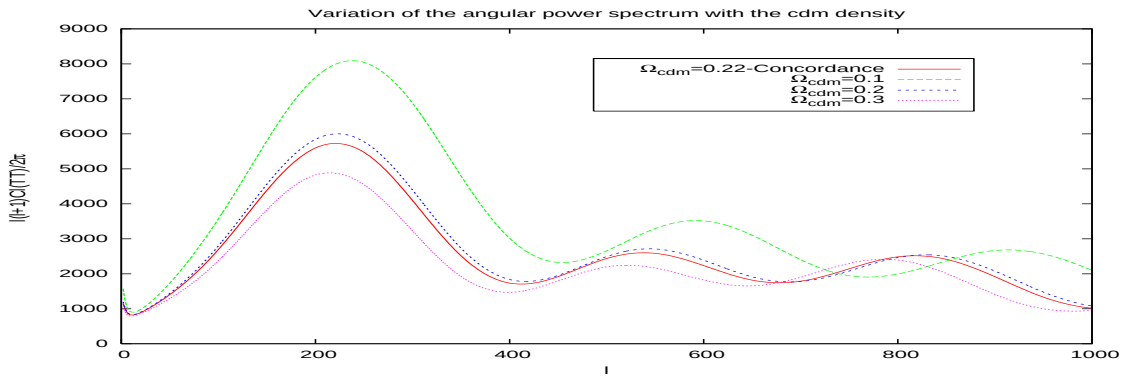

Figure 4.1: Variation of the equilibrium point of the oscillations with $\Omega_{\rm cdm}$. In red (solid line) we plot the power spectrum for the values of the parameters in the currently accepted concordance model.

4.1.2 Implications for cosmology.

We know now that the baryon fraction in the Universe is very low, $\Omega_{\rm b} \sim 0.045$. Even though they play a primordial role in the theory of CMB anisotropies, it is an instructive exercise to study the solutions to the oscillations equation (4.25) when the fraction of baryons is completely negligible- in this way, we study the main effects of the rest of the factors in the oscillations.

If there were no baryons in the primordial Universe, $R = 0$ and (4.25) would be:

$$(\ddot{\Theta}_0 + \ddot{\Psi}) + k^2 c_s^2 (\Theta_0 + \Psi) = 0 \tag{4.31}$$

because for radiation, $c_s^2 = 1/3$. The equation then, has a very simple solution:

$$(\Theta_0 + \Psi)(\eta) = (\Theta_0 + \Psi)(\eta_0)\cos(kc_s\eta) + (\dot{\Theta}_0 + \dot{\Psi})(\eta_0)\sin(kc_s\eta) \tag{4.32}$$

As we see, the initial conditions determine the phase of the solution as well as its amplitude. It is impossible to separate the contribution coming from the intrinsic temperature anisotropy from the one coming from the potential field. We see from Poisson's equation that the potential field in momentum space is directly proportional to the energy density. So this solution illustrates that the amount of CDM directly shifts the amplitude of the oscillations. The dark matter acts then as a spring in a harmonic oscillator. The recovering constant of the spring would be proportional to the amount of dark matter. We see this in Fig. 4.1. Note that the C_ℓ's illustrated have been calculated solving the full set of equations and thus the effect we want to show, although clear, it is not as extreme.

The frequency in the momentum space of the oscillations is $c_s\eta$, *i.e.* the acoustic horizon at time η. Since the photons were frozen at recombination, the position of the peaks in k-space tells us about the size of the acoustic horizon at recombination.

This characteristic scale which can be computed theoretically [77]:

$$\begin{aligned} r_{\rm s}(\eta) &= \int_0^{\eta} c_s d\eta' \Rightarrow \\ r_{\rm s}(a_{\rm rec}) &= \frac{1}{H_0\sqrt{\Omega_{\rm M}}} \int_0^{a_{\rm rec}} \frac{c_s}{\sqrt{a_{\rm eq}+a'}} da' \end{aligned} \tag{4.33}$$

is observed at present with a different size that depends both on the expansion history of the Universe and the curvature through the angular diameter distance, $D_A(z)$ (eq. (1.18)). The multipole number is inversely proportional to the ratio[3]:

$$\ell \simeq \frac{m\pi}{2}\frac{D_A}{r_s} \tag{4.34}$$

where m depends on the initial conditions and could be $m = 1, 3, 5...$ for $(\Theta_0 + \Psi)(\eta_0) = 0$ or $m = 2, 4, 6...$ for $(\dot{\Theta}_0 + \dot{\Psi})(\eta_0) = 0$.

So we see that from the position of the peaks we can get information about the geometry of the Universe and the initial conditions for the gravitational potential and the intrinsic temperature anisotropy.

On figure 4.2 we plot the anisotropies angular spectra for models with different values for the curvature and the Hubble parameters and see how this shifts the position of the peaks.

Variations in the hubble parameter imply variations in age of the Universe. In a younger Universe (higher h) we see things *closer* thus bigger, and the peaks shift to the left. The opposite occurs for older Universes, as it is illustrated in the figure. For models with an open geometry ($\Omega_{\rm K} > 0$, by Eq. (1.26)), the objects appear to be further away than they are, so we see them smaller. The peaks shift to the right then. The opposite occurs for open Universes. We see this in the top panel of Fig. 4.2.

Of course, life is not that easy, and one can easily see how the appropriate shift in the hubble parameter may cancel the effects of a small isocurvature contribution. This is called *degeneracy problem* and we will come back to it later during this thesis. Nevertheless, at this point we must note that this is one of the intrinsic problems of parameter estimation in cosmology. The effect of the variation of the cosmological parameters are similar in some cases, and this leads to an increase in the uncertainties beyond statistical and systematic errors.

Now, we come back to the phase of the oscillations in Eq.(4.34), *i. e.* to the value of the integer m. If the rest of the parameters were fixed, we could learn which was the nature of the primordial conditions for the potentials from the position of the peaks. If they where *isocurvature*, *i.e.* the primordial potentials are not perturbed

[3]This proportionality is not exact due to the decay of the gravitational potential during the radiation domination epoch. It can be quantified in terms of some shifts which are weakly dependent on the cosmological parameters, and have been calculated in [79].

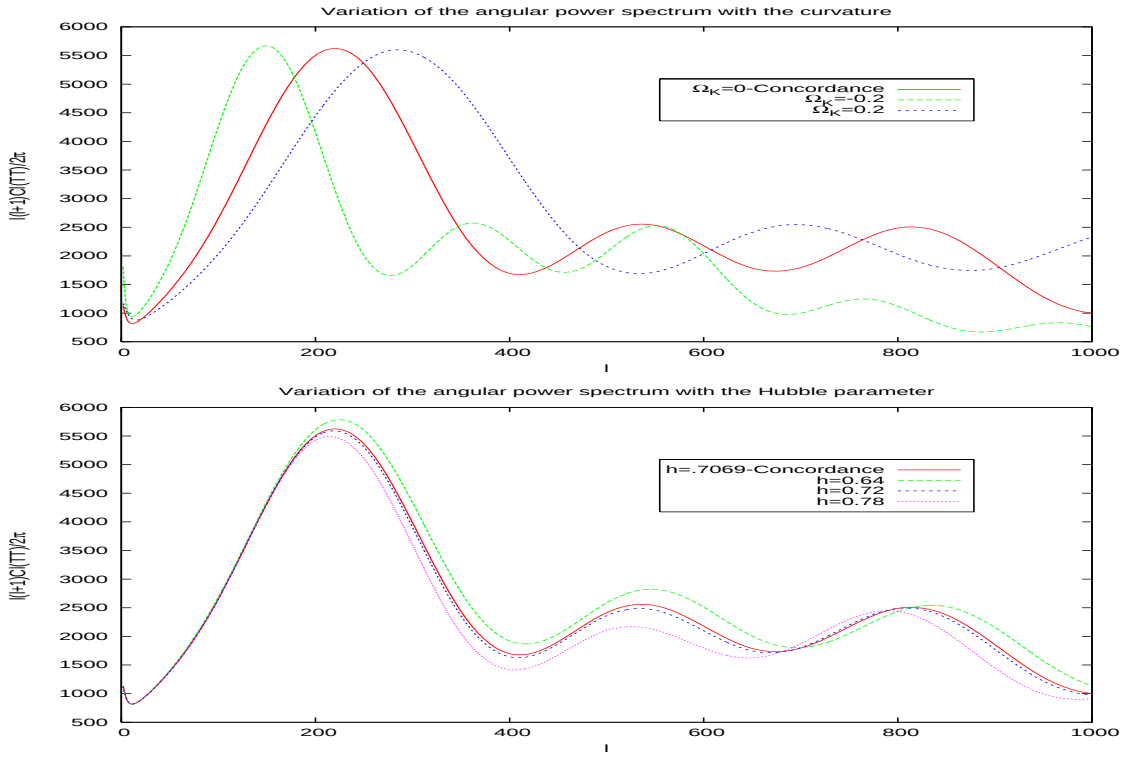

Figure 4.2: Variation of the position of the peaks with $\Omega_{\rm K}$ and h .

initially, then $(\Theta_0 + \Psi)(\eta_0) = 0$ and the sinusoidal mode is excited initially. If the velocity perturbations are the ones which are negligible, *i.e.* they are *adiabatic*, then the oscillations are proportional to a cosine oscillation. We show the difference in the oscillations of the phases in Fig. 4.3 where the shift of $\pi/2$ in the phase can be clearly appreciated.

Note also that for the usual value of the cosmological parameters, the amplitude of the isocurvature modes is two or three orders of magnitude smaller than the adiabatic amplitude, as expected from what was explained in chapter 3. This makes it very easy to "hide" an isocurvature signal inside an adiabatic spectra. This indeed is one of the main reasons why the isocurvature modes are so difficult to rule out given the current observations. Also, as it is the case for the parameters $\Omega_{\rm K}$ and h, a small shift in the position of the peaks due to the contribution of an isocurvature spectrum, could be easily compensated with a variation of h such that its value remains inside allowed current ranges. We study this effect deeper in the upcoming sections and show a way to break the degeneracy.

Now, let us go back to a Universe with a small fraction of baryonic matter, *i.e.* the equation of the primordial oscillator is (4.25) again. We see that the baryons act as a mass therm- this makes the compression peaks more pronounced and thus the first, third, and other odd numbered peaks grow in power.

We illustrate this effect on figure 4.4. Note that the damping caused by the

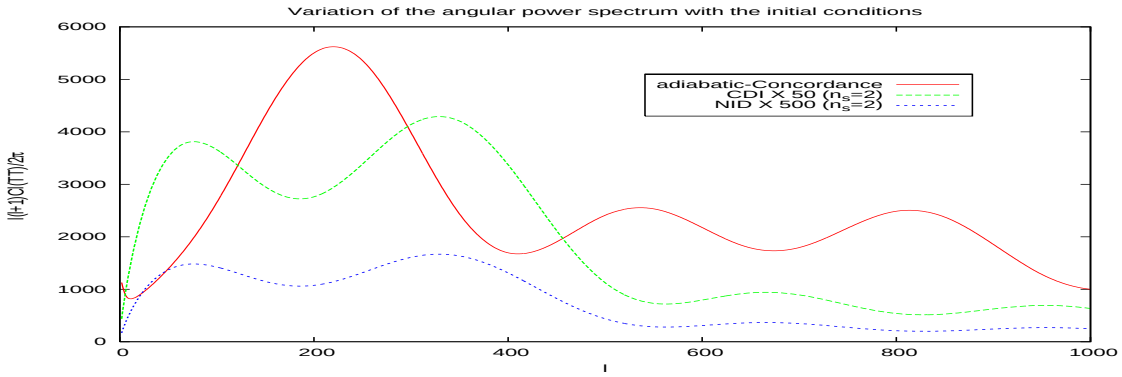

Figure 4.3: Variation of the position of the peaks with the initial conditions. We show adiabatic (red) versus CDI (green) or NID (blue) initial conditions. Note that the isocurvature spectra have been increased in order to be compared to the others. Also, the tilt for the isocurvature spectra has been increased to make visualization easier.

optical depth acts as an exponential envelope for the whole CMB spectrum. Thus the third peak is naturally damped for every model. Still we can see that the third peak in the the model containing $\Omega_b = 0.06$ is as high as the third peak in the concordance model, *even with the damping*. Then, comparing the heights of the second peaks, one understands our point that only the first and third peaks are enhanced.

This has been a very brief review of the basic physics taking part in the CMB spectrum. With it, we just want to give a hand waving physical insight. By no means this is all we need for our analysis, and in practice, it is necessary to use the available boltzmann code `camb` [80]. With it, one computes the theoretical values of the C_ℓ's and they can be subsequently compared to the observed values. We will see the statistical machinery used for the computation of the probabilities in chapter 5 and the results obtained are presented in chapter 6.

Now, we carry on studying experiments and describe the basics of the large scale structure formation in an expanding Universe.

4.2 Large Scale Structure

The perturbations in the metric which seed the anisotropies in the CMB, affect all the fluids present in the Universe at the primordial epoch. In particular, they generate perturbations in the energy density of the non-relativistic matter. These grow via gravitational instability originating ultimately the structures we observe

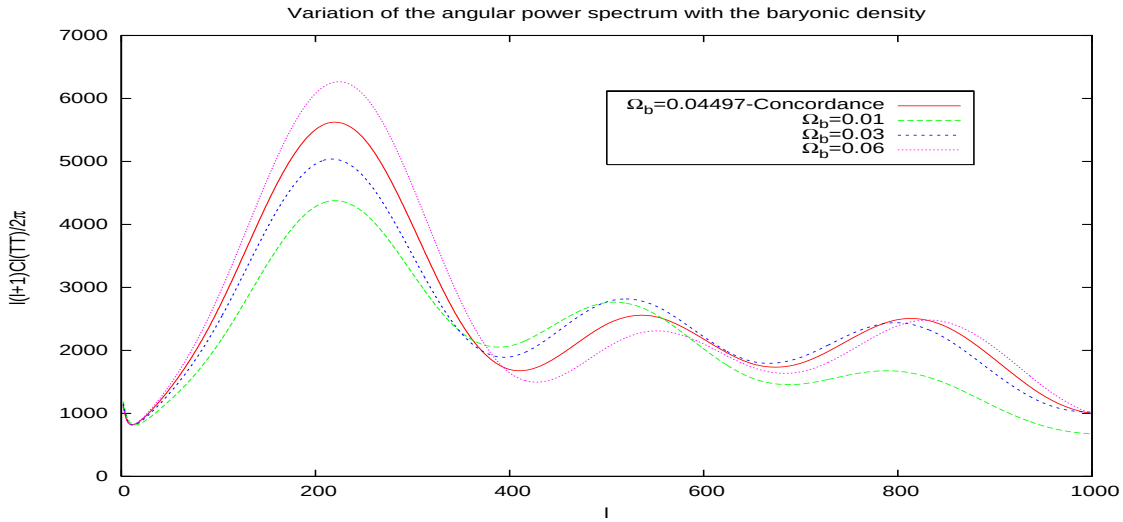

Figure 4.4: Variation of the height of the 1^{st} and the 3^{rd} peaks with $\Omega_{\rm b}$.

today: galaxies, clusters and superclusters.

They start off as tiny perturbations that grow linearly inside the expanding Universe. It is useful to define the *density contrast*:

$$\delta(\mathbf{x},t) \equiv \frac{\rho(\mathbf{x},t) - \langle\rho\rangle}{\langle\rho\rangle} \tag{4.35}$$

Since $\rho_{\rm cdm} \propto T^3$ for usual cold dark matter, we have $\delta(\mathbf{x}, t_{\rm dec}) \propto \Theta(\mathbf{x})$; where Θ has been defined in Eqn. (4.1). Given the observed values for the temperature contrast in the CMB, we get that the density contrast at decoupling should be of order $\mathcal{O} \sim 10^{-5}$. This allows us to deal with the contrasts as small perturbations in a homogeneous energy density background.

Perturbation theory, is thus a powerful tool to study the evolution of δ inside a FRW Universe that undergoes different thermal states (*i. e.* radiation, matter and, eventually, cosmological constant domination).

In this section of the thesis, we review the basics of the temporal evolution of the energy density perturbations and the currently used tools for their study.

For the moment, we neglect the distinction between cold dark matter and baryons, and assume that all non-relativistic matter only interacts gravitationally with the radiation fluid.

We will pay attention to the effects of baryons on the growth structure in the next section of this chapter, where we describe the theory underlying the baryon acoustic oscillations. For the time being we assume the simplest model of a Universe filled by photons and cold non relativistic matter.

As we will see, there are no quadratic evolution equations at least while the evolution is linear. Therefore, the Fourier modes of each perturbation evolve de-

coupled from each other. It is useful thus to define the Fourier components of the perturbation, $\delta_{\mathbf{k}}$:

$$\delta(\mathbf{x}) = \frac{1}{(2\pi)^3}\int d^3\mathbf{k}\delta_{\mathbf{k}}e^{-i\mathbf{kx}} \Rightarrow \delta_{\mathbf{k}} = \int d^3\mathbf{x}\delta(\mathbf{x})e^{i\mathbf{kx}} \tag{4.36}$$

We have dropped the explicit time dependence. It should also be noted that the $1/(2\pi)^3$ normalization for the Fourier transforms is not universal and varies from author to author.

In order to represent data, astrophysicists use the *matter density perturbation power spectrum*. It is defined as:

$$P(k) \equiv \langle|\delta_k|^2\rangle \tag{4.37}$$

where the brackets denote the ensemble average over the whole Universe (ideally, of course). Using relation (4.36) one can see that the power spectrum is proportional to the Fourier transform of the two point correlation function, *i. e.* the probability of finding two objects separated by a given distance.

The power spectrum of the fluctuations in the potential is defined by the quantity $|u_k|^2$ from Chapter 2. Eqns. (2.58) and (2.59) along with (2.52) imply $|u_k|^2 \propto k^{-3}$. This fact, together with Poisson equation (shown below), imply that the primordial power spectrum for the matter density fluctuations is:

$$P(k) \propto k^4\langle|u_k|^2\rangle \propto k \tag{4.38}$$

and we recover the Harrison-Zel'dovich scale invariant power spectrum.

As stated above we will study the linear evolution of perturbations. The effects of the cosmological parameters on the non-linear evolution of structures are not simple to disentangle. The equations are no longer easily solved and simulations are needed in order to predict the behaviour of perturbations when $\delta \gtrsim 1$. Thus, we generally smooth out density perturbations that occur on scales smaller than $\sim 10 - 20$kpc. To do this, the power spectrum is convolved with a *window function* that varies for different analyses and should be taken into account when comparing data to theoretical predictions. The effect of the window function and subtraction of non-linearities from the power spectrum deserves a great deal of literature, and it is not the goal of this thesis to discuss this matter. Thus, we merely point it out and refer the reader to [54], for example, and references therein.

We will focus on the linear equations and derivate the overall behaviour of the power spectrum trying to remark the effects of the cosmological parameters involved on the evolution of the perturbations.

4.2.1 Theory and experiments

When we work in Fourier space, each mode is characterized by a length scale, $\lambda = 2\pi/k$. When this scale is larger than the causal horizon or the sound horizon,

pressure cannot compensate for the effects of gravitational collapse. Evolution then occurs in a different manner from what happens when the perturbations are smaller than the horizon and usual Newtonian fluid dynamics (inside an expanding Universe) can be applied.

Let us start with the former kind. Even though we have used them through out the thesis, we rewrite now all the non-relativistic fluid dynamics equations that we need; Euler, continuitity and Poisson equations:

$$\frac{D\vec{v}}{Dt} = -\frac{1}{\rho}\nabla p - \nabla\Phi \tag{4.39}$$

$$\frac{D\rho}{Dt} = -\rho\nabla\cdot\vec{v} \tag{4.40}$$

$$\nabla^2\Phi = 4\pi G\rho \tag{4.41}$$

where, Φ is the Newtonian gravitational potential and $\vec{v}$ is the velocity of the fluid. $\frac{D}{Dt}$ is the convective derivative [87]:

$$\frac{D}{Dt} = \frac{\partial}{\partial t} + \vec{v}\cdot\nabla \tag{4.42}$$

As stated above, we approach the problem of clustering by studying the behaviour of small perturbations in the energy density, $\delta\rho$, which in turn, induce perturbations on the rest of the relevant quantities: δp, $\delta\vec{v}$ and $\delta\Phi$. Replacing all the quantities by the sum of their background value plus a perturbation (e.g. $\rho \to \rho_0 + \delta\rho$). To first order, the equations for the perturbations are:

$$\frac{d\delta\vec{v}}{dt} = -\frac{1}{\rho_0}\nabla\delta p - \nabla\delta\Phi - H\delta\vec{v} \tag{4.43}$$

$$\frac{d\delta}{dt} = -\rho\nabla\cdot\delta\vec{v} \tag{4.44}$$

$$\nabla^2\delta\Phi = 4\pi G\delta \tag{4.45}$$

where we have used Eqn. (4.35) for the definition of δ and $\frac{d}{dt} = \frac{\partial}{\partial t} + \vec{v_0}\cdot\nabla$. When we change to comoving coordinates (see Eqn.(1.3)) and take into account that pressure and energy density are related through the speed of sound speed (see Eqn. (1.49)) we arrive at a compact equation for the evolution of the density perturbation:

$$\ddot{\delta} + 2H\dot{\delta} = 4\pi G\rho_0\delta - c_s^2\nabla^2\delta \tag{4.46}$$

Switching to Fourier space we finally arrive at:

$$\ddot{\delta}_k + 2H\dot{\delta}_k = \delta_k[4\pi G\rho_0 - c_s^2\frac{k^2}{a^2}] \tag{4.47}$$

If we ignore the effects of the expansion of the Universe (*i.e.* $a = 1$, $\dot{a} = 0$), then (4.47) is easily solved and has the solution:

$$\delta \propto \exp[\pm t\sqrt{4\pi G\rho_0 - c_s^2k^2}] \tag{4.48}$$

From (4.48) we see that there exists a critical scale, λ_J, defined by:

$$\lambda_J = c_s \sqrt{\frac{\pi}{G\rho_0}} \tag{4.49}$$

which separates two evolutionary regimes. If the scale of the perturbation is such that $k < 2\pi/\lambda_J$ its dimension is so large that the gravitational infall time is shorter than the time it takes a soundwave to cover the whole perturbation. Therefore, there is no pressure response and the gravitational growth is unavoidable and exponential. On the other hand, for smaller scales, $k > 2\pi/\lambda_J$, the balance between attractive gravitational forces and the repulsion from pressure makes the amplitude of the perturbation oscillate harmonically without collapsing. The distance λ_J is known as the Jeans length, after Sir James Jeans who first came up with this result during the first half of the 20th century.

Qualitatively, the effects of a dynamical background are to change the energy density and thus, the value of the Jeans lenght with time in such a way that the amplitude of the perturbations may grow or remain constant during different thermodynamical epochs.

Evolution of super-horizon modes

The basic assumption for this modes is that we can ignore the effects of spatial gradients on the perturbations. Therefore we can drop the gradient term in Eqn. (4.47), and the equation for the evolution of the perturbations becomes:

$$\ddot{\delta} + 2H\dot{\delta} = 4f\pi G\rho_0\delta; \text{ with } f = \begin{cases} 1 & \text{during matter domination} \\ \frac{8}{3} & \text{during radiation domination} \end{cases} \tag{4.50}$$

where the relativistic corrections included during the radiation dominated era, are easily derived in [87].

These equations are easily solved under the assumption of a flat Universe. Taking into account the evolution of the densities with redshift (see relations (1.8)) and the Friedmann equation (in (1.14) ignoring the cosmological constant). The growing mode solutions are:

$$\begin{aligned} \delta \propto t^{2/3} \propto \eta^2 \propto a \quad & \text{during matter domination} \\ \delta \propto t \propto \eta^2 \propto a^2 \quad & \text{during radiation domination} \end{aligned} \tag{4.51}$$

Evolution of sub-horizon modes

During the era of matter domination, the evoultion computed above, applies too: the gradient term may be dropped as well, not because the dimension of the perturbation

is much bigger than the Hubble radious, but because the pressure for non-relativistic matter is practically null.

For the evolution of non-relativisitic matter perturbations during radiation domination, we need to approach the solution in a different way. Even though the evolution equation is (4.47) where the gradient term may be dropped, the bottom solution in (4.2.1) does not apply because $\delta \to \delta_m$ and the background is made of radiation and matter, thus $\rho \to (\rho_m + \rho_r)$.

We can find an analytical solution with the change of variable:

$$y \equiv \frac{\rho_{\rm m}}{\rho_{\rm rad}} = \frac{a}{a_{\rm eq}} \Rightarrow \frac{dy}{dt} = H \cdot y \tag{4.52}$$

Then, Eqn.(4.47) becomes:

$$\delta'' + \frac{2+3y}{2y(1+y)}\delta' - \frac{3}{2y(1+y)}\delta = 0 \tag{4.53}$$

where the prime denotes a derivative with respect to y. The solution to this equation is:

$$\delta(y) = (y + \frac{2}{3})\delta_i' + \frac{3}{2}[3\sqrt{1+y} - 2\tanh^{-1}\sqrt{1+y} - 3y\tanh^{-1}\sqrt{1+y}]\delta_i''$$

which has a physical meaning and a very simple interpretation of its growing mode if $\delta_i'' = 0$:

$$\delta(y) \propto y + \frac{2}{3} \tag{4.54}$$

From this solution we see that, the amplitude of a perturbation that enters the horizon at early times, when $\rho_{\rm rad} \gg \rho_{\rm m}$, is frozen because radiation drives such a fast expansion that there is no time for gravitational collapse. Later on, when matter starts being relevant the amplitude $\delta \propto a$ and smoothly matches with the behaviour derived on the previous section [87].

4.2.2 Implications for cosmology.

Putting together all the solutions derived in the previous sections, we can track the evolution of the amplitude of the perturbation during the history of the Universe.

As predicted by the inflationary paradigm, fluctuations are stretched out beyond the horizon, thus, they start off as super-horizon inside a radiation background. Since the comoving horizon during radiation domination grows as $\propto \sqrt{t}$ and the amplitude of the perturbation goes as $\delta \propto a^2 \propto t$, perturbations with wavelength $\lambda < d_{\rm H}(a_{\rm eq})$, enter the horizon before the matter starts to dominate the background energy density. From (4.54) we see that these perturbations are frozen as soon as they cross the horizon. The supression with respect to the modes that were too big

to cross the horizon before the equality epoch is $f = (a_{\rm entry}/a_{\rm eq})^2 \propto 1/k^2$. We show this evolution schematically on the left pannel of Fig. 4.5.

On the right panel, we show the qualitative behaviour of the power spectrum. We know from inflation that (4.38) must hold for large scales, and that is what we observe to the left of the "knee" of the power spectrum. On the other hand, $P(k)$ is related to the amplitude of the perturbations through (4.37), therefore, the factor f previously defined, implies that the supression in power must be $\propto k^{-4}$ and thus, $P(k) \propto k^{-3}$ on the right side of the "knee".

As one may imagine by now, the wavenumber at which the behaviour of the power spectrum changes, is related to the acoustic horizon at matter-radiation equation, $d_s(a_{\rm eq})$ by [85]:

$$k_{\rm knee} = 1/d_H(a_{\rm eq}) = (2\Omega_{\rm M} H_0^2 a_{\rm eq})^{\frac{1}{2}} \tag{4.55}$$

where the second equality comes from the definition of Hubble distance in chapter 1. Inserting $z_{\rm eq} \simeq 2.5 \cdot 10^4 \Omega_{\rm M} h^2$ and using conventional values for the cosmological values, one gets $k_{\rm knee} \sim 0.007 h{\rm Mpc}^{-1}$, as we observe on the righ pannel of Fig.4.5 in a power spectrum that has been calculated using the camb code [80].

With this, we show how the shape, and more specifically the position of the bend in the power spectrum, constrains at least two very important cosmological parameters: $\Omega_{\rm M}$ and h and that is assuming flatness and practically massless neutrinos. These are indeed conservative assumptions, nevertheless it is necessary and worth stating them explicitely.

The specific impact on isocurvature data, stems on the fact that LSS probe scales larger than the maximum probed by CMB experiments. As we saw above, a isocurvature contribution may not show in the CMB observations if the tilt is high enough. But this means that the isocurvature spectrum will have a high power on smaller scales. This could imply a strong difficulty on the model to fit the LSS data. We will see how CMB plus LSS experiments constrained several possible isocurvature models on forthcoming chapters.

4.3 Baryon Acoustic Oscillations

In the previous section we intentionally neglected the effect of baryons in the power spectrum of the matter density fluctuations for two main reasons: 1) baryons suppress power in small and intermediate scales through the Silk damping effect [84, 85]. This is an interesting physical effect but for models with $\omega_{\rm cdm} >> \omega_{\rm B}$ it is of limited importance because baryons can fall into the potential wells generated by the DM that has not been Silk damped since much before recombination [87]. 2) The acoustic wiggles or Baryonic Acoustic Oscillations (BAO) have only been detected

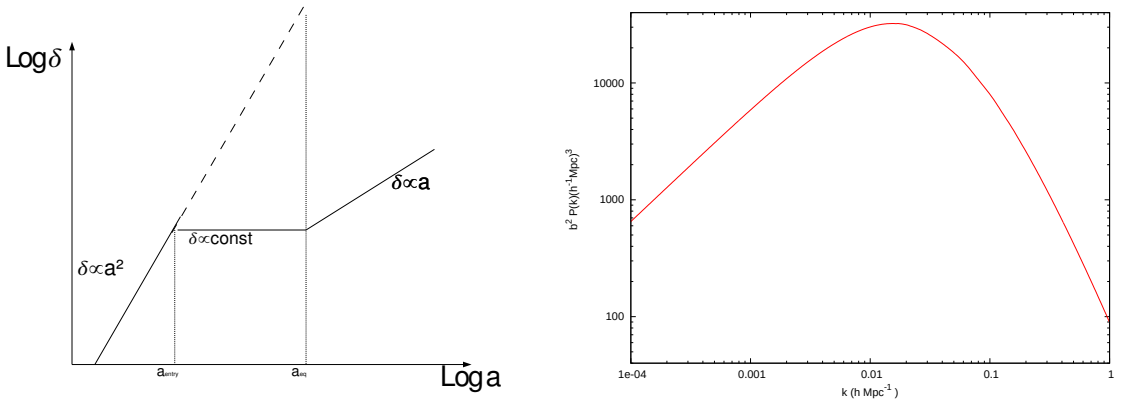

Figure 4.5: (Left) Schematic illustration of a wavelength scale that enters de horizon at $a_{\rm entry}$, during the radiation domination era, freezes out to start growing later, when the matter energy density dominates the Universe. (Right) Matter power spectrum for a ΛCDM Universe. We can see how perturbations with wavelength smaller than $d_H(a_{\rm eq})$ ($k > k_{\rm eq}$) are supressed with respect to the rest of the spectrum. Due to non linearities, the supressed part of the spectrum is not exactly proportional to k^{-3} but this example server us to illustrate the lack of growth on small scales. In figure 4.6 we show the best fit theoretical spectrum to the experimental points, however, we save this plot for the following section because baryons are indeed visible and necessary to explain the whole observed spectrum.

very recently. Phenomenology previous to 2005 was subject to a precision too low to observe them. Thus a treatment that did not take into account the baryonic effects used to be enough for analysing galaxy surveys data.

Fortunately the picture regarding point 2) has changed since BAO were detected in the Luminous Red Galaxies (LRG) two point correlation function in 2005 [88]. Also, forecasts about the future precision for their detection [89] predict high quality and a sharp detection of the peak in the correlation function that may translate into a definition of up to the third peak in the power spectrum. As well as the peak in the correlation function, shown in Fig. 4.7, we also show the whole power spectrum, as a sample of "real data" we work with on figure 4.6 These are the points, taken from reference [86].

The reason why this piece of information had been hiding for so long after they were predicted is because in order to observe any features in the correlation function one needs to probe distances comparable to the correlation distance. As we will see, this distance is of the order of $\sim 100h^{-1}Mpc$ which represented a challenge for observers both in the volume that needed to be probed as well as the kind of objects that were to trace the density. One needs to distinguish clearly evolution from the distance effects.

In this section we review the effects of baryons in the transfer function and study the phenomenology associated to the correlation function or the power spectrum,

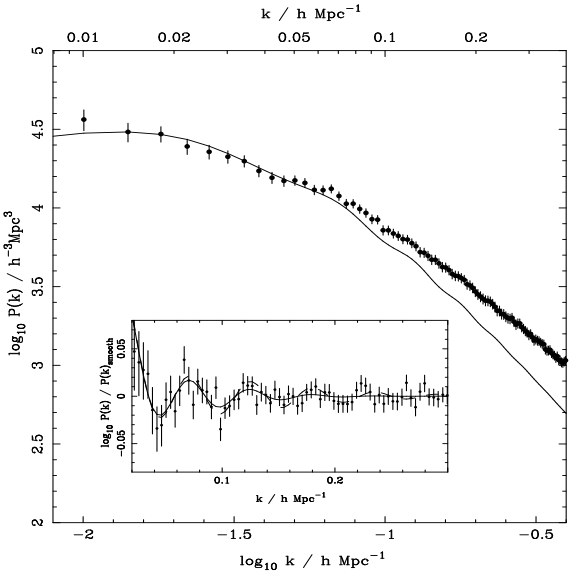

Figure 4.6: This figure, extracted directly from [86] represents the datapoints for the power spectrum observed in by the SDSS telescope collaboration, released in 2006. As we mentioned above, the baryonic wiggles can be clearly seen. In order to explain the current observations, one needs to include indeed, the effects of baryons.

its Fourier transform.

4.3.1 Theory and experiments

On the first section of this chapter we saw that primordial cosmological perturbations excite sound waves in the coupled photon-baryon plasma of the early Universe with a principal harmonic which is the size of the acoustic horizon at the time of recombination (Eq. (4.33)).

This length scale is imprinted on the photons last scattered by the baryons, right before recombination and we can infer its value by studying the temperature distribution of the photons of the CMB, as explained above. However, since the waves were propagated in the baryon-photon plasma and the baryons stop oscillating after recombination, the acoustic waves should also be observable in the baryonic distribution in the Universe. Indeed the BAO have been detected for the first time in the power spectrum of the Luminous Red Galaxies distribution from SDSS DR4 [90]. Thanks to technological advances they will soon be as accessible to us as the anisotropies in the CMB.

Because we know the nature of the BAO, we can predict their characteristic length theoretically. Posterior comparison to observation, provides us with an addi-

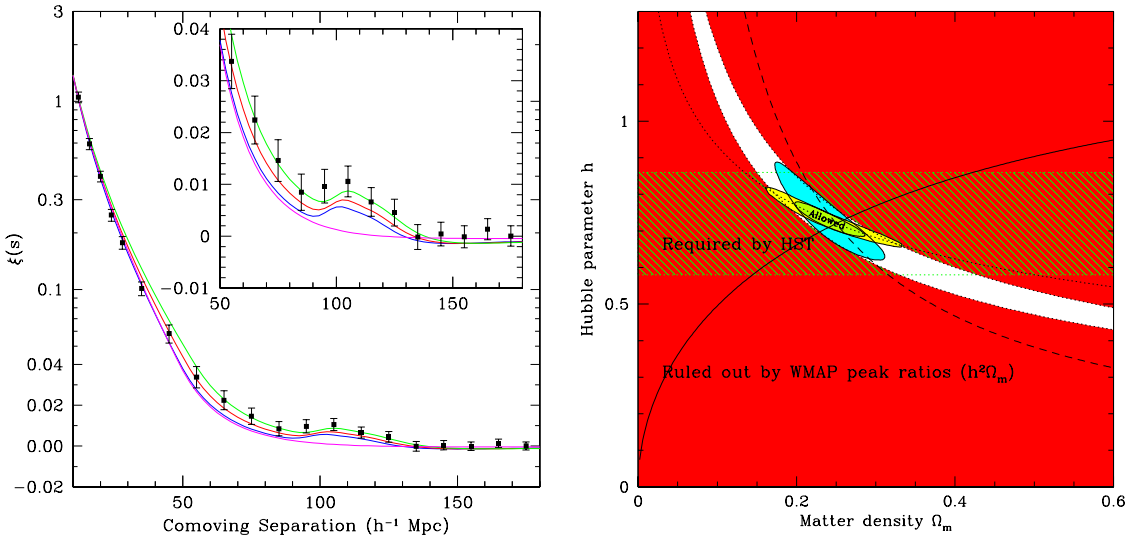

Figure 4.7: (*Left*) This figure has been directly extracted from [88] and shows the experimental points in the correlation function of the SDSS-LRG sample. It is plotted along three theoretical predictions corresponding to $\Omega_{\rm M}h^2 = 0.12$ (top, green), 0.13 (red), and 0.14 (bottom with peak, blue), all with $\omega_{\rm B} = 0.024$ and $n = 0.98$. The magenta line shows a pure CDM model ($\Omega_{\rm M}h^2 = 0.105$), which lacks the acoustic peak (see [88] for a detailed explanation). (*Right*) This figure has been directly extracted from [91] and illustrates how the BAO measurement helps breaking the degeneracy in the $\Omega_{\rm M} - h$ plane present in any CMB-only analysis (See [91] and text for details).

tional measurement of the sound horizon 'standard ruler' [4] at a redshifts other than $z \sim 1100$.

Inserting $c_s \simeq 0.9c/\sqrt{3}$, for a Universe with a baryon density $\Omega_{\rm B}h^2 = 0.02$, $a_{\rm rec} = \frac{1}{1100}$, $a_{\rm eq} = (23900\Omega_{\rm M}h^2)^{-1}$ and $\Omega_{\rm M} = 0.27$ into Eq.(4.33), we find this scale is of the order of $r_{\rm s}(a_{\rm rec}) \sim 100h^{-1}$Mpc. It was expected to find a peak in the correlation function of luminous matter at this scale, a prediction which was confirmed in [88], as shown in Fig. 4.7.

Sometimes and depending on the methodology, it is more convenient to work with the power spectrum instead of the correlation function. These two approaches are exactly equivalent with the smearing in the correlation function due to non-linearities or other uncertainties being equivalent to a failure to detect higher and higher order

[4] Let us remind Eq. (1.18) in which we can see how the ratio of the physical size of a given scale to its angular size observed at a different epoch is a measurement of cosmological contents and expansion history.

peaks (typical experiments predict a detection of 3 to 5 peaks, depending on the redshift and volume of the survey). One advantage of the use of the power spectrum is the fact that errors are, at least theoretically, uncorrelated for different k values.

This is the approach chosen by [91] in which SDSS-LRG data analysed along with the third year of WMAP release [5] finds tighter constrains on $\Omega_{\rm M}$, lowering its error bars by $\sim 30\%$ of the former value of WMAP alone; as well as on Ω_K and, a very striking decrease on the upper bound for the mass of the neutrinos that goes from $\sum m_\nu \leq 1.8$ eV at (95%) c. l. to $\sum m_\nu \leq 1.8$ at the same c. l. for WMAP plus SDSS-LRG dataset. It is not our goal to give an exhaustive description of the BAO theory or phenomenology (see [85] for a very illuminating discussion and useful analytical formulae) but to explain its main power in terms of degeneracy breaking. We will stress the effect on the possible discrimination between purely adiabatic and isocurvature models.

4.3.2 Implications for cosmology.

Interpreting the observed angular separation of acoustic peaks in the temperature power spectrum or the galaxy power spectrum requires knowledge of the sound horizon at last scattering (eq. (4.33)) and of the angular diameter distance to the last scattering surface or the mean redshift of the galaxy survey. The expression for the angular diameter distance is:

$$D_A(z) = \frac{1}{(1+z)} \int_0^z \frac{dz'}{H(z')} \tag{4.56}$$

and, even though the general solution strongly depends on the cosmological parameters, it can be fitted to relatively simple polynomials under some different assumptions and different epochs. They are usually a function of a combination of parameters, rather than of a single one of them, and this leads to important degeneracies. In the context of flat ΛCDM cosmologies, models with the same $\Omega_{\rm M}^{0.29}h$ have the same angular separation between the peaks [92]. This degeneracy induces the familiar 'banana shape' 2-dimensional likelihood contours in the plane spanned by these parameters [91]. It can be partially lifted by measuring the value of the physical matter density, ω_m through the peaks height. However, observation of the baryonic wiggles at a redshifts more recent than 1000 softens the degeneracy more effectively because its direction of degeneracy in the $\Omega_{\rm M} - h$ plane is $h \propto \Omega_{\rm M}^{0.36}$ which is relatively orthogonal to the contours determined by CMB only [91].

We will focus now on how a precise measurement of the position of the peaks in the BAO might help constraining the isocurvature fraction. In particular, we use the curvaton model to illustrate the effects. This time, we measure the isocurvature contribution with the parameter $f_{\rm iso}$ defined as $f_{\rm iso} \equiv \frac{B^2}{A^2} = \frac{\alpha}{1-\alpha}$ following the notation used in chapter 3. In section 4.1 we have seen how the effects of a small isocurvature component could be hidden in a shift in the hubble parameter. To

show this, we plot in figure 4.8 the one-dimensional probability function distribution that we extract from the third year WMAP data [5] and the SDSS DR4 galaxy redshift survey [90]. Comparing the distributions for the two models, we see that

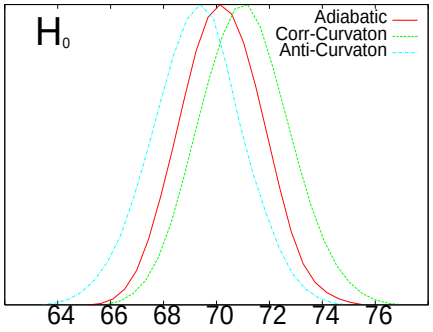

Figure 4.8: One dimensional distributions for the Hubble parameter in three different models: in red (solid) the adiabatic model, in light blue (dot-dashed) the curvaton assuming total anticorrelation, and in green (dashed) the curvaton assuming total correlation.

the inclusion of $f_{\rm iso}$ induces a shift in the position of the peaks that is compensated by a change in H_0 which, in turn, induces a shift on the spectral tilt n_s. All of these adaptation of parameters is small enough to still fit the data used without changing the χ^2/DOF sensibly[5]. It is this feature of the isocurvature models that we would like to test under the inclusion of new pieces of data from BAO.

In order to show how more accurate BAO measurements would add constraints to the isocurvature sector, we compute the C_ℓ's and matter power spectrum for the models described on table 4.1.

Parameter	Ad-ΛCDM	Isocurvature
$\omega_{\rm B}$	0.022	0.023
$\omega_{\rm cdm}$	0.12	0.11
τ	0.089	0.089
H_0	70.6	68.0
A_s	3.06	3.06
n_s	0.967	0.935
$f_{\rm iso}$	–	−0.1

Table 4.1: Value of the parameters for the models shown on Fig.s 4.9. We used a value of $f_{\rm iso}$ outside the 95% c. l. bound to make our point clearer.

[5]The χ^2/DOF for the three models is practically the same. Despite the fact that this is not a good statistic to compare these three models [93], it serves us as an indicator of the problem we want to illustrate.

In Fig. 4.9 we plotted several different power spectra of the two models. On the top panel, along with the WMAP-III data we see how the C_ℓ's are practically indistinguishable. Also, because the spectral tilts are properly fitted, the TE and EE polarization spectra are also the same.

However, we see on the bottom panel how the two models can be discriminated by the position of the peaks in the matter transfer function at redshift 0. We used the prescription given in [91] to plot the baryonic wiggles. The real matter transfer function is normalized to the "non-wiggle" one computed from the analytical formulae given in [85].

The difference in the position of the peaks is was expected because, as pointed out in [91], the degeneracy directions are orthogonal.

This degeneracy rupture would occur for two adiabatic models that fulfilled only one of the proportionality rules described at the beginning of this section, and the fact that isocurvature is introduced neither strengthens nor weakens the effect. Indeed, the amount of isocurvature does not affect the evolution of the perturbations. It is only relevant as a part of the primordial setting of inhomogeneities.

But the rupture does help selecting the value of H_0 and this would in turn select a more precise value of $f_{\rm iso}$. In Fig. 4.10 we show the 2-dimensional likelihood distribution of $f_{\rm iso} - H_0$ marginalized over the other parameters.

It is clear the correlation existing between the isocurvature fraction and the value of the Hubble factor today [6], and we will show how the decrease on the Hubble factor error bars shrinks the volume of the allowed parameter space. We quantify the performance of three different projected surveys in the following section.

4.4 Error bars forecast

We use the universal fitting formulae described in [89] to determine the accuracy with which different planned surveys will measure the acoustic wiggles. In particular, we study the following surveys: ADEPT [94] and WFMOS [95] where redshifts are measured spectroscopically[7]

[6] In order to make this plot, we have analysed together both the totally correlated and anti-correlated sampling. However the MC Markov chains were computed independently from each other, obeying theoretical priors on the possible curvaton models.

[7] We use the following values for the survey parameters. For ADEPT:$1 < z < 2$; Area: 28000 sq degrees; Number of galaxies: 10^8 galaxies; Volume=100.573 $(h/\mathrm{Gpc})^{-3}$; Growth Factor: $D(z = 1.5) = 0.50$. For WFMOS-1 we use: $0.5 < z < 1.3$; Area:2000 sq deg; Number of galaxies: $2.1 \cdot 10^6$ galaxies; Number density: $\bar{n} = 5 \cdot 10^{-4}$ $(h/Mpc)^3$; Volume=3.912 $(h/\mathrm{Gpc})^{-3}$; Growth Factor: $D(z = 0.9) = 0.64$- and for the second version: $2.3 < z < 3.3$; Area:300 sq deg; Number of galaxies: $5.5 \cdot 10^5$ galaxies; Number density: $\bar{n} = 4 \cdot 10^{-4}$ $(h/Mpc)^3$; Volume=1.226 $(h/\mathrm{Gpc})^{-3}$; Growth Factor: $D(z = 2.8) = 0.34$

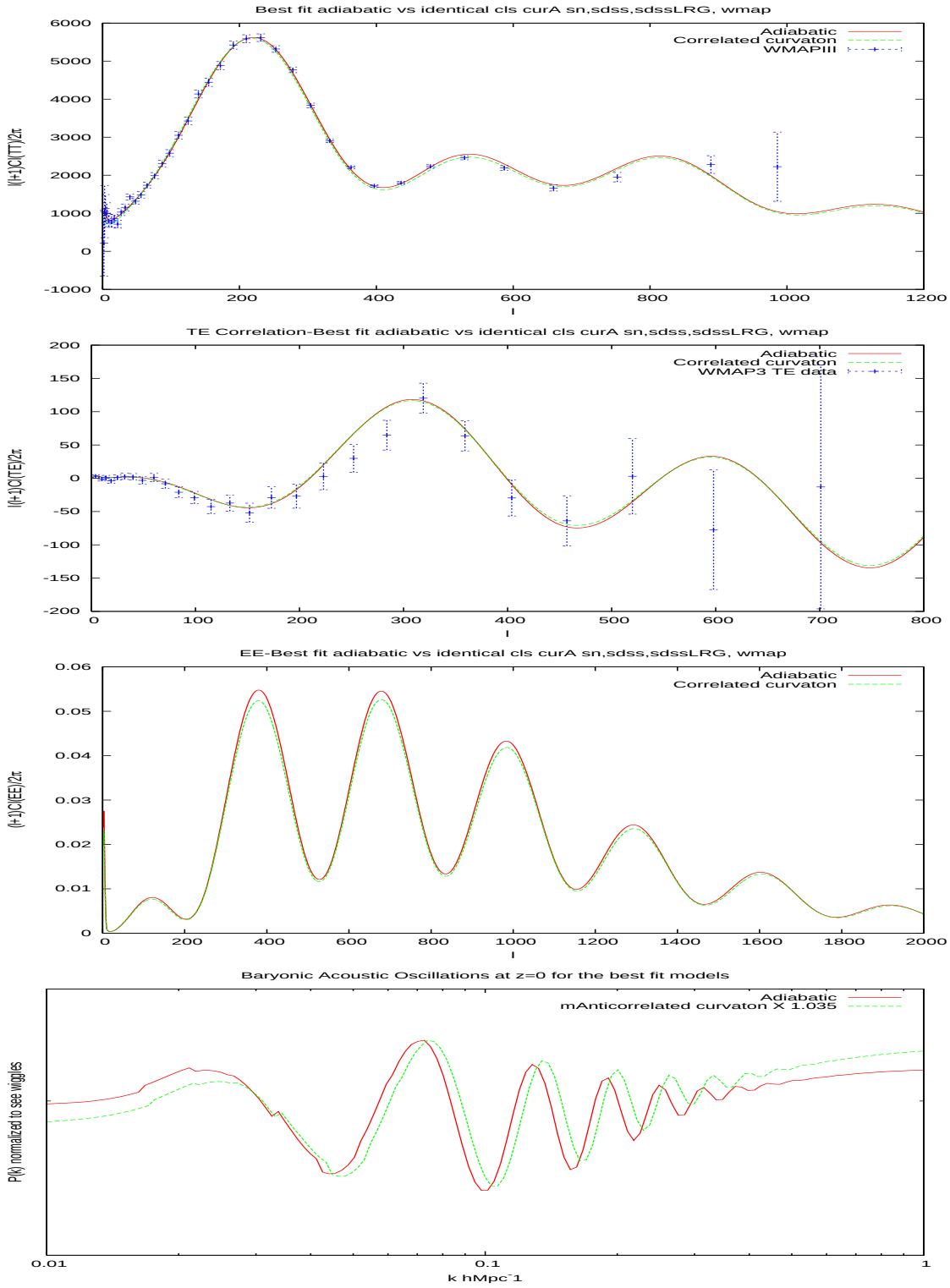

Figure 4.9: Different power spectra for the models described on Table 4.1. In the bottom panel, the amplitude of the isocurvature spectrum has been increased by 3.5% to show more clearly the shifts on the peaks.

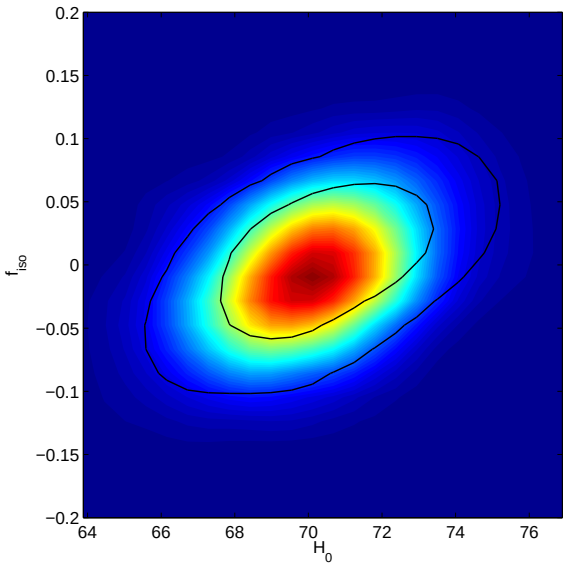

Figure 4.10: Degeneracy on the H-fiso plane for both the correlated and anti-correlated case.

Following [89], we compute the accuracy that will achieved for the measurements of the correlation distance on the radial and tangential directions at a redshift z:

$$x = x_0 \sqrt{\frac{V_0}{V}} \sqrt{\frac{\sigma_r}{\sigma_{r,0}}} \left(1 + \frac{n_{\rm eff}}{n} \frac{D(z_0)^2}{b_0^2 D(z)^2}\right) f_{nl}(z) \tag{4.57}$$

where:

$$\begin{aligned} f_{nl}(z) &= \left(\frac{z_m}{z}\right)^{\gamma} \quad z < z_{\rm m} \\ &= 1 \quad z > z_{\rm m} \end{aligned}$$

accounts for the fact that nonlinearities start smearing the acoustic peak when z goes below a redshift z_m. In [89] they find the values of (x_0, n_0, b,γ, $z_{\rm m}$) by fitting the accuracies with which the acoustic scale was recovered from different realizations created from an underlying linear power spectrum. The values they found are reported on table 1. of [89].

The rest of the parameters are: V, the volume of the survey, n the number density of galaxies in units of $(h/{\rm Gpc})^{-3}$, b_0 is a sort of bias parameter all of them dependent on the survey and the underlying cosmology. $D(z)$ is the growth factor calculated following [97]. σ_r is the redshift error applicable only for photometric surveys. The maximum redshift used for their simulations was $z_{max} = 3.4$ so we are confident that the formulae are valid for the range of redshifts we are studying.

We follow the recipe for calculating the accuracies for the measurements of $H(z)$, the hubble factor at redshift z and $D_A(z)$ the angular diameter distance. We use a

flat ΛCDM fiducial model with $\Omega_\Lambda = 0.7$. We find the following prediction for the error bars:

SURVEY	TANGENTIAL (Error in D_A)	RADIAL (Error in H(z))
ADEPT-$\bar{z} = 1.2$	0.26	0.45
ADEPT-$\bar{z} = 1.5$	0.31	0.54
ADEPT-$\bar{z} = 1.75$	0.28	0.48
WFMOS 1 -$\bar{z} = 0.9$	1.75	3.03
WFMOS 2 -$\bar{z} = 2.8$	9.03	15.72

For the best fit value of the parameters, found for the three different models described above, we find the theoretical values for the angular diameter distance written in table 4.2. We also write the percentage difference of the theoretical value from the *fiducial* adiabatic model. We see that we would be able to distinguish the two models we would be able to rule out the isocurvature models with more than a 3 sigma confidence level with the ADEPT survey.

	Adiabatic	Curvaton-Corr	Curvaton-Anticorr
Redshift	$D_A(z)$	$D_A(z)$	$D_A(z)$
z= 1.2	1710.5	1686.4 ($\sim 2\%$)	1735.3 ($\sim 2\%$)
z=1.27	1744.1	1719.5 ($\sim 1\%$)	1769.3 ($\sim 2\%$)
z= 2.8	1919.8	1597.0 ($\sim 20\%$)	1643.2 ($\sim 16\%$)

Table 4.2: Angular diameter distances (in Mpc) and Hubble factors for the adiabatic ($H^{best} = 70\text{kms}^{-1}\text{Mpc}^{-1}$), curvaton correlated ($H^{best} = 71\text{kms}^{-1}\text{Mpc}^{-1}$) and curvaton anticorrelated ($H^{best} = 69\text{kms}^{-1}\text{Mpc}^{-1}$).

Those are good news indeed, however the ADEPT survey has not even been aproved yet and we cannot hope to get such a good precision in less than 10 years.

On the other hand, the other, less ambitious, WFMOS proyect, would be on the verge of distinguishing between the iso and adiabatic models. Again, this is still an unborn proyect, but it is indeed more economic and somehow more plausible in the near future.

So far, we will not be making use of this piece of data. This section is indeed work in progress, carried out in collaboration with L. Verde and will be published when finished. Nevertheless, it is important to show how this piece of data can imply more tightly constrained errors and should also open (or close) new windows for cosmology.

4.5 Supernovae Type Ia

Supernovae explosions are relatively frequent events in the Universe (the Hubble telescope detects and follows about 10-15 SNae per year at $z \sim 1$ [98]). In particular, in a type IA kind, a white dwarf star, coming from a light weigh binary star progenitor, accretes matter from its companion until it reaches the critical mass superseeding the Chandrasekar limit and a thermonuclear explosion is triggered. This is such a violent event that all previous information about the original star, except maybe for the mass which is very similar in all the cases, is erased and the pattern shown is basically identical in all the cases. The light curves of this kind of supernovae are easily recognizable because they do not show any hydrogen lines in their spectra, but have a broad Si-II absorption line at about 400 nm. Their intrinsic luminosity can be worked out and thus, they are excellent "standard candles" in our Universe and definitely useful to study the expansion history and the energy budget of the Universe.

4.5.1 Theoretical grounds

The observed flux or the number of photons that reach the detector from an event with intrinsic luminosity $\mathcal{L}$ and located at a distance $d_{\rm L}$ is:

$$\mathcal{F} = \frac{\mathcal{L}}{4\pi d_{\rm L}^2} \tag{4.58}$$

where $d_{\rm L}$ is just the luminosity distance defined in eq. (1.19).

As mentioned above, the intrinsic luminosity is well known for a supernovae therefore, once observed is easy to derive their luminosity distance. More precisely, one derives the extinction-corrected distance modulus:

$$\mu_0 = 5 \log d_{\rm L} + 25$$

with $[d_{\rm L}]$ =Mpc [6]. The plot of the supernovae events in the $\mu_0 - z$ plane describes a curve that depends greatly on the expansion history of the Universe. As we know it can be characterized by many different models, and this kind of assumptions do affect the inferred values of the parameters.

A relatively empirical information extraction can be made through the the deceleration parameter, $q(z)$:

$$q(z) = -\frac{\ddot{a}}{a}\frac{1}{H(z)} \tag{4.59}$$

In [6] they perform a two parameter expansion of $q(z)$ in terms of its current value and its derivative measured today:

$$q(z) = q_0 + z dq/dz|_{z=0} \tag{4.60}$$

and they get the 1, 2 and 3 sigma contours shown in the left panel of Fig. 4.11.

For parameter estimation, we compute the value of $d_{\rm L}$ numerically at the redshift of the corresponding supernovae and compare this theoretical value to the observed one to compute the χ^2 of the particular model.

4.5.2 Experiments and implications for cosmology.

There are two main experiments intensively exploited for parameter estimation. These are the Super Nova Search Team Collaboration, carried out by the Hubble telescope [6, 98] and the Supernova Legacy Survey (SNLS) [99], taking place at the CFH Telescope, in Hawaii. All together they add up to about 300 supernovae (which will add up to about 800 by the end of the SNLS project) measured with different precisions (gold and silver sets in the Hubble Telescope Collaboration articles) that constrain the matter and dark energy densities with error bars of the order of $\sim 10\%$ although the amplitudes of the error bars depend crucially on prior assumptions about the rest of the parameters. In particular, the SNLS team finds [100]:

$$\begin{aligned} \Omega_{\rm M} &= 0.271 \pm 0.022 \\ w &= -1.02 \pm 0.11 \end{aligned}$$

at the 68% confidence limit for a joint analysis of their supernovae data plus the BAO from [88] (assuming a flat Universe and a constant equation of state for Dark Energy).

Future surveys, promise to measure about a hundred times more supernovae. The Supernova Acceleration Probe project (SNAP), an planned satellite experiment, aims at observing about 2000 supernovae over the full redshift range to z=1.7 in about three years [101].

The main goal of these projected experiments is to reduce the statistical errors by adding more and more supernovae both in the low and high redshift regime. Allegedly, this would allow for an accuracy in the determination of the values of the constrained parameters of about 1% (again, this value is model dependent).

In Fig.4.11 we show the forecasted errors for the SNAP project as presented on the group homepage. We see how a reduction in the determination of $\Omega_{\rm M}$ and Ω_Λ would shrink the allowed volume inside the space of parameters.

In the first approximation the main power of a supernovae experiment is to break the degeneracy along the line $\Omega_{\rm M}+\Omega_\Lambda = 1$ in the $\Omega_{\rm M}-\Omega_\Lambda$ plane. Only the precision of existing supernovae experiments [6] is enough to lift it and select a value for H_0 making it unnecessary to apply the "Hubble prior" where H_0 had to be set by hand.

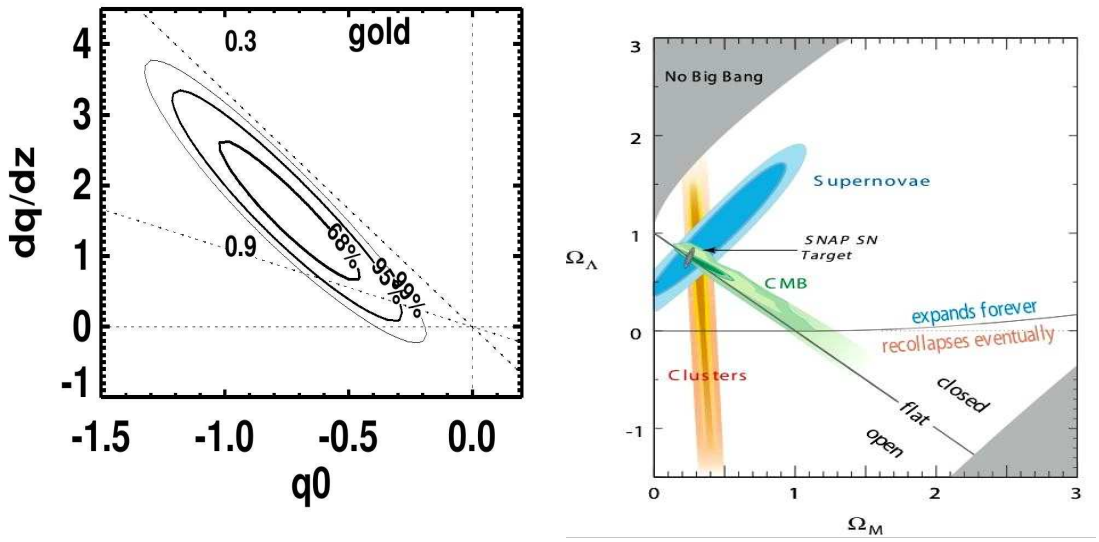

Figure 4.11: Predicted contour likelihood for the SNAP experiment (grey) compared to the rest of the constrains in the $\Omega_{\rm M} - \Omega_\Lambda$ parameter space [101].

More precise experiments will make it possible to study the *temporal evolution* of the Hubble factor thus providing us with a test for the variation of dark energy, the holy grail of cosmology.

In particular, the effect on isocurvature constraints boils down to precisely selecting H_0 and break the degeneracy in the plane $f_{\rm iso} - H_0$, as we will see on following chapters.

Systematic uncertainties

It is important to note that, with the precision of planned supernovae surveys, it is very likely that they become limited by systematics. These errors are inherent to supernovae measurements, thus, more supernovae will not ease the problem. One must also account for the systematic biases which will not increase the errorbars of the inferred values for the parameters, but will shift their values leading us to biased conclusions. Probably, this second kind are the most dangerous and one should be very careful about them.

Examples of sources to the systematics are the host galaxy dust extinction, the flux calibration, gravitational lensing and supernovae evolution [100, 102].

Dust extinction may lead to important dimming in the light of a supernovae. Naturally, the absorption is not uniform in the wavelength and therefore, this effect may be eased by measuring the light at two or more different bands.

The flux calibration is a delicate process by which all the filters must be normalized. This is achieved by the use of laboratory ligth sources or known stars. Of

course, the above the final effect of these sources depends greatly on the specific design of the survey. Studies such as the one performed in [102] show that they could be as important as $\sim 10\%$.

Gravitational lensing effects should be null for a large enough sample of supernovae. However, for regular sizes of redshift bins of about 50 supernovae per bin, this effect could shift the results up to 2%.

In [102] the authors study the effects on the final measurements of different kind of systematics to show that for surveys with specifically designated equipment, where the irreducible error in the magnitudes can below as $\delta_m \simeq 0.02$ mag, the relevant quantities can be bounded with cosmologically significant precision with errors ranging from 1% to 10%.

4.6 Lyman-α forest absorption spectrum

Quasars or the *quasi-stellar objects* are the most powerful astronomical sources of radiation known and are the object of many studies regarding their origin and evolution. These extremely bright objects are believed to correspond to regions of intense activity in the center of active galaxies [87].

In its path to our detectors, the light emitted by the quasar ionizes the clouds of warm ($\sim 10^4$ K) neutral hydrogen, generating characteristic absorption lines on its spectra. Since the main absorber is neutral H, the preferred absorption wavelenght is that of the energy levels of the hydrogen atom, the Lyman series. In particular, the Lyman-α line, corresponding to the excitation of the fundamental level to $n = 1$ shows at a wavelength $\lambda_\alpha = 121.6$ nm. Thus, we should see a lack of light in this wavelenght in the spectrum of a quasar.

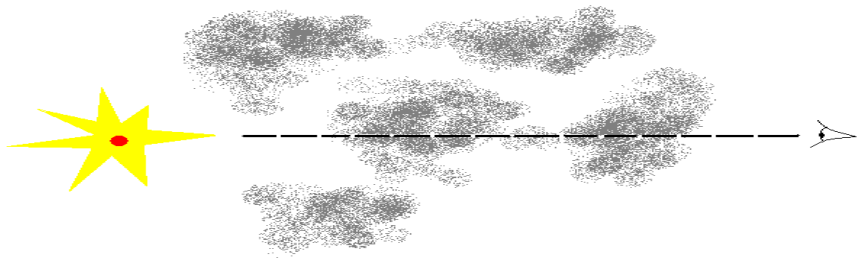

Figure 4.12: Illustration to show how the spectrum of the quasar determines the position and densities of the absorbers encountered in the way.

However, when the light reaches the absorption systems its wavelenght may have been redshifted (according to (1.9)), and more so, the further away the absorber is

from the quasar. We see the lines at wavelengths redshifted from the position of the absorbers, where they were just λ_α.

In this way, the absorption spectra of a quasar is a useful tool cosmologists use to probe the inter galactic medium (IGM), invisible otherwise. We show one of these spectra on Fig. 4.13 downloaded from the SDSS data product web page. We see the strong Lyman-α emission at $\lambda \simeq 580$ nm which means that the quasar is at $z_{\text{emmiter}} \simeq \frac{\lambda}{\lambda_\alpha} - 1 \simeq 3.8$ and the wavelengths and depth of the rest of the absorption lines at $\lambda < 580$ nm determine the position and densities of the hydrogen clouds encountered by light.

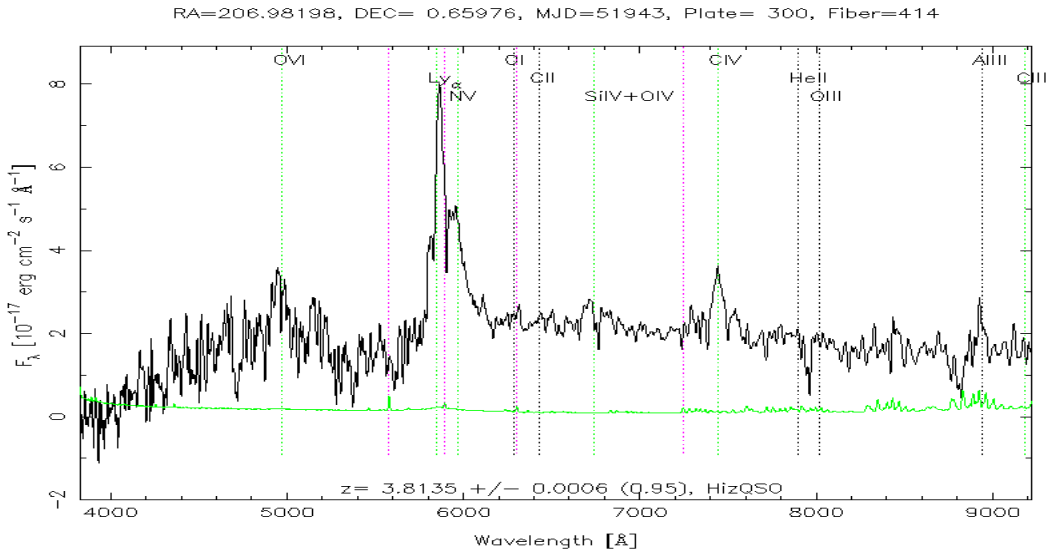

Figure 4.13: Absorption spectrum of a quasar observed by the SDSS telescope, published on the third release. The quasar is at z=3.81. Also plotted, the continuum spectra and the relevant absorption lines [90].

Under some appropriate assumptions, it is possible to extract the power spectrum of the matter probed by the quasar via analytical calculation and hydrodynamical simulations. The Lyman-α forest complements measurements of the dark matter power spectrum[8] via galaxy catalogues at small scales and it has been used extensively as a probe of the matter power spectrum on comoving scales of $(1-40)\,h^{-1}$Mpc [103, 104, 105, 106].

In what follows, we describe how this is done, and in particular, how it is applicable to the study of isocurvature perturbations in the spectra.

[8]The opacity fluctuations in the spectra arise from fluctuations in the matter density and trace the gravitational clustering of the matter distribution in the quasi-linear regime [103].

The Lyman-α optical depth in velocity space u (km/s) is related to the neutral hydrogen distribution in real space as (see e.g. Ref. [107]):

$$\tau(u) = \frac{\sigma_{0,\alpha}\, c}{H(z)} \int_{-\infty}^{\infty} dy\, n_{\rm HI}(y)\ \mathcal{V}\left[u - y - v_{\parallel}(y),\, b(y)\right] dy\ , \tag{4.61}$$

where $\sigma_{0,\alpha} = 4.45 \times 10^{-18}$ cm^2 is the hydrogen Lyα cross-section, y is the real-space coordinate (in km s^{-1}), $\mathcal{V}$ is the standard Voigt profile normalized in real-space, $b = (2k_BT/mc^2)^{1/2}$ is the velocity dispersion in units of c, $n_{\rm HI}$ is the local density of neutral hydrogen and $v_{\parallel}$ is the peculiar velocity along the line-of-sight. The density of neutral hydrogen can be obtained by solving the photoionization equilibrium equation (see e.g. [108]). The neutral hydrogen in the IGM responsible for the Lyman-α forest absorptions is highly ionized due to the metagalactic ultraviolet (UV) background radiation produced by stars and QSOs at high redshift. This optically thin gas in photoionization equilibrium produces a Lyman-α optical depth of order unity.

The balance between the photoionization heating by the UV background and adiabatic cooling by the expansion of the Universe drives most of the gas with $\delta_b < 10$, which dominates the Lyman-α opacity, onto a power-law density relation $T = T_0\,(1+\delta_b)^{\gamma-1}$, where the parameters T_0 and γ depend on the reionization history and spectral shape of the UV background and δ_b is the local gas overdensity ($1 + \delta_b = \rho_b/\bar{\rho}_b$).

The relevant physical processes can be readily modelled in hydrodynamical simulations. The physics of a photoionized IGM that traces the dark matter distribution is, however, sufficiently simple that considerable insight can be gained from analytical modeling of the IGM opacity based on the so called Fluctuating Gunn Peterson Approximation neglecting the effect of peculiar velocities and the thermal broadening [109]. The Fluctuating Gunn Peterson Approximation makes use of the power-law temperature density relation and describes the relation between Lyman-α opacity and gas density (see [110, 104]) along a given line of sight as follows,

$$\begin{aligned} \tau(z) &\propto (1+\delta_b(z))^2\, T^{-0.7}(z) = \mathcal{A}(z)\,(1+\delta_b(z))^{\beta}\,, \\ \mathcal{A}(z) &= 0.433 \left(\frac{1+z}{3.5}\right)^6 \left(\frac{\Omega_b h^2}{0.02}\right)^2 \left(\frac{T_0}{6000\ {\rm K}}\right)^{-0.7} \times \\ &\quad \left(\frac{h}{0.65}\right)^{-1} \left(\frac{H(z)/H_0}{3.68}\right)^{-1} \left(\frac{\Gamma_{\rm HI}}{1.5\times 10^{-12}\ {\rm s}^{-1}}\right)^{-1}\,, \end{aligned} \tag{4.62}$$

where $\beta \equiv 2 - 0.7\,(\gamma - 1)$ in the range $1.6 - 1.8$, $\Gamma_{\rm HI}$ the HI photoionization rate, $H_0 = h\,100$ km/s/Mpc the Hubble parameter at redshift zero. For a quantitative analysis, however, full hydrodynamical simulations, which properly simulate the non-linear evolution of the IGM and its thermal state, are needed.

Equations (4.61) and (4.62) show how the observed flux $F = \exp(-\tau)$ depends on the underlying local gas density ρ_b, which in turn is simply related to the dark

matter density, at least at large scales where the baryonic pressure can be neglected [111]. Statistical properties of the flux distribution, such as the flux power spectrum, are thus closely related to the statistical properties of the underlying matter density field.

The power spectrum of the observed flux in high-resolution Lyman-α forest data provides meaningful constraints on the dark matter power spectrum on scales of $0.003\,\mathrm{s/km} < k < 0.03\,\mathrm{s/km}$, roughly corresponding to scales of $(1-40)\,h^{-1}\mathrm{Mpc}$ (somewhat dependent on the cosmological model). At larger scales the errors due to uncertainties in fitting a continuum (i.e. in removing the long wavelength dependence of the spectrum emitted by each QSO) become very large while at smaller scales the contribution of metal absorption systems becomes dominant (see e.g. [112, 113]).

There are different approaches to solve this problem and we now describe the particular one we used in [15] to asses the use of the Lyman-α flux spectra for constraining isocurvature parameter.

4.6.1 Lyman-α forest data and Isocurvature parameters

Viel, Haehnelt & Springel [105] (VHS) have used numerical simulation to calibrate the relation between flux power spectrum and linear dark matter power spectrum with a method proposed by Croft et al. [104] (C02) and improved by [114] and VHS. A set of hydrodynamical simulations for a coarse grid of the relevant parameters is used to find a model that provides a reasonable but not exact fit to the observed flux power spectrum. Then, it is assumed that the differences between the model and the observed linear power spectrum depend linearly on the matter power spectrum.

Then, hydrodynamical simulations are used to determine a bias function between flux and matter power spectrum: $P_F(k) = b_F^2(k)\,P(k)$, on the range of scales of interest. In this way the linear matter power spectrum can be recovered with reasonable computational resources.[9] This method has been found to be robust provided the systematic uncertainties are properly taken into account [105, 114]. Running hydrodynamical simulations for a fine grid of all the relevant parameters is unfortunately computationally prohibitive (see discussion in [123] on a possible attempt to overcome this problem).

The isocurvature mode contribution can create distortions in the small-scale linear matter power spectrum. Of course, this extra freedom was not taken into account in the definition of the grid of models in VHS. In principle, we should run simulations for a new grid with extra parameters (α, β, n_{iso}, n_{cor}). Alternatively, we can carry a tentative analysis with the same function $b_F(k)$ and the same error bars as in the pure adiabatic case, and check the validity of our results *a posteriori*.

[9] Note that this bias is different from the usual bias between light and matter, and can be strongly scale-dependent.

The idea is simply to select a marginally excluded model with the largest possible deviation from adiabaticity in the matter power spectrum. For this model, we run a new hydrodynamical simulation and we compare $P_F(k)/P(k)$ with the function $b_F^2(k)$ used in the analysis. In case of good agreement, the results will be validated. We expect this agreement to be fairly good on large scales, but deviations should appear on small scales, because of the different non-linear evolution.

4.6.2 Systematics Errors

There is a number of systematic uncertainties and statistical errors which affect the inferred power spectrum and an extensive discussion can be found in [104, 114, 105, 123]. VHS estimated the uncertainty of the overall *rms* fluctuation amplitude of matter fluctuation to be 14.5 % with a wide range of different factors contributing.

We present here a brief summary. The effective optical depth, $\tau_{\rm eff} = -\ln\langle F\rangle$ which is essential for the calibration procedure has to be determined separately from the absorption spectra. As discussed in VHS, there is a considerable spread in the measurement of the effective optical depth in the literature. Determinations from low-resolution low S/N spectra give systematically higher values than high-resolution high S/N spectra. However, there is little doubt that the lower values from high-resolution high S/N spectra are appropriate and the range suggested in VHS leads to a 8% uncertainty in the *rms* fluctuation amplitude of the matter density field (see Table 5 in VHS). Other uncertainties are the slope and normalization of the temperature-density relation of the absorbing gas which is usually parametrised as $T = T_0\,(1+\delta_b)^{\gamma-1}$. T_0 and γ together contribute up to 5% to the error of the inferred fluctuation amplitude. VHS further estimated that uncertainties due to the C02 method (due to fitting the observed flux power spectrum with a bias function which is extracted at a slightly different redshift than the observations) contribute about 5%. They further assigned a 5 % uncertainty to the somewhat uncertain effect of galactic winds and finally an 8% uncertainty due the numerical simulations (codes used by different groups give somewhat different results). Summed in quadrature, all these errors led to the estimate of the overall uncertainty of 14.5% in the *rms* fluctuation amplitude of the matter density field.

For our analysis we use the inferred DM power spectrum in the range $0.003\,\mathrm{s/km} < k < 0.03\,\mathrm{s/km}$ as given in Table 4 of VHS. (Note that, as in [115] we have reduced the power spectrum values by 7% to mimick a temperature-density relation with $\gamma = 1.3$, the middle of the plausible range for γ [116]).

Unfortunately at smaller scales the systematic errors become prohibitively large mainly due to the large contribution of metal absorption lines to the flux power spectrum (see Fig. 3 of Ref. [105]) and due to the much larger sensitivity of the flux power spectrum to the thermal state of the gas at these scales.

In this Chapter, we have briefly reviewed the most relevant experiments used for our analyses. We have done so stressing the phenomenology associated with cosmological parameters. Maybe, these are the most widely used probes, but by no means these are all one can rely on.

In particular, no review of cosmological probes would be complete without references to the galaxy weak lensing. The light rays coming from distant galaxies gets lensed by the clumps of matter it encounters in our way to us. This induces a correlation in the ellipticity of the galaxies where one would expect a zero correlation. The effect is measured in what is called the shear power spectrum [117].

Large optical galaxy surveys measure the shear power spectrum [118] which is then compared to theory and used to impose bounds mainly on the Dark Energy equation of state via the growth structure [119]. The great advantage of this probe is that it is not dependent on the bias between luminous and dark matter since light gets bended by both equally.

Even though it is a rather new tool, its potential seems very promising and current projects such as DES [120] or DUNE [121] are concentrating efforts on measuring the shear power spectrum.

As pointed out by the different sections of this chapter, cosmologists count on a large number of probes and experiments to compare with theory.

It is important to keep in mind that the final observation is the result of a very entangled combination of all the cosmological parameters. This leads to degeneracies in the space of parameters which prevent us from extracting "clean" information about the cosmological model.

Also, we must stress that systematic errors should be carefully considered as they may not only lead to imprecise inferences, but also to erroneous ones as they may bias the results unnoticeably.

Nevertheless, the prospects for the future are very promising with many upcoming experiments and statistical developments that will ease both of the issues numbered above.

In the next chapter, we review the statistical tools necessary to accomplish our goal of determining the cosmological parameters.

Chapter 5

Model selection and Technicalities of Parameter Determination

The volume of cosmological data is continuously increasing, and has been doing so for the past 15 years.

Just for a taste of this development, let us mention that in 1992 the COBE satellite [1] measured the first hints of anisotropies in the CMB. This represented a huge step towards understanding cosmology which was indeed awarded with the Physics Nobel Prize in 2006.

Only 11 years after that, the WMAP team [5], using one of the next generation CMB exploring satellites, measured the same anisotropies with unprecedented precision in such large scales. This allowed for an actual parameter inference from the anisotropies in the CMB with a precision of around 10%. Three years later, more gathered data and a better understanding of the foreground contamination, shrank the error bars to 50% of their previous value.

Ground based interferometers such as VSA [128] or DASI (the first probe that measured CMB polarization) [164] or balloon borne experiments such as Boomerang [165] constrain smaller scale anisotropies with very high precision as well, giving us an elaborate map of the temperature anisotropies on scales that range from the arc minute to tens of degrees [1].

This is an example the impressive revolution in cosmological data collection which, along with measurements in Supernovae of Type Ia or galaxy catalogues, give us the most detailed picture of the cosmos scientists could have hoped for only two decades ago.

Nevertheless, this steep increase in the progress of building measuring devices does not leave us much time to digest and understand data from a statistical point of view- are we ready for mixing all different pieces of data? How do the systematics

[1]For the lowest multipoles, $\ell \lesssim 40$, the precision is always limited by cosmic variance.

affect our inferences? Which parameters are we ready to constrain? And, which is the best way to do that?

These very fundamental questions have been addressed by a considerable number of authors (see, for example [169]) and many advances have been made towards building a specific *language* for cosmological statistics. The lack of data or the fact that an experiment cannot be repeated in any laboratory definitely renders Cosmology a science worth of that effort.

In this chapter we pay special attention to two of the questions posed above, namely, the problem of Model Selection and how to constrain the cosmological parameters.

In section 5.2 we describe the methodology used for parameter estimation, widely used among cosmologists at present. It constitutes a basic pillar upon which this research is founded and this thesis would not be complete without it.

In section 5.3 we formally pose the problem of selecting a number of parameters to be constrained in cosmology and describe some of the tools developed targeting this goal. We also report here our results contributing to this field.

Finally, we present our conclusions in section 5.4.

5.1 Bayesian Probability Theory

The first account of the calculation of a probability as such is found in Jakob Bernoulli's *"Ars Conjectandi"* in 1713. In what could seem a pedestrian compilations of rules and axioms related to game theory, the first definition of a probability is given to be *"a degree of certainty, which is to the certainty as a part to the whole"*. It was specified that if the probability of a particular outcome is p, then, the frequency of occurrence of that event in a series of experiments will be p.

No solution was proposed to solve the problem posed the other way around, *i.e.*, if the frequency of occurrence of a given event is p, what is its probability?

In 1763 Laplace published the posthumous Bayes' Theorem which shed some light to the long standing problem. Using it, one can calculate what is the probability of a hypothesis, $\mathcal{H}$, given some data, D and some prior knowledge about it $\pi(\mathcal{H})$:

$$\mathcal{P}(\mathcal{H}|D) = \frac{P(D|\mathcal{H})\pi(\mathcal{H})}{P(D)} \tag{5.1}$$

where $P(D) = \sum_{\mathcal{H}} P(D|\mathcal{H})\pi(\mathcal{H})$ can be seen as a normalization factor or the probability of the data given all possible hypothesis. In this context, the hypothesis $\mathcal{H}$ can be almost anything, a value for a given parameter or vector or parameters, a model or the statement "I will win the lottery next month". The data, D, is the external piece of information with which we want to update our current knowledge

encoded in π. With the aid of (5.1) one can predict any probability in light of some data and any prior knowledge.

Despite the naturalness of the probability theory built around Bayes' Theorem, it lacked of some mathematical rigour in its axioms and the apparent arbitrariness of the assignation of the prior probabilities. In the 19^{th} century, the problem was drastically solved by assigning probability a new definition:

$$p(A) = \lim_{N\to\infty} \frac{\text{Experiments with outcome A}}{N} \tag{5.2}$$

where N is the total number of experiments. Now, the probability is the relative frequency of occurrence of an event in an ensemble of *identically* prepared systems. All the ambiguity aching the previous definition is removed.

Frequentist statistics have lingered around since then. The apparent objectivity of its methods designates it as a true mathematical science, while the Bayesian approach may seem a more ethereal subjective one. Nevertheless, in the confines of Physics and the openings of Philosophy arises the question of whether inference can ever be a totally subjective operation, free from prejudices or effects coming from the "inferencer". Can the statement "my conclusions are completely independent of my prejudices" ever be true? For a beautiful discussion about the concealed ambiguity of a frequentist analysis see [169].

This is indeed a discussion verging on metaphysics and we are not aiming at providing an exhaustive comparison between the frequentist and the Bayesian approaches. But, given the numerous discussions of frequentists vs bayesianists, we believe it is important to be clear about the fact that many of the discomforts brought up by a Bayesian analysis are simply hidden under the rug for a frequentist approach.

The controversy above remains an open issue but we believe that it is fair to state that one of the approaches could suit different problems better. That is the case for parameter estimation and model selection[2] in cosmology. BPT appears to be the most appealing theory for several reasons:

- Experiments cannot be repeated using an identically prepared system. By assuming ergodicity, cosmological observations are promoted to experiments, but by no means can we assure that these happen under identical settings. In this sense we are violating one of the frequentist assumptions under which, an observable is exactly a random variable.

- Bayesian Probability Theory appears to be the ideal framework to deal with small volumes of data. It even allows one to update current state of knowledge with one single data point. Frequentist set ups generally require a very large number of events in order to draw accurate conclusions from their analyses.

[2]As a matter of fact, only under the Bayesian scope is it possible to assign a probability to a model. A model can never be a random variable with a frequency of occurrence.

- Experiments cannot be chosen specifically to measure a given quantity in the universe. Rather, we are bounded to measure algebraic combinations of them. This difficulty is directly translated into *degeneracies* in the space of parameters. In order to get a physical insight into the effects of each of the parameters it is appropriate to study the effects of different prior assumptions and the Bayesian tools are optimal for these kind of variations.

- Generally, a set of cosmological parameters is determined by merging large amounts of data coming from different observations and which are the result of very different physical processes. The systematics associated with each of these experiments have very diverse origins. Again, BPT provides an unbeatable framework inside which one can be very specific about the statistical weight assigned to each dataset.

- Which estimator to use in a Likelihood Ratio Test, or the threshold one uses to accept or reject a given hypothesis are indeed subjective choices the experimenter has to take. They will be invariably (and probably unawarely) affected by the experimenter's prior knowledge. In this sense, BPT supplies a more structured frame in which to clearly separate ones previous beliefs from data information.

Partly for the reasons above, Cosmology has used a Bayesian framework for the determination of parameters for some time now, and also for Model Selecting.

In what follows, we describe the basics of the statistics tools used for the particular problem of cosmological parameter determination.

5.2 Parameter Determination: Monte Carlo Markov Chains

As we see in Chapter 4 the particular shape of the angular power spectrum is the final result of an accumulation of effects caused by the different parameters, θ. The different effects are quite hard to disentangle from each other. We can arrange the values of the C_ℓ's in a vector data, $\mathbf{D}$, and inquiry about the probability distribution of the parameters given the data, $\mathcal{P}(\theta|\mathbf{D})$. We can compute it with the aid of Bayes' theorem in equation (5.1):

$$\mathcal{P}(\theta|\mathbf{D}) = \frac{\mathscr{L}(\mathbf{D}|\theta)\pi(\theta)}{\int \mathscr{L}(\mathbf{D}|\theta')\pi(\theta')\mathbf{d}\theta'} \tag{5.3}$$

where $\mathscr{L}(\mathbf{D}|\theta)$ is the likelihood function, *i. e.*, the joint pdf for the data given a certain value of θ, evaluated with the data actually obtained in the experiment [171].

Equation (5.3) is the usual way of obtaining the pdf for the parameters in cosmology. In general, the data vector $\mathbf{D}$ comprises more than information in the

temperature anisotropies. Current analyses are done with all kinds of data, some of which were presented on the previous chapter. The denominator of the equation, which is just the normalization or the volume in the space of parameters of the likelihood function, will turn out to be a very relevant quantity for model selection, as we will see later. However for parameter estimation this quantity is useless, and typically it is not even calculated.

The only pending task now is to figure out the shape of $\mathscr{L}(\mathbf{D}|\theta)$. This is not a trivial problem because the way we sample the function can bias the result. In other words, we start off from a completely unknown function and the points we pick to study its shape, may or may not be a fair sample of the whole thing. It is indeed a complicated affair that has brought up much attention from statisticians.

For our purposes, we find most useful the Metropolis-Hastings algorithm [159]. We review now its basic functioning.

5.2.1 The Metropolis-Hastings Algorithm

This is a very efficient algorithm to sample from an unknown probability distribution function. Also one can easily incorporate the prior knowledge about the parameters being constrained. In what follows we may use the likelihood $\mathscr{L}$ or the pdf $\mathcal{P}$ indistinctly.

A sequence of points $\{x_1, x_2..x_N\}$ is generated according to the following procedure:

1. An initial point, x_0 is picked randomly from all the possible positions in the space of parameters.

2. x_{trial} is drawn from a *proposal density* distribution, $q_{trial}(x_0, x_{trial})$, in the vicinity of x_0 . This proposal density is arbitrarily set to control the direction as well as the length of the steps in the parameter space. Once fixed, the proposal density should remain fixed during the rest of the sampling.

3. The likelihood of x_{trial} is computed and compared to the likelihood of x_i. If:

$$\frac{\mathscr{L}(x_{trial})}{\mathscr{L}(x_0)} \geq 1$$

   x_{trial} will be accepted. Then, x_{trial} is set equal to x_1 and the algorithm is repeated using this one as the starting point. If

$$\frac{\mathscr{L}(x_{trial})}{\mathscr{L}(x_0)} = \mathcal{P} \leq 1$$

   the point is accepted as the next sample with probability $\mathcal{P}$. If the point is not accepted the algorithm is repeated all over using x_0 again as the stating point.

4. The process is repeated to get a sequence of points x_{i+1} from x_i on each loop.

This way, the chain walks quasi randomly along the whole volume in the parameter space, but spends more time sampling the peaks of the distributions than the tails. Generally, in Cosmology, we do not expect bimodal distributions or any interesting features on the tails, thus the Metropolis-Hastings algorithm is a very useful tool for us.

In order to optimize the computation time, it is best to sample from several chains simultaneously. With this, we make sure the whole distribution is properly explored. Also, in case the peaks of the distributions are very poorly known (which is not usually the case for Cosmology) one can sample from a *heated* likelihood distribution $\mathscr{L}^\lambda$ where $\lambda = 1/T$. For high temperatures, the likelihood is flattened and although the peaks are less prominent, they are located more rapidly.

The set of points generated using this technique is called a Montecarlo Markov Chain (MCMC).

The more similar the proposal distribution to the unknown probability distribution function (or pdf in short), the more efficient this algorithm becomes. We can use previous and independent knowledge of the pdf to tailor the proposal density to the unknown pdf. There is where the actual power of this method relies, and that is the key point in using this algorithm.

Generally, the first accepted samples of the chain are strongly correlated, thus, a *burn in* phase must be allowed from which no samples are used for computing the pdf for parameter estimation.

The sampling finishes when the chain has *converged*, which is an ambiguous term since there is not a single rule to define convergence. We used the Gelman and Rubin diagnosis, in which convergence is said to be achieved when the variance of the means of the chains approaches the mean of the variances of the chains [172].

We finally arrive at a total number of MCMC picked samples which ranges from $3 \cdot 10^4$ to 10^5. It is the easiest to organise data as a M-dimensional vector in which, along with the coordinates in the parameter space, we also store the likelihood of the point in particular and the *multiplicity* of the sample or how many tries took to jump to that point to the following one.

The marginalized pdf of a parameter, is simply a histogram of the number of samples versus the value of the parameter. For two dimensional contours, the density of points in the plane spanned by the two parameters determines the different confidence levels. Returning to the Bayesian perspective of the probability, the height of the pdf at each particular value of a parameter turns into the plausibility of that value being the true value of the underlying law we are testing.

The Metropolis-Hastings algorithm has been very conveniently adapted for cosmological purposes by A. Lewis in a fortran based code, `cosmoMC` [127]. The code implements the algorithm for sampling a different number of underlying likelihood

distributions and parameter combinations. In particular, it uses the `camb` [80] code to compute the theoretical power spectra generated by the different parameter combinations and compares it to data. After fitting the code to our own necessities, we have used it intensely for all our parameter estimations. Among many other conveniences it allows for a faster likelihood computation by classifying parameters under two categories: "fast" and "slow". The fast ones are those whose values do not affect the evolution of the perturbations, thus the transfer functions do not need to be re-calculated when they are varied This way the new power spectra are quickly retrieved saving time that would be lost in a naive approach where everything is computed on every step.

5.3 Model Selection

It could seem that all we need to go from data to theory is a way to compute the pdf of each of the parameters one wants to constrain, *i.e.*, a *parameter fitting* method. Based on this wrong believe many parameters are determined to a different degrees of accuracy and very little attention is directed at the higher-level inference problem of allowing the data to decide the set of parameters to be used, known as *model comparison* or *model selection* [158, 159]. Such techniques have been widely deployed outside of astrophysics and are playing a relevant role in cosmology [174, 175] only recently.

During the rest of the chapter we give a detailed explanation of what model selection is and present our developments and results addressing this conundrum.

A very simple example

Let us start with a very simple, innocent problem: how well can one fit a sample of N datapoints. We will determine the precision with which the underlying true model of the data points can be recovered.

We obtain a sample of N points, $\{d_i\}_{i=1..N}$, generated randomly from a gaussian distribution with mean $\mu(x) = \hat{A} + x\hat{t}$; where $\hat{A}$ and $\hat{t}$ take different values and we will refer to them as the *amplitude* and the *tilt* respectively. That is, we simulate data gathered on the points $\{x_i\}$ to probe an underlying physical law $m(x) = A + xt$. The dispersion is normalized to $\sigma = 1$.

We want to recover the values of A and t, but hypothetically, we do not know which is the shape of the underlying law, so we calculate the likelihood functions

for models that differ in the number of parameters:

$$\mathscr{L}_{\rm I}(A,\{d_i\}) = \exp[-\frac{1}{2}\sum_{i=1}^{i=N}(A-d_i)^2] \quad (5.4)$$

$$\mathscr{L}_{\rm II}(A,t,\{d_i\}) = \exp[-\frac{1}{2}\sum_{i=1}^{i=N}((A+tx_i)-d_i)^2] \quad (5.5)$$

$$\mathscr{L}_{\rm III}(A,t,b,\{d_i\}) = \exp[-\frac{1}{2}\sum_{i=1}^{i=N}((A+tx_i+bx_i^2)-d_i)^2] \quad (5.6)$$

and find the best fit value of the parameters A, t and b, the later being a hypothetically plausible quadratic component of the law. For model I, parameters t and b are fixed to zero, and for model II, $b=0$ as well.

Firstly, we do the experiment for a sample of 100 and 50 data points and a fiducial model of $(\hat{A},\hat{t})=(25,0.5)$. We compute the χ^2/DOF for each and also the Bayesian Information Criterion razor, the BIC [170, 160]:

$$\mathrm{BIC} = -2\ln\mathscr{L}(\tilde{\theta}) + k\ln N \quad (5.7)$$

where $\tilde{\theta}$ are the values of the parameters in the best fit point and k is the number of parameters of the model. Under the likelihood ratio test (LRT), the best model is that for which the quantity χ^2/DOF is minimized whereas the under the Bayesian information criterion (BIC) we are bounded to choose the model with the lowest value of a quantity that is commonly referred to as BIC. In this way, the BI criterion incorporates a natural Occam's razor since models with more parameters will have a bigger BIC in case the χ^2/DOF are similar.

We report the results on table 5.1. In the second column we write the best fit values for the models and in the third and fourth column we calculate the two quantities relevant for model selection.

Model	$\tilde{A}$	$\tilde{t}$	$\tilde{b}$	χ^2/DOF	BIC
I_{100}	37.5	-	-	55.225	5471.85
II_{100}	24.7	0.508	-	1.008	108.064
III_{100}	24.7	0.513	-10^{-4}	1.018	112.632
I_{50}	38.0	-	-	52.073	2555.5
II_{50}	25.4	0.492	-	0.624	37.807
III_{50}	25.4	0.498	-10^{-4}	0.637	41.696

Table 5.1: Relevant quantities calculated for the three models for data generated from fiducial values $(\hat{A},\hat{t})=(25,0.5)$. The first three rows correspond to a sampling of $N=100$, and the following three are for models with $N=50$.

We compare the numbers in column three in order to perform a likelihood ratio test. Based on it, it can be safely said that model I is ruled out by data and model II

and III compete with a slight difference between the experiments. For the $N = 100$ experiment, $\Delta\chi^2 = 0.01$ whereas for the 50 point one, $\Delta\chi^2 = -0.013$. So, just looking at this column, not much could be said about the preferred model. If we instead apply the BIC, we can definitely select model II as the preferred one and that is good news because model II is precisely the true underlying one.

To show a bit more of the power of the BIC criterion, we perform the same experiment with: a) fewer datapoints ($N = 25$); and b) less steep tilt ($\hat{t} = 0.1$) and write the results on table 5.2 on the first and second 3-row sets, respectively.

Model	$\tilde{A}$	$\tilde{t}$	$\tilde{b}$	χ^2/DOF	BIC
I_{25}	37.9	-	-	56.469	1358.47
II_{25}	24.8	0.506	-	1.067	30.97
III_{25}	24.6	0.525	$3{\cdot}10^{-4}$	1.110	34.08
I_{50}	27.5	-	-	3.004	151.11
II_{50}	25.1	0.095	-	1.120	61.57
III_{50}	25.3	0.074	$4{\cdot}10^{-7}$	1.137	65.20

Table 5.2: Second part experiments. On the top three columns we show the results for 25 datapoints and on the bottom three, we show the results for a experiments where the data were simulated from a $\hat{t} = 0.1$ underlying model.

We see again how, even in these other, not so ideal experiments, the BIC correctly chooses the right model whereas the likelihood ratio test still does not throw much light to the problem.

With this over simplistic example, we get a hint of the power of Bayesian Analysis. In a way, it does make more sense to use a Bayesian approach to address the problem of model selection because it is only inside this scope that one can assign to the probability its most intuitive meaning. For Bayesian, probability means the plausibility of a hypothesis or the degree of belief on a hypothesis to be true. For frequentists, the probability is the frequency of occurrence of an event. A model is not an event that happens thus we cannot assign it a probability in a frequentist fashion. By these two simple definitions, it is easy to see that the appropriate framework or at least, the most coherent one, for model selection would be Bayesian Probability Theory (BPT).

The quantity we have called the BIC, is indeed the asymptotic limit for the *Bayesian Evidence* [158, 159] as $N \to \infty$. While we devote subsection 5.3.1 to the description of this quantity, let us just say, for the moment that this is the quantity that quantifies the goodness of a model inside the BPT.

Also, it must be noted that although the use of the LRT is widely spread among non-specialists, it must be handled with care. Its effectiveness is based upon the fact that we know the distribution towards which the likelihood ratio estimator tends

asymptotically, namely a χ^2 distribution. However this may or may not be the case for each particular problem [146].

It is usually taken for granted that the LRT test will work, but only if the following two conditions are satisfied can the appropriate use of this test be guaranteed [147]:

- Models must be nested.
- The null values of the additional parameters may not be on the boundary of the set of possible parameter values.

The second condition is not fulfilled by models II and III, because we are in principle testing for the possibility that parameters t and b are indeed zero. So, strictly speaking, the LRT has been applied in a misleading manner in this model selection exercise.

Generally, finding evidence for a minor feature in a physical law, is an intricate problem. Detecting a signal on top of a noisy background is, by no means, a trivial problem for statistics[3] and of course cosmological data analysis is not an exception.

Whenever one tries to decide whether or not a particular parameter p should be fixed (for example at $p = 0$), one should use model selection techniques. If one carries out only a parameter-fitting exercise and then examines the likelihood level at which $p = 0$ is excluded, such a comparison fails to account for the model dimensionality being reduced by one at the point $p = 0$, and hence draws conclusions inconsistent with Bayesian inference. This typically overestimates the significance at which the parameter p is needed.

Also for the cases of small amounts of data, regular frequentist approach may not be the most appropriate one. In our toy problem, we tried to ease this ache by using the Bayesian Information Criterion, which evidently falls inside the Bayesian theory for data analysis however this is not a full implementation of Bayesian inference, which appears to be the most appropriate framework for interpreting cosmological data. The correct model selection tool to use in that context is the *Bayesian evidence* , which is the probability of the model in light of the data (i.e the average likelihood over the prior distribution).[4] It has been deployed in cosmological contexts by several authors [162]. The Bayesian evidence can be combined with prior probabilities for different models if desired, but even if the prior probabilities are assumed equal, the evidence still automatically encodes a preference for simpler models, implementing Occam's razor in a quantitative manner.

[3] see for example, [93] where a and possible solution is presented.

[4] The Bayesian Information Criterion can be used as a crude approximation to the ratio of the evidences of two models, also known as the Bayes factor [161], but the existence of parameter degeneracies in cosmological data fitting are likely to violate the conditions for the validity of the approximation.

An example in literature for model selection in data analysis is the level at which is spectral index n_s is needed. Parameter fitting for the first data release of WMAP [4] favoured at a modest (albeit unconvincing) confidence level but its inclusion inside the set of parameters was disfavoured by model selection statistics [160]. As new data came up [5], new analyses reported a mild necessity of the addition of n_s as a parameter: 8 to 1 if other datasets were taken into the analysis and weaker if they were not [178].

In [160] two model selection statistics, known as the Akaike and Bayesian Information Criteria, are applied to some simple cosmological models and it is shown that the simplest model considered was the one favoured by the data. These criteria have recently been applied to models with isocurvature perturbations by Parkinson et al. [154], who concluded that the purely adiabatic model was favoured.

In what follows, we describe our work in [76] where we use the *Bayesian evidence* to compare isocurvature and adiabatic models in light of current data.

5.3.1 Bayesian Model Selection: The Evidence

The Bayesian evidence is the average likelihood of a model over its prior parameter space, namely

$$E = \int \mathscr{L}(\theta)\, \pi(\theta)\, d\theta\,, \tag{5.8}$$

where θ is the parameter vector defining the model, $\mathrm{pr}(\theta)$ the normalized priors on those parameters (typically taken to be top-hat distributions over some range), and $\mathscr{L}(\theta)$ is the likelihood. If we compare (5.8) to (5.1), we see that the evidence is just the normalization factor generally obviated during parameter estimation.

In essence, it asks the question: 'If I consider the possible model parameters I was allowing before I knew about this data, on average how well did they fit the data?'. Generally speaking, models with fewer parameters tend to be more predictive, and provided that for some parameter choices they fit the data well, then the average likelihood can be expected to be higher. On the other hand, a simple model which cannot fit the data for any parameter choices will not generate a good likelihood. The Bayesian evidence therefore sets up the desired tension between model simplicity and ability to explain the data.

Models are ranked in order of their Bayesian evidence, usually using its logarithm. The overall normalization is irrelevant. As the evidence is the (unnormalized) probability of the model, if two models are being compared, the odds of the one with the lower evidence is $1/(1+\exp(\Delta \ln E))$. What constitutes a significant difference is to some extent a matter of personal taste. Jeffrey's [158] rates the importance according to the following table, the decision being against the model with the smaller evidence:

Note that a difference $\Delta \ln E$ of 2.5 corresponds to odds of 1 in about 13, and

$\Delta \ln E$	Significance
< 1	'not worth more than a bare mention'
$1 - 2.5$	'substantial'
$2.5 - 5$	'very strong'
> 5	'decisive'

$\Delta \ln E$ of 5 to odds of 1 in 150.

A significant, but unavoidable, disadvantage of the use of the evidence is that it depends on the prior ranges chosen for the parameters. For instance, if one doubles the range of one parameter by allowing it to vary in a region where the likelihood is negligibly small, then the evidence will half. Indeed, one can make any model disfavoured simply by extending its prior range indefinitely in a direction where there is no hope of fitting the data. From a Bayesian point of view this is unsurprising; of course your belief in a model should be influenced by what you thought of it before the data came along, and the Bayesian analysis has the virtue of forcing you to make your assumptions explicit.

However, the prior width is not as crucial as one might naïvely expect. The main reason is that the likelihood is typically falling off exponentially away from the best fit, while the parameter volume is growing only as a polynomial function. Coming back to toy examples, consider a one-dimensional model for which the likelihood is given by

$$\mathscr{L}(x) = \mathscr{L}_0 \exp\left(-\frac{(x-\mu)^2}{2}\right) , \tag{5.9}$$

and consider two models: model A is $x = 0$ and model B is $x \neq 0$ with a top-hat prior $0 < x < a$. In the case $\mu = 1$, a conventional 1-σ non-detection, the evidence would be unable to strongly distinguish between the models ($|\Delta \ln E| < 2.5$) for up to $a \sim 50$. In the case $\mu = 5$, a conventional 5-σ detection, the evidence would prefer model B for all ranges the evidence will robustly pick up the correct model. Its main advantage is that it is a quantitative measure with clear interpretation within Bayesian statistics, and can be applied in cases where the usual frequentist arguments do not provide us with definite answers. Typically, Bayesian analysis contradicts the frequentist results whenever the latter accepts a parameter in light of a marginally better χ^2 value. If this improvement is not significant, the increase of the volume of the parameter space will clearly penalize the addition of the new parameter and thus decrease the evidence of the extended model.

Generally the evidence is not reparametrization invariant, in the sense that the choice of a flat prior in one parametrization will probably not correspond to a flat prior under another parametrization. The choice of parametrization is a matter of personal preference, though obviously truly robust model selection results should be preserved under reasonable changes in parametrization. In the case of isocurvature perturbations there are different, equally plausible, choices of parametrizations, in

particular geared to dealing with the problem of the cross-correlation angle becoming unconstrained as the isocurvature mode amplitude becomes small. For illustration we will compare the results obtained under two different parametrization choices.

5.3.2 Numerical Implementation: Thermodynamical Integration

The evidence for a given model can be computed by a Markov Chain Monte Carlo method. However it cannot be directly calculated from chains used in parameter estimation (for instance from the program `CosmoMC` [127]), because those chains are sampled from the posterior distribution, which is peaked around the maximum likelihood, and do not carry the necessary information on the likelihood far from the maximum. Equally, one cannot simply sample from the prior distribution, because the dominant contribution from the high-likelihood regions will not be properly sampled. Consequently, a hybrid technique is required, a useful method being thermodynamic integration. [163, 157].

Thermodynamic integration alters the sampling of a Markov chain by introducing a parameter λ, thought of as an inverse temperature, with the acceptance rate governed by the likelihood raised to the power λ. As λ is varied from zero to one, this interpolates between sampling from the prior and the posterior distributions. Defining

$$E(\lambda) = \int \mathscr{L}^{\lambda}(\theta)\ \mathrm{pr}(\theta)\ d\theta\,, \tag{5.10}$$

it can be shown that

$$\ln E = \ln \frac{E(1)}{E(0)} = \int_0^1 \frac{d\ln E}{d\lambda}\, d\lambda = \int_0^1 \langle \ln \mathscr{L} \rangle_{\lambda}\, d\lambda\,, \tag{5.11}$$

where

$$\langle \ln \mathscr{L} \rangle_{\lambda} \equiv \frac{\int \ln \mathscr{L}\ \mathscr{L}^{\lambda}\, \pi(\theta)\, d\theta}{\int \mathscr{L}^{\lambda}\, \pi(\theta)\, d\theta} \tag{5.12}$$

is the average log likelihood over the distribution at temperature $1/\lambda$. The term $\ln E(0)$ equals zero if the prior is normalized, otherwise it acts as a normalization factor since in Eq. (5.8) the priors must be normalized.

Previous work in cosmology has typically evaluated the evidence during the burn-in phase of a chain to be used for parameter estimation. In this process, the temperature is slowly cooled from $\lambda = 0$ to $\lambda = 1$ to facilitate the relaxation of the chain into its stationary distribution and those chain elements are used for evidence computation; they are then discarded and the remaining elements, all sampled at $\lambda = 1$, are used for parameter estimation. This method is ideal for complex inference problems with dimensionality $d \gg 1$ and multimodal likelihood distributions, where a slow burn-in phase is necessary to explore the posterior in an unbiased manner and

thus the evidence calculation comes 'for free'. However, in a typical cosmological problem the likelihood surface is considerably simpler, arguably unimodal, and the number of samples required for a reliable burn-in is much smaller than the number of samples needed for an accurate evidence estimation. Therefore, we choose a different approach in which we heat the chain, using the endpoint of a parameter estimation run as the starting point. Since the volume of parameter space is larger at higher temperatures it should be much easier to ensure that the chain is stationary at each temperature step during heating rather than cooling. We implemented two different heating schedules:

- *Continuous temperature change.* We let the inverse sampling temperature change continuously at each step as

$$\lambda(n) = (1 - \xi)^n, \tag{5.13}$$

  where n is the step number. The single sample taken at that temperature can be viewed as an unbiased (although noisy) estimate of $\langle \ln \mathscr{L} \rangle_\lambda$. This continuous approach obviates the problem of deciding the number of steps per position, transferring it to the step size. When the algorithm decides to stop, the integral is closed to $\lambda = 0$ in the last step. The stopping criterion is that the closure of the integral by the last step would change $\ln E$ by less than a certain threshold, $\epsilon_{\rm stop}$, even for the most extreme likelihood encountered. The choices of ξ and $\epsilon_{\rm stop}$ determine the accuracy and speed of the evidence calculator, and optimum values must be determined empirically. After trying various possibilities we settled for $\xi = 5 \times 10^{-5}$ and $\epsilon_{\rm stop} = 0.001$. We have tested that decreasing either ξ or $\epsilon_{\rm stop}$ further does not affect our results.

- *Stepwise temperature change.* The integrand of Eq. (5.11) is first estimated at $\lambda = 1$ and 0, then at intermediate temperatures given by

$$\lambda_n = \frac{1}{q^n}\,, \tag{5.14}$$

  (q is typically 1.5 – 2 and n an increasing integer). The thermodynamic integral is calculated by the trapezoid rule after each additional point is added. The points are added until the integral converges to a user-specified stopping accuracy $\epsilon_{\rm stop}$. At each temperature the integral is calculated by making a short burn-in at that temperature (typically 400 samples, since the chain must already be roughly burned in from the previous step) and then calculating $\langle \ln \mathscr{L} \rangle_\lambda$ from a further number (typically 1000) of *accepted* samples. This approach has the disadvantage that extra samples are needed for burn-in at each temperature and that there might be systematics associated with stepwise temperature change. However, it is less sensitive to the quality of covariance matrix as a poorer covariance matrix simply results in more samples being taken to get enough accepted samples (note that we cannot do the same for the continuous scheme without biasing the result, unless one is willing to burn-in at *each* 'continuous' temperature change step).

Additionally, we modify the proposal function so that its width scales with λ^{-1} (up to a certain width), which ensures that at high temperatures the chain is sampling randomly from the prior, rather than random-walking with the step-size corresponding to the $\lambda = 1$ posterior.

These two methods have been extensively tested to give results that are consistent and accurate to within a unit of $\ln E$ for a single run. The final numbers for all models were calculated using the continuous temperature change method. Additionally we have performed a comparison with an analytic approximation to the posterior and got results that are also consistent to better than one unit of $\ln E$ in the adiabatic case, though slightly worse in the isocurvature case.

In all cases we find that the number of samples required to accurately estimate the evidence and avoid systematics associated with covariance matrices, proposal widths and similar is unexpectedly large; an order of magnitude larger than what is required for a simple parameter estimation. This makes the computation a challenging task as it is limited by the speed of the likelihood evaluations which require generation of the model power spectra. This also suggests that the uncertainties on evidence values already found in the literature may be underestimated, though we note that the high quality of the WMAP data makes this task considerably more difficult than it was in the pre-WMAP era. Further investigation into evidence estimation methods is clearly warranted and will be a focus of a forthcoming paper.

Other Evidence estimators

Due to the large computational demand of the thermodynamical integration, and its lack of accuracy in some cases, other methods for estimating the evidence of cosmological models have been explored [173, 174, 175, 176].

Most recently, the *Nested sampling* algorithm has been applied to determine a number of evidences and also for accuracy forecasts such as the ones that will be achieved by Planck on measuring the spectral index [177]. This algorithm reduces the problem of computing a multidimensional integral (see Eq. (5.8)) to that of a unidimensional integral in which the variable of integration X is the *mass* in the prior space: $\pi(\theta)d\theta = dX$. Although it has been proved to be more accurate than the thermodynamical integration, it is also computationally intensive, and the computing time does not outperform the former one significantly.

The Savage-Dickey method is another simple exact calculator only useful for comparing nested models. It was introduced in [173], in 1971, and has been most recently applied in [175] to study the significance of $\Omega_{\rm K}$, $n_{\rm s}$ and $f_{\rm iso}$. For nested models the likelihood of the "null model", $\mathscr{L}_0$ is just a slice of the bigger model likelihood at a particular value of the extra parameter, ω. Thus,

$$\mathscr{L}_1(\theta, \omega)|_{\omega=\omega_0} = \mathscr{L}_0(\theta, \omega_0)$$

One computes the Bayes factor as the ratio of the height of the posterior pdf for

Parameter	Prior Range	Model
$\omega_{\rm b}$	(0.018,0.032)	AD-HZ,AD-$n_{\rm s}$,ISO
$\omega_{\rm dm}$	(0.04,0.16)	AD-HZ,AD-$n_{\rm s}$,ISO
θ	(0.98,1.10)	AD-HZ,AD-$n_{\rm s}$,ISO
τ	(0,0.5)	AD-HZ,AD-$n_{\rm s}$,ISO
$\ln[10^{10}\mathcal{R}_{\rm rad}]$	(2.6,4.2)	AD-HZ,AD-$n_{\rm s}$,ISO
$n_{\rm s}$	(0.8,1.2)	AD-$n_{\rm s}$,ISO
$n_{\rm iso}$	(0,3)	ISO
$\delta_{\rm cor}$	$(-0.14,0.4)$	ISO
$\sqrt{\alpha}$	$(-1,1)$	ISO
β	$(-1,1)$	ISO

Table 5.3: The parameters used in the models. The sound horizon θ was used in place of the Hubble parameter. For the AD-HZ model $n_{\rm s}$ was fixed to 1 and $n_{\rm iso}$, $\delta_{\rm cor}$, α and β were fixed to 0. In the AD-$n_{\rm s}$ model, $n_{\rm s}$ also varies. Every isocurvature model holds the same priors for the whole set of parameters.

model 1 to the prior distributions at ω_0. More precisely:

$$B_{01} = \frac{\mathcal{P}(\omega_1)}{\pi\omega_1} \tag{5.15}$$

As we said, this is an exact calculator with the handicap that it can only be used for nested models.

In [76] we use thermodynamical integration to asses the addition of isocurvature parameters in cosmology in light of the following datasets: cosmic microwave anisotropy data from the 1^{st} year release of the WMAP satellite including temperature–polarization cross-correlation [4], VSA [128], CBI [129] and ACBAR [130], matter power spectrum data from the two-degree field galaxy redshift survey (2dFGRS) power spectrum [131] and from the Sloan Digital Sky Survey [7], and the supernovae apparent magnitude–redshift relation [6].

We devote the rest of the chapter to the presentation of our results.

5.3.3 Model Selection for isocurvature parameters

Our principal aim is to compare the evidence of isocurvature models (three different modes — cold dark matter isocurvature (CDI), neutrino isocurvature density (NID), and neutrino isocurvature velocity (NIV) —) with purely adiabatic ones. These modes can exist in any combination, and with correlations both amongst themselves and with the adiabatic modes. We will only allow a single type of isocurvature mode in any model, though we will allow a general spectral index both for the isocurvature modes and for their correlation with the adiabatic ones.

Model	ln(Evidence)
AD-HZ	0.0 ± 0.1
AD-$n_{\rm s}$	0.0 ± 0.1
CDI	-1.0 ± 0.2
NID	-1.0 ± 0.2
NIV	-1.0 ± 0.3

Table 5.4: Evidences for the four different models studied, normalized to the AD-HZ evidence. The absolute value for that model was $\ln E = -854.1$.

The flat prior ranges for all parameters are given in Table 5.3. We consider two adiabatic models. AD-HZ is the simplest model giving a good fit to the data, with a Harrison–Zel'dovich spectrum and five variable parameters. We also computed the evidence for an extended adiabatic model AD-$n_{\rm s}$ in which we let n_s vary.

For each isocurvature model there are four extra parameters. We parametrize the contribution to the temperature and polarization angular power spectra from the adiabatic, isocurvature and correlation amplitudes at the pivot scale ($k_0 = 0.05$ Mpc^{-1}) by α and β as they are defined in Chapter 3 in Eq. (3.21). We also use the parameter $\delta_{\rm cor}$ is related to the spectral tilt of the correlation mode, $n_{\rm cor}$, and its boundaries are fixed by the pivot scale and the $k_{\rm min} = 4 \times 10^{-5}$ Mpc^{-1} and $k_{\rm max} = 0.5$ Mpc^{-1} scales used for the analysis. It is defined as (see Chapter 6):

$$\delta_{\rm cor} \equiv n_{\rm cor} / \ln |\beta|^{-1} \,. \tag{5.16}$$

Thus the priors on the first seven parameters are theoretically motivated, whereas the priors on the last three are automatically set by the model. Throughout the analysis the equation of state parameter of the dark energy was set to -1.

We ran 32 independent computations of the evidence for each model. In all of them the stopping criterion was satisfied after about 2.5×10^5 steps, so the total number of likelihood evaluations was approximately 10^7 per model. The results, given as the logarithm of the evidence, are described in Table 5.4. We have expressed all the calculated evidence values relative to the AD-HZ model, as the absolute value is just a particular of the likelihood code. We see from the table that the evidences are calculated to sufficient accuracy to draw conclusions, but that the comparison is rather inconclusive. Firstly, the two adiabatic models happen to produce the same evidence; as a further consistency check, we also looked at an adiabatic model with the prior range on $n_{\rm s}$ doubled, and found that $\ln E$ fell by 0.4, to be compared with the expected drop of $\ln 2$ that would appear if the likelihood were insignificant throughout the extended range. Secondly, by coincidence all three isocurvature models have the same evidence, with $\Delta \ln E$ being 1.0 relative to AD-HZ in each case. According to the Jeffreys' scale this is just at the edge of being worthy of attention.

Variation under reparametrization

The issue of the non-invariance of the evidence under a transformation in the space of parameters has been studied in some other works [175, 15] and has been addressed as one serious flaw of Bayesian model selection. However, this non invariance should be expected to some extent because changing the basis of parameters typically leads to a different choice of priors. Thus, we see this just as another effect of prior beliefs on posterior inferences. It would be surprising indeed if models in Nature cared about how they were measured but it is a fact that our previous beliefs about the underlying physical reality may alter our inference. A convenient way of dealing with this, is to explicitly cite all the prior assumptions, including parametrization in every information inference analysis.

Various parametrizations have been used in the literature. For instance, a change of pivot scale leads to an $(n_{\rm s} - n_{\rm iso})$–dependent rescaling of α, and to an $n_{\rm cor}$–dependent rescaling of β. Even if the pivot scale is fixed, various definitions of the amplitude parameters can be introduced. The normalization of the isocurvature mode can be parametrized by the ratio of isocurvature to adiabatic primordial fluctuations $f_{\rm iso} \in [0, \infty]$ [149] instead of the fraction of isocurvature contribution to the total primordial spectrum $\alpha \in [0, 1]$ [13]. In this work, as in the parameter estimation one, we chose to vary $\sqrt{\alpha} \in [-1, 1]$ in order to avoid dealing with boundary effects and to have a posterior distribution falling down to zero on the two ends of the prior range. We could nevertheless instead have chosen a flat prior for α. Similarly, the cross-correlation amplitude can be parametrized either by the correlation angle $\beta \in [-1, 1]$, as in Refs. [149, 14], or by the amplitude of the cross-correlation power spectrum $2\beta\sqrt{\alpha(1-\alpha)}$ [151]. The advantage of the latter is that the total power spectrum depends linearly on it, and so it is well constrained by the data, while starting from a flat prior on β we can get a flat posterior distribution if the preferred model is purely adiabatic, so that the value of β does not matter (this point is discussed in detail in Ref. [156] where a third choice is also introduced). Finally, we defined the parameter $\delta_{\rm cor}$ in order to deal with a simple top-hat prior, but we could decide to use instead to impose a flat β–dependent prior directly on $n_{\rm cor}$.

To get a hint of the effect of reparametrization, we recomputed the evidences using a second parameter basis: instead of $(\sqrt{\alpha}, \beta)$ we vary $(\alpha, 2\beta\sqrt{\alpha(1-\alpha)})$ with a flat prior inside the two-dimensional ellipse in which these parameters are defined, and instead of $\delta_{\rm cor}$ we vary $n_{\rm cor}$ within the range $[-0.14\ln(|\beta|^{-1}), 0.4\ln(|\beta|^{-1})]$. Since the prior on $n_{\rm cor}$ is too loose when β is close to zero, we imposed the additional prior over $n_{\rm cor} \in [-1, 1]$.

The results are quoted in Table 5.5, and show differences from the ones that use the original parametrization. Even though the difference is still not big enough to exclude any isocurvature model, we conclude that, as mentioned in Section II, parametrization does matter for the evidence calculation.

Model	ln(Evidence)
AD-HZ	0.0 ± 0.1
CDI	-1.0 ± 0.2
NID	-2.0 ± 0.2
NIV	-2.3 ± 0.2

Table 5.5: Evidences for the four models using the second parametrization, again normalized to the AD-HZ evidence.

Fortunately for this case, we showed in the previous chapter that this apparent mismatch between different parametrizations is asymptotically nonexistent due to the jacobian of the transformation being flat in that limit.

5.4 Conclusions

In this chapter we have briefly reviewed the status of statistics for cosmological purposes. After providing a short insight into Bayesian Probability Theory in the first section, we describe the methods employed for parameter estimation and Model Selection.

Section 5.2 is just a quick review of current computational methods used in cosmology to compute the MonteCarlo Markov Chains. Nothing in this section is original work, but as mentioned above, these computational techniques are an essential part of the methodology followed during this thesis and their presence in this chapter is very well deserved.

On Section 5.3.1, we justify the necessity of model selection in Cosmology and describe our work in this field.

We have carefully calculated the evidence for two adiabatic models and three physically-distinguishable isocurvature models using recent cosmic microwave background, supernovae and large-scale structure data. We find very similar evidences for all the models. For the first parametrization used, the odds of the isocurvature models compared to the adiabatic ones are 1 in about 4. Using a second parametrization of the isocurvature parameters we find the odds for the neutrino cases drop to 1 in 10. Therefore, we conclude that present data are unable to offer a clear verdict for or against the inclusion of isocurvature degrees of freedom. This conclusion is similar to that found by Parkinson et al. [154] using the information criteria. Although the extra parameters introduce extra complexity, these models are still able to satisfactorily fit the present data for a wide range of their parameters and thus the evidence quantifies the common sense that one should allow these models to be considered. We also showed the relevance of the parametrization for evidence computation.

While the present comparison is inconclusive, a key question for future data will be to select between the adiabatic and isocurvature paradigms. Parameter estimation analyses cannot do this, as even if the adiabatic model is correct they can only impose limits on the isocurvature parameters.

For the reasons explained above, we believe that the Bayesian model selection approach, and more generally Bayesian statistics, are the ideal tool to carry out such a selection.

Chapter 6

Results: Constraints on Isocurvature Parameters

During this thesis, we have developed the necessary tools for attacking the problem of isocurvature parameter determination both from a theoretical and a statistical point of view.

Hopefully, we have shown that both are equally important and failing to address any of these issues correctly may lead to erroneous conclusions.

In what follows, we present our work on parameter determination using different pieces of data and different optiques. On the first two analyses, we have adopted a completely phenomenological approach in which we first search for the possible isocurvature signal, and then we concentrate on particular models. Then, we adopt a different angle and first study the problem from a theoretical point of view, *i. e.* we study the possible signature of an axionic density (carrying forward the theoretical analysis from section 3.4 from Chapter 3), and then we specifically investigate its presence.

These two approaches should be equally valid as long as all the prior assumptions are clearly posed. Perhaps, from a model selection point of view, the last approach is better, in which less parameters are fitted obeying strong theoretical priors about the axionic signature. Nevertheless, it is useful to have a first order estimation of how strongly the isocurvature fraction could contribute, taking into account the effects of correlation and different tilts.

As has been mentioned above, on section 6.1, we bound the most general possible isocurvature model using three different pieces of data. On section 6.2, we add a new piece of data, namely the Lyman-α forest spectra and show the impact on the CDI model parameter posteriors. On section 6.3, we put experimental bounds on the model presented in section 3.4 in using, once again several pieces of data.

We will use different combinations of the following datasets: WMAP first and third year releases[4, 5] (WMAP-I, WMAP-III respectively); VSA, CBI and ACBAR

[128, 129, 130] for CMB data at small scales; The 2degree Field GRS [131] (2dF) and the Sloan Digital Sky Survey data releases 2004 [7]; two Supernovae compilations, the Hubble Space Telescope compilation [6] (SnH) and the Supernova Cosmology Project [179] (SnSCS). For the Lyman-α forest data, we use flux power spectra of the Croft et al. [104] (C02) sample and the LUQAS sample of high-resolution Lyman-α forest data [122]. We will usually refer to them by the names assigned above.

In all of the analyses, we assume that neutrinos are massless [183]. The simplest model dealt with consists of the adiabatic model 6 "vanilla" parameters [17] extended in some cases to a constant $w \neq -1$. Then, we also add the amplitude and spectral index of the primordial isocurvature perturbation; the amplitude and spectral index of the cross-correlation angle between the adiabatic and isocurvature modes. In addition, we will treat conservatively the matter-to-light bias of the 2dF and SDSS redshift surveys as two extra free parameters. These will be our assumptions throughout the whole chapter unless otherwise stated.

In general, we follow the procedure described in section 5.2.1 to obtain the probability distribution function for the parameters we want to constrain. The number of chains run varies from analysis to analysis according to our computation capabilities and particular requirements of the situation. In general, the total number of samples gathered is of order $\sim 3 - 8 \cdot 10^4$ and we eliminate about 40% of them in the burn in phase.

6.1 General constraints on isocurvature models from CMB, LSS and SNae data.

In this work (published in [14]) we study the bounds on the three different isocurvature modes described in Chapter 3. We allow for an arbitrary correlation between the adiabatic and isocurvature component with a free tilt for each of the three contributions. We will not assume any specific model of inflation, nor any particular mechanism to generate the perturbations (late decays, phase transitions, cosmic defects, etc.), and thus will allow all five modes — adiabatic (AD), baryon isocurvature (BI), CDM isocurvature (CDI), neutrino isocurvature density (NID) and neutrino isocurvature velocity (NIV) — to be correlated (or not) with each other , and to have arbitrary tilts.

We describe in more detail the analysis performed in Ref [13], constraining the various isocurvature components. We also extend it by including additional observational constraints, and extra free parameters in the model.

In terms of model building, the simplest situation beyond the paradigm of adiabaticity is that of a single isocurvature mode mixed with the adiabatic one. Therefore, we shall not consider more than one isocurvature mode at a time, and our primordial perturbations will be described by three amplitudes and three spectral

indices, associated respectively with the adiabatic, isocurvature and cross-correlated components. This choice is somewhat different from that of Refs. [148, 32, 33], who introduce several modes at a time, but a single tilt for each power spectrum of primordial perturbations. The assumption that all the modes have comparable amplitudes and a common tilt are both difficult to motivate theoretically and, to our knowledge, all proposed mechanisms based on inflation stand far from this case. For instance, double inflation leads to at most one isocurvature mode, always with a tilt differing from the adiabatic one; on the other hand, the curvaton scenario predicts a single tilt, but only one isocurvature mode, fully correlated or anti-correlated with the adiabatic mode. There is also the case of isocurvature perturbations generated by an axionic field during inflation. As we have seen on section 3.4, these are totally uncorrelated from the adiabatic perturbations and scale invariant. Nevertheless in the absence of any theoretical prior, we believe the approach of Refs. [148, 32, 33] is interesting and complementary to ours.

We slightly modified the interface between CAMB and CosmoMC in order to include the cross-correlated power spectra, as well as three independent tilts – in the CosmoMC jargon, the three tilts and the three amplitudes were implemented into the code as "fast parameters" , in order to save a considerable amount of time (see section 5.2.1). The likelihood of each model was then computed using the following data compilation: WMAP-I temperature and polarization data, VSA, CBI, ACBAR, LSS and SDSS and SnH[1], which adds up to 1627 data points.

As described above, and using the general notation of the thesis, the parameter space is: $\mathbf{p} = \{\omega_{\rm cdm}, \omega_b, \tau, \theta, w, n_{\rm ad}, \ln[10^{10}\mathcal{R}_{\rm rad}], \alpha, \beta, n_{\rm iso}, n_{\rm cor}\}$. We need to impose the following condition onto the correlation contribution (see section 3.2):

$$|\cos\Delta| = |\beta| \left(\frac{k}{k_0}\right)^{n_{\rm cor}} \leq 1 \tag{6.1}$$

With this in mind, we choose to define a new parameter:

$$\delta_{\rm cor} \equiv n_{\rm cor}/\ln(|\beta|^{-1}), \tag{6.2}$$

whose boundaries are fixed once and for all by the values of the pivot scale ($k_{\rm pivot} = 0.05$) and the scales ($k_{\rm min}$, $k_{\rm max}$) $=(4\cdot 10^{-4} h{\rm Mpc}^{-1}, 0.15 h{\rm Mpc}^{-1})$ defined by the extent of the dataset used. We will define our results in terms of this new parameter onto with we impose the flat prior $-0.14 \leq \delta_{\rm corr} \leq 0.4$.

We did not devote a specific analysis to the case of the baryon isocurvature modes, which is qualitatively similar to that of CDI modes, since the spectra are simply rescaled by a factor $\Omega_{\rm B}^2/\Omega_{\rm cdm}^2$ ($\Omega_{\rm B}/\Omega_{\rm cdm}$ for the cross-correlation): thus, compared to the AD + CDI case, significantly larger values of α will be allowed in the

[1]We have checked that the inclusion of the HST [144] and BBN priors are irrelevant for the determination of the Hubble parameter and the baryon density; that is, the data from CMB, LSS and SNIa is enough in order to determine these parameters, and therefore we ignored the priors in the final analysis.

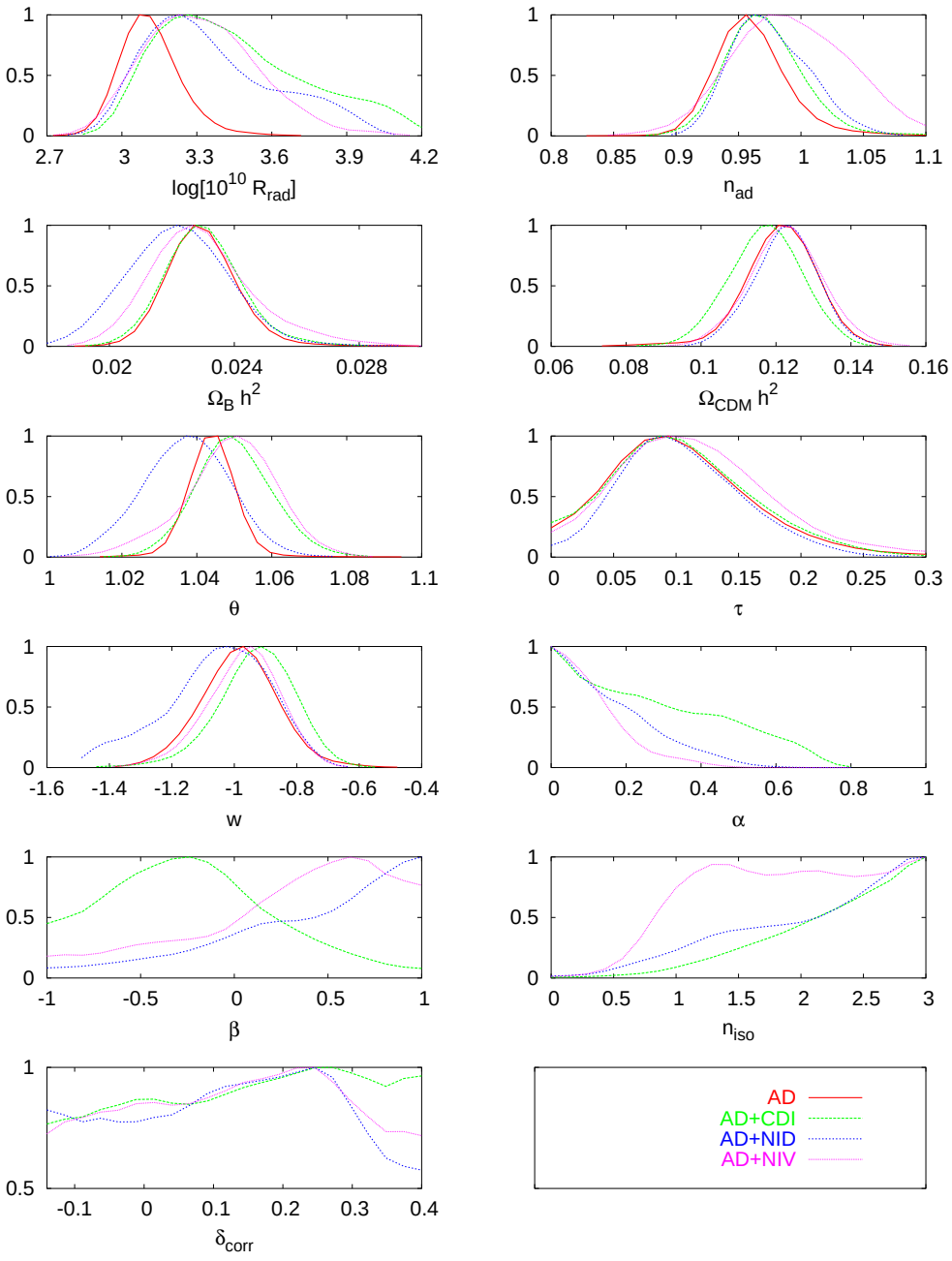

Figure 6.1: The one-dimensional likelihood functions for our basis of eleven independent cosmological parameters (not including the tilts of the two redshift surveys), for the adiabatic mode alone (AD) or mixed with the three different types of isocurvature modes (AD+CDI, AD+NID, AD+NIV). The first seven parameters are those of the standard ΛCDM model, extended to dark energy with a constant equation of state. The last four parameters $(\alpha, \beta, n_{\rm iso}, \delta_{\rm cor})$ describe the isocurvature initial conditions. ($\delta_{\rm cor}$ is define in Eq. (6.2.))

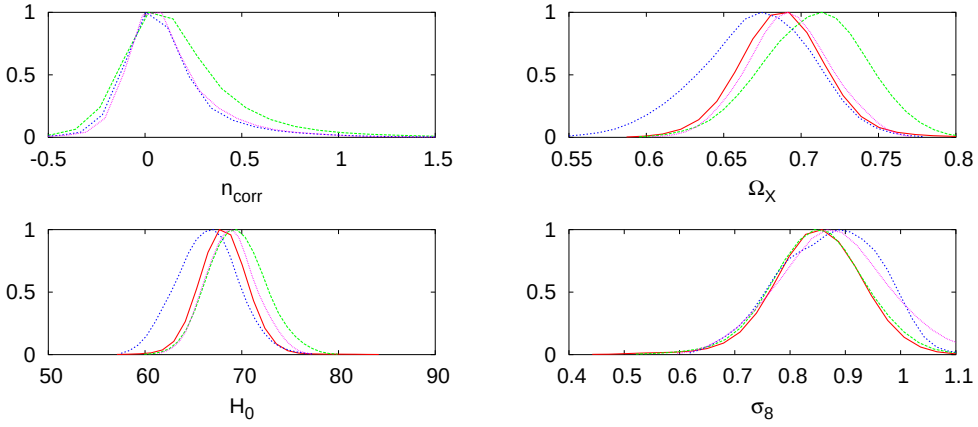

Figure 6.2: Continuation of figure 6.1, showing the 1D likelihood of some derived cosmological parameters, for the same cases. These likelihoods should be considered with care, because the parameters shown here do not belong to the basis used by the Markov chain algorithm. Therefore, the shape of the above likelihoods depends not only on the likelihood of the underlying parameters, but also on the properties of the functions relating them to the parameters of the basis. This explains for instance why $n_{\rm cor} = \delta_{\rm cor}\ \ln(|\beta|^{-1})$ seems to be well-constrained, while $\delta_{\rm cor}$ and β are not.

AD + BI case. Like in other recent analyses, we find that the inclusion of isocurvature modes does not improve significantly the goodness-of-fit of the cosmological model, since in the AD+CDI, AD+NID and AD+NIV cases the minimum χ^2 is always between 1672 and 1674 for 1614 degrees of freedom, to be compared with 1674 for 1618 degrees of freedom in the pure adiabatic case. Therefore, the question is just to study how much departure from the standard picture is allowed, by computing the Bayesian confidence limit on the isocurvature parameters. A more detailed analysis of model comparison with Bayesian Information Criteria [160] was described in Chapter 5 and published in [76].

On Fig. 6.1 we plot the marginalised likelihood for our basis of eleven cosmological parameters, in the cases AD+CDI, AD+NID and AD+NIV, compared with the pure adiabatic case. Figure 6.2 shows the likelihood of some derived parameters. It appears that most parameters are robust against the inclusion of isocurvature perturbations (this is in agreement with the conclusion of Ref. [33] that with only one isocurvature mode present, no significant parameter degeneracy emerges). Our 95% C.L. on α in the three cases is given in Table 6.1.

Note that in the limit $\alpha = 0$, the three parameters β, $n_{\rm iso}$, $\delta_{\rm cor}$ become irrelevant. So, the fact that pure adiabatic models are very good fits implies that these parameters are loosely constrained. This explains why the corresponding likelihoods on Fig. 6.1 are not well-peaked like for other parameters. In addition, these likelihoods should be considered with great care, because it is difficult for the Markov Chains

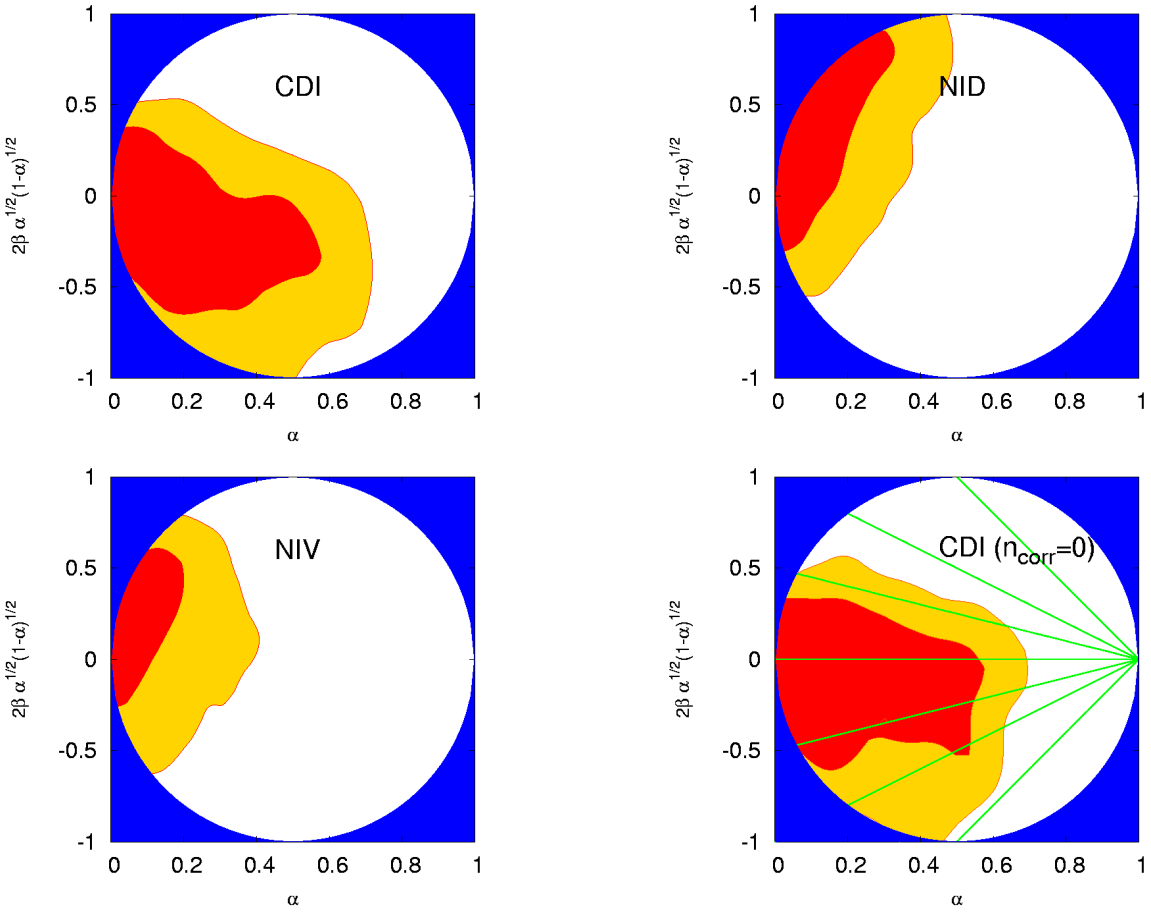

Figure 6.3: The 2-σ contours of α and the cross-correlated mode coefficient $2\beta\sqrt{\alpha(1-\alpha)}$, for a) the CDI isocurvature mode; b) the NID mode; c) the NIV mode; d) the CDI mode, with the constraint $n_{\rm cor} = 0$ and the contours of equal $2(R^2-1)/s_k = 0, \pm 0.5, \pm 1, \pm 2$ from double inflation.

to explore in detail the tails of the multi-dimensional likelihood corresponding to tiny values of α, where basically any value of (β, $n_{\rm iso}$, $\delta_{\rm cor}$) are allowed. Therefore, increasing the number of samples would tend to flatten these likelihoods, while the other ones would remain stable (as we checked explicitly). However, it is clear that all models prefer a large isocurvature tilt and saturate the bound $n_{\rm iso} < 3$ that we fixed in the present analysis. This feature is important for understanding our results and comparing with other analyses, as explained in the last paragraph of this section.

On Fig. 6.3, we plot the two-dimensional confidence levels directly for the isocurvature and cross-correlation coefficients (α, $2\beta\sqrt{\alpha(1-\alpha)}$) in the three cases AD+CDI, AD+NID and AD+NIV. The last plot corresponds to the AD+CDI case with a prior $n_{\rm cor} = 0$ which is relevant for the bounds on double inflation, but the results are not substantially different from the general AD+CDI case. We see that the AD+CDI

model	α	$2\beta\,[\alpha(1-\alpha)]^{1/2}$
AD+CDI	< 0.6	-0.7 to 0.3
AD+NID	< 0.4	-0.2 to 0.8
AD+NIV	< 0.3	-0.4 to 0.6

Table 6.1: The one-dimensional 2-σ ranges on the isocurvature mode coefficients for the various models.

model slightly prefers anti-correlated cases (note that $\beta < 0$ means a positive contribution from the cross-correlated component), while AD+NID and AD+NIV models clearly prefer correlated ones.

On Figure 6.4, we plot the CMB and LSS power spectra for two particular CDI and NID models. In order to get a better understanding of our bounds, we chose models with large values of α, still allowed at the 2-σ level: respectively, $\alpha = 0.53$ and $\alpha = 0.41$. The detailed values of other cosmological parameters are given on Table 6.2.

Parameter	CDI model	NID model
$\omega_{\rm B}$	0.0217	0.0196
$\omega_{\rm cdm}$	0.112	0.131
θ	1.06	(1.01)
τ	0.068	0.131
w	-0.88	-1.44
$\ln[10^{10}\mathcal{R}_{\rm rad}]$	3.73	3.98
$n_{\rm ad}$	0.96	1.02
α	0.53	0.41
$n_{\rm iso}$	2.93	2.95
$n_{\rm cor}$	0.05	0.03
β	-0.62	0.88

Table 6.2: Values for the parameters generating the plots in Fig. 6.4. The χ^2 of the two models is 1675 for the CDI model and 1674 for the NID.

In the CDI example, one can see that the non-adiabatic contributions to all spectra remain tiny, except for the matter power spectrum on scales $k > 0.2h\,{\rm Mpc}^{-1}$, due to the large isocurvature tilt $n_{\rm iso} = 2.93$ of the model. This is an indication that our α bound in the CDI case depends very much on constraints on the small-scale matter power spectrum, while future improvements in the determination of CMB spectra would not reduce it dramatically. We show this in the following section in which we include the Lyman-α forest data to cure this lack of data on small scales [15]. Note that a precise experimental determination of the amplitude parameter σ_8 (which is mainly sensitive to scales around $k = 0.2\,h$ Mpc^{-1}) would probably not

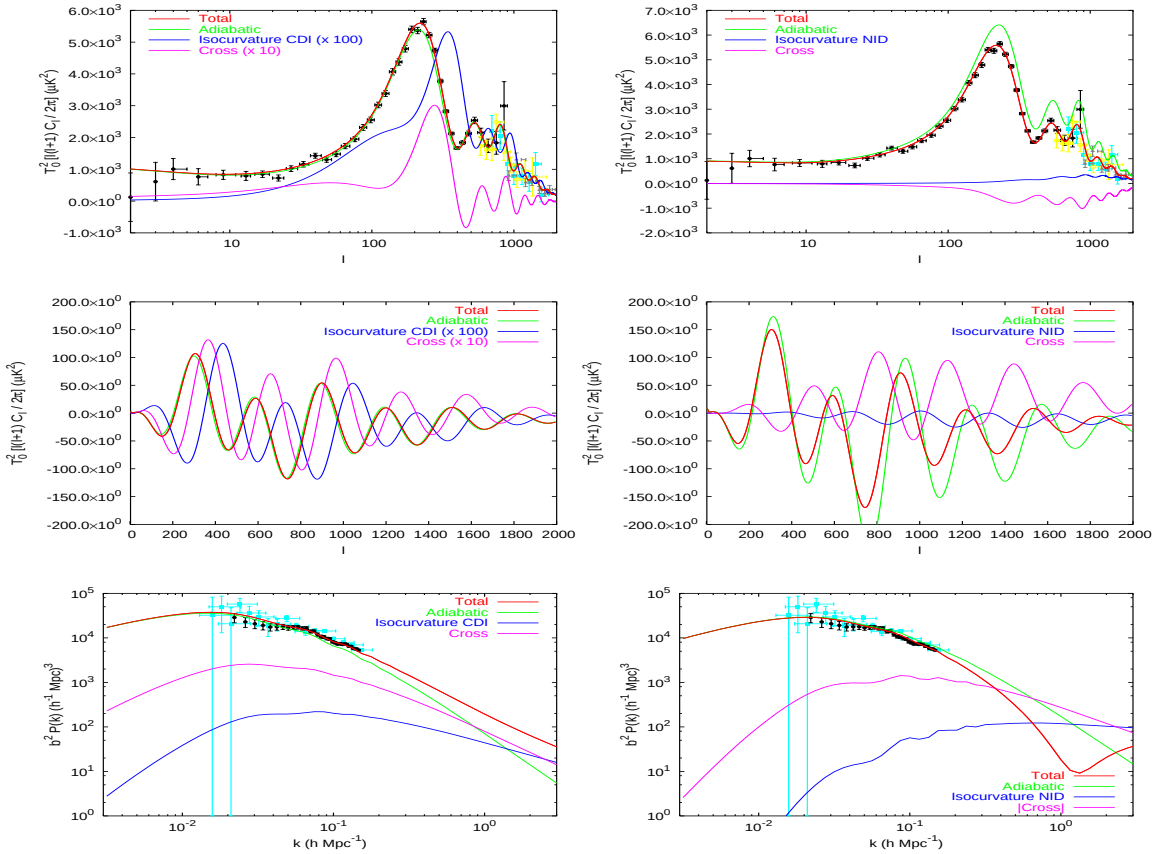

Figure 6.4: Temperature, E-polarization and matter power spectra for two particular CDI and NID models shown on table 6.2. From top to bottom, we show the $C_l^{\rm TT}$, $C_l^{\rm TE}$ and $P(k)$ power spectra, as well as the contribution of each component: adiabatic, isocurvature, cross-correlated, total. The CDI isocurvature and cross-correlated components have been rescaled by a factor indicated in each figure. We also show the data points that we use throughout the analysis, from WMAP (black), ACBAR (grey), CBI (blue), VSA (yellow), 2dF (black) and SDSS (blue).

change things either, since our CDI models have roughly the same σ_8 values as purely adiabatic well-fitting models (see Figure 6.2); on the other hand, any constraint on smaller wavelengths could improve the bounds. This means in particular that our choice not to include the Lyman-α data plays a crucial role in our results.

The same conclusions apply to the NID model of Fig. 6.4. In addition, in the NID case, we see that the non-adiabatic contribution is significant also for small-scale ($l > 200$) temperature and polarization spectra. Indeed, it is well-known that the NID isocurvature and cross-correlated modes can mimic the adiabatic CMB spectra to a better extent than CDI modes (essentially because the amplitude of the secondary peaks is not strongly suppressed). So, in the NID case, future improvement in the CMB data should help to improve the bounds on the isocurvature fraction.

Our bounds are difficult to compare with those of Ref. [33], because of our different parameter space, observational data set and conventions of normalization. In the AD+CDI case, our analysis is closer to the one of the WMAP team [4], although we have more free cosmological parameters ($n_{\rm cor}$, w), more data (SDSS, CBI, VSA) and less constraints on the matter–to–light bias. The 95% limit $\mathcal{B} < 0.33$ obtained by WMAP would correspond to $\alpha < 0.1$ in our notations, which is significantly smaller than our results. Also, The WMAP 1σ bounds on $n_{\rm iso}$ are 1.26 ± 0.5, while we find that the likelihood peaks at our maximum allowed value $n_{\rm iso} = 3$. The most likely explanation is that the use of the Lyman-α data in the WMAP analysis eliminates all our well-fitting models with $n_{\rm iso} > 2$ and large α values. Similar conclusions apply to our previous results [13], in which we did not use any Lyman-α information, but adopted a flat prior $0.6 < n_{\rm iso} < 1.5$ (this was the interval in which our grid of models was computed). Then, most of the well-fitting models of [13] had slightly negative values of $n_{\rm ad} - n_{\rm iso}$. Therefore, translating our previous results in terms of a pivot scale $k_0 = 0.05\,{\rm Mpc}^{-1}$ would lead to a small decrease in the α bounds, making them comparable with the WMAP bound in the CDI case, and smaller than the conservative bounds of this work. We now apply the estimated bounds to two specific, theoretically motivated inflationary models: Double inflation and a massive complex scalar field as the inflaton.

6.1.1 Specific isocurvature models: Double Inflation

We continue the theoretical model development from section 3.2.1 and impose bounds on the double inflationary given the data. Note that in this model it is assumed that the heavy field decays into cold dark matter, and therefore we only have one isocurvature component, CDI. The bounds from CDI will be used to constrain this particular model. We will leave for the future a detailed analysis of other two-field models of inflation.

In order to derive specific constraints, it will be useful to remind the relation between α and β, see Eqns. (3.51) and (3.52):

$$2\beta\sqrt{\alpha(1-\alpha)} = \frac{R^2-1}{s_k/2}\,(1-\alpha)\,, \tag{6.3}$$

which corresponds to a straight line in the contour plot of Fig. 3. This way, one can evaluate the likelihood at which a given value of R is ruled out. We present our results on the bottom right panel of Fig. 6.3 where the green lines fulfill relation (6.3) for different values of R, the ratio between the masses.

For the dataset used, we are able to impose a mild constraint onto R:

$$R < 5 \text{ a } 2\sigma \tag{6.4}$$

Even if the model passes this constraint for a given R, it is possible that the prediction on $n_{\rm ad}$ and $n_{\rm iso}$ from Eqns. (3.2.1) do not agree with the bounds on these

parameters. In our case, the bounds are so loose that any tilt is allowed. Perhaps in the future, with better observational constraints, we may use the information on the tilts to restrict more tightly double inflation models.

6.1.2 Specific isocurvature models: Massive complex field

Another model worth exploring is the particular one in which the two fields have equal masses, corresponding to a massive complex field $\Phi = \frac{1}{\sqrt{2}}(\phi_1 + i\,\phi_2)$. If we rewrite $\Phi = \frac{1}{\sqrt{2}}\sigma\,\exp(i\varphi)$, with modulus σ and phase φ, the lagrangian can be written as

$$\mathcal{L} = \frac{1}{2}(\partial_\mu\sigma)^2 + \frac{1}{2}\sigma^2(\partial_\mu\varphi)^2 - \frac{1}{2}m^2\sigma^2$$

Note that there is no potential for the phase, so it will be free to fluctuate, which will induce a large isocurvature component, as we will see, and which can be used to rule this model out.

In this case, the curvature and entropy perturbations are

$$\mathcal{R}_{\rm rad}(k) = -\frac{\kappa H_k}{\sqrt{2k^3}}\sqrt{s_k}\,e_\sigma(\mathbf{k})\,, \tag{6.5}$$

$$\mathcal{S}_{\rm rad}(k) = -\frac{\kappa H_k}{\sqrt{2k^3}}\frac{1}{\sqrt{s_k}}\,e_s(\mathbf{k})\,, \tag{6.6}$$

with e_σ and e_s orthonormal. Therefore,

$$\alpha = \frac{1}{s_k^2+1}\,, \qquad \beta = 0\,. \tag{6.7}$$

The curvature perturbation has a tilt $n_{\rm ad} = 1 - 2/s = 0.97$, but the isocurvature perturbation has no tilt, $n_{\rm iso} = 1$, and the two modes are uncorrelated, $\beta = 0$. For the moment, this model is not ruled out.

As mentioned above and shown on Fig. 6.4, we believe that the addition of data on scales smaller than those probed by galaxy surveys should be crucial for constraining isocurvature models with a free tilt. Therefore, we include the Lyman-α forest data to our analysis and study new bounds on the CDI model.

6.2 Squeezing the window on isocurvature modes with the Lyman-α forest.

We will use the dark matter power spectrum that Viel, Haehnelt & Springel [105] (VHS) inferred from the flux power spectra C02 sample and the LUQAS sample.

The C02 sample consists of 30 Keck high resolution HIRES spectra and 23 Keck low resolution LRIS spectra and has a median redshift of $z = 2.72$. The LUQAS sample contains 27 spectra taken with the UVES spectrograph and has a median redshift of $z = 2.125$. The resolution of the spectra is 6 km/s, 8 km/s and 130 km/s for the UVES, HIRES and LRIS spectra, respectively. The S/N per resolution element is typically 30-50. Damped and sub-damped Lyman-α systems have been removed from the LUQAS sample and their impact on the flux power spectrum has been quantified by [104]. Estimates for the errors introduced by continuum fitting, the presence of metal lines in the forest region and strong absorptions systems have also been made [113, 104, 180, 112].

The use of state-of-the-art hydrodynamical simulations is a significant improvement compared to previous studies which used numerical simulation of dark matter only [104]. We use the parallel TreeSPH code GADGET-II [182] in its TreePM mode which speeds up the calculation of long-range gravitational forces considerably. The simulations are performed with periodic boundary conditions with an equal number of dark matter and gas particles. Radiative cooling and heating processes are followed using an implementation similar to [108] for a primordial mix of hydrogen and helium. The UV background is given by [124]. To maximise the speed of the simulation a simplified criterion of star formation has been applied: all the gas at overdensities larger than 1000 times the mean overdensity is turned into stars [105]. The simulations were run on COSMOS, a 152 Gb shared memory Altix 3700 with 152 CPUs hosted at the Department of Applied Mathematics and Theoretical Physics (Cambridge).

Parameter basis and priors

We used the same parameter basis as in the previous section. Again, we define the amplitudes parameters at the pivot scale $k_0 = 0.05\,\mathrm{Mpc}^{-1}$. This time, we study a broader set of models. Later on, we show results for different parametrizations for the isocurvature fraction. We could decide to impose a flat prior on $f_{\rm iso}$, or α, or any function of them; different choices are not equivalent, in general. We will come back to the dependence of the final result on the choice of priors in section 6.2.2. Meanwhile, we chose a specific set of parameters which appear linearly in the expression of the observable power spectra, α and $2\beta\sqrt{\alpha(1-\alpha)}$, and that we believe are physically relevant. As already mentioned, these two parameter are defined within an ellipse, in which we assume a flat prior. Taking into account the enlarged reach in the k space we now must adopt a different prior on $\delta_{\rm cor}$ (see Eq. 6.1). Since $k_{\rm min} = 4 \times 10^{-5}\mathrm{Mpc}^{-1}$ and $k_{\rm max} = 2\,\mathrm{Mpc}^{-1}$ we must impose: $-0.14 < \delta_{\rm cor} < 0.27$.

In summary, our basis parameters with flat priors remains the same as in Section 6.1 with three exceptions:

- The bounds on $\delta_{\rm cor}$ are now extended.

- We use $2\beta\sqrt{\alpha(1-\alpha)}$ instead of β alone to parametrize the correlation amplitude.
- We fix $w = -1$.
- Due to the addition of the new Lyman-α data, we must include the Lyman-α calibration parameter $A_{\mathrm{Ly}-\alpha}$ defined in [125], on which we impose the same Gaussian prior $A_{\mathrm{Ly}-\alpha} = 1.0 \pm 0.29$.

Our full parameter space is therefore 13-dimensional. Following the usual procedure, we compute their marginalized Bayesian likelihood. The results are displayed in Fig. 6.5 and Table 6.3 (after marginalization over the 2dF and SDSS bias parameters).

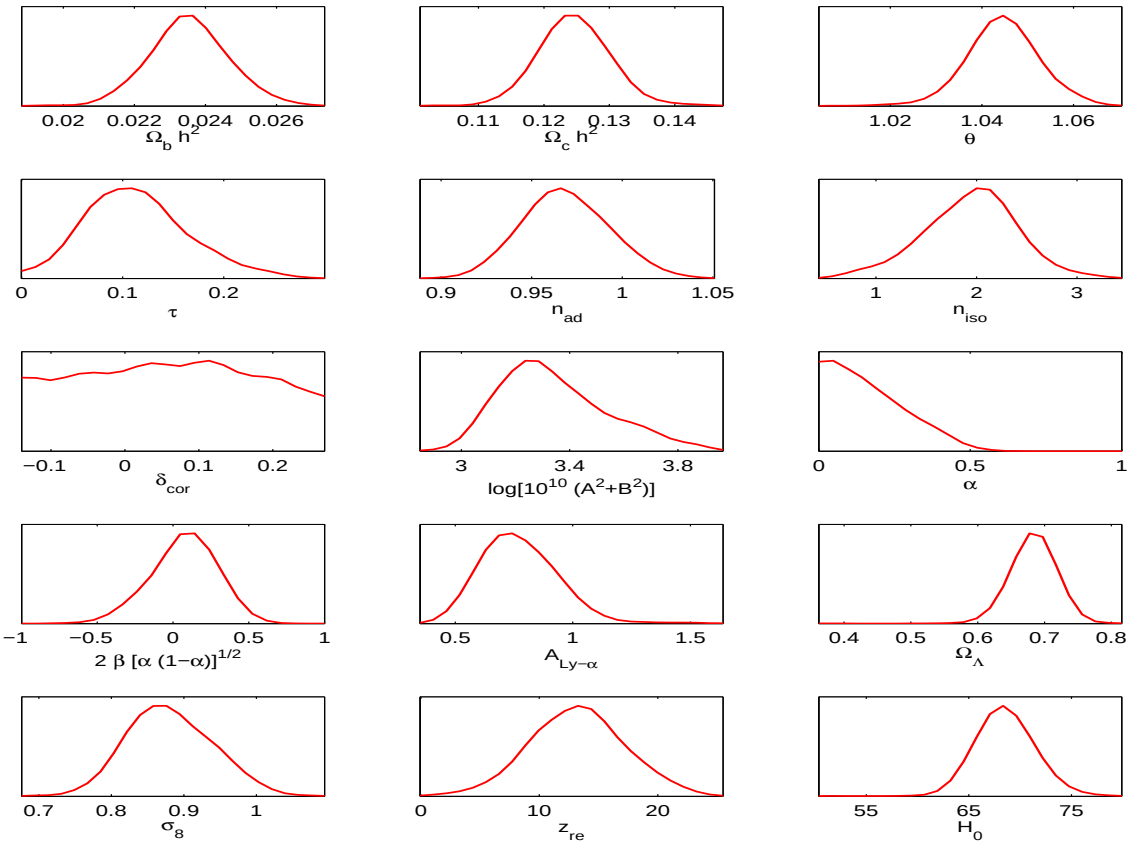

Figure 6.5: Likelihood for the AD+CDI model, using all our data set. The first eleven parameters are independent, while the last four are related parameters (with non-flat priors).

We see that the addition to new data favors purely adiabatic models, but remains compatible with an isocurvature fraction $\alpha < 0.40$ at the 2σ (95%) confidence level

parameter	1σ C.L.
$\Omega_b h^2$	0.0235 ± 0.0011
$\Omega_c h^2$	0.125 ± 0.005
θ	1.045 ± 0.008
τ	0.11 ± 0.05
$n_{\rm ad}$	0.97 ± 0.02
$n_{\rm iso}$	1.9 ± 0.5
$\delta_{\rm cor}$	within prior range
$\log[10^{10}(A^2 + B^2)]$	3.3 ± 0.2
α	< 0.20
$2\beta[\alpha(1-\alpha)]^{1/2}$	0.1 ± 0.2
$A_{{\rm Ly}-\alpha}$	0.8 ± 0.2
Ω_Λ	0.68 ± 0.03
σ_8	0.88 ± 0.06
$z_{\rm re}$	13 ± 4
H_0	69 ± 3

Table 6.3: 1σ confidence limits for the AD+CDI model, using all our data set, for the eleven basis parameters with flat priors, and below, for related parameters.

(CL), with a tilt $n_{\rm iso} = 1.9 \pm 1.0$ (2σ CL). The one-dimensional likelihoods for α, $2\beta\sqrt{\alpha(1-\alpha)}$ must be interpreted with care: the fact that these parameters are defined within an ellipse implies that there is more parameter space available near $\alpha = 0.5$ and $2\beta\sqrt{\alpha(1-\alpha)} = 0$.

More interesting are the two-dimensional likelihood contours for (α, $2\beta\sqrt{\alpha(1-\alpha)}$) displayed in Fig. 6.6, since in this representation the prior is really flat inside the ellipse. From this figure, it is clear that the data prefers an uncorrelated isocurvature contribution. The flatness of the $\delta_{\rm cor}$ likelihood shows that the data give no indication on the tilt of the cross-correlation angle.

6.2.1 Specific impact of the Ly-α data

The Lyman-α forest provides a powerful indication on both the amplitude and the shape of the matter power spectrum for $k > 0.01$ s/km, i.e. roughly larger than $1h$/Mpc. In order to illustrate the importance of this data set in our results, we repeat the same analysis without Lyman-α data. In this case, there are two options: we can either use the 2dF and SDSS galaxy power spectrum data as a constraint only on the *shape* of the matter power spectrum, as already done in the previously; or introduce a bias prior derived e.g. from the third and fourth-order galaxy correlation function of the 2dF catalogue [131, 4], in order to keep an information on the

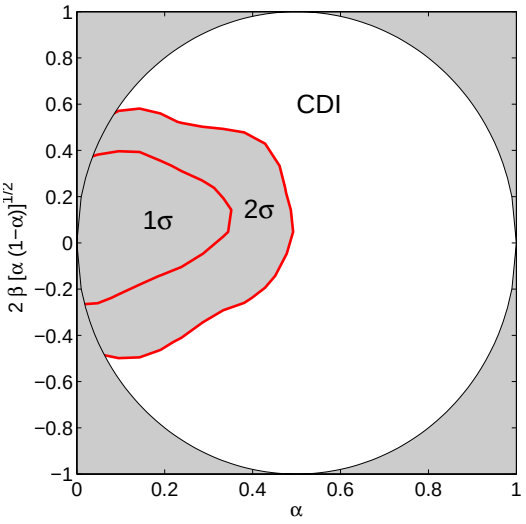

Figure 6.6: Two-dimensional likelihood for the amplitude of the isocurvature mode and of the cross-correlation component, near the pivot scale. We adopted a flat prior within the ellipse (which appears here as a circle) in which these parameters are defined.

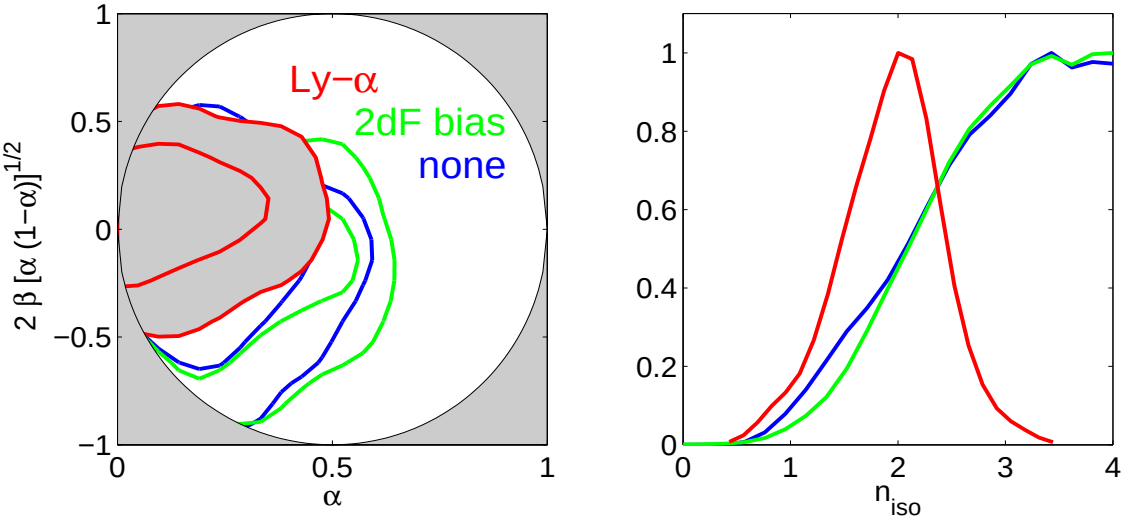

Figure 6.7: Likelihood of the isocurvature-related parameters, for the three combinations of data sets described in section 6.2.1: "Lyman-α" (red), "2dF bias prior" (green) and "none" (blue). *(Left)* Marginalized 1σ and 2σ confidence levels in the $(\alpha, 2\beta[\alpha(1-\alpha)]^{1/2})$ space. *(Right)* Marginalized probability distribution for $n_{\rm iso}$.

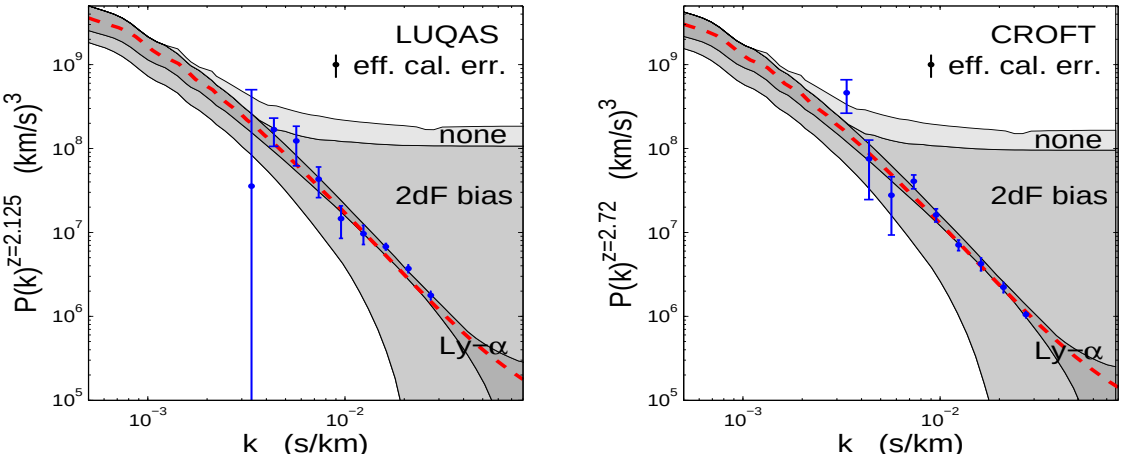

Figure 6.8: Favored ranges for the matter power spectrum $P(k)$ in the three runs "Lyman-α" (dark), "2dF bias prior" (medium) and "none" (light), compared with our Lyman-α data, from the LUQAS quasar spectra *(left)* and from the re-analyzed Croft et al. spectra *(right)*. The bands represent the envelope of all the matter power spectra in the Markov chains (after eliminating models with the worse likelihood). Each power spectrum has been computed at the median redshift of the data and re-expressed in units of km/s. In addition to the statistical errors, the data points share an overall effective calibration error, whose standard deviation is displayed in the top right corners. For the run including the Lyman-α data, each power spectrum has been divided by the value of the calibration parameter. The red dashed curves show the particular power spectrum discussed in section 6.2.1.

amplitude of the matter power spectrum[2].

For these three cases, that we call "Lyman-α", "2dFbias prior" and "none", the 2σ upper bound on α are respectively equal to 0.4, 0.5 and 0.5. The likelihoods for the most interesting parameters are displayed in Fig. 6.7. As expected, the Lyman-α data set is significantly more powerful than the 2dF bias prior for cutting out models with large α, and even more clearly, with large $n_{\rm iso}$ or large anti-correlation, as can be seen in Fig. 4. It is important to note that without these data, all results depend on our arbitrary prior $n_{\rm iso} < 4$: values far beyond this upper bound could still be compatible with the data, as also found in Ref. [156] when using the same pivot scale. In the presence of the Lyman-α data, we get a robust upper bound on $n_{\rm iso}$, and none of our priors play a role in the final results, with the exception of the well-motivated $\delta_{\rm cor}$ prior.

The impact of the Lyman-α data can be understood visually from Fig. 6.8. After running each case, we consider the collection of all matter power spectra in our Markov chains (except models with a bad posterior likelihood $\mathcal{L} < \mathcal{L}_{\rm max}/5$). The gray bands in Fig. 6.8 correspond to the envelope of all these $P(k)$'s, compared to the Lyman-α data points. As expected, when the Lyman-α is not used, the band gets very wide above the wavenumber $k \sim 0.2\ h/{\rm Mpc} \sim 2 \times 10^{-3}\,{\rm s/km}$ (note that for models with $n_{\rm iso} = 4$, the small-scale power spectrum is asymptotically flat). The role of the bias prior is marginal: it simply favors models with the lowest global normalization, but without affecting the isocurvature fraction and tilt. Using the Lyman-α data, we can exclude any break in the power spectrum on scales $k \leq 3\ h/{\rm Mpc} \sim\ 3 \times 10^{-2}\,{\rm s/km}$. This results in much stronger constraints for the parameters $(\alpha, \beta, n_{\rm iso})$, as can be seen from Fig. 4.

Checking the validity of the Ly-α data fitting procedure

We apply the strategy described in section 4.6 of Chapter 4 in order to check the validity of our Lyman-α data fitting procedure. We take the large number of samples contained in our Markov chains, and eliminate all models with a likelihood smaller than $\mathcal{L}_{\rm max}/10$ (in terms of effective χ^2, this corresponds to $\Delta\chi^2 = \chi^2 - \chi^2_{\rm min} > 20$). We then select the model with the largest value of α, which represents the strongest deviation from the purely adiabatic model. The corresponding matter power spectrum is plotted in Fig. 6.8 and has a break around $k \sim 5\ h/{\rm Mpc} \sim 5 \times 10^{-2}\,{\rm s/km}$. Above this wavenumber, the slope of the power spectrum is given by $n_{\rm iso} = 2.7$. For this "extreme" model, we perform a hydrodynamical simulation as described in section 4.6, and compare the bias function $b_F(k)$ with that assumed throughout the analysis. As shown in Fig.6.9, in the range $0.003 < k < 0.3\,{\rm km/s}$ probed by the data, the difference between the two functions is very small with respect to the statistical errors on the data. We conclude that in the present context,

[2]Technically, our bias prior is implemented in the same way as in Ref.[181]: see Eq. (27) and following lines in this reference.

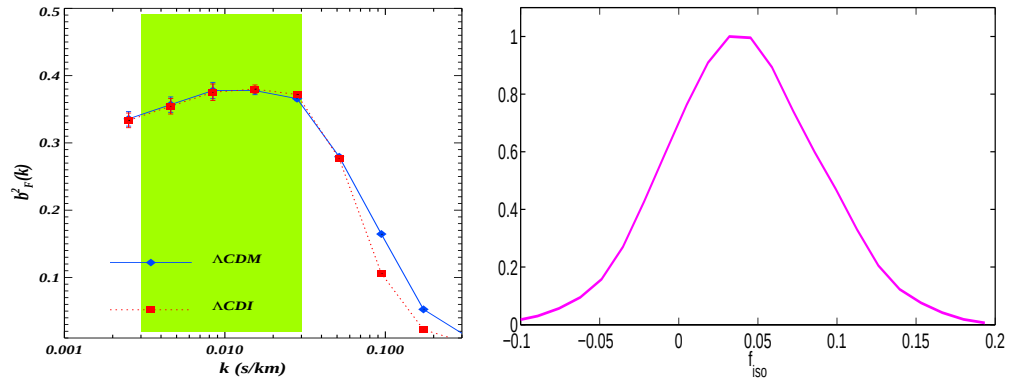

Figure 6.9: (*Left*) The ratio $b_F(k)^2 \equiv P_{\rm flux}(k)/P_{\rm matter}(k)$ at $z = 2.75$, computed from the hydrodynamical simulations as the ratio of the flux power spectrum (averaged over 1000 line-of-sights) over the input linear matter power spectrum. The solid blue curve shows the result for an adiabatic ΛCDM close to the best-fit model, while the dashed red curve was obtained from the "most extreme AD+CDI mixed model" defined in section 6.2.1 and here labelled as ΛCDI. The green band shows the region in which the Lyman-α data is used in the present analysis.(*Right*) Likelihood for $f_{\rm iso}$ in the curvaton model.

our Lyman-α data fitting procedure is robust, and does not introduce an error in the 1σ or 2σ bounds derived for each parameter of the AD+CDI mixed model.

6.2.2 The role of parametrization and priors

The fact of choosing a top-hat prior in the $(\alpha,\, 2\beta\sqrt{\alpha(1-\alpha)})$ parameter space is rather arbitrary. Other groups prefer to take top-hat priors on $f_{\rm iso}$, defined in Chapter 3, and $\cos\Delta = \beta$. Due to the non-linear transformation between the two basis, they are clearly not equivalent in terms of priors.

We checked this issue explicitly with an independent run based on the $(f_{\rm iso}, \cos\Delta)$ basis. The results are summarized in Fig. 6.10. As expected from the Jacobian, the $(f_{\rm iso}, \cos\Delta)$ option gives more weight to models with a small isocurvature fraction. For instance, the run with a flat prior on $f_{\rm iso}$ gives a 1σ bound $f_{\rm iso} < 0.26$, while that with a flat prior on α gives $f_{\rm iso} < 0.66$. However, at the 2σ level, the relative difference is small ($f_{\rm iso} < 0.75$ versus $f_{\rm iso} < 0.87$) because the Jacobian is asymptotically flat.

There is no absolute optimal choice of parameter basis and priors. This intrinsic ambiguity of Bayesian analyses should always be kept in mind, especially when quoting bounds on models which are not strictly needed by the data, which is the case here. However, it is reassuring that the 2σ contours obtained from the the two runs and compared in Fig. 6.10 are roughly in agreement.

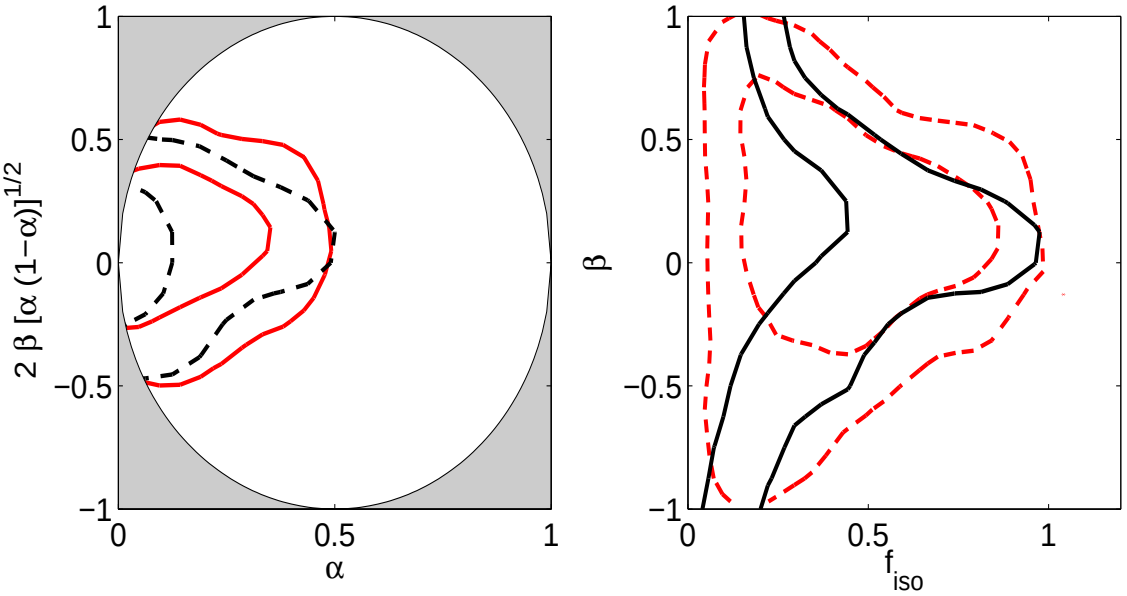

Figure 6.10: Two-dimensional 68% and 95% confidence limits for the CDI mode amplitude and cross-correlation angle (evaluated at the pivot scale). The two plots show the results of two independent runs with different parameter basis and priors. On the left (solid red curves), the parameters are $(\alpha,\, 2\beta\sqrt{\alpha(1-\alpha)})$, with a flat prior within the ellipse. On the right (solid black lines), the parameters are $(f_{\rm iso}, \cos\Delta)$, related to the previous parameters through Eqns.(3.21), with a flat prior within the square. The dashed curves show for comparison the likelihood contours obtained for one parameter set, assuming a flat prior on the *other* parameter set.

6.2.3 Specific isocurvature models: The curvaton

The curvaton hypothesis is an ingenuous way to generate the observed curvature perturbation from a field (the curvaton) different from that which drives inflation (the inflaton) [167]. In practice there is not much difference in the phenomenological signatures left in the CMB and LSS compared to an ordinary inflationary model. However, there are a few cases in which it is possible to leave a "residual" isocurvature component, together with the dominant curvature contribution. More specifically, in the curvaton models in which the curvaton field is responsible for the CDM component of matter, there are various possibilities depending on the time of creation of CDM versus the decay of the curvaton field.

In this section we derive bounds on this specific model. We developed the theoretical part in section 3.3 where the different scenarios were enumerated.

Since case 2) is already excluded at many sigma, and case 3) is essentially identical (except for $n_{\rm iso} = n_{\rm ad}$) to our generic analysis, we will concentrate on case 4) of a maximally anti-correlated mixture of isocurvature and adiabatic modes with equal tilts and $\delta_{\rm cor} = 0$. Our results are summarized on the right panel of Fig. 6.9, which shows the likelihood distribution for the generic curvaton model. We have used $n_{\rm ad} = n_{\rm iso}$, $\delta_{\rm cor} = 0$, and $\beta = \pm 1$, which is equivalent to $\beta = 1$ and $f_{\rm iso}$ positive or negative: $f_{\rm iso} > 0$ corresponds to $\beta = 1$, or positive correlation between $\mathcal{R}_{\rm rad}$ and $\mathcal{S}_{\rm rad}$, i.e. suppression of power in $P(k)$ and in the large-scale CMB temperature spectrum; while $f_{\rm iso} < 0$ corresponds to the opposite anti-correlated case.

We find $f_{\rm iso} = 0.04 \pm 0.09$ at the pivot scale at the 2σ-level, which implies $r > 0.98$ at the same CL (see section 3.3 for the definition of r). In our opinion, such a stringent constraint on the fraction of energy density in the curvaton at decay calls for a tremendous fine tuning (there is no physical reason to expect that the curvaton should decay precisely when it is starting to dominate the total energy density of the universe, within 2%), which makes the curvaton hypothesis in its most attractive scenario very unlikely.

6.2.4 Specific isocurvature models: Double inflation

Another chance to generate an observable isocurvature signature is through the possible presence of two scalar fields driving inflation [35, 36, 72, 73]. The simplest case at hand is that of two massive fields coupled only gravitationally:

$$\mathcal{L} = \frac{1}{2}(\phi_{h;\mu}\phi_h^{;\mu} - m_h^2\phi_h^2) + \frac{1}{2}(\phi_{l;\mu}\phi_l^{;\mu} - m_l^2\phi_l^2) \ , \tag{6.8}$$

where m_h and m_l are the masses of the heavy and light fields respectively.

We assume slow-roll conditions during inflation, and use the number of e-folds

till the end of inflation $s = -\ln(a/a_{\rm end})$ to parametrize the fields as:

$$\phi_h^2 = \frac{s}{2\pi G}\sin^2\theta;\ \phi_l^2 = \frac{s}{2\pi G}\cos^2\theta\ , \tag{6.9}$$

Using the field and Friedmann equations, we can solve for the rate of expansion during inflation:

$$H^2(s) \simeq \frac{2}{3}s\cdot m_l^2[1+(R^2-1)\sin^2\theta]\ , \tag{6.10}$$

where $R = m_h/m_l$, and find the number of e-folds as a function of θ:

$$s(\theta) = s_0\frac{(\sin\theta)^{2/(R^2-1)}}{(\cos\theta)^{2R^2/(R^2-1)}}\ . \tag{6.11}$$

The perturbed Einstein equations can be solved for long wavelength modes in the longitudinal gauge. Assuming that the heavy field decays into CDM whereas the ligth field produces other species, we find the magnitudes of the curvature and entropy perturbation at horizon crossing. During radiation domination and for super-Hubble modes, this gives:

$$\begin{aligned}
\mathcal{R}_{\rm rad}(k) &= -\sqrt{\frac{4\pi G}{k^3}}H_k s_k^{1/2}\Big(\sin\theta_k\, e_h(\mathbf{k}) + \cos\theta_k\, e_l(\mathbf{k})\Big)\\
\mathcal{S}_{\rm rad}(k) &= \sqrt{\frac{4\pi G}{k^3}}H_k s_k^{-1/2}\left(\frac{e_h(\mathbf{k})}{\sin\theta_k} - \frac{R^2\, e_l(\mathbf{k})}{\cos\theta_k}\right)
\end{aligned} \tag{6.12}$$

where $e_i(\mathbf{k})$ are gaussian random fields associated with the quantum fluctuations of the fields, and the subindex k implies the value of the corresponding quantity at horizon crossing during inflation. One typically expects $s_k \simeq 60$. It can be seen from (3.19) that the correlation power spectrum has no scale dependence, and thus, for this model $n_{\rm cor} = 0$, while the adiabatic and isocurvature tilts are described on Eqns. (3.2.1)). Their values, for $s_k = 60$, are typically $n_{\rm ad} = 0.97$ and $n_{\rm iso}$ in the range $[0.97, 0.90]$ for $R \in [1, 4]$. Since $n_{\rm iso} > 0.93$ at 95% c.l., models with large values of R are ruled out.

It was shown in [14] that a relationship between α and β can be found. It can be simply expressed as a straight line in our parameter space:

$$2\beta\sqrt{\alpha(1-\alpha)} = \frac{2(R^2-1)}{s_k}(1-\alpha)\,. \tag{6.13}$$

On the other hand, for these models, the parameters α and β have minimum and maximum values respectively, which only depend on the ratio R and the number of

e-folds s_k,

$$\alpha_{\rm min} = \frac{(R^2+1)^2}{s_k^2+(R^2+1)^2}\,, \tag{6.14}$$

$$\beta_{\rm max} = \frac{R^2-1}{R^2+1}\,, \tag{6.15}$$

$$2\beta\sqrt{\alpha(1-\alpha)}\Big|_{\rm max} = \frac{2s_k(R^2-1)}{s_k^2+(R^2+1)^2}\,. \tag{6.16}$$

Applying the results of our data analysis, we find that the inclusion of the Lyman-α data significantly improves the previous bound on R to $R < 3$ at 95% c.l. This bound comes mainly from a combination of bounds on $2\beta\sqrt{\alpha(1-\alpha)}$ and $n_{\rm iso}$.

We did not find necessary to generate a $n_{\rm cor} = 0$ sampling for this model. In our results, the parameter $\delta_{\rm cor}$ has a flat distribution and thus is unconstrained. We therefore expect similar results when fixing it to zero.

6.3 Bounds on the axionic window

As explained above and in Chapter 3, the existence of an axionic field during inflation (*i. e.* axions generated via the misalignment angle mechanism) could lead to an isocurvature perturbation on large scales with a strenght that would depend on the particular model and the value of the initial misalignment angle.

In this section we continue the theoretical analysis from section 3.4 and challenge the presence of this isocurvature signal in light of the available data. We also consider possible scenarios in which our conclusions would not hold. We must be clear about the fact that we are considering a particular set of hypothesis and if these fail to occur we cannot ensure the validity of our results.

We not only take into account purely cosmological considerations but we also apply constraints on f_a coming also from astrophysical constraints.

6.3.1 Non-Isocurvature bounds on the axionic scale

We now describe bounds on the axionic parameters coming from sources other than the isocurvature component in the CMB. Note that some of the following bounds are generic and apply to every production mechanism or inflationary scenario while some others are rather model dependent. More precisely, we will enumerate the different bounds on the axion parameter space ($M_{\rm inf}$, f_a) associated with the misalignment mechanism of axion production during inflation, $M_{\rm inf}$ being the energy scale during

inflation

$$M_{\rm inf} = \sqrt{\frac{M_{\rm P} H_{\rm inf}}{\sqrt{8\pi/3}}}\,,$$

and $M_{\rm P} \equiv G^{-1/2}$ is the Planck mass. The explicit implications of these bounds are presented on Figs. 6.12.

The scale of inflation

The non-detection of tensor modes [5] imposes a constraint on the inflationary scale. The current bound on the tensor to scalar ratio is:

$$r \sim \left(\frac{4\times 10^4\, H_{\rm inf}}{M_{\rm P}}\right)^2 < 0.3 \quad \text{at } 95\% \text{ c.l.}\,, \tag{6.17}$$

which sets an upper bound on the inflationary scale:

$$M_{\rm inf} < 3\times 10^{16}\ \text{GeV}\,. \tag{6.18}$$

In Figs. 6.12, this constraint corresponds to the hatched forbidden region.

Supernova 1987A bounds

The observed neutrino luminosity from supernova 1987A imposes a bound on the axion luminosity that is saturated for $10^{-2}\,\text{eV} < m_a < 2\,\text{eV}$ [45]. Other astrophysical and laboratory searches rule out an axion heavier than 1 eV (see [42, 45] for a detailed discussion). Therefore, we have:

$$m_a < 10^{-2} - 10^{-3}\ \text{eV}\,, \tag{6.19}$$

or equivalently, $f_a > 10^9 - 10^{10}$ GeV. The forbidden region is (blue-)shaded in Figs. 6.12.

Axionic cosmic strings production

As mentioned before, in the case of symmetry restoration at high energy, axions can be produced from the decay of cosmic strings, and we should impose a bound on their relic density

$$\omega_{\rm a}^{\rm str} \leq \omega_{\rm cdm}\ , \tag{6.20}$$

where ω_i stands for $\Omega_i h^2$ and $\Omega_{\rm a}^{\rm str}$ is taken from Eq. (3.87). Taking $\Omega_{\rm cdm}\, h^2 < 0.123$ (see Eq.(6.33)) we get

$$f_a < 1.25\times 10^{11}\text{GeV}\ . \tag{6.21}$$

This inequality must be imposed in two cases: $f_a > (H_{\rm inf}/2\pi)$, corresponding to symmetry restoration during inflation[3] [67], and $f_a > T_{\rm rh}$, corresponding to symmetry restoration after reheating [58]. Actually, it is worth mentioning that thermal corrections induce a positive mass-squared term $m^2_{\rm eff} = T^2_{\rm rh}/12$, so the precise condition for symmetry restoration is

$$T^2_{\rm rh}/12 \gg \lambda f_a^2 \ . \tag{6.22}$$

Therefore, the usual statement that symmetry is restored whenever $f_a > T_{\rm rh}$ assumes that the self-coupling constant λ is of the order of 0.1. We will proceed with this assumption, but one should keep in mind that the exact condition is model-dependent.

The actual reheating temperature $T_{\rm rh}$ is still unknown. This is the temperature at which the inflaton decays, once its half life has been exceeded by the age of the universe, that is, when $H \sim \Gamma$. Most of the thermal energy comes from perturbative decays of the inflaton and, assuming that the decay products are strongly interacting at high energies, we can estimate the reheating temperature as

$$T_{\rm rh} \simeq 0.1\,\sqrt{\Gamma M_P} \simeq 0.02\,h_{\rm eff}\,\sqrt{m\,M_P} \leq 2\times 10^{11}\ {\rm GeV}\,, \tag{6.23}$$

where $\Gamma = h^2_{\rm eff} m/8\pi$ is the inflaton decay rate, which is typically proportional to the inflaton mass, m, with $h_{\rm eff} \leq 10^{-3}$, in order to prevent radiative corrections from spoiling the required flatness of the inflaton potential [65]. This estimate shows the generic inefficiency of reheating after inflation, where the scale of inflation could be of order 10^{15} GeV and the reheating temperature ends being many orders of magnitude lower. For instance, for Starobinsky type inflation, the weak gravitational couplings give a reheating temperature of order $T_{\rm rh} \sim 10^9$ GeV, while in chaotic inflation models, typical values are of order $10^{10} - 10^{11}$ GeV. We can parametrize the effect on the rate of expansion by introducing an efficiency parameter, $\epsilon_{\rm eff}$, such that $H_{\rm rh} = \epsilon_{\rm eff}\,H_{\rm end}$. Values of ϵ range from 10^{-13} for Starobinsky inflation, to order one for very low scale inflation.

Within certain low scale inflationary models, such as hybrid inflation, the efficiency of reheating can be significant because the rate of expansion at the end of inflation is much smaller than any other mass scale and the inflaton decays before the universe has time to expand, therefore all the inflaton energy density gets converted into radiation.

We can parametrize the effect on the rate of expansion by introducing an efficiency parameter, $\epsilon_{\rm eff}$, such that $H_{\rm rh} = \epsilon_{\rm eff}\,H_{\rm end}$. Values of ϵ range from 10^{-13} for Starobinsky inflation, to order one for very low scale inflation. If the reheating temperature is higher than f_a it could eventually lead to a restoration of the PQ

[3]Note that for simplicity, we impose this condition as if $H_{\rm inf}$ was constant at least during the observable e-folds of inflation (typically, the last sixty e-folds). In principle, the amplitude of quantum fluctuations ($H_{\rm inf}/2\pi$) could fall below f_a precisely during the observable e-folds, see e.g. [69], but we will ignore this possibility here.

symmetry. The subsequent spontaneous symmetry breaking would generate axionic cosmic strings that would not be diluted away by inflation.

In summary, if the PQ symmetry is restored by thermal fluctuations after reheating, i.e.

$$T_{\rm rh} = 0.1\sqrt{H_{\rm rh} M_{\rm P}} = 0.1\sqrt{\epsilon_{\rm eff} H_{\rm inf} M_{\rm P}} > f_a\,, \tag{6.24}$$

then we must impose the condition (6.20). In Figs. 6.12, we have distinguished two cases: one in which the process of reheating the universe is very inefficient ($\epsilon_{\rm eff} \leq 10^{-12}$), and there is no thermal restoration of the PQ symmetry after inflation, and another one in which $\epsilon_{\rm eff} = 10^{-4}$ so that the symmetry might be restored. In both cases the constraint coming from string production and decay corresponds to the triangular (red-)shaded exclusion region.

Cold Dark Matter produced by misalignment

As for axions produced by string decay, the relic density of axions produced by misalignment should not exceed the total cold dark matter density:

$$\omega_{\rm a} \equiv \Omega_a\, h^2 \simeq 1.3\langle\Theta_1^2 f(\Theta_1)\rangle \left(\frac{1\,\mu{\rm eV}}{m_a}\right)^{7/6} = 2.8\times 10^7 \langle\Theta_1^2 f(\Theta_1)\rangle \left(\frac{f_a}{M_{\rm P}}\right)^{7/6} \lesssim\ \omega_{\rm cdm}\,. \tag{6.25}$$

The bounds on $\omega_{\rm cdm}$ from our analysis and considerations about the particular inflationary model put severe constrains on the axion window. First, the inequality (6.25) provides a stringent upper limit on f_a if $\langle\Theta_1^2 f(\Theta_1)\rangle$ is of order one. In particular, in the case of complete quantum diffusion during inflation, we have seen that $\langle\Theta_1^2 f(\Theta_1)\rangle = 1.2\,\pi^2/3$ and

$$f_a \leq 2.5\times 10^{11}{\rm GeV}\left(\frac{\omega_{\rm cdm}}{0.12}\right)^{6/7}. \tag{6.26}$$

This constraint is shown in Figs. 6.12 as a dotted line, excluding the light green region.

In the absence of efficient quantum diffusion, Θ_1 could take any nearly homogeneous value in our Universe: so, it is possible in principle to assume that $\langle\Theta_1^2 f(\Theta_1)\rangle$ is extremely small (this coincidence can be justified by anthropic considerations[4]),

[4]There has been plausible speculations that our presence in the universe may not be uncorrelated with the values of the fundamental parameters in our theories. Such anthropic arguments normally arise in terms of conditional probability distributions of particular observables. In particular, the axion abundance is a natural parameter that could be bounded by those arguments, see e.g. Refs. [69, 139] where it is suggested that the initial misalignment angle should be such that the main CDM component be axionic. In this case, one has a concrete prediction for $R_{\rm a} = \Omega_{\rm a}/\Omega_{\rm cdm} = 1$, and therefore the initial misalignment angle is directly related to the axion mass, see Eq. (6.25),

$$m_a = 9\,\mu{\rm eV}\,\langle\Theta_1^2 f(\Theta_1)\rangle^{6/7}\,. \tag{6.27}$$

Having full diffusion, $\langle\Theta_1^2 f(\Theta_1)\rangle \sim 1.2\pi^2/3$, implies $m_a \sim 30\,\mu$eV, just within reach of present

and to relax the bound on f_a. However, the mean square cannot be fine-tuned to be smaller than the amplitude of quantum fluctuations at the end of inflation. Using Eq. (3.96), we see that $\langle\Theta_1^2\rangle$ can only vary within the range

$$\left(\frac{H_{\rm inf}}{2\pi f_a}\right)^2 \Delta N < \langle\Theta_1^2\rangle < \frac{\pi^2}{3} \,, \tag{6.28}$$

with $\Delta N \sim 30$ is the number of inflationary e-folds associated with scales that reentered the Hubble radius when the QCD transition took place, see Eq. (3.97). This gives a model-independent constraint

$$M_{\rm inf} \leq 2.5\times 10^{15}{\rm GeV}\left(\frac{\omega_{\rm cdm}}{0.12}\right)^{1/4}\left(\frac{30}{\Delta N}\right)^{1/4}\left(\frac{f_a}{10^{12}{\rm GeV}}\right)^{5/24} \tag{6.29}$$

which holds only in the region where

$$\left(\frac{H_{\rm inf}}{2\pi f_a}\right)^2 \Delta N < \frac{\pi^2}{3} \,, \tag{6.30}$$

otherwise it should be replaced by (6.26). This bound excludes the dark green region in Figs. 6.12.

6.3.2 Isocurvature bounds on the axionic scale

As mentioned before, the axionic field induces an isocurvature component in the CMB anisotropies that must be considered when constraining the model. In this work, we assume that axions are the only source of isocurvature modes. Taking expression (3.108) for the isocurvature fraction α, replacing $R_{\rm a}$ by $\omega_{\rm a}/\omega_{\rm cdm}$ and using Eq. (6.25), we obtain

$$\alpha = \frac{0.9\times 10^7 \epsilon_k}{\omega_{\rm cdm}^2}\left(\frac{M_{\rm P}}{f_a}\right)^{5/6} \,. \tag{6.31}$$

The analysis of the next section will provide bounds on α and $\omega_{\rm cdm}$. Also, it will give constraints on the curvature power spectrum $\langle|\mathcal{R}(k)|^2\rangle$, from which one can derive a relation between ϵ_k and $M_{\rm inf}$, using equation (3.103). Therefore, the amplitude of isocurvature modes provides some independent constraints in the ($M_{\rm inf}$, f_a) plane, corresponding to the (yellow-)dashed forbidden region in Figs. 6.12.

We should distinguish here between two cases:

- **Quantum de Sitter fluctuations induce PQ symmetry restoration during inflation**. We have already seen that in this case, the real and imaginary parts of the PQ behave like light fields during inflation, thus leaving a long wave isocurvature perturbation on the axion field. In this case, the above constraint from CMB anisotropies is applicable.

axion dark matter experiments. On the other hand, we might happen to live in an unusual region of the universe with an extremely low value of $\langle\Theta_1^2\rangle$, a large value of f_a and still $R_a = 1$.

Parameter	Prior probability range
$\omega_{\rm B}$	(0.016,0.030)
$\omega_{\rm cdm}$	(0.08,0.16)
θ	(1.0,1.1)
τ	(0.01,0.2)
$n_{\rm ad}$	(0.85,1.1)
A_s	(2.7,4.5)
$\lvert\alpha\rvert$	$(-1,1)$

Table 6.4: Prior probability ranges of the sampled parameters (we sampled from $|\alpha|$ instead to avoid boundary effects near the maximum likelihood region).We set our pivot scale at $k = 0.002$ Mpc^{-1}.

- **Thermal fluctuations induce PQ symmetry restoration after reheating**. If the reheating temperature is much higher than f_a then one expects thermal fluctuations to modify the effective PQ potential and induce a positive mass-squared term, $m_{\rm eff}^2 = T^2/12 \gg \lambda f_a^2$. In this case, the radial part is quickly driven to zero everywhere in the universe. All previous axion fluctuations are erased and we are left with no bounds from axion isocurvature temperature anisotropies. So, for sufficiently large $\epsilon_{\rm eff}$, the isocurvature constraint does not apply above a given line in the ($M_{\rm inf}$, f_a) plane , and the allowed region is split in two parts (as in the right panel of Fig. 6.12).

6.3.3 Axionic window and the Inflationary Model

Under the assumptions stated on section 6.1 (and w fixed to -1) plus the general considerations mentioned above, we want to tighten the current allowed range for f_a. Thus, we need to compute the allowed cold dark matter and isocurvature contribution given several sets of data, namely WMAP-III (TT, TE and EE), VSA, CBI, and ACBAR; large scale structure data from SDSS and 2dF, and the SnSCS experiment.

Our parameter space and the top hat prior probability distribution that was assigned to each parameter are described in table 6.4 where α is measured at a pivot scale $k = 0.002$ Mpc^{-1}. Note that previous studies [14] indicated a very weak sensitivity of this data to $n_{\rm iso}$, while in our model $n_{\rm iso} = 1 - 2\epsilon_k$ is very close to one. So, we safely fix $n_{\rm iso}$ to exactly one without modifying the results. We used the Metropolis-Hastings algorithm implemented by the publicly available code `CosmoMC` [127] to obtain 32 Monte Carlo Markov chains, getting a total of 1.1×10^5 samples. We find a $\chi^2/{\rm DOF} = 1.01$ and the worst variance of chain means over the mean of chain variances value is 1.04 (See Chapter 5 and [172]).

The one dimensional posterior probability distributions for sampled and derived

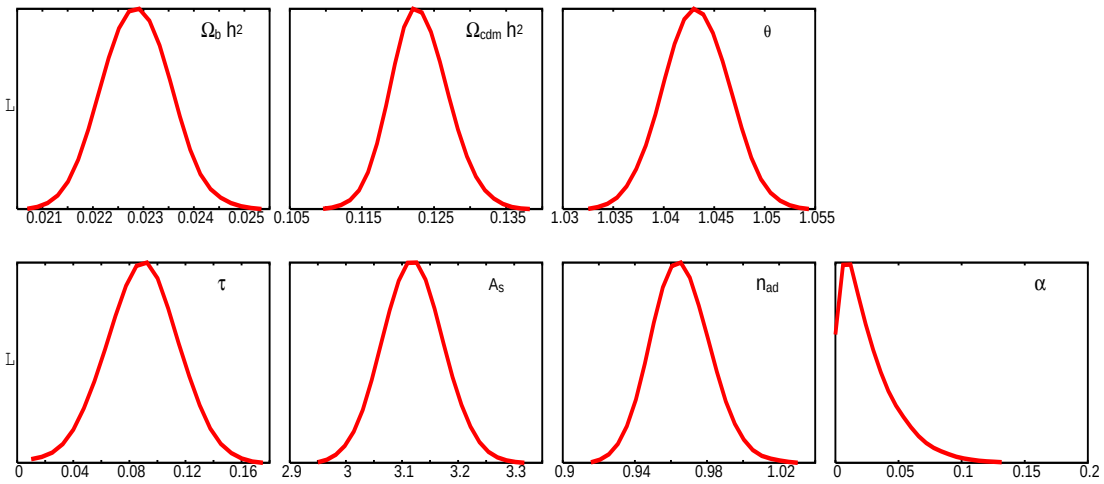

Figure 6.11: The one dimensional distributions of the sampled parameters.

parameters are depicted in Fig. 6.11. In particular, the best-fit value for α is $\alpha = 8 \times 10^{-4}$, and the 2σ bound for the marginalized distribution is:

$$\alpha < 0.08 \text{ at } 95\% \text{ c.l} \tag{6.32}$$

while for $\Omega_{\rm cdm}\, h^2$ we get:

$$\Omega_{\rm cdm}\, h^2 = 0.123 \pm 0.008 \text{ at } 95\% \text{ c.l.} \tag{6.33}$$

Due to the entanglement existing for the axionic scale and the inflationary scale, it is very hard to make a model independent analysis to predict the allowed range inside the parameter of space. As a matter of fact, we do need to consider which inflationary model we assume is taking place to be able to consistently impose bounds on the axionic model. Therefore, we first analyze our results under the least possible assumptions and then we explicitly choose one inflationary model and impose particular bounds under that assumption.

A (nearly) model-independent analysis

At least two bounds in the $(f_a, M_{\rm inf})$ plane are completely model-independent: the upper bound $M_{\rm inf} < 3 \times 10^{16}$ GeV, coming from the non-observation of gravitational waves in the CMB and the lower bound $f_a > 10^{10}$ GeV from astrophysical constraints (see Sec. 6.3.1).

When the PQ symmetry is restored at high energy, we must impose $\omega_{\rm a}^{\rm str} < 0.123$, where $\omega_{\rm a}^{\rm str}$ is taken from Eq. (3.87): this gives $f_a < 1.25 \times 10^{11}$GeV. As explained in Secs. 6.3.1 and 6.3.2, this constraint applies when $(H_{\rm inf}/2\pi) > f_a$ during inflation

and also when $T_{\rm rh} > f_a$ after reheating (the latter bound depends on $\epsilon_{\rm eff}$ in each particular model).

Even if there is no significant axion relic density from string decay, there is one associated with the misalignment angle mechanism. As explained in Sec. 6.3.1, the constraint $\omega_a < 0.123$ gives $f_a < 2.5 \times 10^{11}{\rm GeV}$, unless the misalignment angle is fine-tuned to very small values. In the latter case, there is still a much weaker model-independent bound

$$M_{\rm inf} \leq 2.5 \times 10^{15}{\rm GeV} \left(\frac{f_a}{10^{12}{\rm GeV}}\right)^{5/24} . \tag{6.34}$$

All these bounds are summarized on Figs. 6.12, with thick solid lines for model-independent constraints, and dotted lines for model-dependent ones.

Let us finally discuss the impact of the isocurvature mode limit $\alpha < 0.08$, which applies as long as the PQ symmetry is not restored by thermal corrections, $T_{\rm rh} < f_a$. Our results for the amplitude of the primordial curvature spectrum gives a relation

$$\epsilon_k \sim 3 \times 10^8 \left(\frac{M_{\rm inf}}{M_{\rm P}}\right)^4 . \tag{6.35}$$

Substituting in Eq. (6.31), we see that the constraint $\alpha < 0.08$ finally gives

$$M_{\rm inf} \leq 10^{13}{\rm GeV} \left(\frac{f_a}{10^{12}{\rm GeV}}\right)^{5/24} . \tag{6.36}$$

So, the isocurvature mode limit excludes a large region in parameter space, and *preserves only two regions* The first one is present only if reheating is efficient enough, $\epsilon_{\rm eff} \geq 4 \times 10^{-12}$, and obeys to

$$10^{10}{\rm GeV} < f_a < 1.2 \times 10^{11}{\rm GeV} , \qquad \frac{6 \times 10^{10}{\rm GeV}}{\sqrt{\epsilon_{\rm eff}}} < M_{\rm inf} < 3 \times 10^{16}{\rm GeV} . \tag{6.37}$$

The second one, for which the PQ symmetry is broken during inflation but the isocurvature mode is too small to be excluded by current cosmological data, corresponds to

$$10^{10}{\rm GeV} < f_a < 2.5 \times 10^{11}{\rm GeV} , \qquad M_{\rm inf} < 8 \times 10^{12}{\rm GeV} , \tag{6.38}$$

where we assumed that the average misalignment angle in the observable universe is of order one: otherwise, the upper bound on f_a could be relaxed significantly, while that on $M_{\rm inf}$ would only increase slightly, as f_a to the power 5/24, see Eq. (6.36).

Bounds for chaotic inflation with a quadratic potential

Inflation with a monomial potential $V(\phi) \propto \phi^\alpha$ is usually called chaotic inflation. The latest WMAP results combined with other data sets essentially rule out cases

with $\alpha > 4$, while the quartic case $\alpha = 4$ is only in marginal agreement with the data. Therefore, in this section we only consider the case of a quadratic potential $V(\phi) = \frac{1}{2}m^2\phi^2$, still favored by observational bounds.

Using the COBE normalization, it is possible to prove that the mass should be of order $m \sim 5 \times 10^{-8} M_{\rm P}$, and to show that N_* e-folds before the end of inflation,

$$\phi_*^2 = \frac{N_*}{2\pi} M_{\rm P}^2 \ . \tag{6.39}$$

In particular, between $N_{\rm obs}$ and $N_{\rm QCD}$ the scale of inflation should be in the range

$$3{\times}10^{15}{\rm GeV} < M_{\rm inf} < 4{\times}10^{15}{\rm GeV} \ , \qquad 3{\times}10^{12}{\rm GeV} < M_{\rm inf} < 4{\times}10^{12}{\rm GeV} \ . \tag{6.40}$$

So, if f_a is close to 10^{10} or 10^{11}GeV, one has $H_{\rm inf}/2\pi \geq f_a$ and the PQ symmetry is broken by quantum fluctuations during inflation. Still, the constraint from isocurvature modes applies, unless the symmetry is restored by thermal fluctuations. Reheating after chaotic inflation is expected to lead to a temperature $T_{\rm rh}$ of the order of 10^{10} or 10^{11}GeV, which is precisely the allowed range for f_a. So, if f_a is pushed down to 10^{10}GeV while $T_{\rm rh}$ is pushed up to 10^{11}GeV, a very brief stage of thermal restoration could occur, and could be sufficient for erasing isocurvature perturbations. In fact, the thermal corrections induce a temperature dependent mass $m_{\rm eff} = T^2/12$, which should larger than λf_a^2 in order for symmetry restoration by thermal fluctuations to occur. If λ is not too small (say of order 0.1) then indeed the condition is $T > f_a$, otherwise one has to consider the extra factors.

Note that f_a cannot be much bigger than 10^{11}GeV: if it was the case, thermal symmetry restoration after inflation would be impossible, and given the value of $M_{\rm inf}$ the isocurvature constraint of equation (6.36) would give $f_a \geq 8 \times 10^{23}{\rm GeV} \gg M_{\rm P}$. So, the only possibility for reconciling the PQ axion with chaotic inflation is to lay within a small region with $f_a \sim T_{\rm rh} \sim 10^{10-11}$GeV.

Bounds for low scale inflation

We have seen that unless $\langle \Theta_1^2 \rangle$ is tuned to very small values, which sounds unnatural, a very stringent bound $M_{\rm inf} < 10^{13}$GeV can be derived on the energy scale of inflation. So, we should study the viability of the axion model in the context of low scale inflation. This was essentially the original motivation in Ref. [12] for introducing hybrid inflation. Nowadays, many low scale inflation models can be built in the generic framework of hybrid inflation, see Ref. [30].

For low-scale hybrid inflation, the sign of the tilt $n_{\rm ad} - 1$ is given by that of the second derivative of the potential with respect to the inflaton. The latest bounds on the adiabatic tilt $n_{\rm ad} = 0.987^{+0.019}_{-0.037}$ [5], and our own analysis $n_{\rm ad} = 0.966 \pm 0.033$ (at two sigma) place low-scale hybrid inflationary models with a convex potential in a vulnerable position. This includes the most conventional hybrid inflationary models, with a quadratic mass term for the inflaton. Low-scale hybrid inflation with

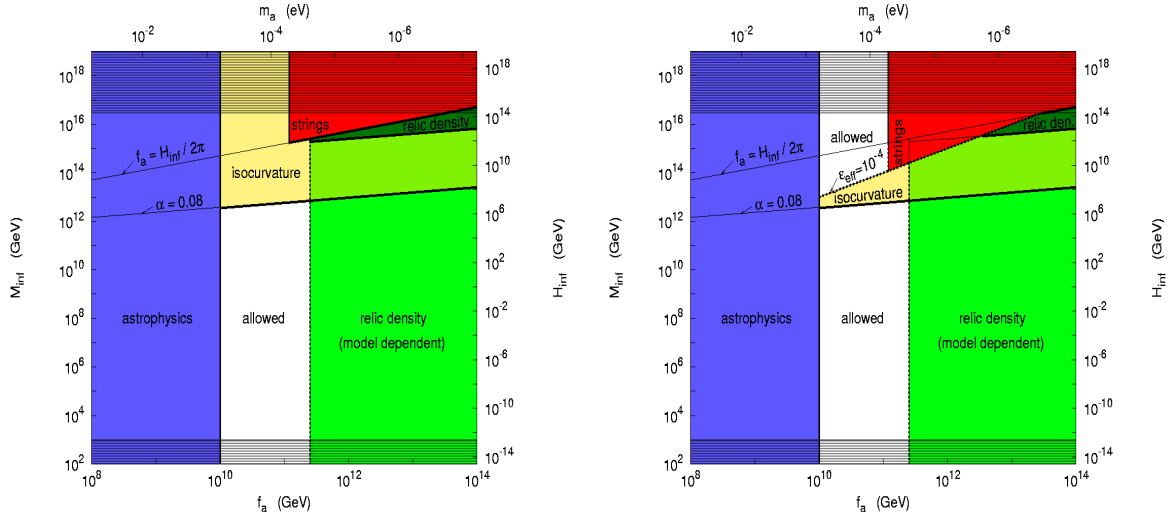

Figure 6.12: On the left panel, we show the bounds in the $(M_{\rm inf},\ f_a)$ plane, assuming that reheating is very inefficient and the PQ symmetry can never be thermally restored ($\epsilon_{\rm eff} \leq 4 \times 10^{-12}$). On the right, we show the same parameter space by assuming that reheating is very efficient ($\epsilon_{\rm eff} = 10^{-4}$) so that the the PQ symmetry is thermally restored above the dotted line. Details are explained in the text.

a concave potential is more favored by the data. One example of such low-scale models is provided by supersymetric inflation with a flat direction and logarithmic loop corrections [135, 30], see also [136]. Here, instead, we chose to study an inverted hybrid inflationary model [137] as a low scale, negative tilt model of inflation.

Our model assumes no particular value for v, the vacuum expectation value of σ, the field whose symmetry breaking is responsible for the end of inflation. Its value is left free and its variation is accounted for as the inflationary energy scale varies. The potential, in terms of the symmetry breaking field σ and the inflaton ϕ, is given by

$$V(\phi,\sigma) = V_0 + \frac{1}{2}M^2\sigma^2 - \frac{1}{2}m^2\phi^2 - \frac{1}{2}g^2\phi^2\sigma^2 + \frac{\lambda}{4}\phi^4 + \frac{\lambda'}{4}\sigma^4 \qquad (6.41)$$

where λ, λ' and g are coupling constants. Although their value is arbitrary in principle, radiative corrections must be under control and this imposes constraints on the coupling constants. The expansion rate during inflation is

$$H^2(\phi) = \frac{8\pi}{3M_{\rm P}^2}V_0\left(1 - \frac{1}{2}\frac{m^2\phi^2}{V_0}\right) \qquad (6.42)$$

With the definition above, freedom of choice is achieved for M and/or λ and there exist a wide range of models that allow for a much lower expansion rate during inflation compared to that assumed for chaotic models. So, even if we assume that inflation is long enough for the quantum diffusion to be complete, a case in which all the bounds of subsection 6.3.3 apply, we can build a successful model of inflation

with $M_{\rm inf} < 10^{13}$GeV. Then, the axion scenario with $10^{10}\text{GeV} < f_a < 10^{12}\text{GeV}$ is viable.

Note that the bounds of subsection 6.3.3 included all the constraints on the axionic window, excepted those related to the reheating mechanism. Reheating can be efficient for the (inverted) hybrid inflation scenario. So, if we want to avoid the generation of cosmic strings, we should impose the bound of Eq. (6.24)

$$M_{\rm inf} < 10 \frac{1}{\sqrt{\epsilon_{\rm eff}}} \left(\frac{3}{8\pi}\right)^{1/4} f_a \,. \tag{6.43}$$

For various possible values of $\epsilon_{\rm eff}$, the regions forbidden by this constraint are shaded on the right plot in Fig. 6.12. This last constraint can cut a part of the allowed window in $(M_{\rm inf}, f_a)$ space, and further reduce the upper bound on $M_{\rm inf}$.

Once all the bounds have been imposed, we are left with a range

$$10^{10}\text{GeV} \lesssim f_a \lesssim 10^{12}\text{GeV} \implies 6\,\mu\text{eV} \lesssim m_{\rm a} \lesssim 600\,\mu\text{eV} \tag{6.44}$$

for the PQ symmetry breaking scale and the mass of the QCD axion.

6.3.4 Possible loopholes

In this subsection we will explore those loopholes we have left open for the axion to be the dominant component of cold dark matter.

Production of cosmic strings during reheating

Even if the reheating temperature of the universe is too low for a thermal phase transition at the Peccei-Quinn scale, it is possible that axionic cosmic strings be formed during preheating if the field responsible for symmetry breaking at the end of inflation is the Peccei-Quinn field. Then, the residual global $U(1)$ symmetry of the vacuum gives rise to axionic cosmic strings. At present there is no prediction for what is the scaling limit of such a mesh of strings produced during preheating. A crucial quantity that requires evaluation is the fraction of energy density in infinite strings produced at preheating, since they are the ones that will give the largest contribution to the axion energy density. It could then be that axionic strings produced at preheating may be responsible for the present axion abundance. We leave for the future the investigation of this interesting possibility.

Axion dilution by late inflation

When imposing bounds on the axion mass from its present abundance, it is assumed that no there is no significant late entropy production or dilution from a secondary

stage of inflation. We truly don't know. It has been speculated that a short period of inflation may be required for electroweak baryogenesis to proceed [138]. In such a case, a few e-folds ($N \sim 5$) of late inflation may dilute the actual axion energy density by a factor $\gamma = e^{-3N} \sim 10^{-7}$, easily evading the bounds.

6.4 Conclusions

Using the measurements of temperature and polarization anisotropies in the CMB by WMAP-I, together with recent data from VSA, CBI, and ACBAR; the matter power spectra from the 2dF galaxy redshift survey and the Sloan Digital Sky Survey, as well as the recent supernovae data from the SN Search Team, one can obtain stringent bounds on the various possible isocurvature components in the primordial spectrum of density and velocity fluctuations.

In section 6.1 we have considered correlated adiabatic and isocurvature modes, and find no significant improvement in the likelihood of a cosmological model by the inclusion of an isocurvature component, see Table 1 and Fig. 3. So, the pure adiabatic scenario remains the most economic and attractive scenario.

In contrast with the WMAP-I analysis, we decided not to include any data from Lyman-α forests initially because constraints on the linear power spectrum coming from these experiments are derived under the assumption of a plain adiabatic ΛCDM scenario. We did not include either strong priors on the isocurvature spectral index, unlike previous analyses [13], and allowed this parameter to vary up to $n_{\rm iso} = 3$. This conservative approach leads to a preference for models with a very blue isocurvature primordial spectrum, and to upper bounds on the isocurvature fraction significantly larger than in other recent analyses: on a pivot scale $k = 0.05\,h\,{\rm Mpc}^{-1}$ the amplitude of the correlated isocurvature component can be as large as about 60% for the cold dark matter mode, 40% for the neutrino density mode, and 30% for the neutrino velocity mode, at 2σ. This leaves quite a lot of freedom, for instance, for double inflation models with two uncoupled massive fields. Assuming that one of these fields decay into Cold Dark Matter, our results simply imply that the mass of the heavy field cannot exceed five times that of the light field at the 2σ confidence level.

Realising of the lack of data at small scales, we decided to add the Lyman-α data. In section 6.2.1 we assess the inclusion of the power spectrum coming from Lyman-α data and we study the impact caused in the results. We find that the systematics induced − in particular, those associated with the recovery of the linear dark matter power spectrum from the flux power spectrum − are greatly compensated by the valuable information on the small-scale matter power spectrum provided by the Lyman-α data.

We see that for the same prior assumptions and space of parameters, we tighten

the constrain on α for the CDI model:

$$\begin{aligned} \alpha &< 0.6 \text{ at } 95\% \text{ c.l. to} \\ \alpha &< 0.4 \text{ at } 95\% \text{ c.l.} \end{aligned} \tag{6.45}$$

when adding the Lyman-α data. Focusing on a particular isocurvature model, we lower the bound on R, the ratio of the masses of the fields for the double inflationary scenario:

$$\text{from R} < 5 \text{ at } 95\% \text{ c.l.} \Longrightarrow \text{R} < 3 \text{ at } 95\% \text{ c.l.} \tag{6.46}$$

by adding the Lyman-α forest data.

The specific impact of the Lyman-α forest data may be most clearly seen on the constraint on the isocurvature tilt which goes from being practically unconstrained to $n_{\rm iso} = 1.9 \pm 1.0$ where the data is added (see Fig. 6.7). A tilt redder than ~ 3 does not allow for a such a high isocurvature component at the pivot scale, that is why we get the reduction shown in (6.45).

In the case of a curvaton scenario where CDM-creation occurs at the decay of the curvaton – a case in which the adiabatic and isocurvature modes are maximally anti-correlated, $\beta = -1$, and $n_{\rm ad} = n_{\rm iso}$ – we find $f_{\rm iso} < 0.05$, still at the 95% confidence level. This requires that the fraction r of the total density in the curvaton field at that time be fine-tuned between 0.98 and one.

It is also worth mentioning that when we omit the Lyman-α forest data our bounds agree very well with those of Ref. [156]. The authors of [156] work with a pivot scale $k_0 = 0.02$ Mpc^{-1}, but they also show how their results are modified when they take $k_0 = 0.05$ Mpc^{-1} like in the present paper: in that case the agreement with us is particularly good. This is a nice crosscheck useful in many cases to compare prior hypothesis and statistical methods.

We also used all the deployed machinery to assemble a bridge between particle physics and observations in cosmology by studying cosmological constraints on the axionic allowed space of parameters.

On the last section of this chapter, we reviewed various bounds on the cosmological scenario in which the cold dark matter is composed of axions plus some other component (like e.g. neutralinos), and the energy density of axions is produced by the misalignment mechanism at the time of the QCD transition. In the model, developed on Chapter 2, a fraction of the cosmological perturbations consists of isocurvature modes related to the quantum perturbations of the axion during inflation. We use this possible signature plus the contribution to dark matter energy density as a tracer of axions in the universe. In that sense, this work is similar to that presented in [140]. However, we make a stronger statement about the generation of isocurvature modes in the case in which the PQ symmetry is restored by quantum fluctuations during inflation, and we significantly improve previous bounds coming from the non-observation of isocurvature modes in the CMB, in particular, given the recent WMAP 3-year data.

A narrow window for the PQ scale $10^{10}\,\mathrm{GeV} < f_a < 10^{12}$ GeV still remains open, but we show that the main consequence of recent data on cosmological perturbations is to limit the possible energy scale of inflation in this context, in order not to have an excessively large contribution of isocurvature perturbations to the CMB anisotropies. In particular, we show that in the axion scenario, the energy scale of inflation cannot be in the range $8 \times 10^{12} < M_{\rm inf} < 5 \times 10^{14}$ GeV, unless one of the two situations occurs: either reheating leads to a temperature $T_{\rm rh} > f_a$, with an efficiency parameter $\epsilon_{\rm eff} \geq 4 \times 10^{-12}$, and there is another allowed region with $6 \times 10^{10} \epsilon_{\rm eff}^{-1/2}\,\mathrm{GeV} < M_{\rm inf} < 3 \times 10^{16}$ GeV; or the misalignment angle is fine-tuned to very small values (this coincidence can be motivated by anthropic considerations) and the upper bound $M_{\rm inf} < 10^{13}$ GeV can be slightly weakened (by at most one order of magnitude).

These bounds may be of interest taking into account particle physics experiments searching for the axion, which may help to put very stringent constraints on inflationary models. Detecting the QCD axion could shed some light on the scale of inflation and possibly into the mechanism responsible for inflation.

In this respect, there is an intriguing possibility that the PVLAS experiment [141] may have observed a pseudo-scalar particle coupled to photons. The nature of this particle is yet to be decided, since its properties seem in conflict with present bounds on the axion coupling to matter [49, 50], see however [142].

This chapter represents the main body of our results in isocurvature parameter constraints, and along with Chapter 5 on Model Selection represents the original work in this thesis.

Both subjects are complementary to each other and are two essential ingredients on any inference problem.

We have also shown the extremely valuable connection between raw data and particle physics models such as the possible detection of the axion on cosmological experiments. Hopefully, this bridge will be more and more firmly established and can ultimately lead to powerful insight on physics beyond the standard model (another significant example being the masses of the neutrinos [183]).

As for the future perspective, it is expected [153] that in the near future, with better data from Planck and other CMB experiments, we will be able to reduce further a possible isocurvature fraction, or perhaps even discover it. The present results also suggest that constraining the linear matter power spectrum on scales which are mildly non-linear today will also be crucial in this respect.

Conclusions and Outlook

Over the development of this thesis, we have tried to address two main issues in contemporary Cosmology. As stated in the title, these are the isocurvature perturbations in Inflationary Cosmology and the problem of Model Selection.

Even though the cosmological paradigm is pretty well settled and it is very successful on explaining the observed phenomenology, many extensions are still possible. To name a few of them, the existence of non-gaussianities in the distribution of the perturbations, the possibility that the spectral tilt depends of the scale, cosmic deffects or the observation of a tensor component in the anisotropies spectrum are broadenings to the most conservative paradigm, challenging to test. Among these, we chose focusing on constraining the reach of yet another extension, the isocurvature perturbations.

We believe this was a necessary analysis that has come in the right time as far as the experimental scenario goes. We are experiencing a time of extreme advances in observational cosmology. Observations are reaching accuracies that were completely new to this science- it is indeed the time to start thinking about how to put bounds on the possible stretches of the model.

To achieve our goals, we initially develop our theoretical tools, underlying models and parametrizations. We study the phenomenology of the isocurvature models. We do so using two different approaches. Firstly, we gather a data compilation and study the possible presence of an isocurvature signal on a model independent way. We put stringent bounds on the contribution at a given scale using a variety of data comprising CMB, LSS and SNae Ia data. One of our main results of this analysis led us to realise of the necessity of the inclusion of data coming from experiments at scales smaller than what we were using [14].

This way, we set our goal on using the latest data on the Lyman-α forest quasar absortion spectra. As expected our results turned out to be much more restringent than what had been obtained previously [15].

We also approached the isocurvature perturbations as a tool for constraining a given particle physics model, namely the axion. That is, isocurvature is not our goal by itself but as an indicator of the existence of this axionic field during inflation. We extend the work of previous analysis and find an allowed window inside the parameter space spanned by the axionic mass and the energy scale of inflation [184].

The other very important problem we tackled in this thesis is one less specific of inflation and more general to data analysis in Cosmology. During the past two or three years cosmologists had grown more and more concerned about the issue of determining how many parameters one should use to describe the Universe given a set of data. We developed a computational tool, the *thermodynamical integration* to calculate the Bayesian Evidence, in order to let the data "speak for themselves" and choose a particular model [76]. All our results and developments on Model Selection are described on chapter 5.

The perspective for future work seems colossal. The research windows that remain open in this field are so many and so interesting that it is indeed difficult to choose only a few. But time is finite for human cosmologists and one needs to focus.

As has been many times stated, cosmology is entering a precision era where a huge variety of data is becoming accessible. I believe it is a fundamental priority to interrelate these very different pieces of data with each other in a such a way that the maximum amount of information possible is exposed.

There is also a great potential in the alliance between observational and theoretical cosmology and particle physics. High precision experiments such as PLANCK enable us to dig out deeper layers in the cosmic puzzle. In my opinion, some of these layers would be directly related to physics beyond the standard model.

Issues that remain an enigma for both cosmology and particle physics such as the nature of dark matter and dark energy or the origin and subsequent evolution (linear and non-linear) of the primordial perturbations, may start to be unveiled with the aid of, for example the study of correlation between LSS and CMB by the ISW effect [185] or the detection of primoridal non-gaussianities in the CMB and LSS anisotropies [186, 187].

In general, it would be interesting to perform a joint analysis of CMB and other datasets to shed some light into the following issues:

The nature of dark energy.

One of the most fascinating enigmas of cosmology is the nature of Dark Energy. Soon we may be able to start discerning between the different models of Dark Energy and explore its nature.

It is crucial to study the different stages and evolution of the universe. Thus, the information contained in the CMB data is necessary, albeit insufficient. It is necessary in order to enable us to *fix* the underlying background cosmology, ie. parameters that do not directly influence the growth of structure and only affect the universe as a homogeneous fluid, in the most precise possible way.

But in addition to this, we need probes that measure the rate of growth of structures and its power spectrum, in a more recent epoch which is when the DE is believed to start being relevant.

Appart from the Supernovae of type Ia, probes such as weak lensing cosmic-shear data or the Sunyaev-Zeldovich (SZ) galaxy cluster catalogues are excellent tools for accurate parameter estimation. Both of them provide an independent measurement of parameters such as Ω_m and thus a way of breaking the degeneracies.

I propose a joint analysis of these pieces of data along with a bayesian model selection of the different parametrizations of the equation of state, w, to study their relevance. With this examination of the data *and* the model one could determine which is the effective model for w that allows us to extract the most information. In the best case scenario, this could even help design the next generation of experiments. Once we know what the data is willing to show, it will be easier to see it.

Baryon Acoustic Oscillation

We discussed in chapter 4 the nature and importance of the BAO in the galaxy distributions. In [88] the mean redshift of the spectroscopic sample is $z_m = 0.35$, but larger catalogues and, apparently, even photometric catalogues, [188], can measure the sound horizon at recombination at higher redshifts with acceptable error bars [89].

The potential of such a variety of rulers is readily understood as a way to impose tighter constraints on the parameters governing the geometry of the universe and the evolution of the equation of state of the Dark Energy. Nevertheless, even if the true underlying model is a cosmological constant, the way in which the allowed region for the standard parameters is squeezed fixes the background cosmology so that extensions to the conventional inflationary model can be tested.

In this sense, precise baryon acoustic oscillation data will be very useful to constrain certain isocurvature models such as the curvaton model or a double inflationary scenario in which both fields have the same mass and behave as one single massive complex scalar field. It is very interesting the capacity of this new piece of information and its usefulness for parameter determination.

Cosmological model selection and information content of data.

As more and more data arrives, we will need to address statistical issues more precisely and uniquely. More precise questions such as the running of the spectral index or even a departure from a scale-invariant spectrum, may get a deceiving answer if not enough data is available [160].

It would be extremely interesting to study the model selection problem and determine whether or not a piece of data is suitable and informative enough so that a certain number and kind of parameters may be extracted from them. It is also very interesting the way in which starting assumptions about our model affect the final results.

Condensing all that was said above, this thesis has served us to address two

different issues.

The first reading should help us understanding the nature of the isocurvature perturbations and how they have indeed been constrained quite tightly using different pieces of data.

On a broader sense, this thesis tries to point out the recent successes of observational cosmology, and the importance of linking experiments and data to theory, in an adequate way, which should be a very fruitful task but by no means trivial. We need to pay special attention to disentangling physics from statistical artifacts and perhaps, come up with new techniques better tailored for cosmology.

This should help our task in this era of progress, spectacular advances and enthralling excitement about which are the mysteries that lay ahead. Only the Universe knows...

Agradecimientos

Es increible que haya llegado el momento de escribir estos agradecimientos... ¡El tiempo pasa tan deprisa!

Me acuerdo de la primera vez que miré al cielo, a las estrellas. Una noche verano de los ochenta en El Espinar mi abuelo Joaquin, posiblemente el primer científico que conocí, señaló hacia arriba. El Universo. Ahí estaba. Impresionante. ¿Qué era todo eso? ¿De dónde habian salido todas esas estrellas? ¡¿Cada una de ellas es como un Sol?! ¿Que se estan alejando de nosotros? ... ¡anda ya!... Pero bueno, entonces, ¿cómo es que todavía las podemos ver? ¿Cuánto tiempo llevan ahí? y... ¡¿cómo empezó todo?!

Cómo empezó todo, sigo sin saberlo, lo que sé es que así empezó todo para mi...

Pasaron los años, años de muy buenos profesores a los que quisiera agradecer su entrega y amor por su profesión. Incluyendo, cómo no, a tantos profesores y profesoras de la Autónoma que no tenían "horas de tutoría" porque su despacho siempre estaba abierto.

Después de una serie de coincidencias y conferencias, acabé llamando a la puerta de mi director de tesis, Juan García-Bellido.

A él es el primero al que debo mencionar en esta lista: gracias por una incesante dedicación y pasión contagiosa por la cosmología, y por tiempo infinito para hablar de física. Gracias por confiar en mi desde el principio y tratarme de tú a tú científicamente. Muchisimas gracias por animarme siempre a viajar, conociendo tantos lugares y personas.

Gracias a mis viajes, he tenido la oportunidad de colaborar con gente excepcional tanto profesional como personalmente. Julien Lesgourgues, que no solo me enseñó los mejores sitos donde comer en Annecy, sino también mucha cosmología y siempre ha sabido crear un ambiente cálido y agradable de trabajo. Andrew Liddle, gracias por conversaciones iluminadoras y un impecable ejemplo a seguir en mi carrera. ¡Me gustó tanto Sussex que volví al año siguiente! Licia Verde muchas gracias por tu paciencia y explicaciones clarísimas. Gracias también a Raul Jiménez, los dos hicisteis de mi estancia en UPenn, dos meses geniales. Gracias a todos por todo-estas visitas han resultado super enriquecedoras en todos los sentidos.

Agradecimientos a todos y todas los no-profesores que han estado conmigo durante estos años. Jose y Enrique, mis compañeros "permanentes" del 514. No tengo

palabras. Gracias por hacerme reir, por escucharme cantar y por hacer que absolutamente todas las mañanas me alegre de entrar en la oficina. A otros habitantes del 514, Fouad, Iñaki, Javi- también me han aguantado lo suyo. Nico, Ernesto y Sergio, cuántos recuerdos! gracias por inolvidables excursiones a la biblioteca de ciencias, experimentos de bolas y consejos de mago de Tex. A todos los otros cohabitantes del 512: Matteo, Jorge, Guillermo... gracias por compartir vuestro entusiasmo por la física, y sobre todo, por la vida. Muchas gracias a Africa por merendar conmigo. A Javi, Jose (María), Tomás, Dani y Chiqui- por relajantes sobremesas comiendo judías. A Luisfer, por cuidar de Wendy y Julieta. A los latticeros: Andres, Alberto, Alfonso y Fermín, por estar siempre al teléfono dispuestos a contestar mis dudas. A todos los "mayores" Ana, Alicia, Edu, Carlos, Sergio, Irene, Juan Pedro... por valiosos consejos y muchas risas. Y la los "pequeños", en especial a Dani y a Javi por entenderme muy bien y por un viaje a Benasque muy divertido. Muchas gracias a mis anfritriones en los departamentos que he visitado en Sussex y en Philadelphia.

Fuera de la física tengo la suerte de contar con muchas personas que han hecho mi vida increible. Mis padres, María y Juan. Gracias por todo. Por el apoyo incondicional, por la confianza y por sentiros orgullosos de mi. Por ser un colchón sobre el que puedo descansar. Esta tesis, trabajo de cuatro años, es para vosotros. Gracias a toda mi familia, en especial a mis abuelos Mary y Juan, que no dejan de sorprenderse cada vez que les cuento mis aventuritas y de que yo vaya a ser "doctora". A mis abuelos Lola y Joaquin, donde quiera que estén. Y a mis primos pequeños: Alicia, Ana, Blanca y Luis, que siempre me reciben con besos y abrazos, aunque pasen semanas sin vernos!

En cuanto al apoyo amistoso-extradepartamental, debo mencionar a unas cuantas personas que han estado conmigo a las duras y a las maduras. María Martín, cuasi-hermana, gracias por cuidarme mucho y por hacerme menos responsable de vez en cuando. Josefina y Maca, hemos compartido risas, llantos, proyectos, bodas... qué os voy a decir que no sepais?! Gracias por estar siempre ahi. Siempre. Inés y Laura, tal vez por vivir con vosotras he dado por hecho el auténtico privilegio que es conoceros y ser vuestra amiga. Gracias por prestar siempre un oido comprensivo, sincero, analítico y solucionador. Han sido tres años geniales. Gracias a Viviana, por una compañía insuperable en Philly y Brighton. A los de físicas, a Cris, Luci, Jose, Elvira, Alvaro, Fer, Jesus, Mery, Luis, Pablo, Miguel...(y más que se me olvidan), por fliparse tanto con la física como con un karaoke.

A Jota, a María Barón, a Luisma, a las chicas del CHAt, a Lucio e Isa, a la Amistad, a María Azcoitia y a todos mis amigos, que tengo la suerte de que no quepan en esta hoja.

Por último, como siempre, el agradecimiento más especial, a Len. Gracias por aprender español, por escucharme y entenderme, por enseñarme, por estar siempre ahi y por aguantar la distancia. Gracias por viajes inolvidables y por muchos más que están por venir.

Bibliography

[1] Fixsen, D.J. et al. Astrophys. J. **473**, 576 (1996)

[2] A. H. Guth, Phys.Rev.D**23**:347 (1981)

[3] A. D. Linde Phys. Lett **108B**389(1982); Phys. Lett **116B**335, 340 (1982)

[4] C. L. Bennett *et al.*, Astrophys. J. Supp. **148**, 1 (2003); D.N. Spergel *et al.*, Astrophys. J. Supp. **148**, 175 (2003). A. Kogut *et al.*, Astrophys. J. Supp. **148**, 161 (2003) [WMAP Collaboration].

[5] D. N. Spergel *et al.*,"Wilkinson Microwave Anisotropy Probe (WMAP) three year results: Implications for cosmology," arXiv:astro-ph/0603449; L. Page *et al.*, "Three year Wilkinson Microwave Anisotropy Probe (WMAP) observations: Polarization analysis," arXiv:astro-ph/0603450; G. Hinshaw *et al.*, "Three-year Wilkinson Microwave Anisotropy Probe (WMAP) observations: Temperature analysis,"arXiv:astro-ph/0603451.

[6] A. G. Riess *et al.* [Supernova Search Team Collaboration], Astrophys. J. **607**, 665 (2004).

[7] M. Tegmark *et al.* [SDSS Collaboration], Astrophys. J. **606**, 702 (2004).

[8] A.R. Liddle and D.H. Lyth, "Cosmological Inflation and Large Scale Structure", Cambridge University Press, 2000

[9] H. Kodama and M. Sasaki, Int. J. Mod. Phys. A **1**, 265 (1986), **2**, 491 (1987); G. Efstathiou and J. R. Bond, Mon. Not. Roy. Astr. Soc. **218**, 103 (1986), ; *ibid* **227**, 33 (1987); P. J. E. Peebles, Nature **327**, 210 (1987);

[10] A. D. Linde, Phys. Lett. B **158**, 375 (1985); L. A. Kofman and A. D. Linde, Nucl. Phys. B **282**, 555 (1987); S. Mollerach, Phys. Lett. B **242**, 158 (1990); A. D. Linde and V. Mukhanov, Phys. Rev. D **56**, 535 (1997); M. Kawasaki, N. Sugiyama and T. Yanagida, Phys. Rev. D **54**, 2442 (1996); P. J. E. Peebles, Astrophys. J. **510**, 523 (1999).

[11] R. D. Peccei and H. Quinn, Phys. Rev. Lett. **38** (1977) 1440; Phys. Rev. **D16** (1977) 1791.

[12] A. D. Linde, Phys. Lett. B **259** (1991) 38.

A. D. Linde, Phys. Rev. D **49** (1994) 748

E. J. Copeland, A. R. Liddle, D. H. Lyth, E. D. Stewart and D. Wands, Phys. Rev. D **49**, 6410 (1994)

L. E. Mendes and A. R. Liddle, Phys. Rev. D **62** (2000) 103511

[13] P. Crotty, J. García-Bellido, J. Lesgourgues and A. Riazuelo, Phys. Rev. Lett. **91**, 171301 (2003).

[14] M. Beltrán, J. García-Bellido, J. Lesgourgues and A. Riazuelo, Phys. Rev. D **70**, 103530 (2004).

[15] M. Beltrán, J. Garcia-Bellido, J. Lesgourgues and M. Viel, Phys. Rev. D **72** (2005) 103515.

[16] C. Brans and R. H. Dicke, Phys. Rev. **124** (1961) 925.

[17] Max Tegmark et.al, Phys.Rev.D **69**:103501,2004

[18] S. Weinberg, "Gravitation and Cosmology", John Wiley and Sons, Inc., 1972

[19] V.F. Mukhanov, H.A. Feldman, R.H. Brandenbeger, Phys. Rept. **215** 203 (1992).

[20] A. Lewis, Phys.Rev.D **70**:043518,2004

[21] M. Kesden, A. Cooray and M. Kamionkowski, Phys. Rev. Lett. **89** (2002) 011304

[22] J. M. Stewart Class. Quantum. Grav **7**, 1169 (1990)

[23] J.Bardeen, Phys.Rev.D **22**:1882,1980

[24] D. Wands, K.A. Malik, D.H. Lyth, A.R. Liddle, Phys.Rev.D**62**:043527,2000

[25] J. Garcia-Bellido, A. D. Linde and D. Wands, Phys. Rev. D **54** (1996) 6040

[26] A. D. Linde, "Particle Physics and Inflationary Cosmology", Harwood Academics, Chur, Switzerland (1990)

[27] J. M. Maldacena, JHEP **0305** (2003) 013

[28] D. H. Lyth, C. Ungarelli and D. Wands, Phys. Rev. D **67** (2003) 023503

[29] A. Albrecht and P. Steinhardt, Phys. Rev. Lett. **48**,1220 (1982)

[30] D. H. Lyth and A. Riotto, Phys. Rept. **314** (1999) 1.

[31] S. Weinberg, Phys. Rev. D**70**:083522,2004

[32] M. Bucher, K. Moodley, and N. Turok, Phys. Rev. D **62**, 083508 (2000); Phys. Rev. Lett. **87**, 191301 (2001).

[33] K. Moodley, M. Bucher, J. Dunkley, P. G. Ferreira, and C. Skordis, Phys. Rev. D**70**, 103520 (2004).

[34] C. Gordon, D. Wands, B. A. Bassett and R. Maartens, Phys. Rev. D **63** 023506 (2001).

[35] J.Silk, M.S.Turner, Phys.Rev D**35**:419 (1987)

[36] D. Polarski and A. A. Starobinsky, Nucl. Phys. **B385**, 623 (1992)

[37] S. Mollerach, Phys. Rev. D **42**, 313 (1990).

[38] A. D. Linde and V. Mukhanov, Phys. Rev. D **56** (1997) 535

[39] D. Lyth and D. Wands, Phys. Lett. B**524**,5 (2002)

[40] S. Gupta, K. A. Malik and D. Wands, Phys. Rev. D **69** (2004) 063513

[41] L. Amendola, C. Gordon, D. Wands and M. Sasaki, Phys. Rev. Lett. **88** (2002) 211302

[42] See e.g. the reviews: J.E. Kim, Phys. Rep. **150** (1987) 1; H.-Y. Cheng, Phys. Rep. **158** (1988) 1; R.D. Peccei, in 'CP Violation', ed. by C. Jarlskog, World Scientific Publ., 1989, pp 503-551; M.S. Turner, Phys. Rep. **197** (1990) 67; G.G. Raffelt, Phys. Rep. **198** (1990) 1.

[43] S. Weinberg, Phys. Rev. Lett. **40** (1978) 223; F. Wilczek, Phys. Rev. Lett. **40** (1978) 279.

[44] C. Vafa and E. Witten, Phys. Rev. Lett. **53** (1984) 535.

[45] Particle Data Group, http://pdg.lbl.gov

[46] W.A. Bardeen and S.-H.H. Tye, Phys. Lett. **B74** (1978) 229; J. Ellis and M.K. Gaillard, Nucl. Phys. **B150** (1979) 141; T.W. Donnelly et al., Phys. Rev. **D18** (1978) 1607; D.B. Kaplan, Nucl. Phys. **B260** (1985) 215; M. Srednicki, Nucl. Phys. **B260** (1985) 689.

[47] J. Kim, Phys. Rev. Lett. **43** (1979) 103; M. A. Shifman, A. I. Vainshtein and V. I. Zakharov, Nucl. Phys. **B166** (1980) 493.

[48] M. Dine, W. Fischler and M. Srednicki, Phys. Lett. **B104** (1981) 199;
A. P. Zhitnitskii, Sov. J. Nucl. **31** (1980) 260.

[49] http://www.phys.ufl.edu/ axion/

[50] http://cast.web.cern.ch/CAST/

[51] K. Zioutas *et al.* [CAST Collaboration], Phys. Rev. Lett. **94** (2005) 121301; L. Duffy *et al.* [ADMX Collaboration], Phys. Rev. Lett. **95** (2005) 091304

[52] D. J. Gross, R. D. Pisarski and L. G. Yaffe, Rev. Mod. Phys. **53** (1981) 43.

[53] P. Fox, A. Pierce and S. D. Thomas, "Probing a QCD string axion with precision cosmological measurements," arXiv:hep-th/0409059.

[54] E. W. Kolb and M. S. Turner,"The Early Universe", Addison-Weseley (1990).

[55] E. Masso, F. Rota and G. Zsembinszki, Phys. Rev. D **66** (2002) 023004.

[56] S. Hannestad, A. Mirizzi and G. Raffelt, JCAP **0507** (2005) 002.

[57] R.A. Battye and E.P.S. Shellard, Phys. Rev. Lett. **73** (1994) 2954; E.P.S. Shellard and R.A. Battye, Phys. Rept. **307** (1998) 227; R.A. Battye and E.P.S. Shellard, Nucl. Phys. Proc. Suppl. **72** (1999) 88

[58] D. Harari and P. Sikivie, Phys. Lett. **B195** (1987) 361; C. Hagmann and P. Sikivie, Nucl. Phys. **B363** (1991) 247; C. Hagmann, S. Chang and P. Sikivie, Phys. Rev. **D63** (2001) 125018.

[59] M. Yamaguchi, M. Kawasaki and J. Yokoyama, Phys. Rev. Lett. **82** (1999) 4578.

[60] M. Y. Khlopov, A. S. Sakharov and D. D. Sokoloff, "The nonlinear modulation of the density distribution in standard axionic Nucl. Phys. Proc. Suppl. **72** (1999) 105.

[61] P. Sikivie, Phys. Rev. Lett. **48** (1982) 1156.

[62] S. Chang, C. Hagmann and P. Sikivie, Phys. Rev. **D59** (1999) 023505.

[63] M. S. Turner, Phys. Rev. **D33** (1986) 889.

[64] P. J. Steinhardt and M. S. Turner, Phys. Lett. **B129** (1983) 51; G. Lazarides, R. Schaefer, D. Seckel and Q. Shafi, Nucl. Phys. **B346** (1990) 193.

[65] A.D. Linde, "Particle Physics and Inflationary Cosmology", Harwood Academic Press (1990).

[66] A. D. Linde and D. H. Lyth, Phys. Lett. B **246** (1990) 353.

[67] D. H. Lyth and E. D. Stewart, Phys. Rev. D **46** (1992) 532.

[68] M. Axenides, R. H. Brandenberger and M. S. Turner, Phys. Lett. B **126** (1983) 178.

[69] A. D. Linde, JETP Lett. **40** (1984) 1333 [Pisma Zh. Eksp. Teor. Fiz. **40** (1984) 496]; Phys. Lett. B **158**, 375 (1985); Phys. Lett. B **201** (1988) 437.

[70] M. S. Turner and F. Wilczek, Phys. Rev. Lett. **66** (1991) 5.

[71] D. Seckel and M. S. Turner, Phys. Rev. D **32** (1985) 3178.

[72] D. Polarski and A. A. Starobinsky, Phys. Rev. D **50**, 6123 (1994);

[73] M. Sasaki and E. D. Stewart, Prog. Theor. Phys. **95**, 71 (1996); M. Sasaki and T. Tanaka, Prog. Theor. Phys. **99**, 763 (1998).

[74] J. García-Bellido and D. Wands, Phys. Rev. D **53**, 5437 (1996); **52**, 6739 (1995).

[75] C. Gordon, D. Wands, B. A. Bassett and R. Maartens, Phys. Rev. D **63**, 023506 (2001); N. Bartolo, S. Matarrese and A. Riotto, Phys. Rev. D **64**, 123504 (2001); D. Wands, N. Bartolo, S. Matarrese and A. Riotto, Phys. Rev. D **66**, 043520 (2002).

[76] M. Beltrán, J. García-Bellido, J. Lesgourgues, A. R. Liddle and A. Slosar, Phys. Rev. D **71** (2005) 063532.

[77] W. Hu and N. Sugiyama, Phys. Rev. D **66** (2002) 010001

[78] W. Hu and S. Dodelson, Ann. Rev. Astron. Astrophys. **40** (2002) 171

[79] W. Hu, M. Fukugita, M. Zaldarriaga and M. Tegmark, Astrophys. J. **549** (2001) 669

[80] A.Lewis, A. Challinor, Phys.Rev.D**66**:023531,(2002). CAMB Code Home Page, `http://camb.info/`

[81] W. T. Hu, arXiv:astro-ph/9508126.

[82] E. R. Switzer and C. M. Hirata, arXiv:astro-ph/0702143; C. M. Hirata and E. R. Switzer, arXiv:astro-ph/0702144;E. R. Switzer and C. M. Hirata, arXiv:astro-ph/0702145.

[83] P. J. E. Peebles and J. T. Yu, Astrophys. J. **162** (1970) 815.

[84] J. Silk, Astrophys. J. **151** (1968) 459.

[85] D. J. Eisenstein and W. Hu, Astrophys. J. **496** (1998) 605

[86] W. J. Percival *et al.*, Astrophys. J. **657** (2007) 645 [arXiv:astro-ph/0608636].

[87] J. A. Peacock, "Cosmological Physics", Cambridge Universty Press, 1999.

[88] D. J. Eisenstein *et al.* [SDSS Collaboration], Astrophys. J. **633** (2005) 560

[89] C. Blake, D. Parkinson, B. Bassett, K. Glazebrook, M. Kunz and R. C. Nichol, Mon. Not. Roy. Astron. Soc. **365** (2006) 255; D. Parkinson, C. Blake, M. Kunz, B. A. Bassett, R. C. Nichol and K. Glazebrook, arXiv:astro-ph/0702040.

[90] The Sloan Digital Sky Survey Home Page: `http://www.sdss.org`

[91] M. Tegmark *et al.*, Phys. Rev. D **74** (2006) 123507

[92] W. J. Percival *et al.* [The 2dFGRS Team Collaboration], Mon. Not. Roy. Astron. Soc. **337** (2002) 1068

[93] R. Protassov, D. A. van Dyk, A. Connors, V. L. Kashyap and A. Siemiginowska, arXiv:astro-ph/0201547. R. S. Pilla, C. Loader and C. Taylor, Phys. Rev. Lett. **95** (2005) 230202

[94] (private communication)

[95] B. A. Bassett, R. C. Nichol and D. J. Eisenstein [WFMOS Collaboration], arXiv:astro-ph/0510272.

[96] J. A. Tyson, D. M. Wittman, J. F. Hennawi and D. N. Spergel, Nucl. Phys. Proc. Suppl. **124** (2003) 21

[97] S. M. Carroll, W. H. Press and E. L. Turner, Ann. Rev. Astron. Astrophys. **30** (1992) 499.

[98] A. G. Riess *et al.*, arXiv:astro-ph/0611572.

[99] P. Astier *et al.*, Astron. Astrophys. **447** (2006) 31

[100] R. Miquel, arXiv:astro-ph/0703459.

[101] Mission homepage: `http://snap.lbl.gov/`

[102] A. G. Kim, E. V. Linder, R. Miquel and N. Mostek, Mon. Not. Roy. Astron. Soc. **347** (2004) 909

[103] H. Bi, Astrophys. J. **405**, 479 (1993); M. Viel, S. Matarrese, H. J. Mo, M. G. Haehnelt and T. Theuns, Mon. Not. Roy. Astron. Soc. **329**, 848 (2002); M. Zaldarriaga, R. Scoccimarro and L. Hui, Astrophys. J. **590**, 1 (2003).

[104] R. A. C. Croft *et al.*, Astrophys. J. **581**, 20 (2002).

[105] M. Viel, M. G. Haehnelt and V. Springel, Mon. Not. Roy. Astron. Soc. **354**, 684 (2004).

[106] P. McDonald *et al.*, arXiv:astro-ph/0407377.

[107] L. Hui, N. Y. Gnedin and Y. Zhang, Astrophys. J. **486**, 599 (1997).

[108] N. Katz, D. H. Weinberg and L. Hernquist, Astrophys. J. Suppl. **105**, 19 (1996).

[109] J. E. Gunn and B. A. Peterson, Astrophys. J. **142**, 1633 (1965); J. N. Bahcall and E. E. Salpeter, Astrophys. J. **142**, 1677 (1965).

[110] M. Rauch, ARA&A **36**, 267 (1998).

[111] L. Hui and N. Gnedin, Mon. Not. Roy. Astron. Soc. **292**, 27 (1997); N. Y. Gnedin and L. Hui, Mon. Not. Roy. Astron. Soc. **296**, 44 (1998).

[112] T. S. Kim, M. Viel, M. G. Haehnelt, R. F. Carswell and S. Cristiani, Mon. Not. Roy. Astron. Soc. **347**, 355 (2004).

[113] P. McDonald *et al.*, arXiv:astro-ph/0405013.

[114] N. Y. Gnedin and A. J. S. Hamilton, Mon. Not. Roy. Astron. Soc. **334**, 107 (2002).

[115] M. Viel, J. Lesgourgues, M.G. Haehnelt, S. Matarrese, A. Riotto, Phys. Rev. D **71**, 063534 (2005).

[116] M. Ricotti, N. Y. Gnedin and J. M. Shull, Astrophys. J. **534**, 41 (2000); J. Schaye et al., Mon. Not. Roy. Astron. Soc. **318**, 817 (2000).

[117] L. van Waerbeke *et al.*, Astron. Astrophys. **358** (2000) 30

[118] I. Tereno, O. Dore, L. Van Waerbeke and Y. Mellier, Astron. Astrophys. **429** (2005) 383; R. Massey *et al.*, arXiv:astro-ph/0701594.

[119] J. Benjamin *et al.*, arXiv:astro-ph/0703570.

[120] Decam Home Page at: `http://decam.fnal.gov/`

[121] A. Refregier *et al.*, arXiv:astro-ph/0610062.

[122] `http://www.ast.cam.ac.uk/~rtnigm/luqas.htm`

[123] M. Viel, M.G. Haehnelt arXiv:astro-ph/0508177

[124] F. Haardt and P. Madau, Astrophys. J. **461**, 20 (1996).

[125] M. Viel, J. Weller and M. Haehnelt, Mon. Not. Roy. Astron. Soc. **355**, L23 (2004).

[126] Max Tegmark, "Doppler peaks and all that: CMB anisotropies and what they can tell us", e-print Archive: astro-ph/9511148

[127] A. Lewis and S. Bridle, Phys. Rev. D **66**, 103511 (2002); CosmoMC home page: `http://www.cosmologist.info`

[128] R. Rebolo *et al.* [VSA Collaboration], Mon. Not. Roy. Astron. Soc. **353**, 747 (2004); C. Dickinson *et al.*, Mon. Not. Roy. Astron. Soc. **353**, 732 (2004).

[129] T. J. Pearson *et al.* [CBI Collaboration], Astrophys. J. **591**, 556 (2003); J. L. Sievers *et al.*, Astrophys. J. **591**, 599 (2003); A. C. S. Readhead *et al.*, Astrophys. J. **609**, 498 (2004).

[130] C. l. Kuo *et al.* [ACBAR Collaboration], Astrophys. J. **600**, 32 (2004); J. H. Goldstein *et al.*, Astrophys. J. **599**, 773 (2003).

[131] J. A. Peacock *et al.* [2dFGRS Collaboration], Nature **410**, 169 (2001); W. J. Percival *et al.*, Mon. Not. R. Astron. Soc. A **327**, 1297 (2001); **337**, 1068 (2002).

[132] S. Brooks and A. Gelman, JCGS, **7**:434-456 (1998).

[133] S. Perlmutter *et al.* [Supernova Cosmology Project Collaboration], "Measurements of Omega and Lambda from 42 High-Redshift Supernovae," Astrophys. J. **517** (1999) 565 [arXiv:astro-ph/9812133].

[134] U. Seljak *et al.*, Phys. Rev. D **71**, 103515 (2005).

[135] G. R. Dvali, Q. Shafi and R. K. Schaefer, Phys. Rev. Lett. **73** (1994) 1886.

[136] R. Allahverdi, K. Enqvist, J. Garcia-Bellido and A. Mazumdar, "Gauge invariant MSSM inflaton," arXiv:hep-ph/0605035.

[137] D. H. Lyth and E. D. Stewart, Phys. Rev. D **54** (1996) 7186.

[138] J. Garcia-Bellido, D. Y. Grigoriev, A. Kusenko and M. E. Shaposhnikov, Phys. Rev. D **60** (1999) 123504.

[139] M. Tegmark, A. Aguirre, M. Rees and F. Wilczek, Phys. Rev. D **73** (2006) 023505.

[140] P. Sikivie, "The search for dark matter axions," arXiv:hep-ph/0606014.

[141] E. Zavattini *et al.* [PVLAS Collaboration], arXiv:hep-ex/0512022.

[142] E. Masso and J. Redondo, JCAP **0509** (2005) 015.

[143] The 2-Degree Field Galaxy Redshift Survey Home Page: `http://aao.gov.au/2df/`

[144] W. L. Freedman *et al.*, Astrophys. J. **553**, 47 (2001)

[145] S. Burles, K. M. Nollett and M. S. Turner, Astrophys. J. **552** (2001) L1

[146] ojo con las distribs chisq

[147] R. Protassov, D. A. van Dyk, A. Connors, V. L. Kashyap and A. Siemiginowska, arXiv:astro-ph/0201547.

[148] R. Trotta, A. Riazuelo and R. Durrer, Phys. Rev. Lett. **87**, 231301 (2001);

[149] H. V. Peiris *et al.* [WMAP Collaboration], Astrophys. J. Supp. **148**, 213 (2003).

[150] C. Gordon and A. Lewis, Phys. Rev. D **67**, 123513 (2003); New Astron. Rev. **47**, 793 (2003).

[151] J. Valiviita and V. Muhonen, Phys. Rev. Lett. **91**, 131302 (2003).

[152] C. Gordon and K. A. Malik, Phys. Rev. D **69**, 063508 (2004).

[153] R. Trotta and R. Durrer, arXiv:astro-ph/0402032.

[154] D. Parkinson, S. Tsujikawa, B. A. Bassett, and L. Amendola, arXiv:astro-ph/0409071.

[155] G. Lazarides, R. R. de Austri and R. Trotta, arXiv:hep-ph/0409335.

[156] H. Kurki-Suonio, V. Muhonen and J. Valiviita, Phys. Rev. D **71**, 063005 (2005).

[157] M. P. Hobson and C. McLachlan, Mon. Not. Roy. Astr. Soc. **338**, 765 (2003).

[158] H. Jeffreys, *Theory of Probability*, 3rd ed, Oxford University Press (1961)

[159] D. J. C. MacKay, *Information theory, inference and learning algorithms*, Cambridge University Press (2003).

[160] A. R. Liddle, Mon. Not. Roy. Astr. Soc. **351**, L49 (2004).

[161] R. E. Kass and A. E. Raftery, Journ. Amer. Stat. Assoc. **90**, 773 (1995).

[162] A. Jaffe, Astrophys. J. **471**, 24 (1996); P. S. Drell, T. J. Loredo, and I. Wasserman I, Astrophys. J. **530**, 593 (2000); M. V. John and J. V. Narlikar, Phys. Rev. D**65**, 043506 (2002); M. P. Hobson, S. L. Bridle, and O. Lahav, Mon. Not. Roy. Astr. Soc. **335**, 377 (2002); A. Slosar *et al.*, Mon. Not. Roy. Astr. Soc. **341**, L29 (2003); T. D. Saini, J. Weller, and S. L. Bridle, Mon. Not. Roy. Astr. Soc. **348**, 603 (2004); A. Niarchou, A. H. Jaffe, and L. Pogosian, Phys. Rev. D**69**, 063515 (2004); P. Marshall, N. Rajguru, and A. Slosar, arXiv:astro-ph/0412535.

[163] J. J. K. Ó'Ruanaidh and W. J. Fitzgerald, *Numerical Bayesian Methods Applied to Signal Processing*, Springer–Verlag, New York, 1996

[164] N. W. Halverson *et al.*, Astrophys. J. **568** (2002) 38

[165] C. B. Netterfield *et al.* [Boomerang Collaboration], Astrophys. J. **571** (2002) 604

[166] R. Bean, J. Dunkley and E. Pierpaoli, Phys. Rev. D **74** (2006) 063503; R. Trotta, arXiv:astro-ph/0608116.

[167] D. H. Lyth and D. Wands, Phys. Lett. B **524**, 5 (2002)

[168] J. Silk and M. S. Turner, Phys. Rev. D **35**, 419 (1987); D. Polarski and A. A. Starobinsky, Nucl. Phys. **B385**, 623 (1992);

[169] T. D. Loredo, "From Laplace to Supernova SN 1987A: Bayesian Inference in Astrophysics", *Maximum-Entropy and Bayesian Methods*, Dartmouth, 1989, ed. P. Fougere pp. 81–142 (1990).

[170] Scharz G., 1978, Annals of Statistics, 5, 461.

[171] W. M. Yao *et. al.*, J. Phys G**33**, 1 (2006)

[172] A. Gelman and D. Rubin, *Statistical Science*, **7**, 457-511 (1992)

[173] J. M. Dickey, 1971, Ann. Math. Stat. **42**, 204

[174] P. Mukherjee, D. Parkinson and A. R. Liddle, Astrophys. J. **638** (2006) L51

[175] R. Trotta, arXiv:astro-ph/0504022

[176] R. Shaw, M. Bridges and M. P. Hobson, arXiv:astro-ph/0701867.

[177] C. Pahud, A. R. Liddle, P. Mukherjee and D. Parkinson, Phys. Rev. D **73** (2006) 123524

[178] D. Parkinson, P. Mukherjee and A. R. Liddle, Phys. Rev. D **73**, 123523 (2006).

[179] S. Perlmutter *et al.* [Supernova Cosmology Project Collaboration], "Measurements of Omega and Lambda from 42 High-Redshift Supernovae," Astrophys. J. **517** (1999) 565

[180] L. Hui, S. Burles, U. Seljak, R. E. Rutledge, E. Magnier and D. Tytler, Astrophys. J. **552**, 15 (2001).

[181] A. Cuoco, J. Lesgourgues, G. Mangano and S. Pastor, Phys. Rev. D **71**, 123501 (2005).

[182] V. Springel, N. Yoshida and S. D. M. White, New. Astr. **6**, 79 (2001); V. Springel, arXiv:astro-ph/0505010

[183] J. Lesgourgues and S. Pastor, Phys. Rept. **429** (2006) 307; K. N. Abazajian and S. Dodelson, Phys. Rev. Lett. **91** (2003) 041301

[184] M. Beltrán, J. Garcia-Bellido and J. Lesgourgues, "Isocurvature bounds on axions revisited." arXiv:hep-ph/0606107. Accepted for publication in Phys. Rev. D.

[185] A. Cabré, E. Gaztañaga, M. Manera, P. Fosalba and F. Castander, Mon. Not. Roy. Astron. Soc. Lett. **372** (2006) L23

[186] P. Vielva, E. Martinez-Gonzalez, R. B. Barreiro, J. L. Sanz and L. Cayon, Astrophys. J. **609** (2004) 22; E. Gaztanaga and J. Wagg, Phys. Rev. D **68** (2003) 021302

[187] F. Bernardeau, S. Colombi, E. Gaztanaga and R. Scoccimarro, Phys. Rept. **367** (2002) 1

[188] C. Blake, A. Collister, S. Bridle and O. Lahav, arXiv:astro-ph/0605303.